frontiers | Research Topics

Consequences of global change in coastal ecosystems from a multidisciplinary perspective

Edited by
Rodolfo Silva, Valeria Chávez, Nobuhito Mori, Tjeerd J. Bouma and Itxaso Odériz

Published in
Frontiers in Marine Science

ISSN 1664-8714
ISBN 978-2-83251-443-6
DOI 10.3389/978-2-83251-443-6

About Frontiers

Frontiers is more than just an open access publisher of scholarly articles: it is a pioneering approach to the world of academia, radically improving the way scholarly research is managed. The grand vision of Frontiers is a world where all people have an equal opportunity to seek, share and generate knowledge. Frontiers provides immediate and permanent online open access to all its publications, but this alone is not enough to realize our grand goals.

Frontiers journal series

The Frontiers journal series is a multi-tier and interdisciplinary set of open-access, online journals, promising a paradigm shift from the current review, selection and dissemination processes in academic publishing. All Frontiers journals are driven by researchers for researchers; therefore, they constitute a service to the scholarly community. At the same time, the *Frontiers journal series* operates on a revolutionary invention, the tiered publishing system, initially addressing specific communities of scholars, and gradually climbing up to broader public understanding, thus serving the interests of the lay society, too.

Dedication to quality

Each Frontiers article is a landmark of the highest quality, thanks to genuinely collaborative interactions between authors and review editors, who include some of the world's best academicians. Research must be certified by peers before entering a stream of knowledge that may eventually reach the public - and shape society; therefore, Frontiers only applies the most rigorous and unbiased reviews. Frontiers revolutionizes research publishing by freely delivering the most outstanding research, evaluated with no bias from both the academic and social point of view. By applying the most advanced information technologies, Frontiers is catapulting scholarly publishing into a new generation.

What are Frontiers Research Topics?

Frontiers Research Topics are very popular trademarks of the *Frontiers journals series*: they are collections of at least ten articles, all centered on a particular subject. With their unique mix of varied contributions from Original Research to Review Articles, Frontiers Research Topics unify the most influential researchers, the latest key findings and historical advances in a hot research area.

Find out more on how to host your own Frontiers Research Topic or contribute to one as an author by contacting the Frontiers editorial office: frontiersin.org/about/contact

Consequences of global change in coastal ecosystems from a multidisciplinary perspective

Topic editors

Rodolfo Silva — National Autonomous University of Mexico, Mexico
Valeria Chávez — National Autonomous University of Mexico, Mexico
Nobuhito Mori — Kyoto University, Japan
Tjeerd J. Bouma — Royal Netherlands Institute for Sea Research (NIOZ), Netherlands
Itxaso Odériz — Environmental Hydraulics Institute (IHCantabria), Spain

Citation

Silva, R., Chávez, V., Mori, N., Bouma, T. J., Odériz, I., eds. (2023). *Consequences of global change in coastal ecosystems from a multidisciplinary perspective*. Lausanne: Frontiers Media SA. doi: 10.3389/978-2-83251-443-6

Table of contents

frontiers | Frontiers in Marine Science

TYPE Editorial
PUBLISHED 11 January 2023
DOI 10.3389/fmars.2022.1130024

OPEN ACCESS

EDITED AND REVIEWED BY
Marta Marcos,
University of the Balearic Islands, Spain

*CORRESPONDENCE
Valeria Chávez
vchavezc@iingen.unam.mx

SPECIALTY SECTION
This article was submitted to Coastal Ocean Processes, a section of the journal Frontiers in Marine Science

RECEIVED 22 December 2022
ACCEPTED 29 December 2022
PUBLISHED 11 January 2023

CITATION
Silva R, Chávez V, Mori N, Bouma TJ and Odériz I (2023) Editorial: Consequences of global change in coastal ecosystems from a multidisciplinary perspective.
Front. Mar. Sci. 9:1130024.
doi: 10.3389/fmars.2022.1130024

Editorial: Consequences of global change in coastal ecosystems from a multidisciplinary perspective

Rodolfo Silva[1], Valeria Chávez[1]*, Nobuhito Mori[2,3], Tjeerd J. Bouma[4,5] and Itxaso Odériz[6]

[1]Instituto de Ingeniería, Universidad Nacional Autónoma de México, Mexico City, Mexico, [2]Disaster Prevention Research Institute, Kyoto University, Kyoto, Japan, [3]School of Engineering, Swansea University, Swansea, United Kingdom, [4]Department of Estuarine and Delta Systems, Royal Netherlands Institute for Sea Research (NIOZ), Texel, Netherlands, [5]Department of Physical Geography, Faculty of Geosciences, Utrecht University, Utrecht, Netherlands, [6]IHCantabria - Instituto de Hidráulica Ambiental de la Universidad de Cantabria, Santander, Spain

KEYWORDS

climate change, coastal ecosystems, ecosystem services, hydrodynamics, sea level rise (SLR)

Editorial on the Research Topic
Consequences of global change in coastal ecosystems from a multidisciplinary perspective

On the need to investigate ecosystems from a multidisciplinary perspective

Ecosystems will play a key role in the future of our planet, as they are capable of great adaptabilty and are resilient to climate (e.g. Bulleri et al., 2018). However, they are also vulnerable to multifactorial disturbances (e.g. anthropic/Gómez et al., 2022). An ecosystem's long-term response to global change (climate change, biodiversity loss, changes in water cycling, etc.) is also affected by the natural, epistemic, and aleatory uncertainty of the environment.

The methods used to evaluate an ecosystem mean that the services it provides are difficult to quantify and predict. While ecosystem conservation strategies should come from a combination of different perspectives, they are commonly tackled *via* independent disciplines, such as coastal management, coastal engineering, ecology, water quality, etc. and therefore, insights into the long-term conservation of our ecosystems is still a key challenge. The starting point to address ecosystem conservation on a changing planet must be a multidisciplinary characterization of the physical and environmental context.

Summary of contributions

Through nine papers, this special issue emphasises the need to address multi-scale problems with multidisciplinary perspectives in which key physical and environmental issues are highlighted:

Biomass loss
Coastal protection
Future scenarios

Biomass loss

Extreme heatwaves at sea may cause ecosystem loss. For example, Magel et al. analyzed the effect of the increase in water temperature on eelgrass and macroalgae in the marine heatwave of 2013-2016 in the northeast Pacific Ocean in four estuaries (Willapa Bay, Washington, and Netarts Bay, Yaquina Bay, and Coos Bay, Oregon). They found that the eelgrass biomass declined for shallower estuaries, with normally higher temperatures. In contrast, there was a neutral or temporarily positive change in aboveground eelgrass biomass in the deeper and colder estuaries.

Similar conclusions were found in another study in the Coos Estuary by Marin Jarrin et al., which also analyzed the impacts of the unusually warm oceanic and atmospheric conditions that occurred from 2014-2016. They found that an increase of at least 1.5°C for over 100 days induced stress and caused eelgrass loss at some stations in this shallow estuary.

At the other end of the temperature spectrum, Ren et al. examined abundance and composition in the bacterial community in Aoshan Bay, in the southern Yellow Sea, during a cold surge in January 2021. They identified differences in the abundance of bacteria in the sea ice and in seawater, presumably from the physical impact of ice formation.

Also associated with biophysical changes, Fang et al., used an integrative model to show that the 304 ton decrease in ragworm biomass in the Western Scheldt estuary (Netherlands) between 1955 and 2010 was driven by alterations in peak current velocities and inundation times in the intertidal habitat, resulting from deepening, dredging and disposal activities.

Coastal protection

Changes in hydrodynamic patterns and ecosystem health may alter valuable ecosystem services, such as coastal protection. On a local scale, Maximiliano-Cordova et al. studied how plants contribute to mitigating dune erosion during a single storm, by monitoring dune evolution on three beaches in the state of Veracruz, Mexico. They found that plants provide dune resistance but that this resistance is site- and species-specific, strongly depending on the pre-storm dune and conditions for species.

Salt-marsh ecosystems also provide valuable coastal protection services, although anthropization and extreme events damage the marsh vegetation and alter this capacity. Reents et al. investigated the response of salt-marsh vegetation to extreme hydrodynamic conditions in a true-to-scale flume experiment. They found salt-marsh vegetation generally had high robustness, although this varied between species: pioneer species showed higher resistance than the high-marsh species.

Future scenarios

As climate change and local and regional anthropization are often responsible for ecosystem loss, McMahon et al. developed a spatially explicit risk model to determine the impacts of various factors on seagrass along the 35,000 km of the Australian coast. They identified two risk hotspots based on climate change (i.e., increase temperature, increased rainfall, and sea level rise), and many other areas at high risk due to multiple threats (e.g., resuspension, industrial pollution, shipping accidents).

Regarding marine species, Diaz-Carballido et al. generated models in Maxent for four climate change scenarios (RCP2.6, RCP4.5, RCP6.0, and RCP8.5) to predict the geographic distribution of 25 carcharhinid sharks that inhabit Mexican waters. They determined that by 2050, climate change will reduce the areas suitable for most of these species.

Loss of ecosystem services can be quantified in terms of economic losses. For example, Fernández-Díaz et al. estimated a loss of 6 billion USD for flooding related to the loss of ecosystem services in Mexico under a scenario of sea level rise of +0.84 m from SSP5-8.5 (2081-2100).

Outlook

While the papers in this special issue do not give a definitive answer as to how coastal ecosystems and their services are affected by climate change processes, they do illustrate how physical and environmental perspectives should be integrated to get a system understanding. We hope this special issue will inspire scientists to document case studies, and to measure key parameters in order to gain a full understanding of how coastal ecosystems function and, over time, feed into predictive models to help better manage them.

Author contributions

RS and VC wrote the first draft of the manuscript. NM, TB and IO revised and edited the manuscript. All authors contributed to manuscript revision, read, and approved the submitted version.

Conflict of interest

The authors declare that the research was conducted in the absence of any commercial or financial relationships that could be construed as a potential conflict of interest.

Publisher's note

References

Bulleri, F., Eriksson, B. K., Queirós, A., Airoldi, L., Arenas, F., Arvanitidis, C., et al. (2018). Harnessing positive species interactions as a tool against climate-driven loss of coastal biodiversity. *PloS Biol.* 16 (9), e2006852. doi: 10.1371/journal.pbio.2006852

Gómez, I., Silva, R., Lithgow, D., Rodríguez, J., Banaszak, A. T., and van Tussenbroek, B. (2022). A review of disturbances to the ecosystems of the Mexican Caribbean, their causes and consequences. *J. Mar. Sci. Eng.* 10 (5):644. doi: 10.3390/jmse10050644

frontiers in Marine Science

ORIGINAL RESEARCH
published: 24 August 2021
doi: 10.3389/fmars.2021.734036

Assessing the Impact of a Winter Storm on the Beach and Dune Systems and Erosion Mitigation by Plants

Carmelo Maximiliano-Cordova[1], M. Luisa Martínez[1], Rodolfo Silva[2], Patrick A. Hesp[3], Roger Guevara[1] and Rosario Landgrave[1]*

[1] Instituto de Ecología, A. C., Xalapa, Mexico, [2] Instituto de Ingeniería, Universidad Nacional Autónoma de México, Ciudad de México, Mexico, [3] Beach and Dune Systems (Beads) Lab, College of Science and Engineering, Flinders University, Bedford Park, SA, Australia

OPEN ACCESS

Edited by:
Juan Jose Munoz-Perez, University of Cádiz, Spain

Reviewed by:
Raul Martell-Dubois, National Commission for the Knowledge and Use of Biodiversity (CONABIO), Mexico
Patricia Lopez-Garcia, University of Cádiz, Spain

****Correspondence:***
Carmelo Maximiliano-Cordova
cmcordova14@gmail.com

Specialty section:
This article was submitted to Coastal Ocean Processes, a section of the journal Frontiers in Marine Science

Received: *30 June 2021*
Accepted: *03 August 2021*
Published: *24 August 2021*

Citation:
Maximiliano-Cordova C, Martínez ML, Silva R, Hesp PA, Guevara R and Landgrave R (2021) Assessing the Impact of a Winter Storm on the Beach and Dune Systems and Erosion Mitigation by Plants. Front. Mar. Sci. 8:734036. doi: 10.3389/fmars.2021.734036

The impact of storms on coastal dunes and beaches and the effects they induce in topography and plant communities are natural processes that contribute to maintaining natural coastal dynamics. However, because coasts are often densely populated, these phenomena are perceived as major threats to human property. To protect human assets sustainably, nature-based defenses have emerged as an option. Coastal dunes act as natural buffers that mitigate the extent of erosion and inland flooding, and their resistance depends on the biogeomorphological feedback between the plants and the dunes. This study aimed to evaluate the effect of one winter storm on beach and dune topography and the plant communities, and to explore the effect of plants in mitigating erosion on beaches with different geomorphological features. The effects on plant communities were evaluated by comparing diversity and plant cover before and after the storm. Later, the role of plants in conferring dune resistance against erosion was examined by measuring erosion on the exposed face of the dunes considering plant cover and plant richness. The results did not show significant differences in plant diversity and plant cover between pre-and post-storm conditions, but turnover of species was recorded. The dune building species were not affected but inland species disappeared. Erosion was reduced when the dunes were higher and, furthermore, plant cover was negatively correlated with erosion on these dunes. The results showed a reduced impact of the storm on the plant communities, which is important as it facilitates the recovery of dunes by the dune-building species and protects them in a subsequent storm. The novelty of this study is that: (a) it demonstrates the species-specific role of plants in mitigating dune erosion in field conditions; (b) it shows the interaction between plant-related features and geomorphological variables in promoting dune resistance to erosion, and (c) it explores the immediate effect of a winter storm on the plant community and dune-building species.

Keywords: coastal erosion, vegetation, foredunes, plant cover, plant diversity, storms, erosion mitigation

INTRODUCTION

Tropical cyclones and winter storms are major drivers in shaping coastal geomorphology through energetic waves, storm surges, set-up, and strong winds which may induce dramatic changes (Coch, 1994; Castelle et al., 2015; Masselink et al., 2016). On wave-dominated sandy coasts, these natural, episodic phenomena are frequently associated with considerable erosion on the beach and dunes (Vellinga, 1982; Carter, 2013; Davidson et al., 2020). After a storm episode, the beach face is lowered and cut back, and a vertical scarp is often seen, due to the loss of sand volume on the dry beach (Hesp, 2002; Carter, 2013; Castelle et al., 2015). However, this sand will return and accumulate on the beach and dunes when calm conditions prevail if the sediment budget is not affected by natural or human processes, and the beach-surfzone has no net sediment deficit (Carter, 2013; Davidson-Arnott et al., 2018). In brief, the coastal response, including the volume of sand that will be eroded during a storm, depends on storm-related features, the cluster of storms (Karunarathna et al., 2014), the synchronicity of environmental variables (e.g., tide, wind direction; Guisado-Pintado and Jackson, 2018, 2019), and factors such as dune height (Pries et al., 2008), the slope of the beach and dunes (Vellinga, 1982), the mechanical characteristics of the bed material (e.g., type of sediment, diameter, and sand density; Overton et al., 1994), the sand volume stored on the beach and dunes (Sigren et al., 2018), the compaction of the foredune (Nishi and Kraus, 1997), the presence of a berm and sand bars (Figlus et al., 2011), the length of foredune ridge (Houser, 2013), and the width of the beach and dunes (Saye et al., 2005; Pries et al., 2008; Davidson et al., 2020).

Besides the geomorphological features of the coast, the impact of storms is also relevant for plant communities and coastal risk management. Plant communities are commonly disturbed by the environmental conditions associated with storms, such as heavy precipitation, flooding, high salinity concentrations, accretion, and erosion (Wolner et al., 2013; Brantley et al., 2014; Cheplick, 2016). The effects of storms on plant communities depend on the spatial and temporal scale of the storm, its magnitude, storm clustering, and the species-specific responses of the plants growing in the different dune habitats (foredunes, interdunes, and back dunes; Judd and Sides, 1983; Gornish and Miller, 2010; Miller et al., 2010; Miller, 2015). Some of these effects include a reduction in plant species richness and diversity (Judd and Sides, 1983; Miller et al., 2010; Cheplick, 2016), species turnover (Synder and Boss, 2002; Miller et al., 2010), changes in species dominance, and their distribution in the dune habitats (Gornish and Miller, 2010), and changes in plant cover or abundance (Cheplick, 2016).

Moreover, because of the biogeomorphological feedback between dunes and plants, the geomorphological responses of the beaches and dunes during storm (but also during dune development and the recovery of the dune) depend on the response of the plant communities and the species-specific response (Stallins and Parker, 2003; Stallins, 2005; Wolner et al., 2013; Brantley et al., 2014). The close interaction between dune plants and coastal dunes occurs because plants entrap, collect, and stabilize sediment, and thus shape dune topography (Moreno-Casasola, 1986; Hesp, 1991, 2002; Hesp et al., 2019). By acting as sediment traps, plants accumulate sand, accelerate accretion, build dunes, withhold sand, and help mitigate erosion. Dune geomorphology depends on factors such as plant zonation (Doing, 1985; Maun and Perumal, 1999; Durán and Moore, 2013), plant density and height (Hesp, 2002; Hesp et al., 2019), and plant architecture (Zarnetske et al., 2012; Charbonneau et al., 2016, 2021). Consequently, different dune types shaped by distinct species could differ in their resistance to erosion (Charbonneau et al., 2021). In addition to burial by sand, plants on the backshore and incipient dunes are also tolerant to salinity (Maun, 1998), so they are likely to survive and recover after the impact of storms, which bring sand movement and flooding with salt water. The resistance and tolerance of plants to storm conditions is of relevance because if dune-building species are harmed, the recovery of the dunes (growth and development) could be arrested and bring about changes in dune morphology. In consequence, storm protection might decrease and the recovery of dunes after the storm could be arrested. Inland vulnerability after subsequent storms may thus increase.

In terms of coastal risk management, when storms are likely to damage human infrastructure and result in the loss of human lives, the above-mentioned biogeomorphological system generated through the dynamic interaction between plants and dunes, becomes highly relevant. This is especially true for coastal green infrastructure solutions whose premise is to protect exposed human interests from ocean hazards, and potentially from sea-level rise, by working with natural processes (Temmerman et al., 2013; Spalding et al., 2014; Chávez et al., 2021). Coastal dunes are often the first natural terrestrial defense against storm impact. Dunes help to reduce the landward extent of erosion, overwashing, the impact of waves (swash, collision, overwash, and inundation; Sallenger, 2000), and the degree of damage to property, by dissipating wave energy, and reducing/preventing floods (Sigren et al., 2018). The protective role of the dunes lies in their natural ability to adjust to the natural disturbances in the littoral (including storm impacts) by changing their morphological configuration (their relative position and form) migrating landward or seaward in response to wind, waves, and sea-level rise (Davidson-Arnott, 2005; Saye et al., 2005).

In addition to the role of plants in promoting the development of these natural barriers, they can also help reduce beach and dune erosion during storms. Laboratory studies have shown that erosion on vegetated dunes is reduced or slowed down, in comparison with dunes without vegetation (Kobayashi et al., 2013; Silva et al., 2016; Figlus et al., 2017; Bryant et al., 2019). It has also been demonstrated that their roots contribute to strengthening the cohesiveness of the sand (Sigren et al., 2014; De Battisti and Griffin, 2020), while the above-ground plant parts slow wave uprush, and reduce wave overtopping and overwashing (Silva et al., 2016; Figlus et al., 2017; Feagin et al., 2019), displace the wave breaking point seawards and deaccelerate the undertow close to the shoreline (Mendoza et al., 2017). Furthermore, Charbonneau et al. (2017) demonstrated that the reduction of erosion is species-specific. These findings are supported by Maximiliano-Cordova et al. (2019), while Odériz et al. (2020) determined that the spatial location of

the plants on the dune affects the erosion patterns, as well as the mass, density, and depth of the roots (Davidson et al., 2020). To our knowledge, only three studies performed in field conditions have tested the effect of plants in conferring dune resistance to wave-induced erosion. Lindell et al. (2017) observed that when plants were removed, wave erosion was greater than that on dunes where the vegetation remained, while Charbonneau et al. (2017) and Biel et al. (2017) documented species-specific dune resistance. Nevertheless, there is a large information gap concerning field conditions which demonstrate how protection offered by plants could depend on the plant- and geomorphological-related features that vary between beaches.

In brief, the impact of even a single storm event is a complex process because it may affect the topography and morphology of the beach and dunes as well as the plant community developing in this environment. In addition, in field conditions, as revealed in findings from laboratory experiments, plants can have a negative impact on erosion and play a protective role. Based on the above, this study aims to: (I) analyze how beach and dune profiles were affected by one winter storm; (II) analyze the impact of this storm on the plant communities established on the beach, the backshore and dunes; (III) examine how pre-existing morphological conditions of the beach-dune complex affect erosion; and (IV) explore whether plant cover and plant species richness help mitigate beach erosion in different dune and beach geomorphologies. Our working hypotheses were: (a) Plant cover and diversity decrease because of the impact of the storm, which also induces changes in species composition and dominance of the dune-building species. (b) Pre-existing beach and dune geomorphological conditions determine storm-induced erosion. Beaches with higher dunes are less likely to be eroded and overwashed than those that are flatter. (c) Plants help mitigate beach and dune erosion, which is expected to decrease with increasing plant cover and species richness. Ultimately, our premise was that the interaction between plants and geoforms modifies beach and dune response to the impact of storms.

MATERIALS AND METHODS

Study Sites

Three beaches located in the central region of the Gulf of Mexico, on the coast of Veracruz (Mexico), were studied: Riachuelos, Navarro, and La Mancha (**Figure 1**). The climate is warm and sub-humid (Martínez et al., 2014) with mean yearly temperatures ranging from 22 to 25°C, and total annual precipitation fluctuating between 1,200 and 1,650 mm (Infante-Mata et al., 2011). The rainy season is from August to September,

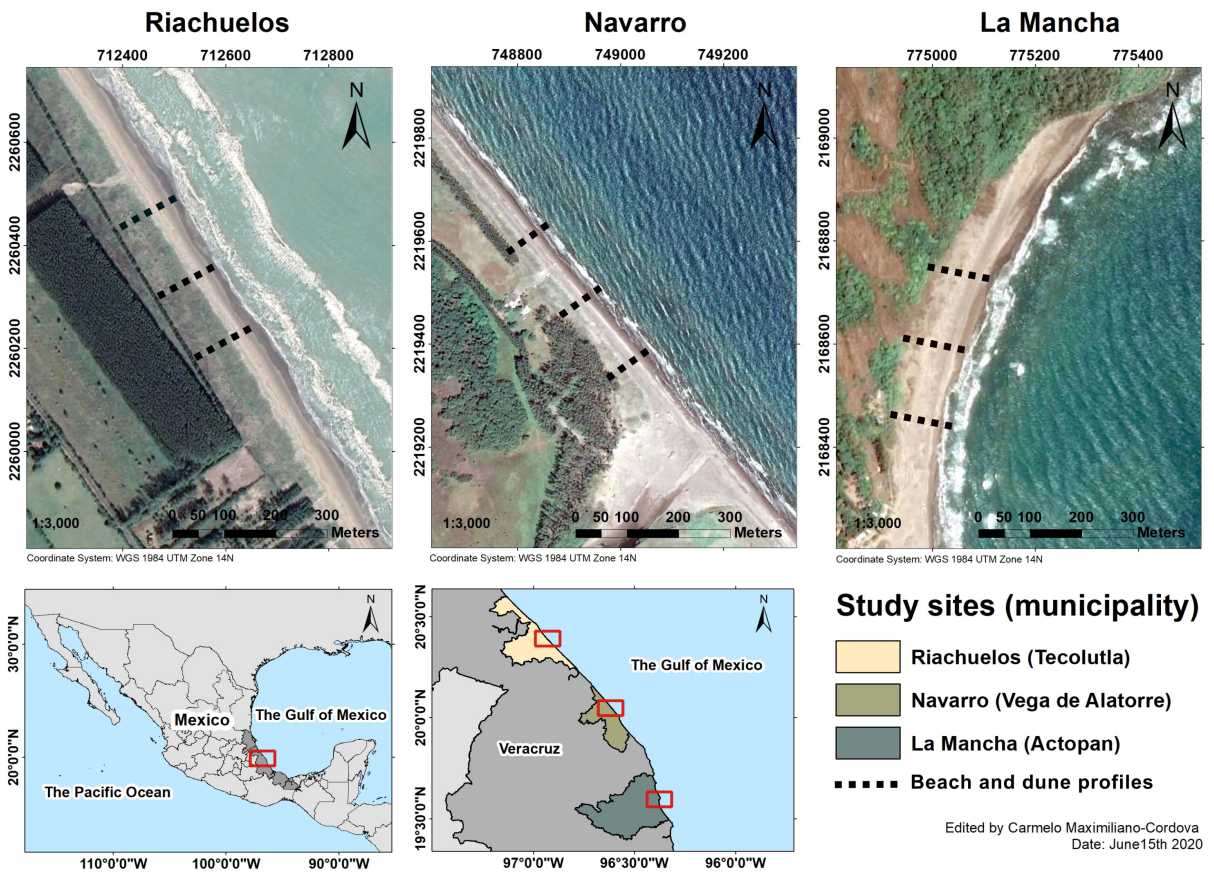

FIGURE 1 | Location of the study sites in the state of Veracruz, Mexico. Images based on satellite images from Google Earth.

coinciding with the season of tropical cyclones (Martínez et al., 2014). Winter storms, known locally as "nortes," occur from November to February and can generate storm surges exceeding 1.5 m and extreme winds of 80 to 100 km/h (Ramírez and Reséndiz, 2002). Both of these phenomena produce energetic waves (Psuty et al., 2009) and can consequently induce dramatic changes in the topography of the beach and dunes.

The three beaches are fed by sand from at least one of the two most important rivers on the central coast of Veracruz. Riachuelos receives sediment from the Tecolutla River while Navarro and La Mancha receive sediments from the Tecolutla and Filobobos rivers. In addition, sediment from adjacent lagoons such as "El Llano" and "La Mancha" is supplied to the beach-dune system of La Mancha. On the central coast of Veracruz, the along-shore sediment is transported from north to south, and its distribution on the coast depends on waves and currents. Aeolian transport is also important, contributing to the alongshore sediment supply, especially in embayed coasts, such as La Mancha (Psuty et al., 2009). Therefore, well-developed dune systems are likely to be found in the study area.

The three beaches are different in terms of their geomorphological features, as well as the dominant vegetation growing on the beach and coastal dunes (**Table 1**). Incipient dunes generated by the creeping vine species *Ipomoea pes-caprae* and the succulent *Sesuvium portulacastrum* are formed on the beach at Riachuelos and La Mancha, with established foredunes behind them. At both sites, the incipient dunes are developed behind the high tide line and do not form a continuous ridge parallel to the coast. At Navarro, there is a well-formed continuous foredune ridge formed by the grass *Panicum amarum* and no incipient dunes are found here. Instead, a second well-formed foredune is developed behind the first one. These geomorphological differences are associated with the dominant plant species growing at each location (in addition to other biophysical variables). They are relevant in determining the response of the beach and dunes to the impact of storms. For instance, a continuous dune ridge is expected to be more resistant to the impact of waves than isolated dunes, which are more susceptible to scarping and erosion (Claudino-Sales et al., 2008). Therefore, the effects of the storm on beach and dune topography, the plant communities, and the effect of the plants in creating dune resistance versus erosion, were explored on different beaches, with different geomorphologies and plant dominance. For simplicity, from here on, although different, both types of dunes are referred to as "dunes."

Storm Conditions

This study focuses on the impacts of a single winter storm event which took place in 2019. Winter storms are milder than tropical cyclones and therefore less destructive. As winter storms occur shortly after the rainy season, the vegetation is fully developed, plant cover is likely to be at a maximum, and plants can more effectively protect the backshore and dunes from erosion. In turn, tropical cyclones occur during the summer, when the vegetation is recovering from the spring-time drought, so they are likely to be less effective in providing protection.

TABLE 1 | Main geomorphological attributes of the beaches studied (* geomorphological features estimated from field surveys performed before the storm).

Features	Riachuelos	Navarro	La Mancha
Geomorphological features*	Exposed open beach	Exposed open beach	Headland-bay beach
Tidal range (Davies, 1964)	Microtidal (<2 m)	Microtidal (<2 m)	Microtidal (<2 m)
Surfzone-beach type (Short and Wright, 1983; Wright and Short, 1984)	Intermediate longshore bar-trough	Intermediate longshore bar-trough	Intermediate rhythmic bar and beach
Beach slope (field observations)	Gentle slope	Steep slope	Gentle slope
Dune types*	Incipient dunes and established foredunes	Foredune	Incipient dunes and established foredunes
Swash zone width (m; mean ± se)*	20.00 ± 1.15	21.66 ± 0.33	33.00 ± 4.72
Backshore width (m; mean ± se)*	32.66 ± 2.90	21.33 ± 0.66	29.33 ± 6.35
Dune system width (m; mean ± se)*	76.33 ± 3.48	33.66 ± 3.48	60.00 ± 6.80
Dune-beach-swash zone width (m; mean ± se)*	129.00 ± 3.78	76.66 ± 3.71	122.33 ± 6.66
Foredune height (m; mean ± se)	2.03 ± 0.28	3.32 ± 0.33	1.06 ± 0.08
Sediment (Flores, 2016)	Fine	Fine	Fine
Sediment size (D_{50}; mm) (Flores, 2016; Martínez et al., 2017)	0.256	0.254	0.222
Sediment roundness (Flores, 2016)	0.871	0.877	0.869
Sediment sphericity (Flores, 2016)	0.827	0.836	0.830
Dominant species on the backshore and embryo dunes (field observations)	*Sporobolus virginicus, Sesuvium portulacastrum, Palafoxia lindenii,* and *Ipomoea pes-caprae.*	*Panicum amarum* and *Sporobolus virginicus*	*Sporobolus virginicus, Sesuvium portulacastrum, Palafoxia lindenii,* and *Ipomoea pes-caprae.*

We studied the effects of winter storm Number 12, which arrived at the Gulf of Mexico on November 12th, 2019. Even though 11 winter storms had previously occurred in the Gulf of Mexico, this was the first of the season to affect the coast of Veracruz. According to the reanalysis of ERA5 (Copernicus Climate Change Service (C3S), 2017), the storm had sustained winds of up to 15.5 m/s, significant waves heights of up to 4.5 m, with a mean wave period of 9 s, and induced 27.95 mm of precipitation. The winds had a predominant Northwest direction, and were mainly moderate in velocity (**Figure 2A**). The prevailing waves arrived from the north and were high (**Figure 2B**). It is important to mention that the lack of bathymetry for the three beaches means that the description of the wave propagation during the storm could not be more accurate.

Fieldwork

The topography and vegetation of the beach and dunes were monitored before and after the impact of a single winter storm, in September and November 2019, respectively. At each study site, three transects were established, perpendicular to the coastline (**Figure 1**). The length of the transects varied depending on the width of the beach, the number of dune ridges, and the limit of private properties at the back of the beach. The transects in Riachuelos and Navarro were set from the toe of the second dune ridge toward the ocean, while in La Mancha they were set from the toe of the stabilized foredune toward the ocean (**Figure 3A**). On each transect, three control points were marked to facilitate their relocation in the post-storm monitoring. The first marker was placed at the beginning of the dune-ocean transect and was considered as the zero reference point ($x = 0$ and $y = 0$ coordinates). The second marker was placed in the middle of the transects and the third in the swash zone of the beach. All three points were georeferenced with a GPS (Garmin GPSMAP®64) and the first and the second points were also marked with aluminum stakes.

Monitoring of Topography (Beach and Dune Profile)

The pre- and post-storm beach and dune profiles were measured along the three transects set on each beach, from the dune toward the ocean (**Figure 3A**), beginning at a previously set point of a known height (our $x = 0$ and $y = 0$ coordinates), with two inclinometers made in the laboratory (**Figure 3B**; Emery, 1961; Krause, 2004). The instruments measured changes in topography between two points set at distances of either 0.5 or 1 m, depending on the topography (**Figures 3B–D**).

The zero-level of the sand surface used as the $x = 0$ and $y = 0$ (height and distance) reference point to measure changes in topography was set based on a 1 m aluminum stake which was marked every 1 cm, with positive and negative numbers, from the zero-line drawn in the middle of the stake. The stake was buried in the sand so that the zero-line coincided with the level of the sand. Following the storm, the topography was measured again, erosion and accretion were registered, and the reference point was adjusted so that the changes in topography could be assessed similar to Davidson-Arnott and Law (1996).

Vegetation Monitoring

Plots (2 × 2 m) were established at two meter intervals to monitor the vegetation along each transect (**Figure 3E**). The first plot was at the $x = 0$, $y = 0$ coordinates used to measure the topography, and subsequent plots were placed at two-meter intervals with the last plot being located at the seaward-most limit of vegetation on the backshore. The corners of each plot were georeferenced and three plots per transect were marked with aluminum stakes to locate them precisely in the post-storm monitoring.

The number of plots monitored per beach and per transect varied, depending on the beach width and the distribution of plants on the foredunes and backshore. Before the storm, 52 plots were monitored at Riachuelos, 24 at Navarro and, 47 at La Mancha. After the storm 54, 24, and 40 plots were monitored, respectively. In each plot, every vascular plant species was identified and the percentage of plant cover per species, the total percentage of plant cover, and the percentage of bare sand were estimated visually (Martínez et al., 2001, 2019). For each plot, the visual percent cover estimations were performed by the same person to avoid bias. When species were unknown, three samples were collected for identification in the herbarium at the Institute of Ecology (XAL), in Xalapa, Veracruz.

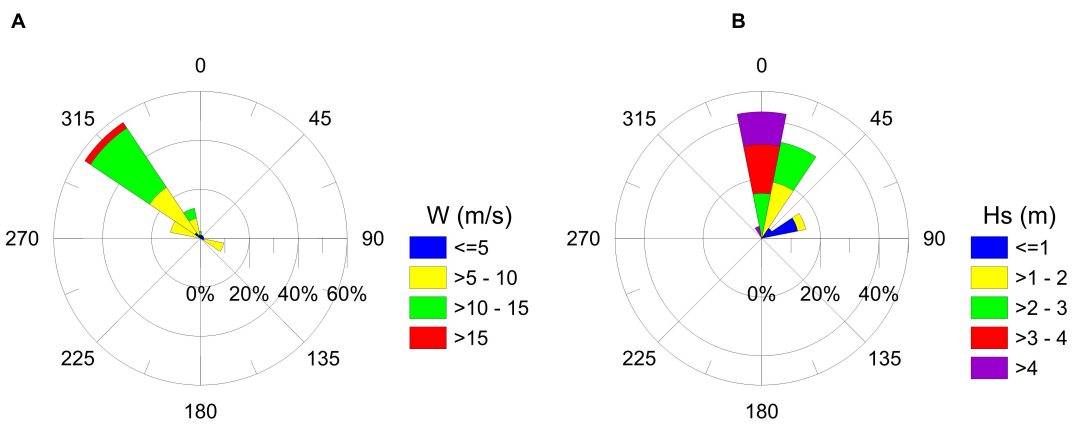

FIGURE 2 | (A) Wind velocity and **(B)** significant wave height roses associated to the Winter Storm Number 12 (November 12–15, 2019).

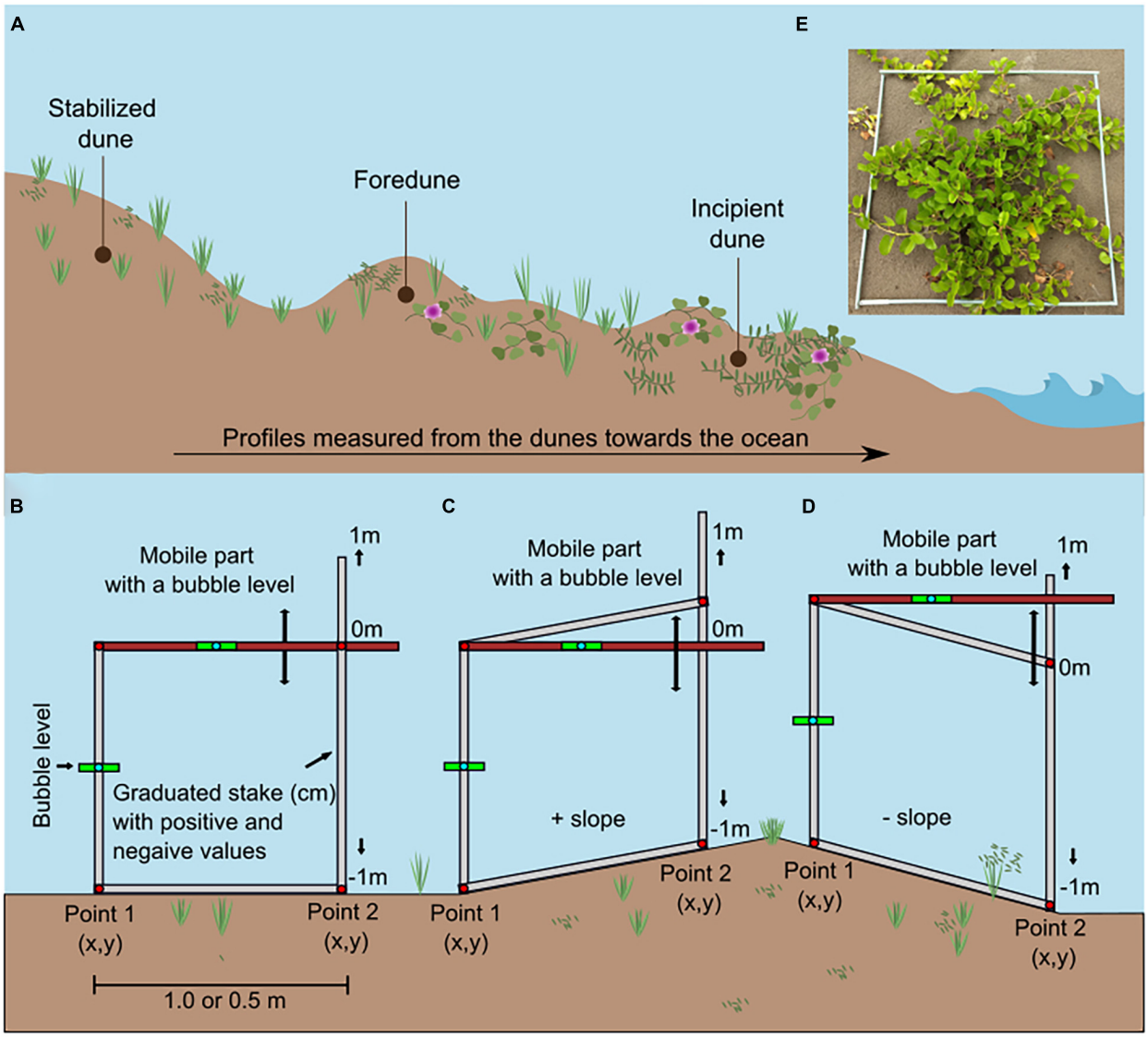

FIGURE 3 | (A) Beach and dune profile showing the direction in which the profiles were measured from the foredune to the swash zone. **(B)** A self-made instrument to measure changes in height (y) between two points separated by a known distance (x). Each time that the user advances, in one-m segments (or 0.5 m segments), changes in height can be measured. Because of the direction in which the profiles were measured (from the dunes to the beach), positive slopes were mainly associated with protected faces of the dune **(C)**, and negative slopes with the exposed face **(D)**. **(E)** Picture showing one of the plots where vegetation was sampled.

Data Analyses

Topography

The beach profiles measured, as explained above, were processed and analyzed with ArcMap 10.5. The *x*, *y* coordinates from each transect were projected as points, transformed into lines, and then into a single polygon, by joining the lines with a straight, horizontal line drawn from the first to the last point. This line was set at a constant height and serves as the baseline of the polygon. Then, the "union" tool of ArcMap was used to overlap the pre-and post-storm profiles. After the overlap, new polygons were created for each pair of profiles, producing new polygons showing accretion, erosion, and no changes in the topography. The area of the new polygons was calculated with the "calculate geometry" tool of ArcMap and then the volume of sand eroded or accreted was calculated for (i) each entire profile, (ii) the frontal dune, backshore, and beach of each profile (measured from the base of the lee slope of the dune to the lowest seaward elevation surveyed) and, (iii) each two-meter segment where the plot to monitor vegetation had been placed.

Beach volume was calculated based on the area of the polygon and by assuming that changes measured in the profile were the same in the adjacent 0.25 m on each side of the transect (0.5 m in total). Thus, changes in the volume were calculated as Eq. 1.

$$V = Ab \times h$$

where V = volume, Ab = base area (polygon area) and, h = height (0.5 m). For the three areas where the volume was calculated, net erosion was estimated by subtracting the total accretion from the total erosion. In the case of the erosion on the entire profile and erosion on the frontal dune and beach, an analysis of variance was performed to see whether the amount of erosion varied between the beaches. The analysis was run in R Studio (R version 3.6.1 "Action of the Toes"; R core Team, 2019).

In addition, for each profile, the maximum height (m) of the first incipient, or foredune, was calculated as the vertical distance from the sea level to the crest of the dune, and with the *x, y* coordinates, the following variables were calculated: width of the backshore (m), slope of the backshore and the stoss slope of the dune. The slopes were calculated as the slope of the line (Eq. 2) and then they were expressed as angle (θ) in sexagesimal degrees (Eq. 3).

$$m = \frac{y2 - y1}{x2 - x1}$$

where *x1* and *y1* represent the coordinates of the first point of the profile (the beginning) and *x2* and *y2* represent the coordinates of the second point (the end) of the segment.

$$\theta = \tan^1(m)$$

It is important to clarify that since the profiles were measured from the dunes toward the ocean, positive values refer to the lee face of the foredunes (the higher the positive number, the steeper the slope on the lee face of the dunes) and negative slopes were measured on the stoss face of the dune (the greater the negative numbers, the steeper the slope in the exposed faces of the embryo dunes). However, for the statistical analysis in which the slopes were considered, the absolute values of the slopes were used. Finally, values close to 0 indicate a gentle or flat slope.

Assessing the Effect of the Winter Storm on the Plant Community

The effect of the winter storm on the plant community was determined based on changes in plant cover, plant diversity, and species dominance. For each sampled plot, and at each observation date, the percentage of species cover was converted into m^2 (Martínez et al., 2001, 2019) as Eq. 4.

$$\frac{\text{Percent plant cover} \times \text{total area of each plot}}{100}$$

Then, plant cover per species (m^2), total plant cover (m^2), and species richness were used to evaluate: (i) the changes in plant cover, (ii) plant diversity, and (iii) the Relative Importance Value (RIV).

Plant cover

Two paired sample *t*-tests were performed (i) to look for differences in overall plant cover between pre- and post-storm conditions at each site by considering all the plots located on the dunes and backshore, and (ii) to explore the changes in seaward vegetation established on the dunes closest to the ocean (incipient dunes for Riachuelos and La Mancha and foredunes for Navarro). To achieve this, first, we added total plant cover per transect so that for each beach, we had three plant cover values before the storm and three after the storm, which were compared with a *t*-test for each site. Then, we focused the analyses on the three vegetated plots located closest to the ocean (per transect) and followed the same procedure that was used for the complete transects. The tests were run in R studio (R version 3.6.1 "Action of the Toes"; R core Team, 2019).

Alpha-diversity

Alpha diversity was evaluated using the concept of "effective numbers of species" (Jost, 2006; Eq. 5), a method that is equivalent to Hill's number (Hill, 1973). This method has mathematical properties that accurately capture the diversity concept, the replication principle is met and the magnitude of the differences in diversity between two communities can be interpreted adequately (Jost, 2006; Cultid-Medina and Escobar, 2016).

$${}^qD \equiv \left(\sum_{i=1}^{S} P_i^q\right)^{1/(1-q)}$$

Where:

${}^qD$ is the diversity of the community according to the chosen diversity index (Jost, 2006). It depends on the proportional abundance per species (P_i) and the exponent q (Jost, 2006; Cultid-Medina and Escobar, 2016). The exponent and superscript q is called the "order of diversity" and indicates the sensitivity to common and rare species (sensitivity to species abundance). For the study, the q values used were: 0 (${}^\circ D$) which is the species richness, 1 (${}^1D$) which is the common species (Shannon diversity), and 2 (${}^2D$) which is the number of dominant species (Simpson diversity; Jost, 2006).

The values of the three orders of diversity were measured before and after the storm and were compared. Because the methods established by Jost (2006) and Hill (1973) were used, the comparison is only possible if the sample coverage is the same in the two communities (Chao and Jost, 2012). Therefore, it is necessary to know the sample coverage, which is a measure indicating the proportion of the statistical population represented by the species sampled (Eq. 6; Chao and Jost, 2012). Thus, before estimating and comparing diversity, sample coverage ($\hat{C}m$) was calculated.

$$\hat{C}m = \left(1 - \frac{f1}{n}\left[\frac{(n-1)f1}{(n-1)f1 + 2f2}\right]\right) \times 100$$

Where *f1* and *f2* are the numbers of singletons and doubletons, respectively, and n is the abundance of the sample. The values of sample coverage range from 0 (minimal completeness) to 100 (maximum completeness). When the completeness value is close to 100, and it is similar to the species assemblages to be compared, then diversity values (${}^qD$) can be compared directly (Chao and Jost, 2012; Cultid-Medina and Escobar, 2016). Finally, comparisons between the different orders of diversity (0, 1, and 2) were performed, considering the overlap between the confidence intervals (CI) at 95% (Cumming et al., 2007). Data analyses were performed with the iNEXT library (Hsieh et al., 2016) in R studio (R version 3.6.1 "Action of the Toes"; R core Team, 2019).

Beta-diversity

For each site, beta-diversity (variations in species composition) was evaluated as the total dissimilarity between two species assemblages at two-time steps (the pre-and post-storm; Baselga, 2010). The total dissimilarity was computed as the Jaccard Index (β_{jac}; Eq. 7). Additionally, its two partition components, species turnover (β_{jtu}; Eq. 8), and nestedness (β_{jne}; Eq. 9) were considered (Baselga, 2010, 2012; Baselga and Orme, 2012).

Jaccard dissimilarity (Eq. 7):

$$\beta_{jac} = \frac{a + c}{a + b + c}$$

Turnover component of Jaccard dissimilarity (Eq. 8):

$$\beta_{jtu} = \frac{2\min(b, c)}{a + 2\min(b, c)}$$

Nestedness-resultant component of Jaccard dissimilarity (Eq. 9):

$$\beta_{jne} = \frac{\max(b, c) - \min(b, c)}{a + b + c} \times \frac{a}{a + 2\min(b, c)}$$

where:

a is the number of shared species in both sites (in this study, on both dates), *b* is the number of species present on the first date but not on the second, and *c* is the number of species present on the second date but not on the first (Jaccard, 1912; Baselga, 2012). The index ranges from 0 (null dissimilarity) to 1 (complete dissimilarity; Baselga, 2012). The analysis was run with the betapart library (Baselga and Orme, 2012) in R studio (R version 3.6.1 "Action of the Toes"; R core Team, 2019).

Relative importance value

Relative importance value was calculated per site by adding relative frequency (the number of plots where each species was observed, divided by the total number of plots) and relative cover (the total cover per species, divided by the total plant cover). The result was divided by 2 to obtain a value ranging from 0 (very scarce) to 1 (very abundant), which facilitates comparisons between species and sites or dates (Brower and Zar, 1977).

Pre-Existing Conditions and Beach-Dune Erosion After the Winter Storm

First, we explored the effect of pre-existing morphological conditions on beach and dune erosion by incorporating the geomorphological parameters measured in the field, and calculated from the field surveys, into a Principal Component Analysis (PCA). With this, we explored the relative contribution of each variable to the geomorphological variability between the three beaches. We also looked for possible correlated variables. From this prior analysis we intended to select the most relevant variables, to statistically assess the variables most related with erosion. Furthermore, to show that the most relevant variable can vary greatly on the beaches, an analysis of variance was performed to compare the beaches studied. Once the variables were selected, we ran a Generalized Linear Mixed-Effects Model (GLME) to evaluate the net erosion on the entire beach profile, as a function of the most relevant geomorphological variables. In this model, the variable site (beach identity) was used as a random component.

Second, to see whether plants mitigated erosion, linear regression analyses were performed using the information from the vegetated plots located closest to the ocean. This decision was made because it has been demonstrated that plant cover is positively correlated with the distance from the beach. Then, to avoid errors of comparison, plots that were directly impacted by storm surges and waves, and had reduced vegetation cover, were not compared with the plots further inland that had higher vegetation cover. Thus, at Riachuelos and La Mancha, three plots per transect were considered, whereas at Navarro only two plots per transect were analyzed because the beach is narrower. The plots selected were all on the stoss slope of the dunes and backshore.

The following variables were evaluated for each beach with the linear regressions: plant cover, plant richness, and the overlap cover index. This index was estimated, as the plant cover is only the cover visible in a 2D aerial view. When dunes (in this case the plots) are covered by one or more species that do not overlap, plant cover is a good proxy to study its effects on mitigating erosion. In this case, the maximum plant cover value is ≤ 4 m^2, because this is the maximum area of each plot. However, when two or more species coexist and overlap in a plot, plant cover is stratified, since the plant cover of taller species could be on top of the plant cover of shorter species. The total plant cover of all species found in a plot could be more than 4 m^2 because of the juxtaposition of species. When this occurs, the cover could be highly relevant in reducing the erosion induced by waves. Therefore, a value for this stratification (overlap) was calculated (Eq. 10) to test its possible effects in reducing erosion.

$$\text{Overlap cover index} = \text{Total plant cover} + (2 \times \text{overlap})$$

Where:

Total plant cover = the addition of plant cover per species in the plot.

Overlap = the addition of plant cover and bare sand (if it was present) minus the total area of the plot (4 m^2).

Two is a constant number, used only to magnify the resulting values.

The analyses were run in R Studio (R version 3.6.1 "Action of the Toes"; R core Team, 2019), the PCA was run with the "rda" library of the "Vegan" package (Oksanen et al., 2019), and the GLME was run with the "glmer" function of the "lme4" package (Bates et al., 2015). Finally, the analysis of variance and the linear regressions were performed with the "lm" function.

RESULTS

Erosion Induced by a Single Winter Storm Event

The impact of the storm varied between the sites. Based on field observations after the storm and analyses of the beach and dune profiles, washover penetration was documented at Riachuelos

and La Mancha, where the dominant regime of wave impact, based on Sallenger (2000), was swash and overwash, but only over the incipient dunes. However, in La Mancha, there was lateral variation in the storm impacts, and collision regime was also observed. At Navarro, there was no evidence of washover penetration, and only the collision regime was observed on the foredunes (**Figures 4–6**).

Erosion was the dominant process taking place during the storm along each transect. No net accretion (income of sand to the system) was documented (**Figure 7**), and the accretion was only of the sand stored on the dunes, repositioned along the transects. Only in La Mancha, profile 1, was accretion observed on the backshore, whereas on the other beaches accretion took place on the back of the dunes. At Riachuelos erosion occurred not only on the stoss slope of the foredunes and backshore, but also on the back of the dunes (**Figure 7**). At Navarro, erosion mainly occurred on the stoss slope of the foredune, and slight accretion was observed on the back of the foredunes (**Figure 7**). At La Mancha, erosion took place on the backshore, and incipient dunes (**Figure 7**).

In terms of the total net erosion (the sum of the erosion taking place on all three transects for each beach), Riachuelos had the highest value, followed by La Mancha, and then Navarro. Nonetheless, the analysis of variance ($P \leq 0.05$) did not show any statistical differences for the erosion taking place on the three beaches (F value = 0.44; P = 0.66; **Figure 8A**). The same trend was seen for the net erosion taking place on the dunes closest to the ocean (F value = 0.16; P = 0.84; **Figure 8B**).

Response of the Plant Community to the Impact of the Winter Storm

Plant Cover

There was no clear impact of the storm on the vegetation. Plant cover increased in Riachuelos and Navarro, but decreased in La Mancha, although these differences were not statistically significant (**Table 2**). The same trends were observed on the seaward plots (**Table 2**).

Alpha Diversity

A total of 32 species were recorded on all the beaches in the two sampling periods, with 28 species occurring in both periods.

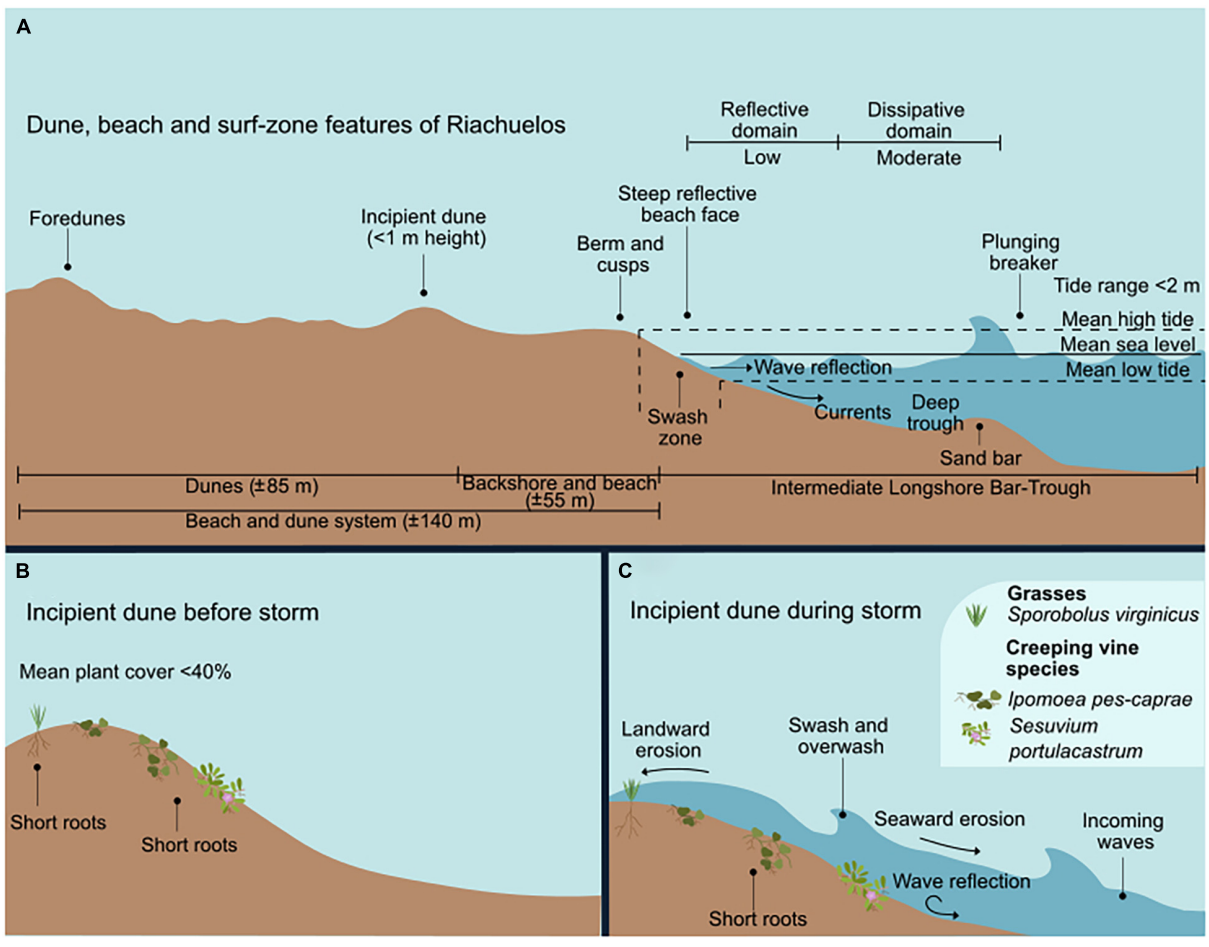

FIGURE 4 | The surf-zone and dunes of Riachuelos. **(A)** Dune, beach, and surf-zone features. **(B)** The incipient dunes and species before the storm. **(C)** The incipient dune during the storm, showing the wave-induced erosion.

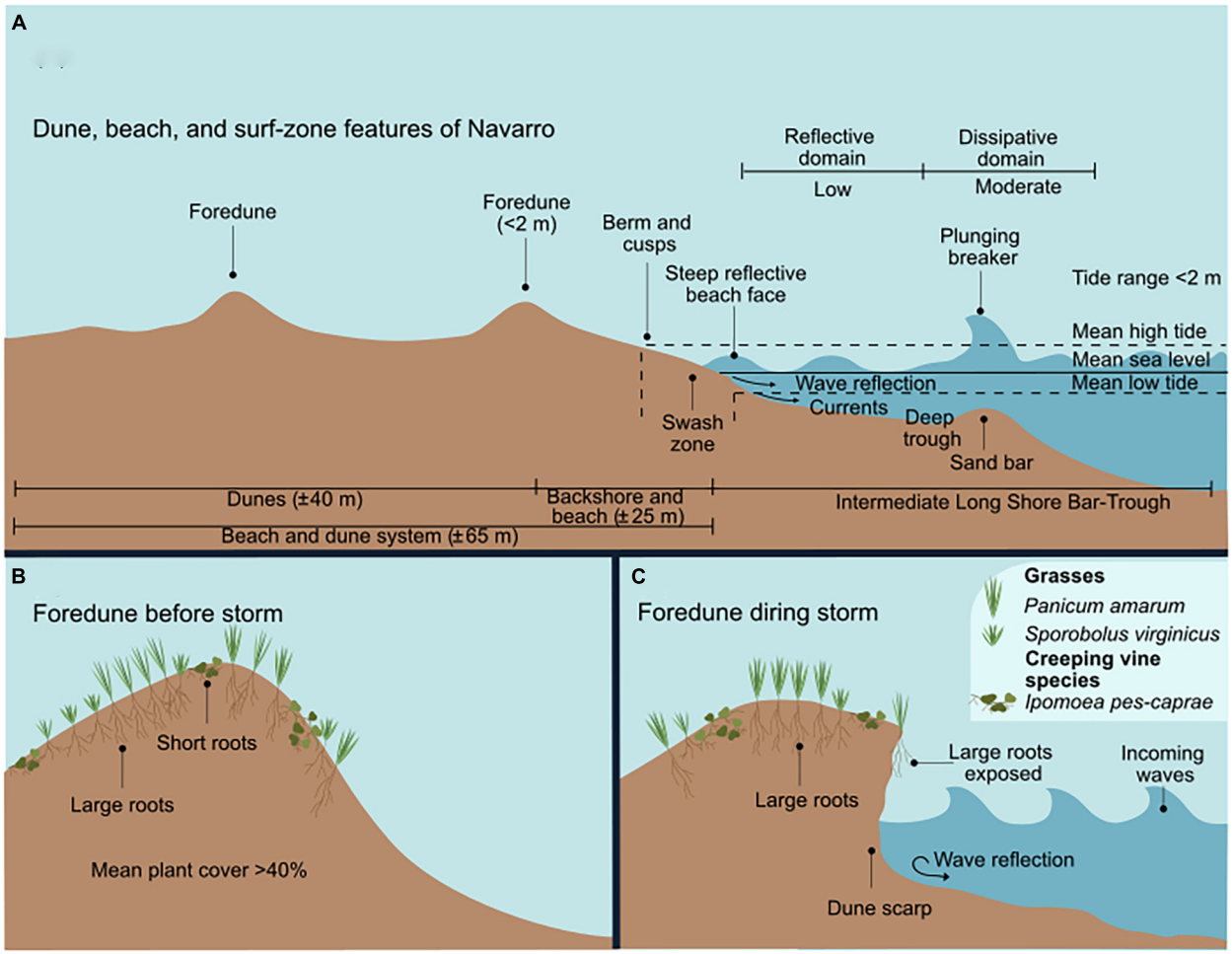

FIGURE 5 | The surf-zone and foredunes of Navarro. **(A)** Dune, beach, and surf-zone features. **(B)** The foredunes and species before the storm. **(C)** The foredunes during the storm, showing the wave-induced erosion.

There were variations between the sites: 18 species were recorded in Riachuelos, 15 in Navarro, and 24 in La Mancha. On the three beaches, the sample coverage (evaluated as part of the diversity analysis to make the comparisons between the two sampling periods) was ≥96%. Thus, diversity comparisons of each order of diversity were done directly, and no extrapolation or interpolation methods were necessary (Chao and Jost, 2012). In Riachuelos, we observed a slight increase in the three orders of diversity. Species richness (^{0}D) increased from 16 to 18 before and after the storm, respectively. The number of common species (^{1}D) increased from 10 to 11 and the dominant species (^{2}D) from 8 to 9. The species that appeared after the storm, prompting the increase in species richness were the inland grass *Cenchrus echinatus* and forb *Cyperus rotundus*. In contrast, no changes were observed in Navarro (**Figure 9A**). Before and after the storm, species richness was 14, the number of common species was 10, and the dominant species 9. Finally, in La Mancha, the three orders of diversity decreased after the storm. Species richness (^{0}D) was the order with the greatest change, since it decreased from 21 to 17; while the common and dominant species varied from 12 to 11 and from 9 to 8, respectively. The inland species *Bidens pilosa*, *Commelina erecta*, *Euphorbia dioica,* and the beach plant *Oenothera drummondii* are the four species that disappeared after the storm. Despite the slight changes observed in Riachuelos and Navarro, the analyses performed with the 95% CI did not reveal significant differences for any order of diversity (^{0}D, ^{1}D, and ^{2}D) in any of the beaches studied (**Figure 9A**), which means that in terms of alpha diversity, the plant communities were not significantly affected by the winter storm.

There were, however, slight differences in the RIV between pre- and post-storm conditions. On the three beaches, the grass *Sporobolus virginicus* was the dominant species before the storm. However, after it, this species became the third and second most dominant species in Riachuelos and Navarro, respectively, being replaced by *Croton punctatus* and *P. amarum,* respectively, (**Figure 9B**). In La Mancha, *S. virginicus* continued to be the most dominant species and its dominance slightly increased after the storm. Of the three beaches, La Mancha had the fewest changes in species ranking (**Figure 9B**). Concerning the species with geomorphological relevance being considered

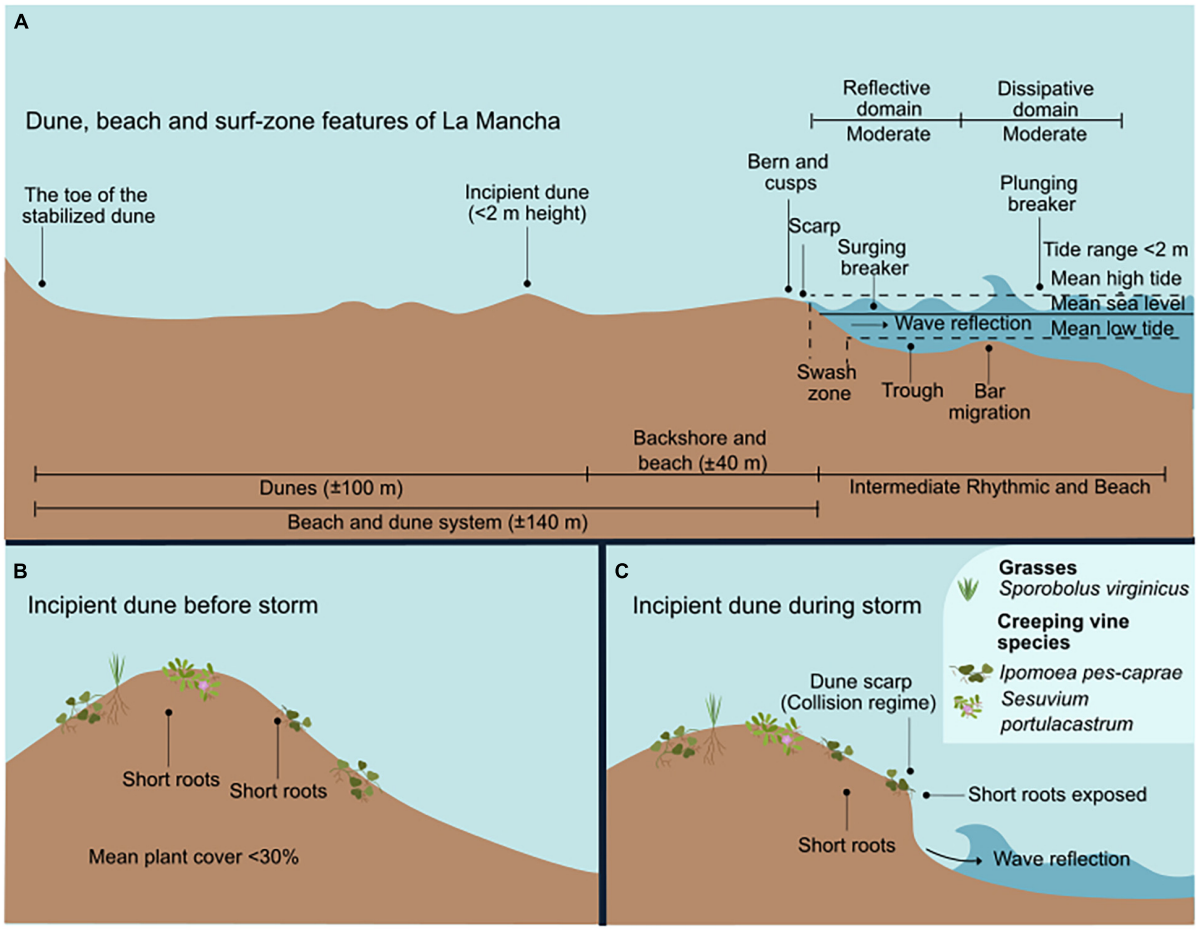

FIGURE 6 | The surf-zone and dunes of La Mancha. **(A)** Dune, beach, and surf-zone features. **(B)** The incipient dunes and species before the storm. **(C)** The incipient dunes during the storm, showing the wave-induced erosion.

dune-building plants, in Riachuelos, we observed that some had lower RIV (*Ipomoea pes-caprae* and *S. virginicus*) after the storm, while others (*Palafoxia lindenii*) remained unchanged. In contrast with Riachuelos, in Navarro *Ipomoea pes-caprae* and *S. portulacastrum* remained unchanged and the RIV of *P. lindenii* decreased. Furthermore, on this beach, the dune building and sand stabilizer grass, *P. amarum,* was the most dominant species after the storm, replacing *S. virginicus.* In La Mancha, as was previously mentioned, no major changes were observed and the two important dune building species (*S. virginicus* and *P. lindenii*) remained the most dominant. Finally, and coinciding with our observations at Riachuelos, in La Mancha the importance value of *Ipomoe pes-caprae* also fell.

Beta Diversity

The Jaccard index was used to show changes in species composition on the three beaches, after the winter storm. The Jaccard dissimilarity (B_{jac}) in Riachuelos (0.11), Navarro (0.13), and La Mancha (0.41) showed that La Mancha had the greatest dissimilarity values between the pre- and post-storm species assemblages, while Riachuelos and Navarro had lower values, closer to 0 which indicates less dissimilarity. The turnover component (β_{jtu}) in Riachuelos was zero while Navarro (0.13) and La Mancha (0.30) had almost similar values to those for the total dissimilarity. Regarding the nestedness component (β_{jne}), Riachuelos had the same value (0.11) that the total dissimilarity, while Navarro had a zero value and La Mancha 0.11. These results indicate that changes in species assemblages were site-dependent. In Riachuelos, the arrival of two new species was recorded, however, no species disappeared (nestedness), while in Navarro changes were due to species turnover and the number of species did not vary between pre-and post-storm species assemblages. Finally, in La Mancha, dissimilarities due to species turnover and nestedness were observed, however, the first was dominant.

Species turnover before and after the storm varied between sites. In Ricahuelos, the two new species found after the storm were *C. echinatus* and *C. rotundus.* In Navarro, *Erigeron longipes* was present before the event but absent after it, while *Palafoxia texana* appeared after the storm. In La Mancha, *E. longipes, B. pilosa, C. erecta, O. drummondii, Lantana camara* and *Schizachyrium scoparium* were observed before the storm but were absent after it. The species present after the storm, but

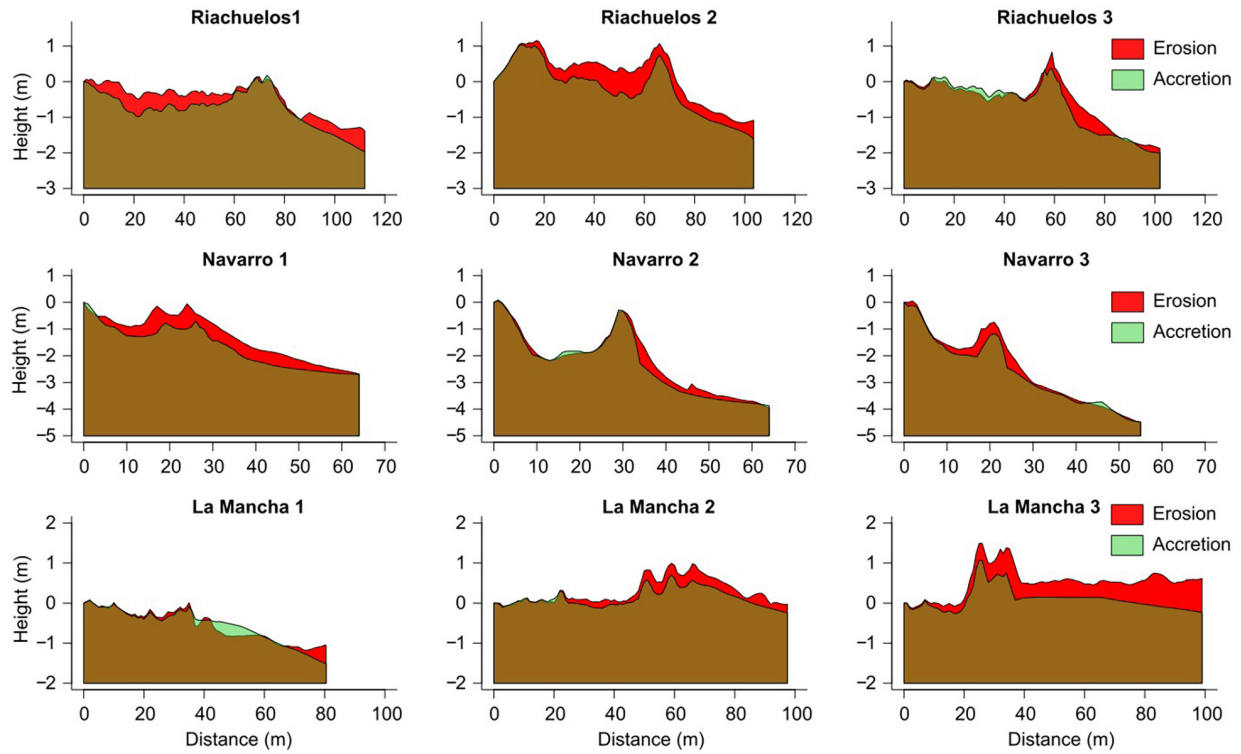

FIGURE 7 | Pre-and post-storm profiles on Riachuelos, Navarro, and La Mancha. Note that scale in axes *y* and *x* is not the same for all the beaches because of the differences in length and height of the beach and dune systems.

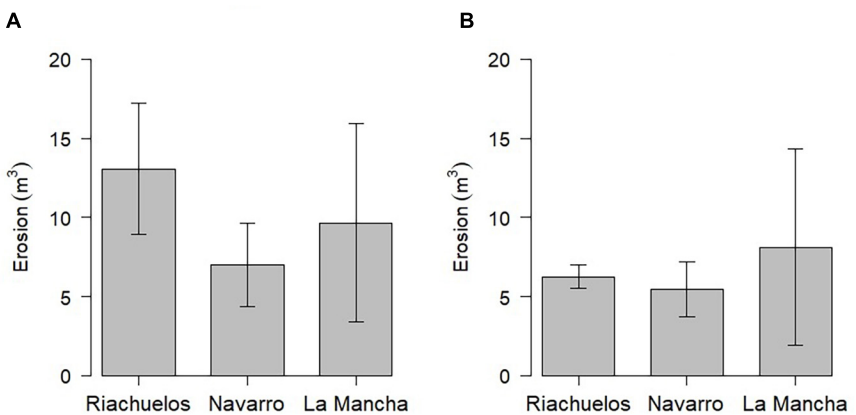

FIGURE 8 | Erosion at the study sites: **(A)** mean erosion on the three transects; **(B)** mean erosion on the frontal dunes (from the lee slope to the windward slope) and the lowest seaward point surveyed.

absent before it, were *Parthenium hysterophorus, Macroptilium atropurpureum* and *C. rotundus.*

Pre-Existing Conditions Related to Beach-Dune Erosion and the Role of Plants

The PCA shows differences between the geomorphological features of the beaches studied. Axis 1 and Axis 2 accounted for 70 and 17% of the total data variability, respectively, (**Figure 10A**). Dune height, the stoss slope of the dune and slope of the backshore appear on the positive extreme of Axis 1. A strong correlation was found between dune height and the slope of the backshore (r^2 = 0.85), and dune height and the stoss slope of the dune (r^2 = 0.76). Beach width was associated with Axis 2 and no strong correlations were observed with dune height (r^2 = –0.35), backshore width (r^2 = –0.56), or the stoss slope of the dune (r^2 = –0.53).

TABLE 2 | Mean plant cover, *p*-value, and *t*-test value for all the plots on the three beaches, and in the frontal plots.

	All plots			Seaward plots		
	Plant cover (mean ± se) (m^2)	***P*-value (≤0.05)**	***t***	**Plant cover (mean ± se) (m^2)**	***P*-value (≤0.05)**	***t***
Riachuelos	Bs 55.6 ± 6.8 As 87.9 ± 7.9	0.052	–4.19	Bs 10.0 ± 1.1 As 12.4 ± 1.9	0.11	–2.75
Navarro	Bs 26.1 ± 3.8 As 38.8 ± 6.9	0.07	–3.45	Bs 7.4 ± 0.2 As 11.4 ± 1.8	0.16	–2.15
La Mancha	Bs 42.7 ± 8.6 As 39.7 ± 13.2	0.057	0.65	Bs 5.6 ± 1.4 As 5.7 ± 0.4	0.95	–0.06

Before the storm (Bs) and After the storm (As).

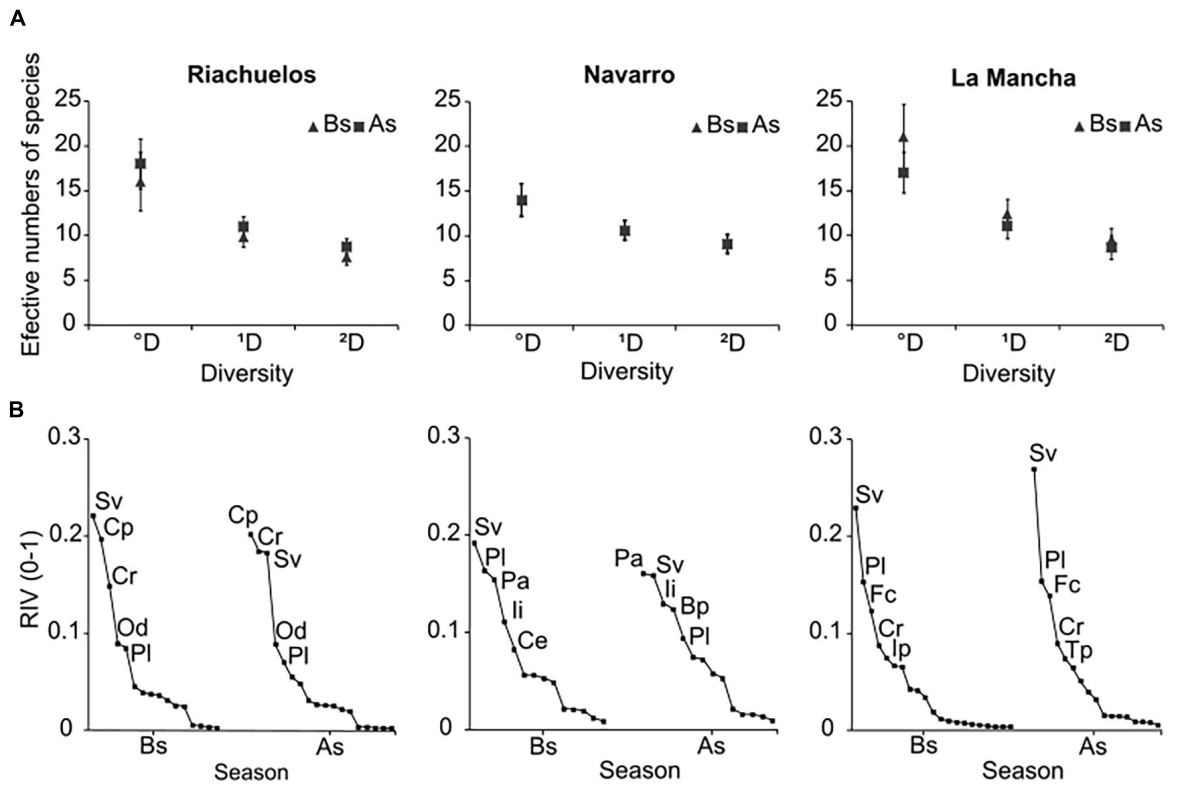

FIGURE 9 | (A) Plant diversity on the three beaches before (Bs) and after the storm (As). Species richness (^{0}D), the number of common species (^{1}D), and the dominant species (^{2}D) in the community were evaluated. Error bars correspond to the 95% CI. **(B)** Relative Importance Value (RIV) on the three beaches before (Bs) and after the storm (As). Only the five most dominant species on each beach are shown. Letters next to the point denote the name of the species: Sv (*Sporobolus virginicus*), Cp (*Croton punctatus*), Cr (*Canavalia rosea*), Od (*Oenothera drummondii*), Pl (*Palafoxia lindenii*), Pa (*Panicum marum*), Ii (*Ipomoea imperati*), Ce (*Cenchrus echinatus*), Bp (*Bidens pilosa*), Fc (*Fimbristylis cymosa*), Ip (*Ipomoea pes-caprae*), and Tp (*Trachypogon plumosus*).

In the biplot, the points that corresponded to Navarro were located on the positive extreme of Axis 1, while the points from Riachuelos and La Mancha were located in the center of the plot and toward the negative extreme of the same axis (**Figure 10A**). This shows that the beach at Navarro is narrower, and the dunes are higher, with steeper exposed face slopes, compared to Riachuelos and La Mancha. These results coincide with the field observations and the metrics shown in **Table 1**. Finally, the analysis of variance to compare the dune heights of the beaches (the variable with most contribution and associated correlation with the other geomorphological variables) also shows that they were statistically different for the beaches, with Navarro having the highest dunes and La Mancha the lowest ($P = 0.002$; **Figure 10B**).

Based on this information and the correlation analyses, dune height and backshore width were selected as good predictors to evaluate the effect of the geomorphological variables in erosion using the GLME. The results showed a significant effect

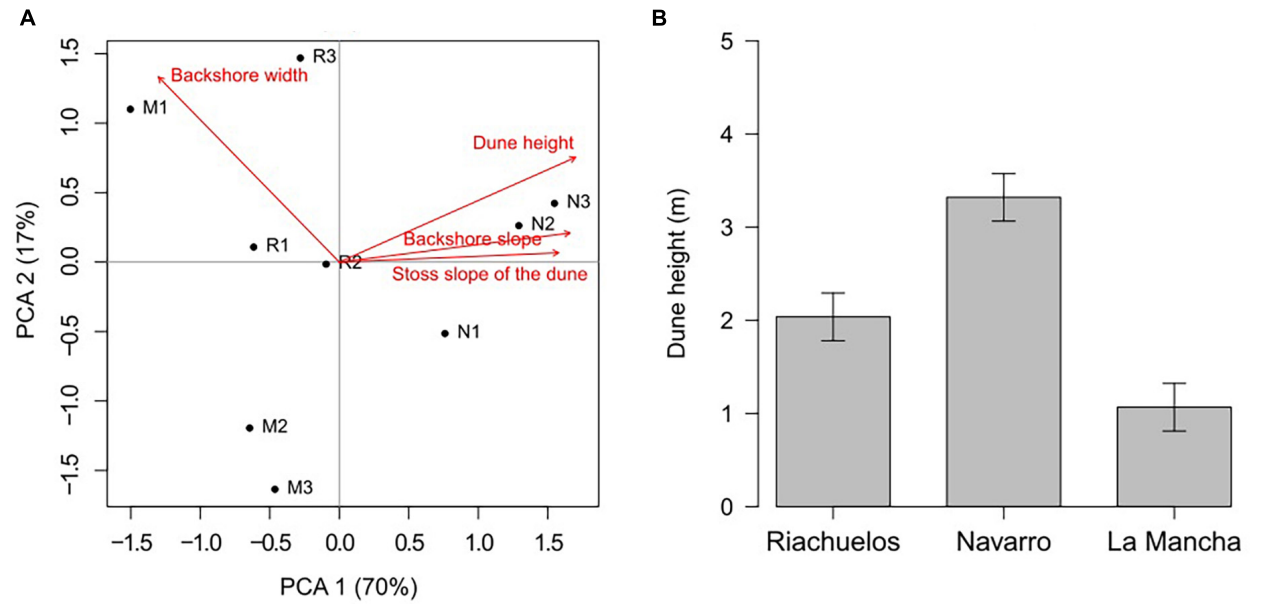

FIGURE 10 | (A) Geomorphological variables included in the Principal Component Analyses. **(B)** Mean height of the frontal dunes on the three beaches (incipient dunes for Riachuelos and La Mancha, and foredunes at Navarro).

of dune height (Chisq = 20.51, $P < 0.001$), backshore width (Chisq = 58.81, $P < 0.001$) and the interaction of both variables (Chisq = 9.39, $P = 0.002$). Erosion was greater on the beaches fronted by lower dunes (**Figure 11A**), and narrower beaches also tended to lose more sediment (**Figure 11B**). The interaction of both variables indicates that narrower beaches with higher dunes are less prone to erosion, however, in some cases when beach width increased, the erosion was also less.

Finally, the linear regressions performed to explore the effect of plant cover, plant richness and the overlap cover index in mediating erosion, only showed a significant negative correlation between plant cover and erosion in Navarro ($r^2 = 0.84$, $P = 0.009$; **Figure 11C**) and a significant positive correlation between bare sand and erosion ($r^2 = 0.84$, $P = 0.009$; **Figure 11D**). On this beach, severe erosion occurred when plant cover was reduced on the exposed face of the dunes.

DISCUSSION

This study is novel because it: (a) demonstrates the species-specific role of plants in mitigating dune erosion in field conditions; (b) shows the interaction between plant-related features and geomorphological variables in mitigating dune erosion, and (c) explores the immediate effect of a winter storm on beach and dune topography, the plant community, and dune-building species. This is relevant because previous work has focused on laboratory experiments and seldom explored the interaction between plant-related features with geomorphological attributes after exposure to a storm.

Our results are partially in accordance with our working hypotheses. We expected that: (a) plant cover and diversity would decrease after the impact of the storm and species dominance would change; (b) pre-existing beach and dune geomorphological conditions would determine storm-induced erosion; and (c) plants would help mitigate beach and dune erosion. We found that the winter storm did not have a significant impact on plant cover and diversity, but species composition and dominance varied for pre- and post-storm conditions. Beach and dune erosion did not vary significantly among sites, although it was less intense at Playa Navarro, where the highest dunes were observed. The correlation between erosion and plant cover was significantly negative only in Navarro.

Impacts of the Storm on Beach and Dune Morphology

Coinciding with previous findings, our results show that pre-existing conditions (dune and beach geomorphology before the storm) are relevant in determining the run-up, and the outcome of the storm on the beach and dune topography (Pries et al., 2008). Erosion was lower on the beaches with higher frontal dunes, but higher on narrower beaches (Vellinga, 1982; Saye et al., 2005; Pries et al., 2008; Keijsers et al., 2014). In Navarro, the narrowest beach with the highest dunes, erosion was induced through collision regime, and the resistance to flooding from the storm surge was conferred because the higher foredune ridge prevented inland flooding (Sallenger, 2000). In contrast, in Riachuelos and La Mancha, the lower dunes were more likely to be overwashed and inundated, although the width of the beach helped to reduce the effect of the storm surge (Keijsers et al., 2014) and consequent destruction of the incipient dunes. These results coincide with the previous findings of Houser et al. (2008) who observed that areas with lower dunes are more prone

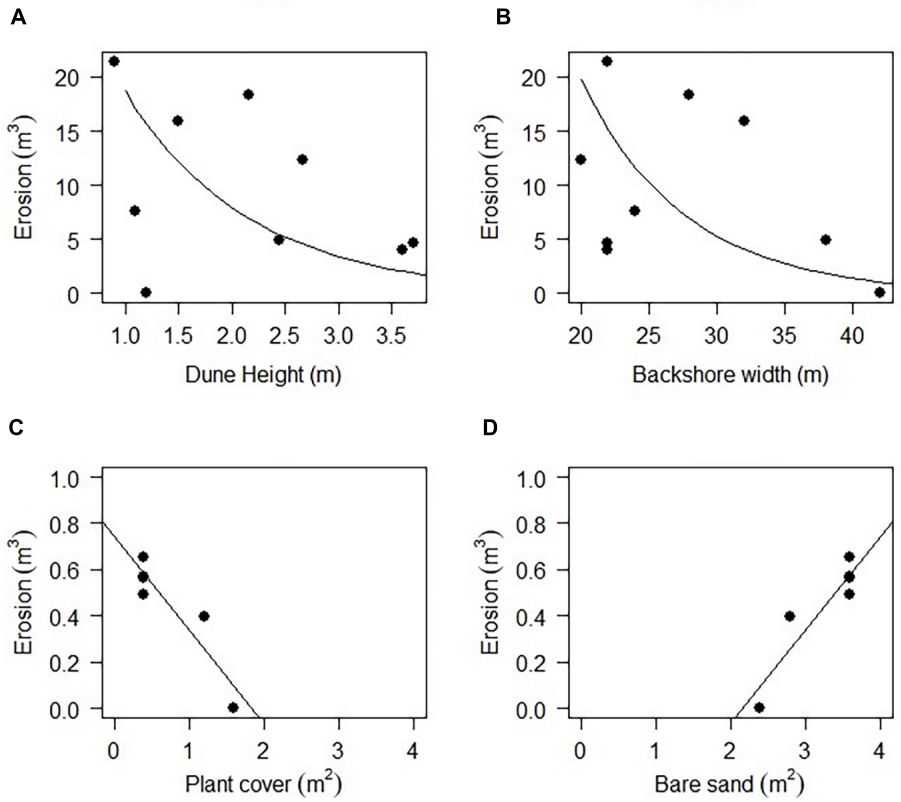

FIGURE 11 | Erosion as a function of **(A)** dune height, **(B)** backshore width, **(C)** plant cover and **(D)** bare sand.

to overwashing, while the well-developed foredunes tend to be eroded on the exposed face.

Impacts of the Winter Storm on the Beach and Dune the Plant Communities

One of the most relevant characteristics of nature-based defense for coastal protection is that natural ecosystems are capable of recovering naturally after disturbances, such as storms. Indeed, storms are natural events that are part of the natural dynamics of the coasts. Although natural, the stress induced by winter storms and tropical cyclones (e.g., hurricanes) on the coast (e.g., inundation, high salinity concentration, overwash, scarping and erosion, and burial) may have positive or negative impacts on plant communities (Rodgers et al., 2009; Miller, 2015). Consequently, we hypothesized that plant cover and alpha diversity would decrease after the impact of the winter storm. Additionally, we also expected to observe changes in species composition and dominance, with the most tolerant species becoming dominant after the storm.

Species richness was not altered by the storm, although species composition did change. Most of the species involved in species turnover were inland species (e.g., *B. pilosa* and *E. dioica*), with low incidence, abundance, and plant cover, and which were negatively affected by the storm. In turn, the abundance of dune builder plants increased after the storm. These results coincide with previous findings by Miller et al. (2010), who demonstrated that beach and dune species are highly resistant to storm conditions. These authors also recorded species turnover after a storm, mostly owing to the arrival of grasses and forbs. They noted that (i) major changes in plant cover on the incipient dunes are more related to temperature and drought, rather than to the action of waves, and (ii) species with higher occurrence are more likely to respond positively to storms. In accordance with this, the present study shows that in the three study sites, plant cover of the most dominant dune-building species (for example, *Canavalia rosea, C. punctatus, Ipomoea pes-caprae, S. virginicus,* and *P. lindenii*), increased after the storm, probably due to the rain brought by the storm, but also perhaps because of a positive response to burial by sand (Martínez et al., 2002) in the overwash areas where accretion occurred. It is important to mention that the coast of Veracruz faced a severe drought in the year when the study took place. Thus, when the rain from the winter storm reached the coast, it was beneficial, rather than harmful, for the plants (personal field observations).

Furthermore, the fact that the dune building species *Ipomoea pes-caprae, P. lindenii, S. virginicus, S. portulacastrum,* and *P. amarum* were little or not affected by the storm is relevant because, besides being effective dune builders (Devall, 1992; Stallins, 2002; Lonard and Judd, 2011; Lonard et al., 2013), these species are known to help mitigate wave-induced dune erosion (Silva et al., 2016; Feagin et al., 2019; Maximiliano-Cordova et al., 2019). This means that these species maintain their protective

role by building dunes and by resisting the impact of the storm. However, this also depends on factors such as the sediment budget and the storm incidence.

Pre-Existing Conditions and the Effect of Plants in Mitigating Erosion

Experiments previously performed in wave flume conditions have shown the effectiveness of vegetation in mitigating erosion induced by storm waves (e.g., Kobayashi et al., 2013; Sigren et al., 2014; Silva et al., 2016; De Battisti and Griffin, 2020). However, to date, only the studies conducted by Charbonneau et al. (2017), Lindell et al. (2017), and Biel et al. (2017) have demonstrated the protective role of plants in field conditions. To contribute to this field, the aim and novelty of the present study were to explore the effect of plant-related features (plant cover, overlap cover index, and plant richness), in mitigating erosion in different beaches with varying morphological features, in order to understand under what conditions plants confer dune resistance against erosion. This study shows that plant richness and the overlap cover did not affect erosion, except on one beach, where plant cover was negatively correlated with erosion on the exposed face of the dunes.

The differences in erosion observed at the three study sites and the protective role of vegetation may be associated with beach-dune morphology (Sallenger, 2000; Saye et al., 2005; Pries et al., 2008) as well as the dominant species, because protection may be species- and site-specific (Charbonneau et al., 2017; Maximiliano-Cordova et al., 2019). Our results show that the dominant species varied between beaches. The incipient dunes of La Mancha and Riachuelos were covered by the creeping vine *Ipomoea pes-caprae,* while the foredunes of Navarro were covered by the tall grass *P. amarum*. Even though experimental evidence has demonstrated the efficiency of both species in mitigating beach and dune erosion in laboratory conditions (Silva et al., 2016; Figlus et al., 2017; Maximiliano-Cordova et al., 2019), it is possible that in field conditions, the architecture of *P. amarum* is better at mitigating erosion as its plant cover increases because the dunes that develop around this plant are higher and the plants effectively trap sediment that would otherwise be eroded. Nevertheless, there is a threshold in the protective effect beyond which, erosion will not be mitigated (Odériz et al., 2020).

The mechanisms involved in the protective role of vegetation are diverse. Previous laboratory experiments have demonstrated that dune plants primarily reduce the velocity of beach erosion by attenuating wave swash and run-up with their stems and leaves (Mendoza et al., 2017; Feagin et al., 2019), but they do not compensate for the sediment deficit of the submerged beach (Silva et al., 2016; Odériz et al., 2020). Feagin et al. (2019) observed that plant roots also attenuated waves and reduced erosion. Furthermore, Mendoza et al. (2017) explored the mechanisms through which plant cover decreased dune erosion. Their findings show that where plants were present, the wave breaking point was displaced seawards, and bed velocities close to the shoreline were lower, associated with a reduction of the wave energy reflected on the beach. Both phenomena help explain the protective role of vegetation on the beach, which provides a slight, but relevant, contribution to the resilience and resistance of the beach profile.

Hydrodynamic changes are species-specific (Bouma et al., 2013), and hence, plant cover and architecture will play a differential role in modifying the impact of waves. For instance, *I. pes-caprae* mitigates wave impact and provides dune resistance (Silva et al., 2016; Feagin et al., 2019; Maximiliano-Cordova et al., 2019), but when plant cover increases, the results are unpredictable (Silva et al., 2016). In some cases, the maximum plant cover of this species could induce an increase in the coefficients of wave reflection, and as a consequence, induce greater dune erosion (personal observations). Instead, *P. amarum* mitigates turbulence as plant cover increases (Figlus et al., 2017). In laboratory conditions, it was demonstrated that *P. amarum* and the similar *Ammophila arenaria* were more efficient in mitigating erosion than forb species because of differences in their aerial architecture and below-ground biomass (Figlus et al., 2017; De Battisti and Griffin, 2020). These trends probably apply to our results. For example, *I. pes-caprae* has long branches that extend over the surface of the sand and abundant shallow adventitious roots that grow a few centimeters below the surface (Devall, 1992). In turn, *P. amarum* is a tall grass with dense and compact roots. The plant architecture and below-ground roots of both help mitigate the impact of storms, and retain sediment, thus reducing erosion.

Finally, the protective role of plants is the result of reciprocal interaction between plants and dunes which converts them into a dynamic bio-shield that determines the extent of the storm-induced effects. Indeed, beach and dune resistance is an accumulative process that depends on the biogeomorphological feedback between the plants and the dunes (Stallins and Parker, 2003; Durán and Moore, 2013; Charbonneau et al., 2021). In brief, our results show that plant cover can help mitigate erosion. However, this protective role is species- and site-dependent; influenced by local geomorphological characteristics.

Caveats of the Study

Spatio-Temporal Dynamics

In temperate coasts, it is possible that the abundance and diversity of plant species vary over time because of seasonal changes during which annual species may be present or absent, and plant cover varies drastically, depending on the weather conditions. Unlike temperate coasts, in the tropics there are almost no noticeable seasonal changes. For instance, annual plants are absent; all species are perennial, and thus, they do not disappear seasonally. This means that without disturbances that cause major disruptions, plants remain present even during the dry season, although their cover may decrease. Also, there is no successional species turnover on the beach and incipient dunes because of the recurrent disturbance events which repeatedly set vegetation trends back to early pioneer stages. Therefore, in our case, a spatio-temporal relationship is likely to occur simultaneously, between the state of the vegetation and geomorphological changes, because plant cover is highest when storms occur (Martínez et al., 2001).

One Single Storm

It is also important to acknowledge the limitations of a study with only one single storm event. It is certainly necessary to explore the cumulative effects of subsequent storms with different intensities, as well as the time elapsed between them, because this affects the possibility of plant recovery after the disturbance events. In addition, long-term studies will contribute to the understanding of the dynamic interaction between plants and geoforms. We also lacked information on the bathymetry of the study sites, and this would have been useful to describe the impact regime of the waves during the storm and the redistribution of the sediment along the surf zone.

Number of Replicates

The significant correlations between different environmental variables (dune height, backshore width, plant cover, and bare sand) and observed erosion were performed with a relatively reduced number of replicates. This was due to the fact that we chose the plots closest to the ocean to test the impact of storm-induced waves on the dunes, with and without vegetation, because the impact of waves decreases inland. Certainly, these results would be strengthened with a greater number of replicates, both within each beach and by adding more beaches. Nevertheless, the general trends are statistically significant and reveal interesting trends in field conditions which coincide with laboratory experiments, as well as the relatively small number of field observations performed previously (Feagin et al., 2019).

Applicability Worldwide

The study was only performed in three sites (three beaches), all located on the Gulf of Mexico. Nevertheless, the results can be extended worldwide, specifically to sandy coasts with vegetated dunes, and which are exposed to storms (winter storms or tropical cyclones; see for example, Costanza et al., 2021; Castelle et al., 2015; Masselink et al., 2016). While sandy beaches are heterogeneous, and dune-building plant species vary between regions. Nevertheless, sediment dynamics and the tolerance of dune building plants to salinity and sand movement is similar between species (Maun, 1998). Therefore, the response of the beach-dune system to the impact of storms is likely to be parallel in coastal regions beyond the Gulf of Mexico. Thus, in tropical and temperate latitudes, the interaction between geomorphological features, plants and storms are likely to share similarities. Nevertheless, further field observations are necessary to confirm this assumption.

CONCLUSION

This study aimed to evaluate the impact of a single winter storm on beach and dune morphology and plant communities, and to explore whether plants help in reducing wave-induced erosion in field conditions. The results show that: (1) erosion and accretion occurred on the three beaches studied, but that the patterns depend on the local geomorphological attributes and pre-existing conditions. Erosion was less intense where dunes were higher, although the beach was narrower (Navarro). On the other hand, wider beaches with more gentle slopes and shorter incipient dunes (Riachuelos and La Mancha) and were more eroded. (2) The impact of the winter storm on the plant communities established on the backshore and dunes was most often observed on typical inland plant species. Dune-building plants were not only tolerant to the storm, but they also increased their plant cover, demonstrating their ability to tolerate harsh storm conditions. (3) The protective role of plant-cover and species richness in mitigating erosion was site-dependent, and was only significant where erosion was less intense, which coincided with higher dunes and a narrower beach. The results from this study show that in field conditions, plants can confer dune resistance. However, this protective role is not linear because it is site- and species-specific, and depends on pre-existing geomorphological conditions and the plant species growing on the beach and dunes. Finally, concerning the applicability of this study, our results help understand the circumstances under which plants contribute to mitigating dune erosion. This is relevant as there is growing global interest in protecting coasts and mitigating erosion by means of ecosystem-based solutions.

DATA AVAILABILITY STATEMENT

The raw data supporting the conclusions of this article will be made available by the authors, without undue reservation.

AUTHOR CONTRIBUTIONS

CM-C conceived the manuscript, collected field data, performed the statistical analyses, wrote the first draft, and edited the manuscript. MM conceived, reviewed, and edited the manuscript. RS reviewed and edited the manuscript and oversaw the project administration. PH reviewed and edited the manuscript. RG performed the statistical analyses, reviewed, and edited the manuscript. RL helped with data curation and analysis. All authors contributed to the article and approved the submitted version.

FUNDING

The present research has been developed under the framework of CEMIE-Océano (Mexican Centre for Innovation in Ocean Energy), project FSE-2014-06-249795 financed by CONACYT-SENER-Sustentabilidad Energética. CM-C received a graduate studies scholarship from CONACYT (584584).

ACKNOWLEDGMENTS

We are thankful to Valeria Chávez for her contribution to the acquisition of ERA-5 data to perform the analysis of wave and wind conditions during the storm. Andrea Perez-Campos contributed to the design of the supplementary material.

REFERENCES

Baselga, A. (2010). Partitioning the turnover and nestedness components of beta diversity. *Glob. Ecol. Biogeogr.* 19, 134–143. doi: 10.1111/j.1466-8238.2009.00490.x

Baselga, A. (2012). The relationship between species replacement, dissimilarity derived from nestedness, and nestedness. *Glob. Ecol. Biogeogr.* 21, 1223–1232. doi: 10.1111/j.1466-8238.2011.00756.x

Baselga, A., and Orme, C. L. (2012). Betapart: an R package for the study of beta diversity. *Methods Ecol. Evol.* 3, 808–812. doi: 10.1111/j.2041-210X.2012.00224.x

Bates, D., Mächler, M., Bolker, B. M., and Walker, S. C. (2015). Fitting linear mixed-effects models using lme4. *J. Stat. Softw.* 67, 1–48. doi: 10.18637/jss.v067.i01

Biel, R. G., Hacker, S. D., Ruggiero, P., Cohn, N., and Seabloom, E. W. (2017). Coastal protection and conservation on sandy beaches and dunes: context-dependent tradeoffs in ecosystem service supply. *Ecosphere* 8:e01791. doi: 10.1002/ECS2.1791

Bouma, T. J., Temmerman, S., van Duren, L. A., Martini, E., Vandenbruwaene, W., Callaghan, D. P., et al. (2013). Organism traits determine the strength of scale-dependent bio-geomorphic feedbacks: a flume study on three intertidal plant species. *Geomorphology* 180–181, 57–65. doi: 10.1016/j.geomorph.2012.09.005

Brantley, S. T., Bissett, S. N., Young, D. R., Wolner, C. W. V., and Moore, L. J. (2014). Barrier island morphology and sediment characteristics affect the recovery of dune building grasses following storm-induced overwash. *PLoS One* 9:104747. doi: 10.1371/journal.pone.0104747

Brower, J. E., and Zar, J. H. (1977). *Field and Laboratory Methods for General Ecology*. Dubuque: Wm. C. Brown Company Publishers.

Bryant, D. B., Anderson Bryant, M., Sharp, J. A., Bell, G. L., and Moore, C. (2019). The response of vegetated dunes to wave attack. *Coast. Eng.* 152:103506. doi: 10.1016/j.coastaleng.2019.103506

Carter, R. W. G. (2013). *Coastal Environmets: An Introduction to the Physical, Ecological and Cultural Systems of Coastlines*. Available online at: https://www.elsevier.com/books/coastal-environments/carter/978-0-08-050214-4 (accessed February 26, 2021)

Castelle, B., Marieu, V., Bujan, S., Splinter, K. D., Robinet, A., Sénéchal, N., et al. (2015). Impact of the winter 2013-2014 series of severe Western Europe storms on a double-barred sandy coast: beach and dune erosion and megacusp embayments. *Geomorphology* 238, 135–148. doi: 10.1016/j.geomorph.2015.03.006

Chao, A., and Jost, L. (2012). Coverage-based rarefaction and extrapolation: standardizing samples by completeness rather than size. *Ecology* 93, 2533–2547. doi: 10.1890/11-1952.1

Charbonneau, B. R., Dohner, S. M., Wnek, J. P., Barber, D., Zarnetske, P., and Casper, B. B. (2021). Vegetation effects on coastal foredune initiation: wind tunnel experiments and field validation for three dune-building plants. *Geomorphology* 378:107594. doi: 10.1016/j.geomorph.2021.107594

Charbonneau, B. R., Wnek, J. P., Langley, J. A., Lee, G., and Balsamo, R. A. (2016). Above vs. belowground plant biomass along a barrier island: implications for dune stabilization. *J. Environ. Manage.* 182, 126–133. doi: 10.1016/j.jenvman.2016.06.032

Charbonneau, B. R., Wootton, L. S., Wnek, J. P., Langley, J. A., and Posner, M. A. (2017). A species effect on storm erosion: invasive sedge stabilized dunes more than native grass during Hurricane Sandy. *J. Appl. Ecol.* 54, 1385–1394. doi: 10.1111/1365-2664.12846

Chávez, V., Lithgow, D., Losada, M., and Silva-Casarin, R. (2021). Coastal green infrastructure to mitigate coastal squeeze. *J. Infrastruct. Preserv. Resil.* 2, 1–12. doi: 10.1186/s43065-021-00026-1

Cheplick, G. P. (2016). Changes in plant abundance on a coastal beach following two major storm surges. *J. Torrey Bot. Soc.* 143, 180–191. doi: 10.3159/TORREY-D-15-00030

Claudino-Sales, V., Wang, P., and Horwitz, M. H. (2008). Factors controlling the survival of coastal dunes during multiple hurricane impacts in 2004 and 2005: santa Rosa barrier island, Florida. *Geomorphology* 95, 295–315. doi: 10.1016/J.GEOMORPH.2007.06.004

Coch, N. K. (1994). Geologic effects of hurricanes. *Geomorphology* 10, 37–63. doi: 10.1016/0169-555X(94)90007-8

Copernicus Climate Change Service (C3S) (2017). *ERA5: Fifth Generation of ECMWF Atmospheric Reanalyses of the Global Climate. Copernicus Climate Change Service Climate Data Store (CDS), 2018/12.* Available online at: https://cds.climate.copernicus.eu/cdsapp#W/home (accessed June 18, 2020).

Costanza, R., Anderson, S. J., Sutton, P., Mulder, K., Mulder, O., Kubiszewski, I., et al. (2021). The global value of coastal wetlands for storm protection. *Glob. Environ. Chang.* 70:102328. doi: 10.1016/J.GLOENVCHA.2021.102328

Cultid-Medina, C. A., and Escobar, F. (2016). Assessing the ecological response of dung beetles in an agricultural landscape using number of individuals and biomass in diversity measures. *Environ. Entomol.* 45, 310–319. doi: 10.1093/EE/NVV219

Cumming, G., Fidler, F., and Vaux, D. L. (2007). Error bars in experimental biology. *J. Cell Biol.* 177, 7–11. doi: 10.1083/jcb.200611141

Davidson, S. G., Hesp, P. A., and Silva, G. M. (2020). Controls on dune scarping. *Prog. Phys. Geogr. Earth Environ.* 44, 923–947. doi: 10.1177/0309133320932880

Davidson-Arnott, R. G. D. (2005). Conceptual model of the effects of sea level rise on sandy coasts. *J. Coast. Res.* 21, 1166–1172. doi: 10.2112/03-0051.1

Davidson-Arnott, R. G. D., Hesp, P. A., Ollerhead, J., Walker, I., Bauer, B., Delgado-Fernandez, I., et al. (2018). Sediment budget controls on foredune height: comparing simulation model results with field data. *Earth Surf. Process. Landforms* 43, 1798–1810. doi: 10.1002/esp.4354

Davidson-Arnott, R. G. D., and Law, M. N. (1996). Measurement and prediction of long-term sediment supply to coastal foredunes. *J. Coast. Res.* 12, 654–663.

Davies, J. L. (1964). A morphogenic approach to world shorelines. *Zeitschrift für Geomorphol.* 8, 127–142. doi: 10.1127/zfg/mortensen/8/1964/127

De Battisti, D., and Griffin, J. N. (2020). Below-ground biomass of plants, with a key contribution of buried shoots, increases foredune resistance to wave swash. *Ann. Bot.* 125, 325–334. doi: 10.1093/aob/mcz125

Devall, M. S. (1992). The biological flora of coastal dunes and wetlands. 2. Ipomoea pes-caprae (L.) Roth. *J. Coast. Res.* 8, 442–456.

Doing, H. (1985). "Coastal fore-dune zonation and succession in various parts of the world," in *Ecology of Coastal Vegetation*, eds W. G. Beeftink, J. Rozema, and A. H. L. Huiskes (Dordrecht: Springer), 65–75. doi: 10.1007/978-94-009-5524-0_7

Durán, O., and Moore, L. J. (2013). Vegetation controls on the maximum size of coastal dunes. *Proc. Natl. Acad. Sci. U.S.A.* 110, 17217–17222. doi: 10.1073/pnas.1307580110

Emery, K. O. (1961). A simple method of measuring beach profiles. *Limnol. Oceanogr.* 6, 90–93. doi: 10.4319/lo.1961.6.1.0090

Feagin, R. A., Furman, M., Salgado, K., Martínez, M. L., Innocenti, R. A., Eubanks, K., et al. (2019). The role of beach and sand dune vegetation in mediating wave run up erosion. *Estuar. Coast. Shelf Sci.* 219, 97–106. doi: 10.1016/j.ecss.2019.01.018

Figlus, J., Kobayashi, N., Gralher, C., and Iranzo, V. (2011). Wave overtopping and overwash of dunes. *J. Waterw. Port Coast. Ocean Eng.* 137, 26–33. doi: 10.1061/(ASCE)WW.1943-5460.0000060

Figlus, J., Sigren, J. M., Power, M. J., and Armitage, A. R. (2017). Physical model experiment investigating interactions between different dune vegetation and morphology changes under wave impact. *Proc. Coast. Dyn.* 470–480.

Flores, P. (2016). *Evaluación de la Opresión Costera y sus Consecuencias en las Playas Arenosas y Dunas Costeras de Veracruz*. Master's Thesis. Xalapa, Mexico: Instituto de Ecología, A. C.

Gornish, E. S., and Miller, T. E. (2010). Effects of storm frequency on dune vegetation. *Glob. Chang. Biol.* 16, 2668–2675. doi: 10.1111/j.1365-2486.2009.02144.x

Guisado-Pintado, E., and Jackson, D. W. T. (2018). Multi-scale variability of storm Ophelia 2017: the importance of synchronised environmental variables in coastal impact. *Sci. Total Environ.* 630, 287–301. doi: 10.1016/j.scitotenv.2018.02.188

Guisado-Pintado, E., and Jackson, D. W. T. (2019). Coastal impact from high-energy events and the importance of concurrent forcing parameters: the cases of storm Ophelia (2017) and storm Hector (2018) in NW Ireland. *Front. Earth Sci.* 7:190. doi: 10.3389/feart.2019.00190

Hesp, P. A. (1991). Ecological processes and plant adaptations on coastal dunes. *J. Arid Environ.* 21, 165–191. doi: 10.1016/s0140-1963(18)30681-5

Hesp, P. A. (2002). Foredunes and blowouts: initiation, geomorphology and dynamics. *Geomorphology* 48, 245–268. doi: 10.1016/S0169-555X(02)00184-8

Hesp, P. A., Dong, Y., Cheng, H., and Booth, J. L. (2019). Wind flow and sedimentation in artificial vegetation: field and wind tunnel experiments. *Geomorphology* 337, 165–182. doi: 10.1016/j.geomorph.2019.03.020

Hill, M. O. (1973). Diversity and evenness: a unifying notation and its consequences. *Ecology* 54, 427–432. doi: 10.2307/1934352

Houser, C. (2013). Alongshore variation in the morphology of coastal dunes: implications for storm response. *Geomorphology* 199, 48–61. doi: 10.1016/j.geomorph.2012.10.035

Houser, C., Hapke, C., and Hamilton, S. (2008). Controls on coastal dune morphology, shoreline erosion and barrier island response to extreme storms. *Geomorphology* 100, 223–240. doi: 10.1016/j.geomorph.2007.12.007

Hsieh, T. C., Ma, K. H., and Chao, A. (2016). iNEXT: an R package for rarefaction and extrapolation of species diversity (Hill numbers). *Methods Ecol. Evol.* 7, 1451–1456. doi: 10.1111/2041-210X.12613

Infante-Mata, D., Moreno-Casasola, P., Madero-Vega, C., Castillo-Campos, G., and Warner, B. G. (2011). Floristic composition and soil characteristics of tropical freshwater forested wetlands of Veracruz on the coastal plain of the Gulf of Mexico. *For. Ecol. Manage.* 262, 1514–1531. doi: 10.1016/j.foreco.2011.06.053

Jaccard, P. (1912). The distribution of the flora in the alpine zone. *New Phytol.* 11, 37–50. doi: 10.1111/j.1469-8137.1912.tb05611.x

Jost, L. (2006). Entropy and diversity. *Oikos* 113, 363–375. doi: 10.1111/j.2006.0030-1299.14714.x

Judd, F. W., and Sides, S. L. (1983). The effect of Hurricane Allen on the near-shore vegetation of South Padre Island. *Southwest. Nat.* 28, 365–369. doi: 10.2307/3670799

Karunarathna, H., Pender, D., Ranasinghe, R., Short, A. D., and Reeve, D. E. (2014). The effects of storm clustering on beach profile variability. *Mar. Geol.* 348, 103–112. doi: 10.1016/j.margeo.2013.12.007

Keijsers, J. G. S., Poortinga, A., Riksen, M. J. P. M., and Maroulis, J. (2014). Spatio-temporal variability in accretion and erosion of coastal foredunes in the Netherlands: regional climate and local topography. *PLoS One* 9:e91115. doi: 10.1371/journal.pone.0091115

Kobayashi, N., Gralher, C., and Do, K. (2013). Effects of woody plants on dune erosion and overwash. *J. Waterw. Port Coast. Ocean Eng.* 139, 466–472. doi: 10.1061/(asce)ww.1943-5460.0000200

Krause, G. (2004). The "Emery-Method" revisited: performance of an inexpensive method of measuring beach profiles and modifications. *J. Coast. Res.* 20, 340–346. doi: 10.2112/1551-5036(2004)20[340:teroai]2.0.co;2

Lindell, J., Fredriksson, C., and Hanson, H. (2017). Impact of dune vegetation on wave and wind erosion: a case study at Ängelholm Beach, South Sweden. *Vatten Tidskr. för vattenvård /J. Water Manag. Res.* 73, 39–48.

Lonard, R. I., and Judd, F. W. (2011). The biological flora of coastal dunes and wetlands: panicum amarum S. Elliott and Panicum amarum S. Elliott var. amarulum (A.S. Hitchcock and M.A. Chase) P. Palmer. *J. Coast. Res.* 27, 233–242. doi: 10.2112/JCOASTRES-D-09-00129.1

Lonard, R. I., Judd, F. W., and Stalter, R. (2013). The biological flora of coastal dunes and wetlands: sporobolus virginicus (C. Linnaeus) K. Kunth. *J. Coast. Res.* 29, 706–716. doi: 10.2112/JCOASTRES-D-12-00139.1

Martínez, M. L., Moreno-Casasola, P., Espejel, I., Jimenéz-Orocio, O., Infante-Mata, D., and Rodríguez-Revelo, N. (eds) (2014). *Diagnóstico de las Dunas Costeras de México*. Guadalajara: CONAFOR.

Martínez, M. L., Silva, R., Lithgow, D., Mendoza, E., Flores, P., Martínez, R., et al. (2017). Human Impact on coastal resilience along the coast of Veracruz. *Mexico. J. Coast. Res.* 2017, 143–153. doi: 10.2112/SI77-015.1

Martínez, M. L., Vázquez, G., and Colón, S. S. (2001). Spatial and temporal variability during primary succession on tropical coastal sand dunes. *J. Veg. Sci.* 12, 361–372. doi: 10.2307/3236850

Martínez, M. L., Vázquez, G., Favila, M. E., and Álvarez-Molina, L. (2019). Variation in different measures of diversity during primary succession on a tropical coastal dune. *Plant Ecol. Divers.* 12, 489–505. doi: 10.1080/17550874.2019.1628114

Martínez, M. L., Vázquez, G., White, D. A., Thivet, G., and Brengues, M. (2002). Effects of burial by sand and inundation by fresh-and seawater on seed germination of five tropical beach species. *Can. J. Bot.* 80, 416–424. doi: 10.1139/b02-027

Masselink, G., Castelle, B., Scott, T., Dodet, G., Suanez, S., Jackson, D., et al. (2016). Extreme wave activity during 2013/2014 winter and morphological impacts along the Atlantic coast of Europe. *Geophys. Res. Lett.* 43, 2135–2143. doi: 10.1002/2015GL067492

Maun, M. A. (1998). Adaptations of plants to burial in coastal sand dunes. *Can. J. Bot.* 76, 713–738. doi: 10.1139/b98-058

Maun, M. A., and Perumal, J. (1999). Zonation of vegetation on lacustrine coastal dunes: effects of burial by sand. *Ecol. Lett.* 2, 14–18. doi: 10.1046/j.1461-0248.1999.21048.x

Maximiliano-Cordova, C., Salgado, K., Martínez, M. L., Mendoza, E., Silva, R., Guevara, R., et al. (2019). Does the functional richness of plants reduce wave erosion on embryo coastal dunes? *Estuaries Coasts* 42, 1730–1741. doi: 10.1007/s12237-019-00537-x

Mendoza, E., Odériz, I., Martínez, M. L., and Silva, R. (2017). Measurements and modelling of small scale processes of vegetation preventing dune erosion. *J. Coast. Res.* 77, 19–27. doi: 10.2112/si77-003.1

Miller, T. E. (2015). Effects of disturbance on vegetation by sand accretion and erosion across coastal dune habitats on a barrier island. *AoB Plants* 7:lv003. doi: 10.1093/aobpla/plv003

Miller, T. E., Gornish, E. S., and Buckley, H. L. (2010). Climate and coastal dune vegetation: disturbance, recovery, and succession. *Plant Ecol.* 206, 97–104. doi: 10.1007/s11258-009-9626-z

Moreno-Casasola, P. (1986). Sand movement as a factor in the distribution of plant communities in a coastal dune system. *Vegetatio* 65, 67–76. doi: 10.1007/BF00044876

Nishi, R., and Kraus, N. C. (1997). "Mechanism and calculation of sand dune erosion by storms," in *Coastal Engineering 1996*, ed. L. E. Billy (New York, NY: American Society of Civil Engineers), 3034–3047.

Odériz, I., Knöchelmann, N., Silva, R., Feagin, R. A., Martínez, M. L., and Mendoza, E. (2020). Reinforcement of vegetated and unvegetated dunes by a rocky core: a viable alternative for dissipating waves and providing protection? *Coast. Eng.* 158:103675. doi: 10.1016/j.coastaleng.2020.103675

Oksanen, J., Blanchet, F. G., Friendly, M., Kindt, R., Legendre, P., McGlinn, D., et al. (2019). *vegan: Community Ecology Package*. Available online at: https://cran.r-roject.org/package=vegan (accessed March 5, 2020).

Overton, M. F., Pratikto, W. A., Lu, J. C., and Fisher, J. S. (1994). Laboratory investigation of dune erosion as a function of sand grain size and dune density. *Coast. Eng.* 23, 151–165. doi: 10.1016/0378-3839(94)90020-5

Pries, A. J., Miller, D. L., and Branch, L. C. (2008). Identification of structural and spatial features that influence storm-related dune erosion along a barrier-island ecosystem in the Gulf of Mexico. *J. Coast. Res.* 24, 168–175. doi: 10.2112/06-0799.1

Psuty, N. P., Martínez, M. L., López-Portillo, J., Silveira, T. M., García-Franco, J. G., and Rodríguez, N. A. (2009). Interaction of alongshore sediment transport and habitat conditions at Laguna La Mancha, Veracruz, Mexico. *J. Coast. Conserv.* 13, 77–87. doi: 10.1007/s11852-009-0060-0

R core Team (2019). *R: A Language and Environment for Statistical Computing*. Available online at: https://www.r-project.org/ (accessed March 5, 2010).

Ramírez, M. G., and Reséndiz, I. N. R. (2002). Seguimiento de nortes en el litoral del Golfo de México en la temporada 1999-2000. *Rev. Geográfica* 131, 5–19.

Rodgers, J. C., Murrah, A. W., and Cooke, W. H. (2009). The impact of Hurricane katrina on the coastal vegetation of the Weeks Bay Reserve, Alabama from NDVI data. *Estuaries Coasts* 32, 496–507. doi: 10.1007/s12237-009-9138-z

Sallenger, A. H. Jr. (2000). Storm impact scale for barrier islands. *J. Coast. Res.* 16, 890–895.

Saye, S. E., van der Wal, D., Pye, K., and Blott, S. J. (2005). Beach-dune morphological relationships and erosion/accretion: an investigation at five sites in England and Wales using LIDAR data. *Geomorphology* 72, 128–155. doi: 10.1016/j.geomorph.2005.05.007

Short, A. D., and Wright, L. D. (1983). "Physical Variability of Sandy Beaches," in *Sandy Beaches as Ecosystems*, eds A. McLachlan and E. Theuns (Berlin: Springer), 133–144. doi: 10.1007/978-94-017-2938-3_8

Sigren, J. M., Figlus, J., and Armitage, A. R. (2014). Coastal sand dunes and dune vegetation: restoration, erosion, and storm protection. *Shore Beach* 82, 5–12.

Sigren, J. M., Figlus, J., Highfield, W., Feagin, R. A., and Armitage, A. R. (2018). The effects of coastal dune volume and vegetation on storm-induced property

damage: analysis from hurricane Ike. *J. Coast. Res.* 34, 164–173. doi: 10.2112/jcoastres-d-16-00169.1

Silva, R., Martínez, M. L., Odériz, I., Mendoza, E., and Feagin, R. A. (2016). Response of vegetated dune-beach systems to storm conditions. *Coast. Eng.* 109, 53–62. doi: 10.1016/j.coastaleng.2015.12.007

Spalding, M. D., Ruffo, S., Lacambra, C., Meliane, I., Hale, L. Z., Shepard, C. C., et al. (2014). The role of ecosystems in coastal protection: adapting to climate change and coastal hazards. *Ocean Coast. Manag.* 90, 50–57. doi: 10.1016/j.ocecoaman.2013.09.007

Stallins, J. A. (2002). Dune plant species diversity and function in two barrier island biogeomorphic systems. *Plant Ecol.* 165, 183–196. doi: 10.1023/A:1022224216705

Stallins, J. A. (2005). Stability domains in barrier island dune systems. *Ecol. Complex.* 2, 410–430. doi: 10.1016/j.ecocom.2005.04.011

Stallins, J. A., and Parker, A. J. (2003). The influence of complex systems interactions on barrier Island dune vegetation pattern and process. *Ann. Assoc. Am. Geogr.* 93, 13–29. doi: 10.1111/1467-8306.93102

Synder, R. A., and Boss, C. L. (2002). Recovery and stability in barrier island plant communities. *J. Coast. Res.* 18, 530–536.

Temmerman, S., Meire, P., Bouma, T. J., Herman, P. M., Ysebaert, T., and De Vriend, H. J. (2013). Ecosystem-based coastal defence in the face of global change. *Nature* 504, 79–83. doi: 10.1038/nature12859

Vellinga, P. (1982). Beach and dune erosion during storm surges. *Coast. Eng.* 6, 361–387. doi: 10.1016/0378-3839(82)90007-2

Wolner, C. W. V., Moore, L. J., Young, D. R., Brantley, S. T., Bissett, S. N., and McBride, R. A. (2013). Ecomorphodynamic feedbacks and barrier island response to disturbance: insights from the Virginia Barrier Islands, Mid-Atlantic Bight, USA. *Geomorphology* 199, 115–128. doi: 10.1016/j.geomorph.2013.03.035

Wright, L. D., and Short, A. D. (1984). Morphodynamic variability of surf zones and beaches: a synthesis. *Mar. Geol.* 56, 93–118. doi: 10.1016/0025-3227(84)90008-2

Zarnetske, P. L., Hacker, S. D., Seabloom, E. W., Ruggiero, P., Killian, J. R., Maddux, T. B., et al. (2012). Biophysical feedback mediates effects of invasive grasses on coastal dune shape. *Ecology* 93, 1439–1450. doi: 10.1890/11-1112.1

Conflict of Interest: The authors declare that the research was conducted in the absence of any commercial or financial relationships that could be construed as a potential conflict of interest.

Publisher's Note: All claims expressed in this article are solely those of the authors and do not necessarily represent those of their affiliated organizations, or those of the publisher, the editors and the reviewers. Any product that may be evaluated in this article, or claim that may be made by its manufacturer, is not guaranteed or endorsed by the publisher.

frontiers in Marine Science

ORIGINAL RESEARCH
published: 15 December 2021
doi: 10.3389/fmars.2021.747833

Hindcasting Ecosystem Functioning Change in an Anthropogenized Estuary: Implications for an Era of Global Change

Xiaoyu Fang[1,2†], Francesco Cozzoli[3,4†], Sven Smolders[5], Antony Knights[6], Tom Moens[1], Karline Soetaert[6] and Carl Van Colen[1†]*

[1] Marine Biology Research Group, Department of Biology, Ghent University, Ghent, Belgium, [2] School of Biological and Marine Sciences, University of Plymouth, Plymouth, United Kingdom, [3] Research Institute on Terrestrial Ecosystems (IRET) – National Research Council of Italy (CNR), Rome, Italy, [4] Laboratory of Ecology, Department of Biological and Environmental Sciences and Technologies, University of the Salento, Lecce, Italy, [5] Flanders Hydraulics Research, Department of Mobility and Public Works, Flemish Government, Antwerp, Belgium, [6] Department of Estuarine and Delta Systems, NIOZ Royal Netherlands Institute for Sea Research, Yerseke, Netherlands

OPEN ACCESS

Edited by:
Rodolfo Silva, National Autonomous University of Mexico, Mexico

Reviewed by:
Debora Lithgow, Instituto de Ecología (INECOL), Mexico
Itxaso Odériz, National Autonomous University of Mexico, Mexico

***Correspondence:**
Carl Van Colen
carl.vancolen@ugent.be

† These authors have contributed equally to this work

Specialty section:
This article was submitted to Coastal Ocean Processes, a section of the journal Frontiers in Marine Science

Received: *26 July 2021*
Accepted: *17 November 2021*
Published: *15 December 2021*

Citation:
Fang X, Cozzoli F, Smolders S, Knights A, Moens T, Soetaert K and Van Colen C (2021) Hindcasting Ecosystem Functioning Change in an Anthropogenized Estuary: Implications for an Era of Global Change. Front. Mar. Sci. 8:747833. doi: 10.3389/fmars.2021.747833

Understanding how altered hydrodynamics related to climate change and anthropogenic modifications affect ecosystem integrity of shallow coastal soft-sediment environments requires a sound integration of how species populations influence ecosystem functioning across heterogeneous spatial scales. Here, we hindcasted how intertidal habitat loss and altered hydrodynamic regimes between 1955 and 2010 associated with geomorphological change to accommodate expansion in anthropogenic activities in the Western Scheldt altered spatial patterns and basin-wide estimates of ecosystem functioning. To this end we combined an empirically derived metabolic model for the effect of the common ragworm *Hediste diversicolor* on sediment biogeochemistry (measured as sediment oxygen uptake) with a hydrodynamic and population biomass distribution model. Our integrative modeling approach predicted an overall decrease by 304 tons in ragworm biomass between 1955 and 2010, accounting for a reduction by 28% in stimulated sediment oxygen uptake at the landscape scale. Local gains or losses in habitat suitability and ecosystem functioning were primarily driven by changes in maximal current velocities and inundation regimes resulting from deepening, dredging and disposal practices. By looking into the past, we have demonstrated how hydro- and morphodynamic changes affect soft-sediment ecology and highlight the applicability of the integrative framework to upscale anticipated population effects on ecosystem functioning.

Keywords: soft-sediment biogeochemistry, bioturbation, animal – ecosystem function relationships, metabolic theory of ecology, Western Scheldt estuary

INTRODUCTION

Coastal ecosystems are at the frontline of environmental change. Expanding human activities, accelerating sea level rise, and changing wind climates modify hydrodynamic patterns that define the delicate balance in physical exchange processes that underpin the ecology of these shallow ecosystems (Birchenough et al., 2015; Khojasteh et al., 2021). Consequently, worldwide loss in

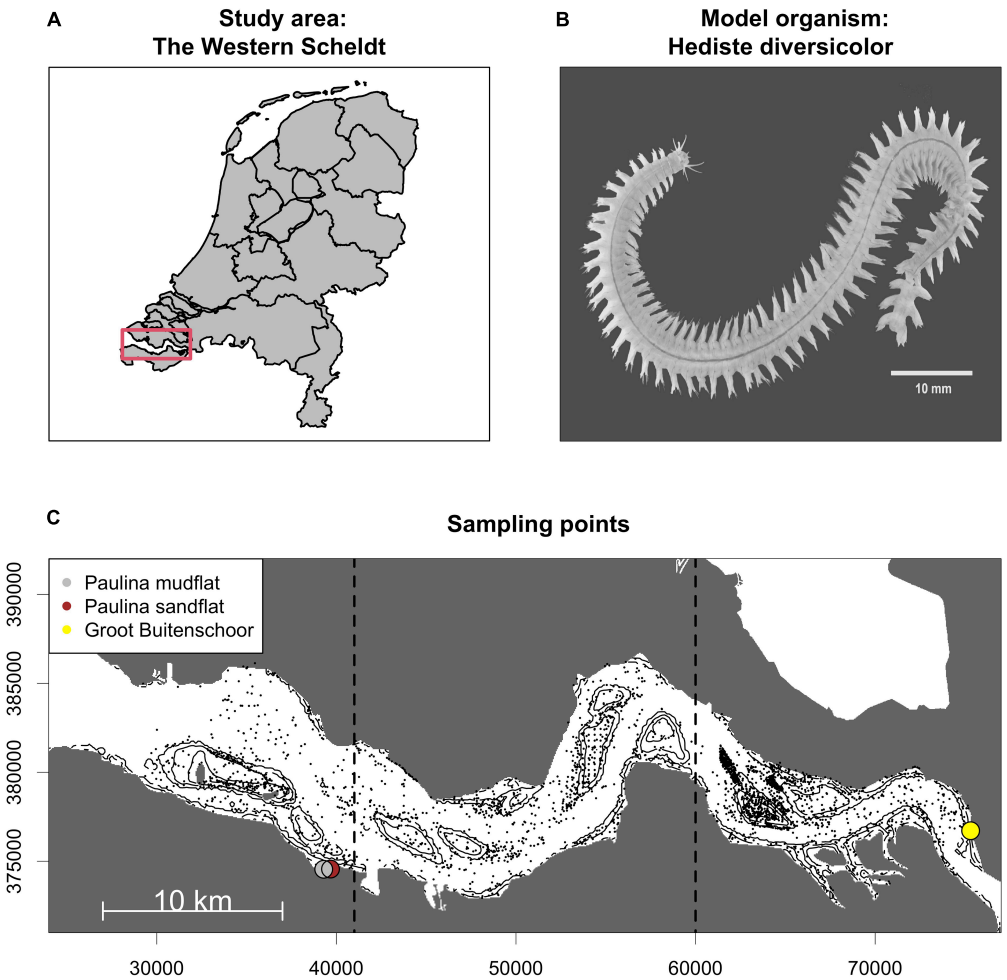

FIGURE 1 | Study area: the Western Scheldt estuary (Netherlands) **(A)**; model organism: *Hediste diversicolor*, common ragworm **(B)**; sampling points: the colored dots show the sampling points used for oxygen uptake measurements **(C)**. The smaller black dots mark the location of the 3051 benthic samples collected between 2006 and 2010 and used to fit the *H. diversicolor* potential biomass distribution model. Coordinates are in Amersfoort - EPSG:4289.

ecosystem integrity during the Anthropocene has reduced some of the critical services provided by the biodiversity of these highly productive ecosystems to society (Barbier et al., 2011 and references therein). According to the definition of Reiss et al. (2009), the concept of "ecosystem functioning" describes the combined effects of the natural processes that sustain an ecosystem and it is determined by the interplay of abiotic (physical and chemical) and/or biotic factors. A key ecosystem function of coastal ecosystems is the efficient processing of nutrient inputs from terrestrial sources, which could otherwise cause eutrophication and disrupt marine food webs. Soft-sediment dwelling animals (further referred to as macrobenthos, typically including crustaceans, bivalves, and bristle worms) play pivotal roles in the biogeochemical cycling of estuaries and coastal ecosystems by channeling nutrients and carbon assimilated into their biomass to higher trophic levels such as wading birds and fish. Additionally, these burrowing animals alter biogeochemistry at the sediment-water interface *via* respiration, excretion, and indirectly through their sediment reworking and ventilation activities (i.e., bioturbation; Kristensen et al., 2012) that importantly stimulate the microbial mineralization of sedimentary organic matter (Snelgrove et al., 2018).

Multiple anthropogenic pressures increasingly affect the water column and sediment processes involved in macrobenthos-mediated biogeochemical cycling (Knights et al., 2015). Key examples are dredging and disposal practices that induce bathymetric, hydrodynamic, and sedimentological changes of the seabed that affect the distribution and bioturbation effects of macrobenthos (e.g., Mermillod-Blondin and Rosenberg, 2006; Cozzoli et al., 2017). Accordingly, quantifying the implications of anthropogenic change to shallow coastal and estuarine sediments for the delivery of ecosystem services, requires a sound integration of the contributions of macrobenthos to biogeochemical cycling, and sediment ecosystem functioning in general. Although the functional role of macrobenthos can exhibit a strong context-dependency across environmental gradients (e.g., Cassidy et al., 2020), logistical constraints typically

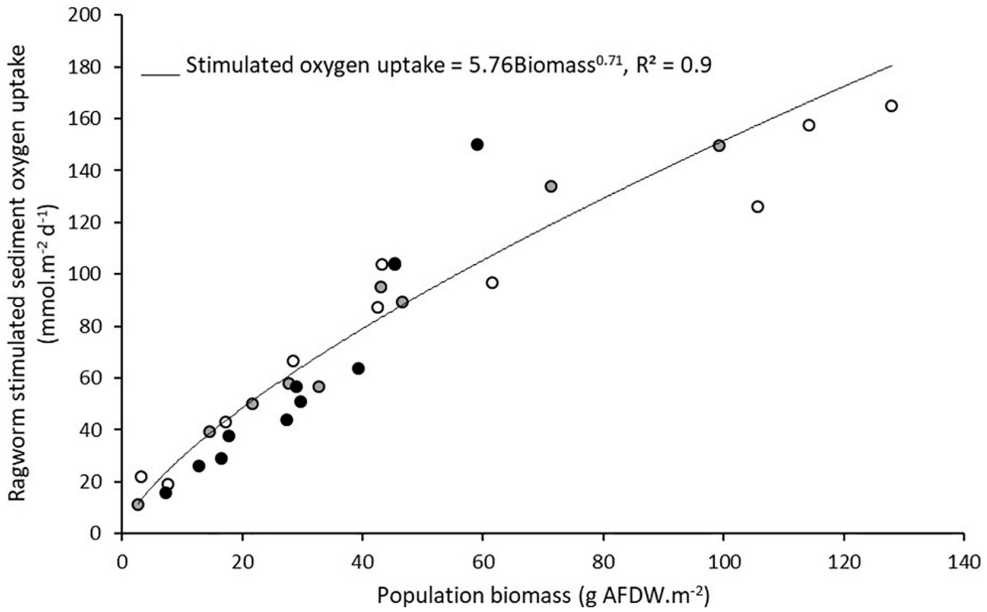

FIGURE 2 | Stimulated sediment oxygen uptake by ragworm biomass in each experiment. Sediments were collected from three locations with varying physical characteristics (**Supplementary Material 1**). The fitted line is an allometric power function relating biomass and ecosystem functioning. Data from Fang et al. (2021) are included in this figure.

limit replication of empirical studies across the landscape that can impede spatial upscaling of functioning at the ecosystem level and beyond. However, when the functional role of populations across spatial gradients is well understood, a promising way to estimate larger-scale functional implications of changing environments is the integration of species ecosystem functioning models with predictive population distribution models across environmental gradients, even when the underlying mechanisms are complex and difficult to unravel (e.g., Ellis et al., 2006). Such integrated modeling framework can extrapolate changes on population level to ecosystem functioning across heterogeneous spatial scales, or can make predictions for different time periods. Hydrodynamic variables are amongst the most important determinants for macrobenthos distributions (Ysebaert et al., 2002), but they are rarely measured with full spatial coverage therefore limiting landscape applications, let alone that the temporal changes that occurred during the Anthropocene has been recorded. Coupled hydro- and morphodynamic models fill this gap as they describe water motion, sediment transport and bed-level changes by numerically solving a coupled set of mathematical equations (Smolders et al., 2013).

To demonstrate this approach we integrated a metabolically supported species-ecosystem functioning model with species distribution predictions to assess the spatial and temporal variation in ecosystem functioning in the Western Scheldt (Netherlands) as an exemplar study (**Figure 1A**). The Western Scheldt is a coastal plain estuary of high ecological and economic importance protected under the EU Water Framework and the Floods Directive. The estuary has underwent severe geomorphological changes since the 1950s (De Vriend et al., 2011) to accommodate safe navigation of larger ships to the port of Antwerp, the second-largest marine harbor in Europe. Ecosystem functioning was measured using sediment oxygen uptake, which is a good proxy for total sediment metabolism (Canfield et al., 1993) and includes the direct and indirect contributions of macrobenthos to biogeochemical cycling (Glud, 2008). We specifically considered the contribution to sediment metabolism of the benthic ragworm *Hediste diversicolor* (**Figure 1B**); a species widely distributed across the coasts of the Americas and Europe including the intertidal river banks and shoals of the Western Scheldt (Ysebaert et al., 2003) and the bioturbation activities of which importantly stimulate sediment biogeochemical cycling (e.g., Kristensen, 2001). We first established an ecosystem functioning model by empirically quantifying the contribution of ragworm population biomass to stimulated sediment oxygen uptake across a diversity of sediment types. Then we extrapolated stimulated ecosystem functioning across the spatially heterogeneous landscape by integrating the ragworm ecosystem functioning model with a ragworm biomass distribution model based on hydrodynamic predictor variables. Lastly, we estimated spatio-temporal variability in ecosystem functioning between 1955 and 2010 as a result of anthropogenically driven loss and/or change in habitat suitability related to hydrodynamical modifications.

MATERIALS AND METHODS

Ragworm – Ecosystem Functioning Model

Using laboratory experiments to characterize ecosystem-functioning under various natural biomasses, we previously

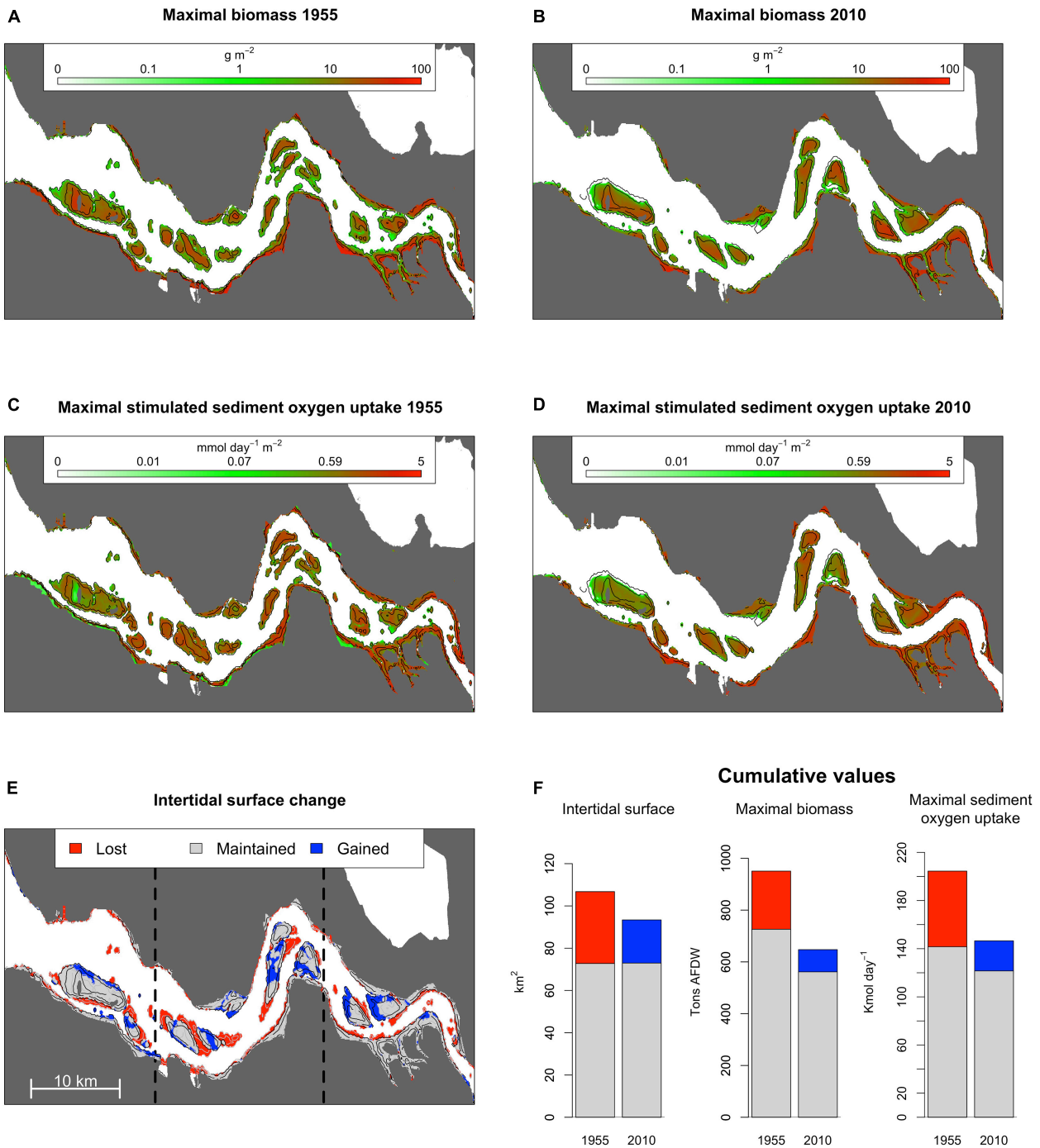

FIGURE 3 | Maximal expected ragworm biomass in 1955 **(A)** and 2010 **(B)** as estimated from a 0.95 quantile distribution model. Maximal stimulated sediment oxygen uptake in 1955 **(C)** and 2010 **(D)** as estimated from the allometric scaling relation between ragworm biomass and stimulated sediment oxygen uptake. Distribution of lost, gained, and prevailing intertidal habitats between 1955 and 2010 are presented in **(E)**. Bar charts in **(F)** summarize basin-wide implications of anthropogenic change for intertidal surface area, ragworm biomass, and the cascading effect on sediment oxygen uptake for lost (red), gained (blue), and prevailing (gray) areas.

demonstrated that stimulatory ragworm bioturbation effect on sediment oxygen uptake varies proportionally with population biomass in sandy and muddy sediments of tidal flat in the lower region of the estuary (Fang et al., 2021). Because macrobenthos activity can vary with salinity (Verdelhos et al., 2015; but see Murray et al., 2017), a third experiment (presented here) with ragworms collected in the upper region of the Western Scheldt (**Supplementary Material 1**) was undertaken following the same

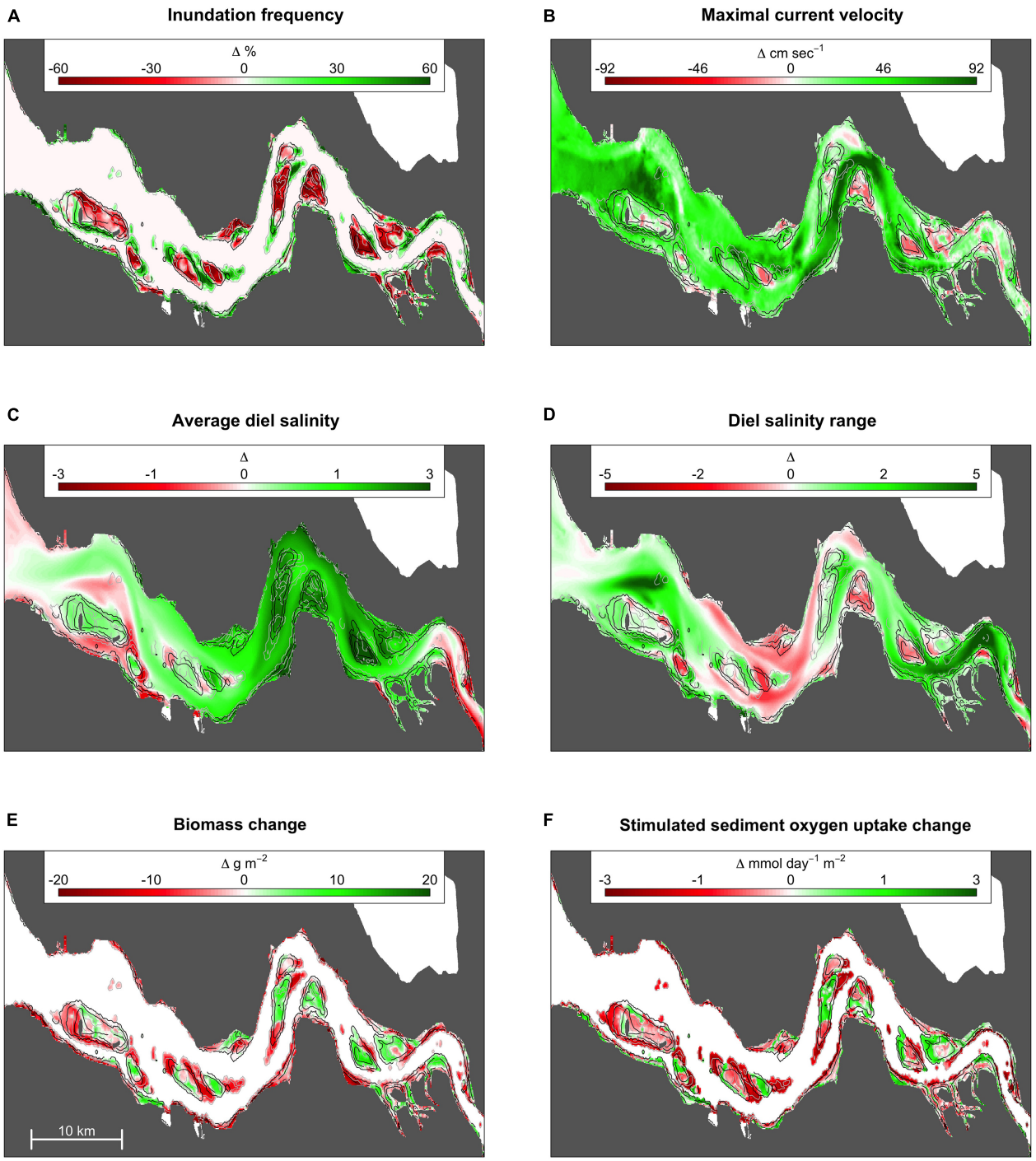

FIGURE 4 | Hydrodynamic **(A–D)**, biomass **(E)**, and ecosystem functioning **(F)** changes between 1955 and 2010. Average values for hydrodynamic variables for the total basin, the prevailing and the lost intertidal habitats are presented according to inundation frequency categories (0–100, >66, 33–66, <33% of a full tidal cycle) in **Supplementary Material 5**. Negative values (red color) imply a decreasing of the predicted hydrodynamic variable value between 1955 and 2010, while positive value (green color) imply an increase.

methods reported in Fang et al. (2021). Briefly, total sediment oxygen uptake was measured in 11 plexiglass microcosms (height 12.2 cm, inner diameter 3.6 cm) filled with 1 mm sieved sediment to a depth of 6 cm, topped with seawater (salinity = 19.4) and seeded with variable densities of differently sized individuals (**Supplementary Material 2**). Sediment oxygen uptake was calculated from the decline in dissolved oxygen concentrations over time; these were measured continuously in the airtight

closed microcosms using calibrated oxygen optodes (Pyroscience OXROB10). The ragworm contribution to sediment ecosystem functioning was calculated for each microcosm by subtracting the oxygen uptake in one microcosm without ragworms. Analysis of covariance (ANCOVA) was used to compare the ragworm effect on ecosystem functioning between sediment types while controlling for biomass. Ragworm population biomass was normalized using log transformation in all experiments to meet assumptions of the homogeneity of regression slopes and the homogeneity of variances.

Upscaling Ragworm – Ecosystem Functioning Effects

Four hydrodynamic variables, namely: (1) yearly averages of maximal tidal current velocity ($m{\cdot}s^{-1}$); (2) salinity; (3) diel variation in salinity; and (4) inundation time (% of submersion during a full tidal cycle) – all known determinants of ragworm distribution (Ysebaert et al., 2003) were predicted across a 20 m triangular spatial grid overlaying detailed bathymetric maps of the Western Scheldt for 1955 and 2010 using the 2Dh TELEMAC hydrodynamic model (Smolders et al., 2013). Subsequently these hydrodynamic variables were extracted from the 2010 hydrodynamic scenario for 3051 locations sampled between 2006 and 2011 in the Western Scheldt (BIS dataset, NIOZ-Yerseke Monitor Taskforce, **Figure 1C**). Ragworm biomass distribution in the estuary was then predicted based on the observed biomass in the sampled locations and using the four physical variables extracted by the 2Dh TELEMAC hydrodynamic model as explanatory variables. To this end we used quantile regression, a preferred method for species distribution modeling when only a subset of possibly limiting governing variables are available (Cade and Noon, 2003). We predicted ragworm biomass using the upper (0.95) quantile to describe change in niche potential in response to environmental drivers, after Vaz et al. (2008). The distribution model was fitted up to second degree interaction terms between explanatory variables and subsequently simplified using a stepwise bi-directional elimination procedure (Venables and Ripley, 2002; **Supplementary Material 3**). The explanatory variable submersion time, expressed as a fraction between 0 and 1, was linearized *via* arcsin transformation. Similarly to Cozzoli et al. (2014), to validate our forecast for the 95th quantile of the *H. diversicolor* biomass distribution, the whole dataset was iteratively sampled with replacement (9999 iterations). Due to sampling with replacement, some observations are repeated and others remain unpicked. The model was fitted on the sampled observations (training dataset) and used to predict the unpicked ones (validation dataset). The distribution of the coefficients estimated through the iterations of the pseudoreplication procedure was used to estimate the significance and confidence intervals of the estimates of the distribution model. The predicted values were discretized in 10 logarithmic classes, for which the corresponding 95th sample quantile of the validation data was calculated. To finally asses the validity of the model, observed and predicted quantiles were plotted against each other and checked for linear correlation (**Supplementary Material 4**).

The relationship between ecosystem functioning and ragworm biomass (Stimulated oxygen uptake = $a\text{Biomass}^b$, where a is the quantified coefficient and b the allometric scaling exponent; see section "Results") was used to convert the ragworm population effect on sediment oxygen uptake and constrained to the inundation time (i.e., the period of the tidal phase when bioturbation can stimulate sediment oxygen uptake from the water column). The predicted biomass distribution and ragworm-stimulated oxygen uptake maps were generated for 1955 and 2010 to evaluate the implications of deepening, dredging and disposal practices that increasingly occurred since 1955 (De Vriend et al., 2011). The pseudoreplication test previously described and used to validate the biomass distribution model requires a large training and validation dataset. Consequently, in this study we were able to validate the biomass distribution model only. A much greater number of field observations should be collected to properly validate the predicted ecosystem functioning scenario.

RESULTS AND DISCUSSION

Ragworm-Ecosystem Functioning Model

The biomass-dependent stimulation of sediment oxygen uptake by ragworms did not vary between sediment types (ANCOVA: biomass effect $F_{1,24}$, $p < 0.001$; sediment type effect $F_{2,24}$, $p = 0.24$; biomass × sediment type interaction $F_{2,24}$, $p = 0.40$), despite differences in granulometry, organic matter content or salinity (**Supplementary Material 1**) and a combined stimulatory effect per gram biomass increased sediment metabolism to the power 0.71 (**Figure 2**) across all environmental contexts. This uniformity likely results from the fact that burrow ventilation by ragworms is restricted to the lumen and a few mm in the burrow wall (Nielsen et al., 2004) and suggests that the ragworm bioturbation effect on sediment ecosystem functioning is proportional to its energetic requirements corroborating the allometric scaling exponent of ∼0.75 for the relation between body size and metabolism that is evidenced across taxonomic groups (Brown et al., 2004). Cozzoli et al. (2018) further support this theory by demonstrating that sediment resuspension can be ascribed to the overall metabolic rate of bioturbating populations.

Habitat Change and Ecosystem Functioning

Maximum ragworm biomass occurred in the most elevated intertidal areas (**Figures 3A,B**) corroborating this species' preference for low-energy environments, i.e., low current velocities and low inundation time (Ysebaert et al., 2002). These conditions are usually associated to fine sediments, i.e., mud or silt, and high organic matter sediment load (Cozzoli et al., 2013). In contrast, ragworm-mediated sediment oxygen uptake peaked at intermediate surface elevations (**Figures 3C,D**) due to the opposing patterns in inundation time and ragworm biomass along the intertidal elevation gradient, that both positively relate to stimulated ecosystem functioning.

Anthropogenically induced changes in fluvial geomorphology between 1955 and 2010 (**Figure 3E**) increased seawater

penetration into the estuary, modified local daily salinity fluctuations, and altered the inundation time and current velocities in the intertidal region (**Figures 4A–D**). Overall, channel deepening and erosion of lower intertidal areas led to the permanent inundation of 34 km^2, accounting for the direct loss of 216 tons of potential intertidal ragworm biomass, or 22% of the potential biomass achievable in 1955 (**Figure 3F**). This was, in part, offset by creation of 20 km^2 of new intertidal habitat (i.e., previously fully submersed habitat) in close proximity to the shoals (**Figure 3E**) and potentially inhabited by 85 tons, or 13% of ragworm biomass present in 2010. The overall decrease in intertidal habitat surface was stronger in the marine and intermediate sectors of the estuary (respectively, shrinking of 19 and 17% of the intertidal surface present in 1955) than in the riverine one (shrinking of 9%) (**Figure 3E**).

The 73 km^2 of prevailing intertidal habitat underwent a distinct increase in average maximum current velocity, especially in the most elevated intertidal habitats (1955; 0.16 ± 0.10 SD $m{\cdot}s^{-1}$ vs. 2010; 0.31 ± 0.11 SD $m{\cdot}s^{-1}$; **Figure 4** and **Supplementary Material 5**), reducing their suitability for ragworms. Similarly, newly developed intertidal habitats in 2010 had a higher maximal current velocity as compared to the lost habitat (gained habitat; 0.43 ± 0.12 SD $m{\cdot}s^{-1}$ vs. lost habitat; 0.11 ± 0.12 SD $m{\cdot}s^{-1}$), and experience a longer submersion time (+11%) in comparison to the lost habitats. The change in hydrodynamics was more drastic for the marine and intermediate portion of the estuary (respectively, average increases of 74 and 84% in maximum current velocity between 1955 and 2010) than for the riverine sector (increase of 25% only) (**Figure 4B** and **Supplementary Material 5**). Differently, the riverine sector of the estuary experienced the strongest increase in daily salinity variation, with an increase of 73% between 1955 and 2010 in the intertidal area (**Figure 4D** and **Supplementary Material 5**).

Collectively, direct habitat loss and change in habitat suitability over time reduced ragworm population biomass by 32% between 1955 and 2010, causing a predicted reduction in ecosystem functioning by 28% across the estuary (1955; 204 $Kmol{\cdot}day^{-1}$ vs. 2010; 147 $Kmol{\cdot}day^{-1}$)(**Figure 3F**). The joint effect of larger intertidal habitat loss and stronger increase in tidal current velocity made so that the strongest reduction in ragworm population biomass was predicted in the marine and central sectors of the estuary (respectively decrease in potential ragworm biomass of 43 and 38% from 1955 to 2010) than in the riverine one (decrease in potential ragworm biomass of 20%) (**Figure 4E** and **Supplementary Material 5**). This implies a predicted reduction in ecosystem functioning of 36 and 34% in the marine and central sectors of the estuary, respectively. The decrease in ecosystem functioning in the riverine sector was of 16% only (**Figure 4F** and **Supplementary Material 5**).

In addition to basin-wide estimates, our approach hindcasted changes in biomass at a smaller scale, with the implications for ecosystem functioning primarily depending on the local interplay of biomass and inundation time. For example, geomorphological changes generally reduced habitat suitability for ragworms on the river banks whereas implications for biomass and ecosystem functioning were more variable on the shoals with, e.g., predicted gains in habitat suitability toward the brackish part of the estuary where reductions in inundation time co-occurred with lowered current velocities (**Figures 4E,F**).

CONCLUSION

By combining quantitative estimates of functioning under varying environmental contexts, spatio-temporal data describing hydrodynamic conditions, and modeling tools, we have shown how small-scale studies can be upscaled from a population perspective to the larger spatial (landscape) scales necessary to underpin effective ecosystem-based management in the current era of global change. The integrative modeling framework can be applied to predict functional implications of hydrodynamic change resulting from, e.g., alternative dredge disposal strategies, sea level rise, or river flooding regimes. By looking in the past in the specific case study presented here, we demonstrated how particularly the ultimate balance between maximal current velocities and inundation time in the intertidal habitat will define faunal-mediated functioning in future estuaries and soft-sediment shorelines. Finally, the allometric scaling of ecosystem functioning with population biomass corroborates the metabolic theory of ecology, supporting the possibly wider application of the integrated framework to assess ecosystem functioning change.

DATA AVAILABILITY STATEMENT

The original contributions presented in the study are included in the article/**Supplementary Material**, further inquiries can be directed to the corresponding authors.

AUTHOR CONTRIBUTIONS

CV and XF conceived and designed the study, analyzed the experimental data, and wrote the first draft of the manuscript. XF ran the experiment. SS developed the hydrodynamic model. XF and FC modeled the species and ecosystem functioning distributions. All authors contributed to manuscript revision, read, and approved the submitted version.

FUNDING

This work was funded by a MARES Ph.D. grant to XF (2012-1720/001-001-EMJD). The research leading to results presented in this publication was carried out with infrastructure funded by EMBRC Belgium – FWO project GOH3817N. Extra funding for this project was obtained from the Special Research Fund (BOF) from Ghent University through GOA-project 01G02617.

SUPPLEMENTARY MATERIAL

The Supplementary Material for this article can be found online at: https://www.frontiersin.org/articles/10.3389/fmars.2021.747833/full#supplementary-material

REFERENCES

Barbier, E. B., Hacker, S. D., Kennedy, C., Koch, E. W., Stier, A. C., and Silliman, B. R. (2011). The value of estuarine and coastal ecosystem services. *Ecol. Monogr.* 81, 169–193. doi: 10.1890/10-1510.1

Birchenough, S. N. R., Reiss, H., Degraer, S., Mieszkowska, N., Borja, Á, Buhl-Mortensen, L., et al. (2015). Climate change and marine benthos: a review of existing research and future directions in the North Atlantic. *Wiley Interdiscip. Rev. Clim. Change* 6, 203–223. doi: 10.1002/wcc.330

Brown, J. H., Gillooly, J. F., Allen, A. P., Savage, Van M., and West, G. B. (2004). Toward a metabolic theory of ecology. *Ecology* 85, 1771–1789. doi: 10.1890/03-9000

Cade, B. S., and Noon, B. R. (2003). A gentle introduction to quantile regression for ecologists. *Front. Ecol. Environ.* 1, 412–420. doi: 10.1890/1540-9295(2003)001[0412:AGITQR]2.0.CO;2

Canfield, D. E., Jorgensen, B. B., Fossing, H., Glud, R., Gundersen, J., Ramsing, N. B., et al. (1993). Pathways of organic-carbon oxidation in 3 continental-margin sediments. *Mar. Geol.* 113, 27–40. doi: 10.1016/0025-3227(93)90147-N

Cassidy, C., Grange, L. J., Garcia, C., Bolam, S. G., and Godbold, J. A. (2020). Species interactions and environmental context affect intraspecific behavioural trait variation and ecosystem function. *Proc. R. Soc. B Biol. Sci.* 287:20192143. doi: 10.1098/rspb.2019.2143

Cozzoli, F., Bouma, T. J., Ottolander, P., Lluch, M. S., Ysebaert, T., Herman, P. M. J., et al. (2018). The combined influence of body size and density on cohesive sediment resuspension by bioturbators. *Sci. Rep.* 8:3831. doi: 10.1038/s41598-018-22190-3

Cozzoli, F., Bouma, T. J., Ysebaert, T., and Herman, P. M. J. (2013). Application of non-linear quantile regression to macrozoobenthic species distribution modelling: comparing two contrasting basins. *Mar. Ecol. Prog. Ser.* 475, 119–133. doi: 10.3354/meps10112

Cozzoli, F., Eelkema, M., Bouma, T. J., Ysebaert, T., Escaravage, V., and Herman, P. M. (2014). A mixed modeling approach to predict the effects of environmental modification on species distributions. *PLoS One* 9:e89131. doi: 10.1371/journal.pone.0089131

Cozzoli, F., Smolders, S., Eelkema, M., Ysebaert, T., Escaravage, V., Temmerman, S., et al. (2017). A modeling approach to assess coastal management effects on benthic habitat quality: a case study on coastal defense and navigability. *Estuar. Coast Shelf Sci.* 184, 67–82. doi: 10.1016/j.ecss.2016.10.043

De Vriend, H. J., Wang, Z. B., Ysebaert, T., Herman, P. M. J., and Ding, P. (2011). Eco-morphological problems in the yangtze estuary and the Western Scheldt. *Wetlands* 31, 1033–1042. doi: 10.1007/s13157-011-0239-7

Ellis, J., Ysebaert, T., Hume, T., Alf Norkko, T., Bult, P. M., Herman, J., et al. (2006). Predicting macrofaunal species distributions in estuarine gradients using logistic regression and classification systems. *Mar. Ecol. Prog. Ser* .316, 69–83. doi: 10.3354/meps316069

Fang, X. Y., Moens, T., Knights, A., Soetaert, K., and Colen, C. V. (2021). Allometric scaling of faunal-mediated ecosystem functioning: a case study on two bioturbators in contrasting sediments. *Estuar. Coast Shelf Sci.* 254:107323. doi: 10.1016/j.ecss.2021.107323

Glud, R. N. (2008). Oxygen dynamics of marine sediments. *Mar. Biol. Res.* 4, 243–289. doi: 10.1080/17451000801888726

Khojasteh, D., Glamore, W., Heimhubber, V., and Felde, S. (2021). Sea level rise impacts on estuarine dynamics: a review. *Sci. Tot. Environ.* 780:146470. doi: 10.1016/j.scitotenv.2021.146470

Knights, A. M., Piet, G. J., Jongbloed, R. H., Tamis, J. E., White, L., Akoglu, E., et al. (2015). An exposure-effect approach for evaluating ecosystem-wide risks from human activities Ices. *J. Mar. Sci.* 72, 1105–1115. doi: 10.1093/icesjms/fsu245

Kristensen, E. (2001). Impact of polychaetes (*Nereis* and *Arenicola*) on sediment biogeochemistry in coastal areas: past, present, and future developments. *Abstr. Pap. Am. Chem. Sci.* 221:U538. doi: 10.1186/1467-4866-2-92

Kristensen, E., Penha-Lopes, G., Delefosse, M., Valdemarsen, T. B., Quintana, C. O., Banta, G. T., et al. (2012). What is bioturbation? The need for a precise definition for fauna in aquatic sciences. *Mar. Ecol. Prog. Ser.* 446, 285–302. doi: 10.3354/meps09506

Mermillod-Blondin, F., and Rosenberg, R. (2006). Ecosystem engineering: the impact of bioturbation on biogeochemical processes in marine and freshwater benthic habitats. *Aquat. Sci.* 68, 434–442. doi: 10.1007/s00027-006-0858-x

Murray, F., Solan, M., and Douglas, A. (2017). Effects of algal enrichment and salinity on sediment particle reworking activity and associated nutrient generation mediated by the intertidal polychaete hediste diversicolor. *J. Exp. Mar. Biol. Ecol.* 495, 75–82. doi: 10.1016/j.jembe.2017.06.002

Nielsen, O. I., Gribsholt, B., Kristensen, E., and Revsbech, N. (2004). Microscale distribution of oxygen and nitrate in sediment inhabited by Nereis diversicolor: spatial patterns and estimated reaction rates. *Aquat. Microb. Ecol.* 34, 23–32. doi: 10.3354/ame034023

Reiss, J., Bridle, J. R., Montoya, J. M., and Woodward, G. (2009). Emerging horizons in biodiversity and ecosystem functioning research. *Trends Ecol. Evol.* 24, 505–514. doi: 10.1016/j.tree.2009.03.018

Smolders, S., Cozzoli, F., Plancke, Y., Ides, S., Meire, P., and Temmerman, S. (2013). "A 2Dh hydrodynamic model of the Scheldt estuary in 1955 to assess the ecological past of the estuary," in *Proceedings of the 20th TELEMAC-MASCARET User Conference, October 16-18, 2013 (ISBN 978-3-939230-07-6)*, Karlsruhe, Germany.

Snelgrove, P. V. R., Soetaert, K., Solan, M., Thrush, S., Wei, C. L., Danovaro, R., et al. (2018). Global carbon cycling on a heterogeneous seafloor trends. *Ecol. Evol.* 33, 96–105. doi: 10.1016/j.tree.2017.11.004

Vaz, S., Martin, C. S., Eastwood, P. D., Ernande, B., Carpentier, A., Meaden, G. J., et al. (2008). Modelling species distributions using regression quantiles. *J. Appl. Ecol.* 45, 204–217. doi: 10.1111/j.1365-2664.2007.01392.x

Venables, W. N., and Ripley, B. D. (2002). *Modern Applied Statistics with S*, 4th Edn. New York, NY: Springer. doi: 10.1007/978-0-387-21706-2

Verdelhos, T., Marques, J. C., and Anastacio, P. (2015). The impact of estuarine salinity changes on the bivalves scrobicularia plana and cerastoderma edule, illustrated by behavioral and mortality responses on a laboratory assay. *Ecol. Indic.* 52, 96–104. doi: 10.1016/j.ecolind.2014.11.022

Ysebaert, T., Herman, P. M. J., Meire, P., Craeymeersch, O., Verbeek, H., Heip, C. H. R., et al. (2003). Large-scale spatial patterns in estuaries: estuarine macrobenthic communities in the schelde estuary, nw europe. *Estuar. Coast Shelf Sci.* 57, 335–355. doi: 10.1016/S0272-7714(02)00359-1

Ysebaert, T., Meire, P., Herman, P. M. J., and Verbeek, H. (2002). Macrobenthic species response surfaces along estuarine gradients: prediction by logistic regression. *Mar. Ecol. Prog. Ser.* 225, 79–95. doi: 10.3354/meps225079

Conflict of Interest: The authors declare that the research was conducted in the absence of any commercial or financial relationships that could be construed as a potential conflict of interest.

frontiers in Marine Science

ORIGINAL RESEARCH
published: 27 January 2022
doi: 10.3389/fmars.2021.745501

Evaluation of Shifts in the Potential Future Distributions of Carcharhinid Sharks Under Different Climate Change Scenarios

Pedro Luis Diaz-Carballido[1], Gabriela Mendoza-González[2], Carlos Alberto Yañez-Arenas[3] and Xavier Chiappa-Carrara[3,4]**

[1] Posgrado en Ciencias del Mar y Limnología, Universidad Nacional Autónoma de México, Mexico City, Mexico, [2] CONACYT-Facultad de Ciencias, UMDI-Sisal, Universidad Nacional Autónoma de México, Mérida, Mexico, [3] Facultad de Ciencias, Universidad Nacional Autónoma de México, Mexico City, Mexico, [4] Escuela Nacional de Estudios Superiores–Mérida, Universidad Nacional Autónoma de México, Mérida, Mexico

OPEN ACCESS

Edited by:
Nobuhito Mori,
Kyoto University, Japan

Reviewed by:
Oscar Sosa-Nishizaki,
Center for Scientific Research and Higher Education at Ensenada (CICESE), Mexico
Daniel Philip Crear,
National Marine Fisheries Service (NOAA), United States

***Correspondence:**
Gabriela Mendoza-González
gabriela.mendoza@ciencias.unam.mx
Xavier Chiappa-Carrara
chiappa@unam.mx

Specialty section:
This article was submitted to Coastal Ocean Processes, a section of the journal Frontiers in Marine Science

Received: 22 July 2021
Accepted: 16 December 2021
Published: 27 January 2022

Citation:
Diaz-Carballido PL, Mendoza-González G, Yañez-Arenas CA and Chiappa-Carrara X (2022) Evaluation of Shifts in the Potential Future Distributions of Carcharhinid Sharks Under Different Climate Change Scenarios. Front. Mar. Sci. 8:745501. doi: 10.3389/fmars.2021.745501

Climate change is currently considered one of the main phenomena affecting marine species through expansion or contraction of their distribution. Being ectothermic organisms, sharks of the family Carcharhinidae could be highly susceptible to the effects of climate change. These sharks are of great ecological importance, which is reflected in their role in the integrity of coastal and oceanic ecosystems as top predators that act to maintain the stability of the food chain, as well as providing economic value through fishing, consumption, and ecotourism. Currently, their populations are threatened by fishing pressure and anthropogenic activities, including meeting the demand for shark fins. Despite the ecological and economical importance of carcharhinid sharks, knowledge regarding how they are impacted by climate change remains scarce. Ecological niche modeling is a tool that allows analysis of future potential distributions under different climate change scenarios and could contribute to future planning activities and improved conservation outcomes for sharks. We generated models in Maxent in order to predict the potential geographic distribution of 25 carcharhinid sharks that inhabit Mexican waters, projecting this onto future climate change scenarios (RCP2.6, RCP4.5, RCP6.0, and RCP8.5) to calculate the potential losses and gains in their distribution areas by the year 2050. The greatest shifts in suitable areas were observed for the sharks *Triaenodon obesus* (gained area) and *Carcharhinus porosus* (lost area). Overall, under all four RCP future scenarios, six species presented gains in suitable area and 19 species presented losses. The greatest loss of suitable area for carcharhinid sharks was found with RCP8.5; however, under this high-emissions global warming scenario, seven species actually showed an increase in distribution area. Our results therefore indicate that climate change could reduce suitable areas for most of the species by 2050. Assessment of the distribution of shark species under climate change is urgently required in order to prioritize conservation efforts toward the most vulnerable species and to ensure the natural function of marine ecosystems, thus maintaining the important ecosystem services they provide to human society.

Keywords: ecological niche modeling (ENM), suitable area, sharks, RCP, carcharhinid, climate change

INTRODUCTION

Climate change is currently considered one of the main phenomena that influence the phenology and physiology of some marine species, through modification of environmental variables (Parmesan and Yohe, 2003; Jones et al., 2013; Poloczanska et al., 2013). The tropical marine fauna is among the groups of animals most sensitive to climate change, since the members evolved in a relatively stable thermal environment (Rosa et al., 2014) and are expected to respond to environmental change by shifting their distributions to areas more conducive to maintaining a physiological optimum (Hobday, 2010; Tittensor et al., 2010; Cheung et al., 2012, 2015; Hazen et al., 2013; Nakamura et al., 2013; Robinson et al., 2015; Fogarty et al., 2016).

Regarding the modification of environmental variables, the global average sea surface temperature is predicted to rapidly rise by 1–3°C, as a result of the greenhouse effect (IPCC, 2013). Changes in sea surface temperature are often accompanied by variations in salinity, which is another environmental variable that could be modified by climate change. For instance, decreased salinity can be due to the melting of glaciers and ice sheets, while increased salinity can be produced by higher sea surface temperatures and evaporation (Durack et al., 2012). Variations in salinity are also related to large-scale changes in water movement and it has been speculated that increased wind stress due to climate change could lead to increased coastal currents and upwelling (Bakun, 1990).

Recent evaluations of species distribution have assessed the potential impacts of climate change on both terrestrial and marine organisms (Peterson et al., 2011; Jones et al., 2013; Wabnitz et al., 2018). One taxonomic group of marine fishes that has been put at risk by the rapid environmental modification imposed by climate change is Chondrichthyes (sharks, rays, and chimeras) (Field et al., 2009). Some studies of shark species in particular have described potential changes in their distribution in response to projected changes in climate, which are related to the reduced or increased availability of suitable habitat and poleward shifts in their distribution (Hare et al., 2016; Tanaka et al., 2021). Other studies have evaluated the potential distribution of carcharhinid sharks with climate change using species distribution modeling and generally report a reduction or shift in suitable area for future distributions under different climate change scenarios (Jones et al., 2013; Lezama-Ochoa et al., 2016; Gonzalez-Pestana, 2018; Birkmanis et al., 2020; Crear et al., 2020).

In this context, ecological niche models (ENM) can be employed to describe the geographic and ecological aspects of species and are widely used to assess potential future distributions using a correlative approach between species presence records and environmental variables (Jones and Cheung, 2015; Chefaoui et al., 2019). To assess shifts in future species distributions using ecological niche modeling, it is common to use environmental variables from different future scenarios derived from general circulation (GCMs) and atmosphere-ocean general circulation (AOGCMs) models (Wiens et al., 2009; Harris et al., 2014; Peterson et al., 2018). In the Special Report on Emissions Scenarios (SRES), the Intergovernmental Panel on Climate Change (IPCC) published a family of greenhouse gas scenarios (A1, A2, B1, and B2) that comprise storylines of different demographic, societal, economic, and technical change that assume different future increases in greenhouse gas emissions (IPCC, 2000). These initial emission scenarios were recently updated in the IPCC Fifth Assessment Report (AR5) by replacement with Representative Concentration Pathways (RCPs) that refer to radiative forcing (2.6, 4.5, 6.0, and 8.5 W/m^2 by 2,100) and represent alternative greenhouse gas concentration trajectories. These RCPs include a mitigation scenario involving an initial increase in temperature followed by a decline (RCP2.6), two intermediate scenarios (RCP4.5 and RCP6.0), and finally an extreme scenario with very high annual greenhouse gas emissions and a very marked temperature increase (RCP8.5) (IPCC, 2013).

The consequences of climate change could also be reflected in the integrity of the ecosystem due to the close inter-dependency between it and the sharks. This relationship signifies that, in coastal and oceanic habitats, the sharks keep the food web healthy, maintain the carbon cycle and comprise one of the largest groups of apex predators. Sharks occupy a high trophic level in marine habitats and play a key role in the structure, function, and health of marine ecosystems (Davidson and Dulvy, 2017). Food webs are essential for the stability, maintenance, and control of the populations of the commercial and non-commercial species that occupy the lower trophic levels, indirectly affecting the economy. Given all of these functions, sharks also help to preserve the stability of ecosystems (such as coral reefs) and thus maintain the provision of their ecosystem services (Motivarash et al., 2020).

In addition to the effects of climate change on sharks, populations of their functionally important species assemblages have declined because of rising fishing pressure, increasing their risk of global extinction (Pacoureau et al., 2021). The depletion of sharks could also be the result of indirect anthropogenic threats, including loss or contamination of their habitat (Worm and Tittensor, 2011; Sguotti et al., 2016). This factor can be added to the disadvantages conferred by their intrinsic low phenotypic plasticity (Rosa et al., 2014) and life history patterns (e.g., slow growth, reduced fecundity, late sexual maturity, and long gestation time) (Cortés, 2000). Carcharhinids are subject to high fishing mortality as a result of intentional and incidental capture in a variety of fisheries (Bond et al., 2012; Dulvy et al., 2014), of which there are high levels in Mexico (Sosa-Nishizaki et al., 2020). Intentional fishing of Carcharhinids is mainly conducted to obtain liver oil, cartilage, meat, or fins, for example, in the case of *Carcharhinus falciformis* and *Prionace glauca* (Camhi et al., 2008; Santana-Morales et al., 2020). Furthermore, shark cage diving is currently a prominent feature of ecotourism activities in various parts of the world, including Mexico (Haas et al., 2017; Cisneros-Montemayor et al., 2020).

The members of the Carcharhinidae family include around 12 genera and 50 species, distributed worldwide in both tropical and temperate marine waters. This study focused on 25 carcharhinid sharks that inhabit the waters of Mexico and other areas of the world (Castro, 2011; Saldaña-Ruiz et al., 2019). Of these, 16% are categorized as vulnerable (VU), 52% as near threatened (NT),

16% as data deficient (DD) and 4% as not evaluated (NE) by the International Union for Conservation of Nature (IUCN, 2020).

As the climate continues to warm and change, its effects on vulnerable species should be examined via studies of ecological niche modeling (Hill et al., 2011; Bellard et al., 2012; Lezama-Ochoa et al., 2016; Davidson and Dulvy, 2017). Despite the possible impacts of climate change on shark distribution and their ecological importance and economic value, information on elasmobranch fish remains scarce (Rosa et al., 2014; Davidson and Dulvy, 2017). Knowledge of potential distribution shifts under different scenarios could support scientists and decision makers in the development of appropriate strategies to reduce climate change impacts on biodiversity through actions of early intervention, such as the design of potential protection areas that could become zones of suitable habitat under future climatic conditions (Bellard et al., 2012; Pacifici et al., 2015; Wilkening et al., 2019). The aim of this study was to use ecological niche modeling to evaluate potential changes in the global geographic distribution areas of the 25 carcharhinid sharks that inhabit Mexican waters, considering the climate change scenarios RCP2.6, RCP4.5, RCP6.0, and RCP8.5 for the year 2050. This information could help identify the species that are most vulnerable to climate change and quantify the percentage range of gains/losses over time in order to estimate their risk of extinction and thus inform the creation of a network of protected areas to ensure their persistence.

MATERIALS AND METHODS

Species distribution modeling through estimation of the ecological niche is a correlative approach that uses species presence records (occurrence data of the entire life stages of species) and environmental variables that describe the climatic features of the area in which the species is distributed (Soberón and Nakamura, 2009). In the following sections, we address the different steps that we used to model the potential geographic distribution of carcharhinid sharks under different climate change scenarios.

Occurrence Data

Occurrence records of the complete known distribution of the species in the coastal and marine areas of the Atlantic, Pacific, and Indian Oceans were obtained from the databases of Global Biodiversity Information Facility (GBIF[1]), speciesLink[2], VertNet[3] and the Ocean Biogeographic Information System (OBIS[4]). We also used occurrences from Del Moral-Flores et al. (2015) and the ichthyological collections of CNPE–IBUNAM[5] and CIICMYLP-UNAM[6]. Most of the occurrence records comprised preserved specimens or human observations recorded from 1960 to 2017.

[1]http://www.gbif.org
[2]www.splink.org.br
[3]www.vertnet.org
[4]www.iobis.org
[5]www.unibio.unam.mx
[6]www.icmyl.unam.mx

A thorough inspection of each occurrence record was conducted in R 3.4.4 (R Core Team, 2018) in order to eliminate duplicate records and those with no specified location. We also cross-checked each occurrence record with the information available in the published literature in order to eliminate those that originated outside the known distribution or within the land mask of the Global Self-Consistent, Hierarchical, High resolution Shoreline (GSHHS) database (Wessel and Smith, 1996) in a Geographic Information System (GIS) (ArcMap 10.5). To reduce the effects of sampling bias, we filtered a large number of points grouped into specific areas using the function 'GridSample' of the 'dismo' package. This function divides the area in which the model is calibrated (see Section "M Area" for definition of calibration area) into different grid cell sizes and selects a number of occurrences in each cell as defined by the user. In this record filtering procedure, we selected a grid cell size of one or two degrees, depending on the lower or higher number of occurrence points (respectively), and one occurrence in each cell to maintain the best visual compromise between the largest possible number of occurrence data and a suitable level of homogeneity, according to Voda et al. (2015). This record thinning procedure eliminates the number of occurrences derived from repeated sampling events in the same area (Hijmans, 2012; Hijmans and Elith, 2013), but was not applied to those species with $<$100 occurrence points.

Environmental Data

Since the model is correlative, the algorithm obtains the environmental information relative to each point of occurrence (species presence record) that provides an estimate of the general environmental profile of the species. For this analysis, we used the known distribution of each species (at the regional or global scale, see "M Area" Section) (**Table 1**), current environmental data layers expressed for the entire current period (2000–2014), and future climate projection layers (2040–2050) obtained from the repository Bio-ORACLE (Ocean Rasters for Analysis of Climate and Environment)[7]. These layers were developed specifically to model marine species distributions (Tyberghein et al., 2011; Assis et al., 2017). The repository contains ocean rasters for analysis of climate and environment derived from both satellite-based and *in situ* data in regular two- and three-dimensional spatial grids, at a spatial resolution of 5 arcmins ($\sim$9.2 km^2). We selected environmental variables based on published information pertaining to species-habitat associations of carcharhinid sharks and their availability in the repository. Under this criterion, we used six different predictors for the variables of temperature, salinity, and current velocity, based on monthly averages for the current period: the long term average (mean); the minimum (min) and maximum (max) records; the long-term average of the minimum (ltmin) and maximum (ltmax) records per year; and range (range), which is the average of the absolute difference between the minimum and maximum records per year (Assis et al., 2017). These provide a total of 18 surface environmental variables, which we used to generate our models (**Supplementary Table 1**). In addition, we used their future projections based on the four RCP (RCP2.6, RCP4.5, RCP6.0, and RCP8.5) for the year

[7]https://www.bio-oracle.org/

TABLE 1 | List of modeled species, divided into groups according to their M area.

Group	*Species*	Initial	Filtered	Calibration/evaluation	Number of MEOW and buffer	Know distribution
1	*Carcharhinus cerdale*	20	20	14/6	13	EP
	Nasolamia velox	168	63	44/19	37	EP
	Rhizoprionodon longurio	736	235	164/71	18	EP
2	*Carcharhinus acronotus*	349	102	71/31	17	WA
	Carcharhinus isodon	555	40	28/12	18	WA
	Carcharhinus perezi	306	79	55/24	18	WA
	Carcharhinus porosus	268	58	41/17	50	WA
	Rhizoprionodon porosus	185	109	74/33	20	WA
	Rhizoprionodon terraenovae	891	118	83/35	21	WA
3	*Carcharhinus brachyurus*	1718	184	129/55	144	AO, PO, MS
	Carcharhinus brevipinna	1051	194	136/58	123	AO, IP, MS
	Carcharhinus leucas	12462	86	60/26	138	CS
4	*Carcharhinus signatus*	906	119	84/35	44+ buff.	AO
	Negaprion brevirostris	5158	98	69/29	16	AO, EP
5	*Carcharhinus albimarginatus*	4193	221	155/66	110+ buff.	IP
	Carcharhinus altimus	815	213	149/64	142	CS
	Carcharhinus obscurus	2782	301	211/90	152+ buff.	CS
	Carcharhinus plumbeus	3114	300	210/90	156+ buff.	AO, IP, MS
	Triaenodon obesus	1659	137	98/39	109+ buff.	IP, EP
6	*Carcharhinus falciformis*	8185	600	421/179	182+ buff.	CL
	Carcharhinus galapagensis	587	144	101/43	170+ buff.	CL
	Carcharhinus limbatus	3609	340	239/101	173+ buff.	CS
	Carcharhinus longimanus	2334	404	283/121	168+ buff.	CS
	Galeocerdo cuvier	4939	559	391/168	174+ buff.	CS
	Prionace glauca	7119	1110	777/333	206+ buff.	CS
	TOTAL	64109	5826			

Initial number of occurrences, the number after filtering, and those used to conduct the calibration and evaluation process. Number of marine ecoregions (MEOW) used for constructing the M areas and including the buffer. Known distribution of species [AO (Atlantic Ocean), WA (western Atlantic), PO (Pacific Ocean), EP (eastern Pacific), IP (Indo-Pacific), MS (Mediterranean Sea), CL (Circumtropical), and CS (Cosmopolitan)].

2050. We calibrated the models of the 25 carcharhinid sharks with two different sets of variables created as potential predictors of niche models ('set_1' and 'set_2'). The former comprised all of the variables and the latter only the non-correlated variables. For 'set_2,' collinearity was reduced in order to avoid instability in parameter estimation and bias in the inference statistics (Dormann et al., 2012). In order to reduce collinearity among variables, we used the variance inflation factor (VIF). This factor excludes the highly correlated predictor variables from the set through a stepwise procedure based on the square of the multiple correlation coefficient and produced by regressing one predictor variable against all other predictor variables. Predictor variables greater than 10 VIF in value were removed and used to form 'set_2.' A VIF value greater than 10 is a signal that the predictor variables have high collinearity (Montgomery and Peck, 1992). This value statistically indicates a significant multicollinearity and is used in studies of niche modeling (Naimi and Araújo, 2016; Pradhan, 2016). However, the modeling algorithm we used (MaxEnt) compensates for high collinearity of variables using a method for regularization that addresses feature selection in order to assign relative contributions by weighting the variables throughout the analysis (Elith et al., 2011; Mendoza-González et al., 2016). For this reason, we also used 'set_1.'

M Area

The M areas represent the geographic regions where the models are calibrated (calibration area) and are accessible to a species or population via dispersal over extended time periods (Peterson and Soberón, 2012; Banks, 2017). The importance of considering the M area when estimating ecological niches has been demonstrated, since it helps when transferring correlative models to other areas and has no effect on the calibration and validation processes (Barve et al., 2011; Peterson et al., 2018). Various different approaches can be adopted in order to calibrate the study area correctly, including the use of polygons, buffers, or distances based on species dispersal ability, among others. However, the question of how to better define the calibration area remains to be addressed (Simões et al., 2020). We developed an M area for each species based on the 232 marine ecoregions for coastal and shelf areas of the world (MEOW) of Spalding et al. (2007). The criterion used to define the extent of the species distribution was based on ecological delimitation and

dispersal abilities for two cases. The first case considered only the MEOW for the species that are distributed in the coastal and shelf areas, and which presented specific characteristics such as homogeneous composition of species, upwelling, nutrient inputs, temperature regimes, etc. (Spalding et al., 2007). These MEOW were selected when they contained at least one point of occurrence for each species, and they were then grouped to form the species M area (M areas independent for each species). For some sharks, the known distribution was found in small areas within the MEOW but far from their limits; however, we still considered the complete extension of the MEOW, since they are considered biogeographic units within which the sharks could spread out given their dispersal capacities. In the second case, when the occurrence points were beyond the limits of MEOW, such as for non-coastal sharks, the M area was estimated through a 100 km radius buffer created around each occurrence, based on the dispersal ability of other pelagic and carcharhinid sharks (Speed et al., 2010; Acuña-Marrero et al., 2017; Spaet et al., 2017). Regarding the possible mobility of organisms through this region, we used a sea currents raster mask (Sun, 2018) as a basis for joining the resulting separated buffer areas with the marine ecoregions. In both cases of M area, we considered the total area of accessibility of the species (Barve et al., 2011).

Finally, we identified the following distributions for our study species: AO (Atlantic Ocean), WA (western Atlantic), PO (Pacific Ocean), EP (eastern Pacific), IP (Indo-Pacific), MS (Mediterranean Sea), CL (Circumtropical), and CS (Cosmopolitan). The number of marine ecoregions involved in constructing the M region per species, for which a buffer was applied, is shown in **Table 1**. The resulting model maps are presented in six groups depending on the M area of the species. The first three correspond to distributions only in MEOW and the second three correspond to distributions in MEOW and the generated buffers: (1) distribution in the eastern Pacific Ocean (EP), (2) distribution in the western Atlantic Ocean (WA), (3) distribution in the Mediterranean Sea and some oceans (AO, PO, MS, and IP), (4) distribution in eastern Pacific and/or Atlantic Ocean (AO, EP), (5) distribution in some ocean regions including the Mediterranean Sea (IP, CS, AO, MS, and EP), and (6) distribution in all ocean regions (Atlantic, Pacific, and Indian) including the Mediterranean Sea (with distributions CL and CS).

Construction of Models

For model calibration, we used MaxEnt 3.4.1 (Phillips et al., 2006), an algorithm based on the maximum entropy approach that is commonly used to estimate the potential distribution of species by correlating presence-only data with sets of environmental variables (Elith et al., 2010). This algorithm is very flexible and has many parameters that can be changed by users; however, the models are often constructed based on simple protocols by using the default parameter settings (i.e., auto-features) in the traditional platform, which could ultimately produce non-optimal (over-complex or over-simplistic) models. This could present a problem, particularly when dealing with a small number of occurrence points, in which case the recommendation is to evaluate the best potential combination of multiple parameterizations that can produce good fits for small data sets (Warren and Seifert, 2011; Radosavljevic and Anderson, 2014; Morales et al., 2017). Given the time-consuming nature of performing this task manually, we ran Maxent in R (R Core Team, 2018) using the kuenm package[8] as an automated tool that allows users to generate many Maxent candidate models with varying calibration settings (feature classes, regularization multiplier, and sets of environmental variables) to obtain a species-specific parameterization, thus increasing the robustness of models over a much shorter time (Cobos et al., 2019). Feature classes (FC) are defined as transformations applied to the different covariates used in models to allow modeling of complex relationships. A regularization multiplier (RM) is a parameter that adds new constraints or imposes penalties on the model to prevent over-complexity and/or overfitting (Elith et al., 2010). Prior to the calibration process, the dataset of each species was randomly partitioned into training (70%) and validation (30%) data (Mendoza-González et al., 2016). The calibration process for candidate model creation was performed with a parameter setting using the *kuenm-cal function* using a combination of 15 feature classes (all potential combinations of four feature classes: linear, quadratic, product, and hinge); nine values of the regularization multiplier (1, 1.5, 2, 2.5, 3, 3.5, 4, 6, and 10) and the two sets of environmental variables ('set_1' and 'set_2'). Two models were created for each parameter setting: one based on the complete filtered and thinned dataset of occurrences, and the other based only on the training data. The former is used to calculate model complexity and the latter to calculate significance and omission rates (Cobos et al., 2019). Likewise, the Jackknife function of Maxent was used to identify the percentage of contribution from each environmental variable (Phillips et al., 2006). Candidate model evaluation and best model selection were developed using the *kuenm-ceval function*. This function completes the process of calibration by evaluating and selecting models according to the following hierarchical evaluation criteria: (1) statistical significance of the model, using the area under the curve ratio (AUC) of the partial receiver operating characteristic (ROC) tests, with 500 iterations and 50% of the data used for bootstrapping, in which the AUC ranges from 1 to 2 (1 representing a random model, 2 representing a better than random performance); (2) model performance: predictive ability with omission rates (OR) $\leq$ 5%, which is our level of confidence in the training data; and (3) model complexity: based on the Akaike Information Criterion (AIC), which indicates how well the models fit to the data while penalizing complexity to favor more parsimonious and less overfitted models. Finally, we used the *kuenm-mod function*, which generated final continuous models of probability (suitability) with the parameter sets selected as best, including one model per species that met the three hierarchical evaluation criteria (AUC, OR, and AIC) and its corresponding environmental set (1 or 2). Once the model that best projected the distributions of the current time period was determined, it was used to transfer the projections

[8]https://github.com/marlonecobos/kuenm

to the four RCP scenarios of the future for each species (Cobos et al., 2019).

Projections to Future Scenarios (RCP)

The best final models per species in the current period were projected to the four RCPs (2.6, 4.5, 6.0, and 8.5) for the year 2050 using the *kuenm-cal function*. These scenarios are based on average data from different Atmosphere-Ocean General Circulation Models (AOGCMs: CCSM4, HadGEM2-ES, and MIROC5) available in Bio-ORACLE (see Text Footnote 7) (Assis et al., 2017).

Three different strategies can be used to extrapolate the models to the future: (1) truncation, which considers all conditions outside the calibration data range as unsuitable; (2) clamping, which extrapolates the marginal values in the calibration area as the prediction for more extreme conditions; and (3) actual extrapolation, which extends the response curve based on trends obtained from the calibration conditions (Qiao et al., 2019). In order to choose the optimum strategy, we calculated the climatic analogy (environmental similarity) between the present and future scenarios through the extrapolation risk in model transfers via mobility-oriented parity (MOP), which calculates the environmental difference between current (calibration region) and future (transfer region) scenarios (Owens et al., 2013). Since the MOP analysis indicated large areas of uncertainty for the projection of models under future scenarios, we used the truncated response, thus strongly reducing the combinations of environmental conditions under which models are calibrated in the present (Owens et al., 2013; Cobos et al., 2019). This step was applied using the *kuenm-mop function* implemented by kuenm (Cobos et al., 2019).

Current and future binary maps [suitable areas (1) – unsuitable areas (0)] were obtained by thresholding the final continuous models (present and future) using the criterion of 5% of allowed omission in the training presence (Cooper and Soberón, 2018). This cut-off threshold value for generating the binary maps utilizes the suitability values less than or equal to 5% in the presence points (training data) to classify absence (0) and those that exceed this value to classify presence (1). This percentage value was determined based on a fixed allowable omission error rate among the calibration data, assuming that up to 5% of the occurrence data may have included errors that misrepresented the environments used by the species. This value is considered appropriate when input data are heterogeneous and uncontrolled in origin (Anderson et al., 2003; Peterson et al., 2008; Costa et al., 2009) and is also the parameter that measures error associated with the presence localities dataset (Costa et al., 2009). Shifts in suitable areas for the current and different future scenarios were then obtained per species, through spatial analysis in a GIS (ArcMap 10.5), to produce three categories: (i) lost or contraction areas (areas suitable at present but not in the future), (ii) gained or expansion areas (areas unsuitable at present but suitable in the future), and (iii) maintained or stable suitable areas (areas suitable at present and in the future). These areas were then mapped, and percentage values for the gained, lost and maintained suitable areas for each species in each of the four future RCP scenarios calculated as the proportion of each category in relation to the total area of study, which is the M area of each species (area of category/total area * 100). We calculated the total shift of suitable areas by subtracting the loss of suitable area per species from the total percentages of gain, under all four future scenarios.

RESULTS

A total of 64,109 presence records were compiled for the 25 species of carcharhinid sharks, and 5,826 occurrences remained after data cleaning. After filtering, the occurrence records ranged from 20 (*Carcharhinus cerdale*) to 1,110 (*Prionace glauca*) (**Table 1**). The lowest number of marine ecoregions used for constructing the accessible or M area was 13 and the highest was 206, including the buffer (**Table 1**). Following calibration of the 25 species models with the two different sets of variables, the best qualified according to the metrics described in the previous section were selected to be modeled with 'set_1' (18 species: all predicted variables) and 'set_2' (seven species: non-correlated variables only, **Supplementary Table 2** and **Table 2**).

A total of 270 candidate models were created per species, considering the combinations of 15 feature classes, nine regularization multipliers and two environmental data sets. The model evaluation presented statistical significance ($P < 0.05$), with the AUC ratios of partial ROC > 1 and some close to 2, indicating good model performance. Indeed, the performance in most of our models met the defined permissible omission rate threshold or better than random expectation (omission rates $\leq$ 5%), except for *C. falciformis* (0.07), *Carcharhinus signatus* (0.08), *Galeocerdo cuvier* (0.06), and *T. obesus* (0.07) (**Table 2**). According to the jackknife test results, there were differences among the species in terms of the relative importance of the environmental predictors (EP) used to construct the models. For example, the relative importance values of "Range surface temperature" (ST_range) and "Minimum surface current velocity" (CV_min) were highest in six species, "Maximum surface temperature" (ST_max) and "Average of the maximum records of temperature per year" (ST_ltmax) presented their highest values in three species, and "Mean surface temperature" (ST_mean) and "Range surface salinity" (SS_range) had their highest values in two species (**Table 2**). The final continuous models for the 25 species with the optimal parameterizations and the occurrences used for calibration were mapped (**Supplementary Figures 1–25**).

The mobility-oriented parity (MOP) analyses revealed areas with strict extrapolation risk or non-analogous environmental combinations for all species. For this reason, we decided to employ truncated estimates to create the future scenario maps (for all RCP scenarios) for each species. In this paper, we present the suitable areas gained, lost, and maintained, relative to the current species distribution, using binary maps only for the two most contrasting scenarios of low (RCP2.6) and high (RCP8.5) greenhouse gas emissions (**Figures 1–6**). Binary maps that present this information for all four RCP scenarios (2.6; 4.5; 6; and 8.5) are provided in 100 future maps for all species (**Supplementary Figures 26–50**).

TABLE 2 | Optimal parameters in kuenm models for each species, divided into groups according to their M area: regularization multiplier (RM), feature classes (FC) [linear (l), quadratic (q), product (p), and hinge (h)], set of environmental variables (Pred. Sets), AUC ratio of Partial ROC (AUC), omission rate accepting 5% error in training data (OR ≤ 5%).

Group	Species	RM	FC	Pred. sets	AUC ratio	OR 5%	No. of param	EP (%)
1	*C. cerdale*	1.5	lqp	set_1	1.9	0	3	ST_ltmin 27.9%
	N. velox	1	q	set_1	1.7	0	9	ST_ltmax 33.6%
	R. longurio	2	l	set_2	1.6	0.04	9	ST_range 37.3%
2	*C. acronotus*	6	lqh	set_1	1.3	0.03	14	CV_min 32.7%
	C. isodon	1.5	lq	set_1	1.8	0	10	ST_range 32%
	C. perezi	1.5	l	set_1	1.3	0	9	CV_min 40.2%
	C. porosus	1	q	set_1	1.4	0	14	SS_min 39.9%
	R. porosus	1.5	q	set_1	1.2	0	9	CV_min 43.6%
	R. terraenovae	1	lq	set_1	1.4	0.03	10	CV_min 37.6%
3	*C. brachyurus*	6	lh	set_2	1.3	0.02	19	ST_range 50.8%
	C. brevipinna	2.5	lph	set_1	1.2	0.03	72	CV_min 21.6%
	C. leucas	1.5	lq	set_1	1.3	0.04	11	ST_range 39.5%
4	*C. signatus*	3	lqp	set_1	1.1	0.08	37	SS_ltmin 17.4%
	N. brevirostris	1	lq	set_2	1.1	0.03	11	ST_range 23.7%
	C. albimarginatus	2	lp	set_1	1.2	0.05	35	ST_ltmax 20.1%
	C. altimus	1.5	lqh	set_1	1.2	0.05	22	SS_range 38.3%
	C. obscurus	3	qp	set_1	1.1	0.04	35	ST_range 22.5%
	C. plumbeus	4	lh	set_2	1.2	0.03	8	ST_max 40.1%
	T. obesus	6	h	set_2	1.1	0.07	36	CV_min 37.7%
6	*C. falciformis*	6	l	set_1	1.1	0.07	10	ST_mean 52.6%
	C. galapagensis	6	h	set_1	1.1	0.05	11	ST_mean 60.8%
	C. limbatus	6	p	set_1	1.2	0.05	29	SS_range 19.8%
	C. longimanus	3.5	pq	set_2	1.2	0.05	38	ST_max 34.8%
	G. cuvier	1	l	set_2	1.1	0.06	10	ST_max 42.1%
	P. glauca	3.5	lqph	set_1	1.1	0.05	89	ST_ltmax 44.2%

Number of parameters (No. of param.). Environmental predictor with the greatest percentage contribution to the model (EP%).

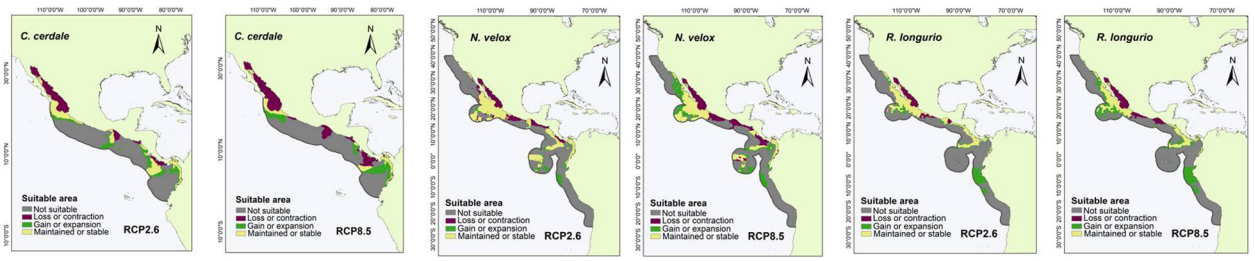

FIGURE 1 | Suitable areas maintained, gained, and lost by the year 2050 under low (RCP2.6) and high (RCP8.5) greenhouse gas emission scenarios in species with an M area in the eastern Pacific Ocean: *Carcharhinus cerdale, Nasolamia velox,* and *Rhizoprionodon longurio*.

For the species with distribution in the eastern Pacific Ocean (EP, group one), the area of greatest loss for the three species corresponded to the Gulf of California, while those of greatest gain were closer to the equator (**Figure 1**). For the species with distribution in the western Atlantic Ocean (WA, group two), the areas of greatest loss generally occurred in the northern Gulf of Mexico, with only *Carcharhinus perezi* showing areas of considerable gain in both scenarios. For the three species with distribution in the Mediterranean Sea and some oceans (AO, PO, MS, IP, and group three), there was a very wide area of maintenance or stability. In comparison, the areas of contraction or loss were very small, and corresponded to Southeast Asia (**Figure 3**). For the species with distribution in eastern Pacific and/or Atlantic Ocean (AO, EP, and group four), the areas of greatest loss generally occurred in the northern Gulf of Mexico for both species, while *C. signatus* and *Negaprion brevirostris* presented areas of loss in west Africa and in the Gulf of California, respectively (**Figure 4**). For the species with distribution in some ocean regions including the Mediterranean Sea (IP, CS, AO, MS, EP, and group five), the areas of loss for *Carcharhinus albimarginatus*, *Carcharhinus altimus*, and *Carcharhinus obscurus* were regionalized in South Asia. This is in

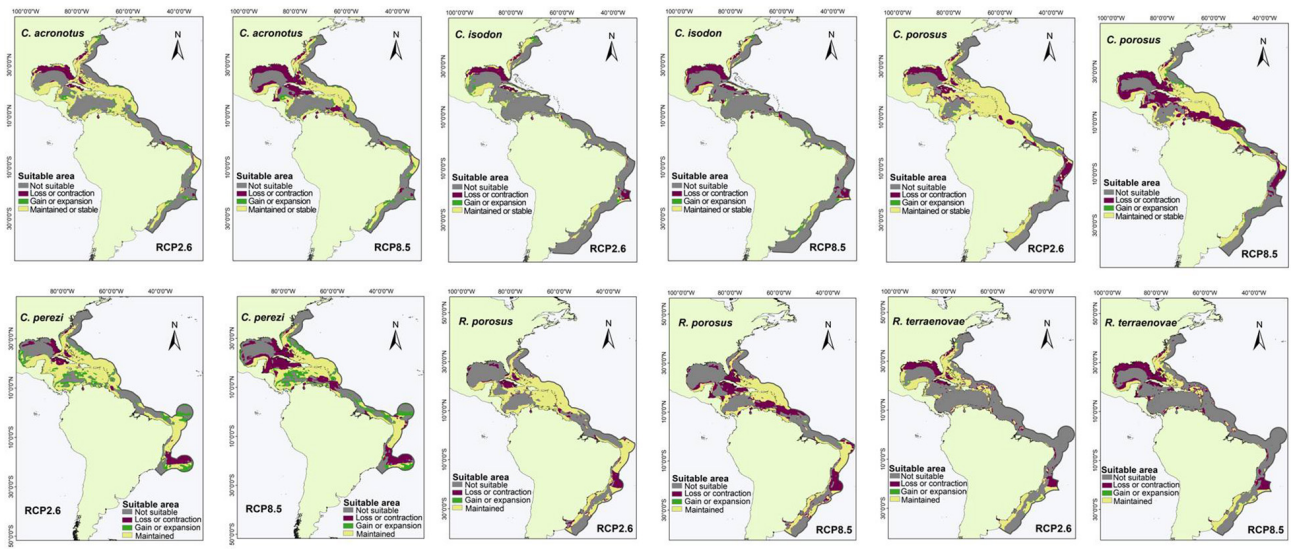

FIGURE 2 | Suitable areas maintained, gained, and lost by the year 2050 under low (RCP2.6) and high (RCP8.5) greenhouse gas emission scenarios in species with an M area in the western Atlantic Ocean: *Carcharhinus acronotus, Carcharhinus isodon, Carcharhinus porosus, Carcharhinus perezi, Rhizoprionodon porosus,* and *Rhizoprionodon terraenovae*.

contrast to *Carcharhinus plumbeus* and *T. obesus*, which generally presented maintained and gained areas across almost all of their distribution (**Figure 5**). Similar to the previous group, for the species with distribution in all ocean regions (Atlantic, Pacific, and Indian), including the Mediterranean Sea (with distributions CL, CS, group six), the unsuitable areas were found in South Asia, except for the species *Carcharhinus longimanus* and *G. cuvier*, which presented large maintained areas. The six species in this group presented gained areas in the extreme north and south of their respective M areas (**Figure 6**).

For all of the species in general, considering the four RCP scenarios, the highest gain in suitable area was found for *T. obesus*, while the highest loss in suitable area was for *C. porosus* and the highest maintained suitable area was for *G. cuvier* (**Table 3**). Under all four RCP future scenarios, the total shifts (gain – loss) presented losses in suitable areas for 13 species but gains for six species. However, under at least one RCP future scenario, 19 species showed losses while 11 presented gains. In most species, the main future losses of suitable area were observed under the extreme scenario RCP8.5 (**Figure 7**). For sharks in group one, *C. cerdale* showed a loss of suitable area under all climate change scenarios. In group two, all of the species presented losses in suitable area, except *C. perezi*, which showed small gains in all RCP except for RCP8.5. For groups three and four, the species showed loss of suitable area, except for *Carcharhinus leucas* and *N. brevirostris*, respectively, which showed low percentages of gain in suitable areas. Groups five and six presented the species with highest percentages of gain (**Figure 7**). On average, under all four RCP future scenarios, *Carcharhinus porosus* (in group two) was the species that presented the highest losses, while *T. obesus* (in group five) presented the highest gains (**Figure 7**).

DISCUSSION

The results of this study show that most of the species presented a shift in their distribution in response to the projected changes in climate. The suitable area for carcharhinid sharks showed a general trend of decline in the future for most species, although the suitable area of some species is expected to increase. In general, the loss of suitable area is predominantly found around the equatorial band, the Gulf of Mexico, and the Indian Ocean; in contrast, the areas that present gains in suitability are predominantly on the periphery of the M areas.

Regarding changes in environmental variables and shifts in range, in our study, temperature range, and other variables related to temperature, made the highest contributions to the niche models. This supports the findings of other studies on shark distributions (Lezama-Ochoa et al., 2016; Birkmanis et al., 2020). Being ectothermic organisms, in common with other teleost fishes, the physiological functions of many sharks are controlled and determined by temperature and their thermal tolerance limits. This makes them susceptible to negative impacts as a result of climate change (Rosa et al., 2014; Schlaff et al., 2014). Unlike bony fish, the k-selected life strategy of the Chondrichthyans, characterized by long generation times and low fecundity, impedes their adaptation to rapid environmental change imposed upon them as a result of human activities (Wheeler et al., 2021). In addition, the projected negative future change (loss of suitable area) in our modeled species could be related to some theoretical expectations, in which the physiology and behavior of ectothermic and tropical species are strongly affected by temperature gradients (Chin et al., 2010; Feary et al., 2013; Rosa et al., 2014; Schlaff et al., 2014). This could be because tropical species live close to their thermal limits, and have a lower capacity for acclimation compared to temperate

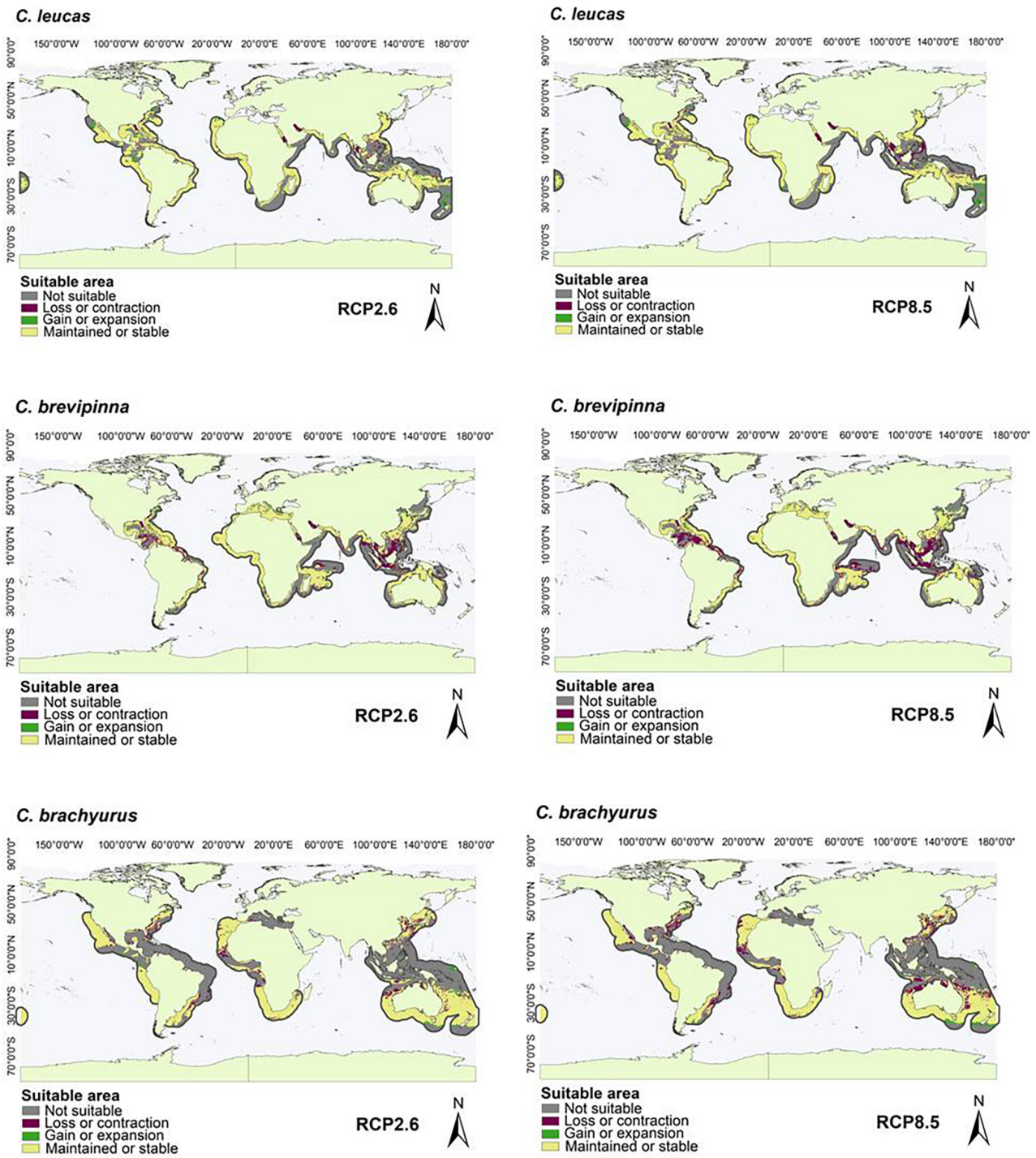

FIGURE 3 | Suitable areas maintained, gained, and lost by the year 2050 under low (RCP2.6) and high (RCP8.5) greenhouse gas emission scenarios in species with an M area in the Mediterranean Sea and some Oceans (Atlantic, Pacific, and Indian): *Carcharhinus leucas, Carcharhinus brevipinna,* and *Carcharhinus brachyurus*.

species, implying their possible vulnerability to even slight increases in habitat temperature (Cheung et al., 2009; Comte and Olden, 2017). However, vulnerability to rising temperatures will depend mostly on the thermal tolerance and acclimation capacity of the organism in question (Rodriguez-Dominguez et al., 2019), and these are parameters that remain unknown for most species. With regard to shifts in shark distributions related to changes in salinity, the long-term impacts on sharks are not well understood. However, these impacts are known to depend on the duration of exposure. For instance, some

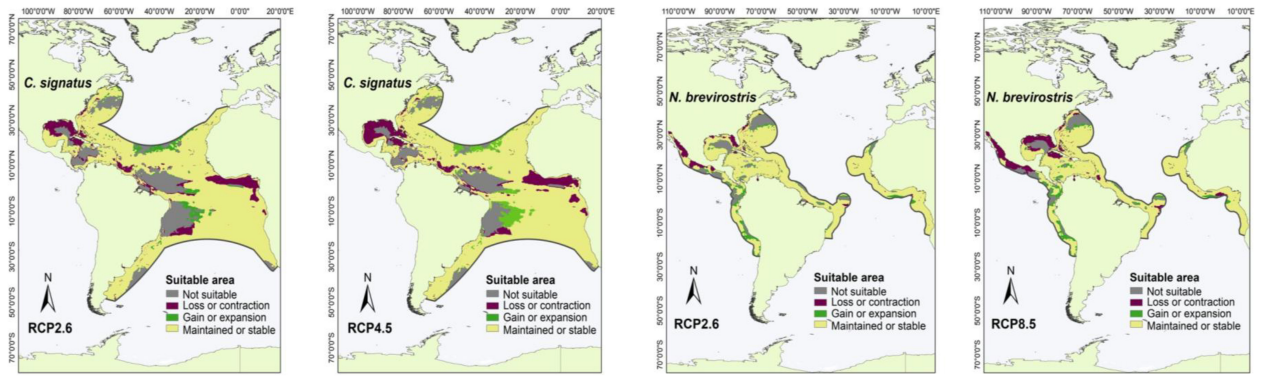

FIGURE 4 | Suitable areas maintained, gained, and lost by the year 2050 under low (RCP2.6) and high (RCP8.5) greenhouse gas emission scenarios in species with occurrence points outside of marine ecoregions and M areas in the Pacific and/or Atlantic Ocean: *C. signatus* and *N. brevirostris*.

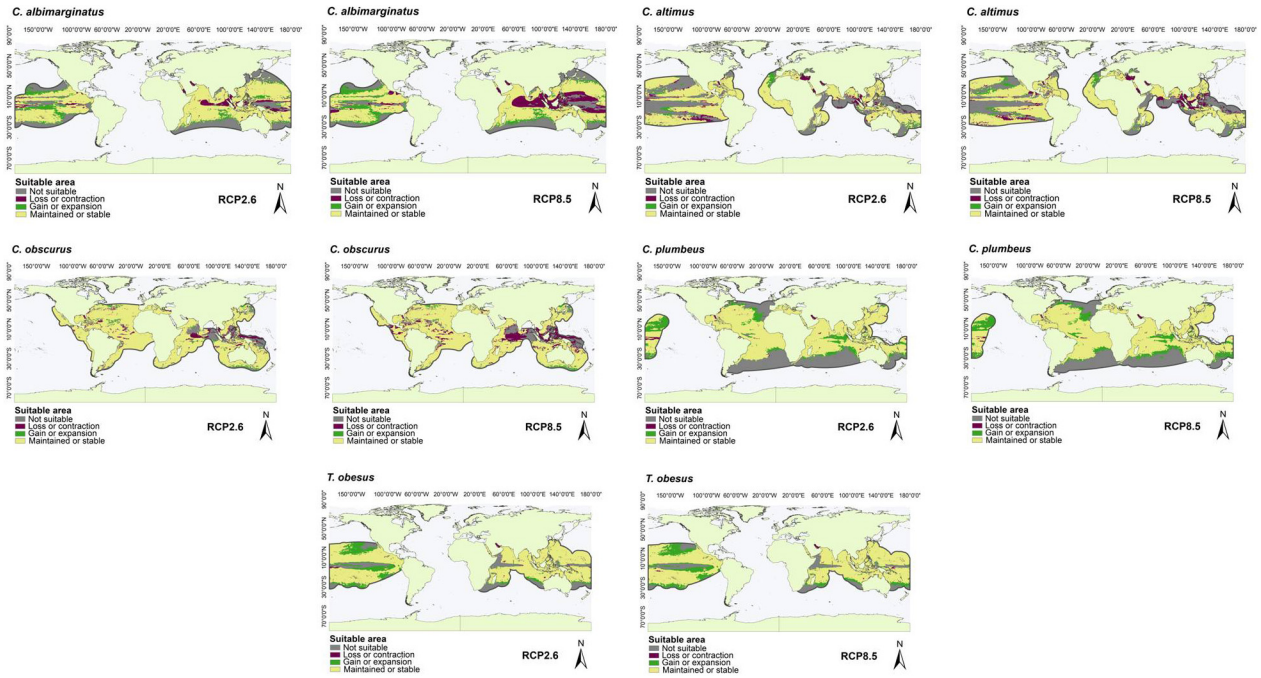

FIGURE 5 | Suitable areas maintained, gained, and lost by the year 2050 under low (RCP2.6) and high (RCP8.5) greenhouse gas emission scenarios in species with occurrence points outside of marine ecoregions and M areas in some regions of the Oceans (Atlantic, Pacific, and Indian), including the Mediterranean Sea: *C. albimarginatus, C. altimus, C. obscurus, C. plumbeus,* and *T. obesus*.

sharks can tolerate decreased salinity, although this implies increased energy costs to maintain osmotic balance, and they tolerate increases in salinity by retaining more salts such as urea in their blood (Yates et al., 2015; Dwyer et al., 2019; Vedor et al., 2021). Such exposure to salinity levels beyond the preferred range of the sharks could affect their physiology, as well as their abundance and distribution (Drymon et al., 2013). The range of a marine fish is also influenced by ocean currents, although this aspect has received scant attention in the context of climate change (Feary et al., 2013). Distribution shifts could also be related to the oceanographic conditions of each ocean, since climate change can impact the strength, direction, and behavior of the main currents (Hoegh-Guldberg and Bruno, 2010). Ocean currents have also been described as an oceanographic predictor for certain species of sharks, given their active behavior and use of these currents in the search for food (Bradie and Leung, 2017; Ranintyari et al., 2018; Báez et al., 2019).

A few attempts have been made to estimate the potential current or future distribution areas of carcharhinid sharks using Maxent, or other modeling approaches, in which the decrease of suitable area has also been reported. Jones et al. (2013) applied three species distribution models projected to one climate change scenario (SRES A2 to 2050), with two sets

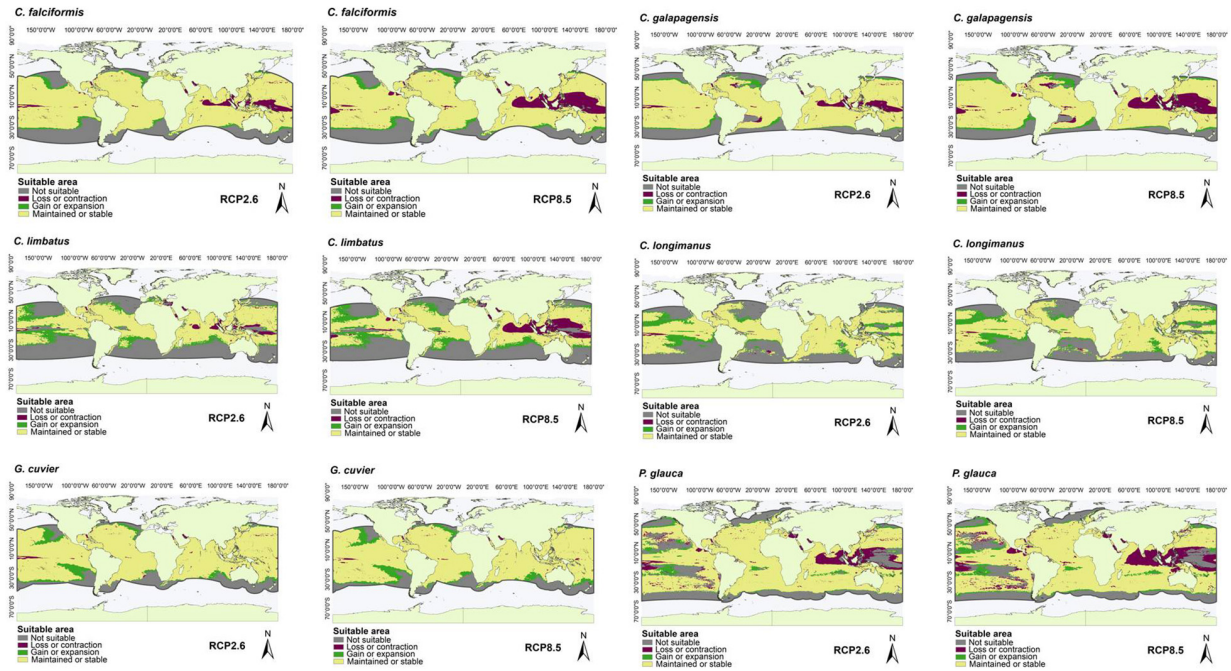

FIGURE 6 | Suitable areas maintained, gained, and lost by the year 2050 under low (RCP2.6) and high (RCP8.5) greenhouse gas emission scenarios with occurrence points outside of marine ecoregions and M areas in all regions of the oceans (Atlantic, Pacific, and Indian), including the Mediterranean Sea: *C. falciformis, Carcharhinus galapagensis, C. limbatus, C. longimanus, G. cuvier,* and *P. glauca*.

of variables to determine the potential impacts on commercial fish in the North Sea, finding a contraction in total suitable area of 11.6% for Angel sharks (*Squatina squatina*) and other elasmobranchs, such as rays. Gonzalez-Pestana (2018) predicted habitat suitability for smooth hammerheads (*Sphyrna zygaena*) under current and future climate change scenarios for the period 2040–2050, indicating that the suitable habitat for this species will shift to a more coastal distribution in the future. For carcharhinid sharks, Lezama-Ochoa et al. (2016) found that *Carcharhinus falciformis* presents losses in suitable area, under SRES A2 climate change scenarios for 2100, of 15.5% in the Atlantic Ocean, 9.9% in the Pacific Ocean, and a minimum change of 1.4% in the Indian Ocean. Our results for *C. falciformis* showed that the maximum loss in suitable area was 10% under RCP8.5 and the minimum was 4.3% under RCP2.6. Although the effects of RCP8.5 could be compared to the SRES A2 scenario of the IPCC (2013), we did not evaluate the shift in potential distribution for each ocean separately. Birkmanis et al. (2020) predicted a decrease in suitable areas for *C. falciformis* under the RCP4.5 and RCP8.5 scenarios (2050–2099) on the coast of Australia, and reported the same in this region for *C. obscurus*, *C. longimanus,* and *P. glauca*. In contrast to these results, our study found a general increase in suitable area for *C. longimanus* under all RCP scenarios. This discrepancy could be due to the fact that our study considered the known worldwide distribution, which is the same distribution that was used as the calibration and projection area. However, distribution shifts can be observed at the regional level, showing a reduction in the distribution area of this species within the Australian EEZ, which coincides with that reported by Birkmanis et al. (2020).

The projected expansions of suitable areas for some species under the RCP8.5 and RCP4.5 scenarios may contrast with previous studies that suggest a greater contraction of suitable areas under severe future climate scenarios (Perry et al., 2005; Dulvy et al., 2008). Such differences in the predictions may be due to the thermal tolerance of the species coupled with their high capacity for movement, which provides the opportunity to move to higher latitudes and avoid the increase in water temperature. In this regard, Sunday et al. (2015) state that the high movement capacity and the latitudinal range of the species have positive relationships with their distribution area under climate change. Other studies conducted with carcharhinid sharks (Lezama-Ochoa et al., 2016; Birkmanis et al., 2020), in which no gain area was reported, contrast with our results, possibly due to the difference in the geographic regions for which modeling was conducted, the diverse size of the study areas (M area from Birkmanis et al., 2020) or the specific future scenarios used [for example, SRES A2 from Jones et al. (2013) and Lezama-Ochoa et al. (2016)]. Nevertheless, our results are congruent with some bioclimatic theories that predict an overall expansion of niches with climate change in some tropical fish (Genner et al., 2004), and also support the general trend of gain in areas as a result of climate change-induced temperature rises (i.e., poleward shifts) (Booth et al., 2011). In addition, Coro et al. (2016) found that endangered and near threatened species of some wide-range elasmobranchs, such as *Alopias vulpinus* and *Alopias pelagicus*, showed positive trend

TABLE 3 | Percentage of not suitable (NS), gained (G), lost (L), and maintained (M) areas, and total shift (TS) in the potential geographic distribution of each species under the RCP future scenarios, divided into groups according to their M area.

		RCP2.6					RCP4.5					RCP6.0					RCP8.5				
Group	**Species**	**NS**	**G**	**L**	**M**	**TS**	**NS**	**G**	**L**	**M**	**TS**	**NS**	**G**	**L**	**M**	**TS**	**NS**	**G**	**L**	**M**	**TS**
1	*C. cerdale*	60.3	10.6	13.3	15.8	−2.7	60.4	10.5	21.1	8	**−10.5**	59.4	11.4	14.3	14.8	−2.9	59.4	11.5	20.6	8.5	−9.1
	N. velox	61.3	5.3	9.4	24	−4.1	59.7	6.8	14.1	19.3	−7.3	62.9	3.7	11.4	22	−7.7	52.4	14.2	12.9	20.5	1.3
	R. longurio	67.3	9.4	5.6	17.7	3.8	65	11.7	9.7	13.6	2	69.2	7.6	6.4	16.9	1.2	61.9	14.9	8	15.3	6.9
2	*C. acronotus*	49.8	5.2	7.3	37.7	−2.1	48.1	6.9	10.2	34.9	−3.3	49.7	5.3	7.1	37.9	−1.8	49.4	5.6	15.9	29.1	**−10.3**
	C. isodon	72.6	3.6	8.4	15.4	−4.8	71.8	4.4	9.6	14.2	−5.2	72.6	3.6	7.8	16	−4.2	72.7	3.5	13	10.9	−9.5
	C. perezi	32.4	12.5	9	46.1	3.5	32.1	12.8	11.9	43.2	0.9	32.5	12.4	8	47.2	4.4	31.4	13.5	21.9	33.3	−8.4
	C. porosus	35.6	2.2	12.9	49.3	**−10.7**	36.4	1.3	16.4	45.8	**−15.1**	35.5	2.2	10.8	51.4	−8.6	35.7	2.1	28.3	33.9	**−26.2**
	R. porosus	44.8	0.7	8.8	45.8	−8.1	44.9	0.6	11.1	43.5	**−10.5**	45.0	0.4	9.5	45.1	−9.1	45.0	0.4	21.3	33.3	**−20.9**
	R. terraenovae	67.8	0.7	10.3	21.2	−9.6	68.2	0.3	12.2	19.3	**−11.9**	67.9	0.6	9.5	22	−8.9	68.2	0.4	15.8	15.7	**−15.4**
3	*C. leucas*	39.1	3.9	3.2	53.8	0.7	38.3	4.7	4.1	52.9	0.6	38.9	4.1	2.8	54.2	1.3	38.7	4.3	5.2	51.8	−0.9
	C. brachyurus	50.1	1.4	5.4	43.1	−4	49.9	1.6	7.7	40.9	−6.1	50.0	1.5	6	42.5	−4.5	50.2	1.3	8.7	39.8	−7.4
	C. brevipinna	35.2	1.6	11.2	52.1	−9.6	35.2	1.6	13.6	49.6	**−12**	35.4	1.3	10.8	52.5	−9.5	35.1	1.7	15.7	47.6	**−14**
4	*C. signatus*	16.9	3.9	9.1	70.1	−5.2	14.8	6	10.6	68.6	−4.6	18.4	2.5	7.9	71.3	−5.4	18.0	2.9	16.8	62.4	**−13.9**
	N. brevirostris	11.1	6.2	4.8	***77.9***	1.4	10.4	7	9.4	***73.3***	−2.4	12.2	5.1	4.7	***78***	0.4	10.1	7.2	11.4	***71.3***	−4.2
5	*C. albimarginatus*	24.9	9.3	5.7	60.1	3.6	23.3	10.9	11.1	54.8	−0.2	25.0	9.2	6.6	59.3	2.6	22.0	12.2	13.9	52	−1.7
	C. altimus	31.3	3.7	5.9	59	−2.2	30.3	4.8	7.4	57.6	−2.6	30.9	4.2	6.3	58.7	−2.1	29.9	5.1	7.6	57.3	−2.5
	C. obscurus	10.6	2.6	6	***80.8***	−3.4	10.4	2.8	7.9	***78.9***	−5.1	11.2	2	7.7	***79.1***	−5.7	11.1	2.1	11.6	***75.2***	−9.5
	C. plumbeus	23.9	10.9	1	64.2	9.9	21.0	13.8	0.8	64.5	**13**	23.6	11.1	0.9	64.4	10.2	21.7	13.1	0.8	64.4	**12.3**
	T. obesus	15.4	12.6	0.9	71.1	**11.7**	14.2	13.8	0.9	71.1	**12.9**	16.8	11.3	0.9	71.1	**10.4**	14.2	13.9	0.8	71.2	**13.1**
6	*C. falciformis*	19.0	3.5	4.3	73.2	−0.8	18.3	4.2	8	69.4	−3.8	18.9	3.6	5.3	72.2	−1.7	17.9	4.6	10	67.5	−5.4
	C. galapagensis	17.6	3.7	5.1	73.6	−1.4	16.5	4.8	9.3	69.4	−4.5	17.5	3.8	6.3	72.5	−2.5	16.0	5.3	11.4	67.3	−6.1
	C. limbatus	38.1	10.5	2.8	48.5	7.7	36.3	12.3	6.5	44.9	5.8	38.3	10.3	3.6	47.8	6.7	35.8	12.8	8.4	43	4.4
	C. longimanus	33.7	10.8	0.9	54.7	9.9	31.3	13.1	0.5	55	**12.6**	33.8	10.7	0.7	54.8	**10**	32.3	12.2	0.6	54.9	**11.6**
	G. cuvier	13.2	6.7	1	***79***	5.7	12.8	7.1	0.8	***79.3***	6.3	13.3	6.6	0.8	***79.2***	5.8	12.1	7.8	0.8	***79.3***	7
	P. glauca	20.0	5.1	8.1	66.8	−3	19.1	6	10.4	64.5	−4.4	20.2	4.9	8.6	66.3	−3.7	18.7	6.4	11.9	63	−5.5

M values in bold italics denote the largest maintained areas. TS values in bold font denote percentages > 10, highlighting the larger shifts (negative and positive) within each RCP scenario.

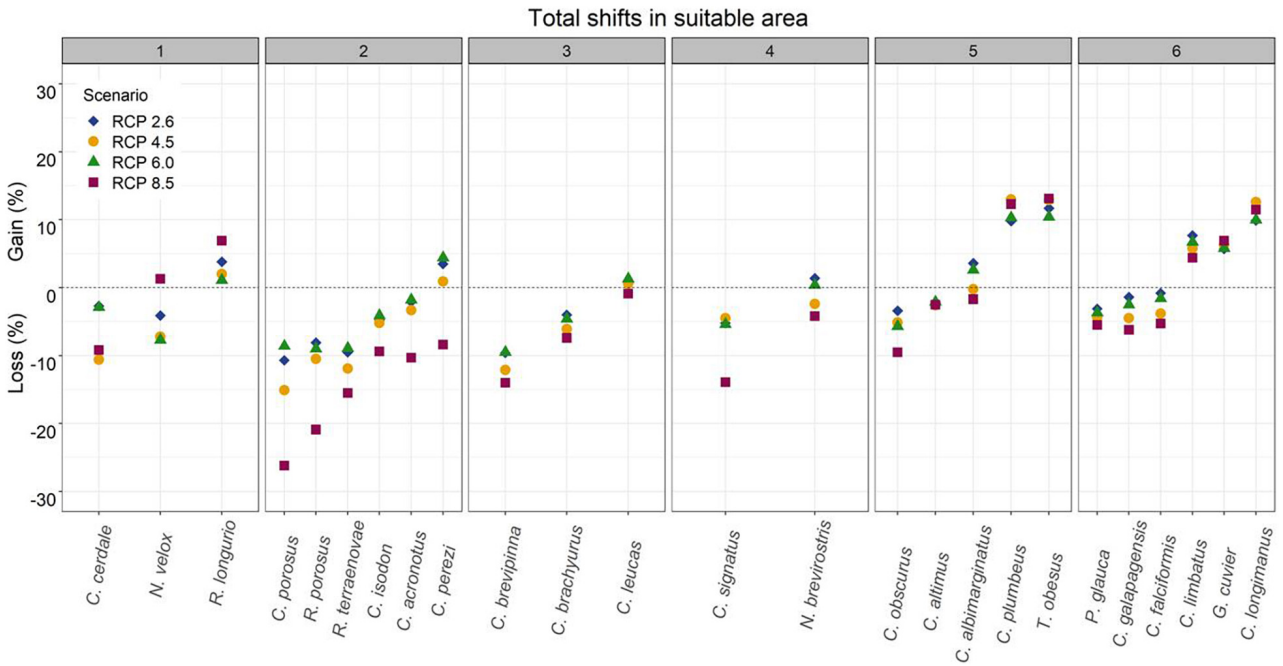

FIGURE 7 | Total shifts in suitable areas for 25 carcharhinid shark species under future climate change scenarios (RCP2.6, RCP4.5, RCP6.0, and RCP8.5) for 2050, divided into groups according to their M area.

variation and gains in suitable area under future distribution projections in the niche models of AquaMaps for 2050[9]. This agrees with our study, in which species of wide distribution presented gains in suitable area, although one of the species of narrow distribution also showed such gains. On the other hand, large marine organisms are constrained not only by their physiological limits but also by their mobility and the accessibility of thermal refuges. This could be the reason why *Carcharhinus limbatus*, a shark with a preference for deeper waters during daylight hours, showed gains in suitable area probably through the requirement of the species to avoid the increased water temperatures (Barnes et al., 2016).

Regarding the losses and gains of suitable area found for carcharhinid sharks, the relationship between species niche properties as indicators of species sensitivity and climate change has been proved (Thuiller et al., 2005), as well as some hypotheses regarding which species will be more sensitive. For example, Rosa et al. (2014) indicated that the more active pelagic sharks would experience greater negative physiological impacts from increasing ocean temperatures than their benthic counterparts. This could be because more active pelagic lifestyles correlate with higher metabolic rates (which are temperature dependent) compared to those of the less active benthic or bathyal species. For instance, we found percentages of suitable area loss for *Rhizoprionodon terraenovae*, an obligate-ram ventilator that must move by swimming at speed or finding a swift current in which to linger in order to continually force water through its gills to breathe (Parsons and Hoffmayer, 2005), and for *Carcharhinus isodon*, which is described as an active shark (Kells and Carpenter, 2011). Nevertheless, *C. plumbeus* is an obligate ram-ventilating apex predator that, in our study, presented gains in suitable area under all RCP scenarios (Crear et al., 2019). In contrast, we found a low percentage of loss in suitable areas presented by the sedentary species *T. obesus* (Whitney et al., 2012). There is also evidence that suggests negative effects on suitable area in species that are restricted to a single habitat throughout their life cycle, such as in the case of sharks strictly associated with coral reefs (Kibria et al., 2017; Heupel et al., 2019). This was consistent with the reef shark *C. perezi* under scenario RCP8.5, but disagrees with that found for the other scenarios and for the other reef shark *T. obesus*, which presented gains under all RCPs. With respect to these gains in suitable area, Heupel et al. (2019) state that there is a need to focus on reef sharks in order to better predict consequences for their populations, given that coral reefs are the habitats most threatened by climate change. It should also be considered that species present complex and dynamic geographical structures that are difficult to model (Coro et al., 2016).

In addition to the effect of climate change due to the physiological and biological characteristics of the species, their shifts in distribution could be related to their biological interactions with other organisms (Gervais et al., 2020), since the first response of species to altered environmental conditions is to adjust their behavior (Wong and Candolin, 2015). One such adjustment is distribution shifts in apex predators such as the large sharks (Heard et al., 2017) because novel combinations of prey species could generate reorganization of species, even

[9]www.aquamaps.org

among the trophic webs (Lurgi et al., 2012; Cameron et al., 2019). It has also been observed that expansion of the distribution range is dominated by dietary generalist species (Evans and Moustakas, 2018; Bartley et al., 2019). In our results, *G. cuvier* and *C. longimanus* (which presented the greatest gain in suitable area) have been defined as generalist predators or species that exploit abundant food resources (Matich et al., 2011). In contrast, the shark *C. leucas* presents more specialized dietary profiles (Matich et al., 2011) and, according to our results, has presented few changes in its distribution.

The occurrence of a shift in species distribution can lead to pervasive and often unexpected consequences for both biological communities and human society (Pecl et al., 2017). A change generated by the distribution or extinction of sharks, as top predators that regulate the populations of other species, could significantly affect the health of seagrass beds, coral reefs, and other vital marine habitats, with a consequently impact on the fishery and ecotourism industries and economy in some regions (Motivarash et al., 2020). Hammerschlag et al. (2019) state that researching ecosystem services and their relationship to top predators is challenging, but is nevertheless important in order to determine how changes associated with climate change in aquatic systems will affect the ecological functions and ecosystem services provided by predators.

Knowledge of the future potential distribution of vulnerable and key species such as sharks could be of value to the design of conservation programs that focus on sites that present the ecological features required by these species in order to face climate change. Niche and distribution modeling offer useful information for incorporation into strategies of environmental management, especially with regard to marine conservation and planning (Marshall et al., 2014). It is therefore important to investigate the impact of climatic change in shark distribution shifts in order to adequately assess their future management in Marine Protected Areas. This is important in terms of the protection of mobile marine species, such as chondrichthyan fishes, among others, especially if such changes require a reassessment of their interactions with fisheries (Carlisle et al., 2019).

METHODOLOGICAL CAVEATS

Predicting and mapping the contractions and expansions of suitable areas for threatened and endangered species is critical for monitoring and restoring their natural populations (De Oliveira et al., 2019). Several studies have modeled the potential future distribution of species; however, there are multiple sources of variation and uncertainty in the geographic predictions and their interpretation that are associated with the methodology (Peterson et al., 2018; Alkishe et al., 2020). To avoid this, in this study, we modeled the potential distribution of the study species based on different sets of environmental variables, a more robust metric of statistical significance such as the partial ROC, and the mobility-oriented parity (MOP) (Peterson et al., 2008; Owens et al., 2013; Cobos et al., 2019). Moreover, although there were many areas of strict extrapolation of risk conditions in the future that show a non-analog environment (MOP results), the truncated response used in our models acts to strongly reduce the combinations of environmental conditions under which models are calibrated in the present (Owens et al., 2013) and projected to future RCP scenarios, in order to reduce uncertainty (Thuiller et al., 2004). As a consequence, this study improves the general understanding of the ecological niche and potential distribution of carcharhinid sharks and estimates their distribution under the reliable climate change scenarios featured in recent literature. According to our evaluation results and expert knowledge on this group of sharks, and by modeling presence-only data, the models obtained are informative and adequately describe the current potential distributions (Cobos et al., 2019), which indicates their utility in terms of making further projections and predicting shifts in habitat suitability (Warren and Seifert, 2011).

Another caveat is related to the small sample sizes for some species of sharks used to create the niche models. In this regard, Pearson et al. (2007) emphasize that these models should only be interpreted as regions that have environmental conditions similar to those in which the species is known to occur. However, this kind of model created in Maxent has previously generated good results, even with small sample sizes (<10) (Phillips et al., 2006) such as some of those used in our study. The integration of ecologically relevant predictors and variables in a 3-dimensional space (e.g., primary productivity, dissolved oxygen throughout the water column) significantly affects shark distributions with climate change (Deutsch et al., 2015; Feitosa et al., 2020; Vedor et al., 2021). Where this information is available, it could therefore be considered to significantly increase the performance and transferability of the niche models (Regos et al., 2019). However, despite the fact that remotely sensed data has recently become more available, environmental predictors remain limited for the marine environment and therefore probably lack important ecological factors (Werkowska et al., 2016). This is a general problem for marine ecological niche modeling in contrast to 2-dimensional modeling for terrestrial species, since most oceanographic layers are only representative of the uppermost layers of the water column (Whittock et al., 2016; Assis et al., 2017; Melo-Merino et al., 2020). In addition, some studies that model future species distributions recommend the use of other variables, such as dispersal capacity, genetic adaptation, species behavioral plasticity, and biotic interactions (Robinson et al., 2011; Bentlage et al., 2013; Sirois-Delisle and Kerr, 2018; Brodie et al., 2019; Gómez-Ruiz and Lacher, 2019). Certain studies have attempted to solve this problem by using oceanographic variables at multiple depths in the current distribution (Bentlage et al., 2013; Duffy and Chown, 2017) and applying future scenarios evenly throughout the entire water column (Crear et al., 2020). However, these environmental layers are still not available in all areas and under different climate change scenarios and were therefore excluded from this study. Despite this limitation, the environmental variables that were used in this study (temperature, salinity, and current velocity) have been described as important factors that affect current marine habitats and thus future shark distributions (Rosa et al., 2014; Ranintyari et al., 2018; Vedor et al., 2021).

CONCLUSION

Our results show the usefulness of correlative models based on the ecological niche theory in terms of modeling the future potential distribution of carcharhinid sharks through presence records and environmental variables. We conclude that climate change will have important effects on the distribution of carcharhinid sharks by the year 2050, highlighting losses of suitable area for most species. The carcharhinid sharks presented the greatest loss of suitable area under the severe future climate scenario RCP8.5. The shark species with the greatest loss of suitable area was *C. porosus* and the shark with the highest gain in suitable area was *T. obesus*. Species distribution modeling approaches, such as that utilized in this study, represent an attempt to identify changes in the distribution patterns of carcharhinid sharks and can provide basic primary information of potential value to the improvement of decision-making processes in biodiversity conservation. The preservation of sharks as key elements in the present and future is important to the maintenance of ecosystem services of great value to human society, as well as to conserve the natural function of the marine ecosystems.

DATA AVAILABILITY STATEMENT

The original contributions presented in the study are included in the article/Supplementary Material, further inquiries can be directed to the corresponding author/s.

ETHICS STATEMENT

Ethical review and approval was not required for the animal study because we work with databases. At no time do we work with living organisms.

AUTHOR CONTRIBUTIONS

PLD-C, GM-G, CY-A, and XC-C contributed to the conception and design of the study. PLD-C organized the database and performed the statistical analysis. PLD-C and GM-G wrote the drafts of the manuscript. All authors contributed to manuscript revision, read, and approved the submitted version.

FUNDING

This study was supporded by CEMIE-Océano (Mexican Centre for Innovation in Ocean Energy), project FSE-2014-06-249795 financed by CONACYT SENER Sustentabilidad Energética.

ACKNOWLEDGMENTS

We thank the Postgraduate Program in Marine Sciences and Limnology, UNAM, the Mexican National Council of Science and Technology (CONACyT), which granted a fellowship to PLD-C, and the Mexican Centre for Innovation in Ocean Energy (CEMIE-Océano, CONACYT project 249795). We also thank Felipe Galván, Andrés Lira, and the referees for their valuable and careful suggestions that greatly contributed to improving this work. Finally, we would like to express our gratitude to Keith MacMillan for correcting the English style of the manuscript.

SUPPLEMENTARY MATERIAL

The Supplementary Material for this article can be found online at: https://www.frontiersin.org/articles/10.3389/fmars.2021.745501/full#supplementary-material

REFERENCES

Acuña-Marrero, D., Smith, A. N. H., Hammerschlag, N., Hearn, A., Anderson, M. J., Calich, H., et al. (2017). Residency and movement patterns of an apex predatory shark (*Galeocerdo cuvier*) at the Galapagos Marine Reserve. *PLoS One* 12:e0183669. doi: 10.1371/journal.pone.0183669

Alkishe, A., Cobos, M. E., Peterson, A. T., and Samy, A. M. (2020). Recognizing sources of uncertainty in disease vector ecological niche models: an example with the tick. *Rhipicephalus sanguineus* sensu lato. *Perspect. Ecol. Conserv.* 18, 91–102. doi: 10.1016/j.pecon.2020.03.002

Anderson, R. P., Lew, D., and Peterson, A. T. (2003). Evaluating predictive models of species' distributions: criteria for selecting optimal models. *Ecol. Model.* 162, 211–232. doi: 10.1016/S0304-3800(02)00349-6

Assis, J., Tyberghein, L., Bosch, S., Verbruggen, H., Serrao, E. A., and De Clerck, O. (2017). Bio-ORACLE v2.0: extending marine data layers for bioclimatic modelling. *Glob. Ecol. Biogeogr.* 27, 277–284. doi: 10.1111/geb.12693

Báez, J. C., Barbosa, A. M., Pascual, P., Ramos, M. L., and Abascal, F. (2019). Ensemble modeling of the potential distribution of the whale shark in the Atlantic Ocean. *Ecol. Evol.* 10, 175–184. doi: 10.1002/ece3.5884

Bakun, A. (1990). Global climate change and intensification of coastal ocean upwelling. *Science* 247, 198–201. doi: 10.1126/science.247.4939.198

Banks, W. E. (2017). The application of ecological niche modeling methods to archaeological data in order to examine culture-environment relationships and cultural trajectories. *Quaternaire* 28, 271–276. doi: 10.4000/quaternaire.7966

Barnes, C. J., Butcher, P. A., Macbeth, W. G., Mandelman, J. W., Smith, S. D. A., and Peddemors, V. M. (2016). Movements and mortality of two commercially exploited carcharhinid sharks following longline capture and release off eastern Australia. *Endanger. Species Res.* 30, 193–208. doi: 10.3354/esr00730

Bartley, T. J., McCann, K. S., Bieg, C., Cazelles, K., Granados, M., Guzzo, M. M., et al. (2019). Food web rewiring in a changing world. *Nat. Ecol. Evol.* 3, 345–354. doi: 10.5281/zenodo.1158733

Barve, N., Barve, V., Jiménez-Valverde, A., Lira-Noriega, A., Maher, S. P., Peterson, A. T., et al. (2011). The crucial role of the accessible area in ecological niche modeling and species distribution modeling. *Ecol. Model.* 222, 1810–1819. doi: 10.1016/j.ecolmodel.2011.02.011

Bellard, C., Bertelsmeier, C., Leadley, P., Thuiller, W., and Courchamp, F. (2012). Impacts of climate change on the future of biodiversity. *Ecol. Lett.* 15, 365–377. doi: 10.1111/j.1461-0248.2011.01736.x

Bentlage, B., Peterson, A. T., Barve, N., and Cartwright, P. (2013). Plumbing the depths: extending ecological niche modelling and species distribution modelling in three dimensions. *Glob. Ecol. Biogeogr.* 22, 952–961. doi: 10.1111/geb.12049

Birkmanis, C. A., Freer, J. J., Simmons, L. W., Partridge, J. C., and Sequeira, A. M. M. (2020). Future distribution of suitable habitat for pelagic sharks in

Australia under climate change Models. *Front. Mar. Sci.* 7:570. doi: 10.3389/fmars.2020.00570

Bond, M. E., Babcock, E. A., Pikitch, E. K., Abercrombie, D. L., Lamb, N. F., and Chapman, D. D. (2012). Reef sharks exhibit site-fidelity and higher relative abundance in marine reserves on the Mesoamerican Barrier Reef. *PLoS One* 7:e32983. doi: 10.1371/journal.pone.0032983

Booth, D. J., Bond, N., and Macreadie, P. (2011). Detecting range shifts among Australian fishes in response to climate change. *Mar. Freshw. Res.* 62, 1027–1042. doi: 10.1071/mf10270

Brodie, S. J., Thorson, J. T., Carroll, G., Hazen, E. L., Bograd, S. J., Haltuch, M. A., et al. (2019). Trade-offs in covariate selection for species distribution models: a methodological comparison. *Ecography* 42, 1–14. doi: 10.1111/ecog.04707

Bradie, J., and Leung, B. (2017). A quantitative synthesis of the importance of variables used in MaxEnt species distribution models. *J. Biogeogr.* 44, 1344–1361. doi: 10.1111/jbi.12894

Cameron, E. K., Sundqvist, M. K., Keith, S. A., CaraDonna, P. J., Mousing, E. A., Nilsson, K. A., et al. (2019). Uneven global distribution of food web studies under climate change. *Ecosphere* 10:e02645. doi: 10.1002/ecs2.2645

Camhi, M. D., Pikitch, E. K., and Babcock, E. A. (2008). *Sharks of the Open Ocean: Biology, Fisheries and Conservation*. Oxford: Blackwell Publishing, 536.

Carlisle, A. B., Tickler, D., Dale, J. J., Ferretti, F., Curnick, D. J., Chapple, T. K., et al. (2019). Estimating space use of mobile fishes in a large marine protected area with methodological considerations in acoustic array design. *Front. Mar. Sci.* 6:256. doi: 10.3389/fmars.2019.00256

Castro, J. I. (2011). *The Sharks of North America*. Oxford: Oxford University Press, 613.

Chefaoui, R. M., Serebryakova, A., Engelen, A. H., Viard, F., and Serrão, E. (2019). Integrating reproductive phenology in ecological niche models changed the predicted future ranges of a marine invader. *Divers. Distrib.* 25, 688–700. doi: 10.1111/ddi.12910

Cheung, W. W. L., Brodeur, R. D., Okey, T. A., and Pauly, D. (2015). Projecting future changes in distributions of pelagic fish species of Northeast Pacific shelf seas. *Prog. Oceanogr.* 130, 19–31. doi: 10.1016/j.pocean.2014.09.003

Cheung, W. W. L., Meeuwig, J. J., Feng, M., Euan, H., Lam, V. W. H., Langlois, T., et al. (2012). Climate-change induced tropicalisation of marine communities in Western Australia. *Mar. Freshw. Res.* 63, 415–427. doi: 10.1071/MF11205

Cheung, W. W. L., Sarmiento, J. L., Kearney, K., Watson, R., and Pauly, D. (2009). Projecting global marine biodiversity impacts under climate change scenarios. *Fish Fish.* 10, 235–251. doi: 10.1111/j.1467-2979.2008.00315.x

Chin, A., Kyne, P. M., Walkers, T. I., and McAuley, R. B. (2010). An integrated risk assessment for climate change: analysing the vulnerability of sharks and rays on Australia's Great Barrier Reef. *Glob. Change Biol.* 16, 1936–1953. doi: 10.1111/j.1365-2486.2009.02128.x

Cisneros-Montemayor, A. M., Becerril-García, E. E., Berdeja-Zavala, O., and Bocos, A. (2020). Shark ecotourism in Mexico: scientific research, conservation, and contribution to a Blue Economy. *Adv. Mar. Biol.* 85, 71–92. doi: 10.1016/bs.amb.2019.08.003

Cobos, M. E., Peterson, A. T., Barve, N., and Osorio-Olvera, L. (2019). kuenm: an R package for detailed development of ecological niche models using Maxent. *PeerJ* 7:e6281. doi: 10.7717/peerj.6281

Comte, L., and Olden, J. D. (2017). Climatic vulnerability of the world's freshwater and marine fishes. *Nat. Clim. Change* 7, 718–722. doi: 10.1038/NCLIMATE3382

Cooper, J. C., and Soberón, J. (2018). Creating individual accessible area hypotheses improves stacked species distribution models performance. *Glob. Ecol. Biogeogr.* 27, 156–165. doi: 10.1111/geb.12678

Coro, G., Magliozzi, C., Ellenbroek, A., Kaschner, K., and Pagano, P. (2016). Automatic classification of climate change effects on marine species distributions in 2050 using the AquaMaps model. *Environ. Ecol. Stat.* 23, 155–180. doi: 10.1007/s10651-015-0333-8

Cortés, E. (2000). Life history patterns, correlations in sharks. *Rev. Fish. Sci. Aquac.* 8, 299–344. doi: 10.1080/10408340308951115

Costa, G. C., Nogueira, C., Machado, R. B., and Colli, G. R. (2009). Sampling bias and the use of ecological niche modeling in conservation planning: a field evaluation in a biodiversity hotspot. *Biodivers. Conserv.* 19, 883–899. doi: 10.1007/s10531-009-9746-8

Crear, D. P., Brill, R. W., Bushnell, P. G., Latour, R. J., Schwieterman, G. D., Steffen, R. M., et al. (2019). The impacts of warming and hypoxia on the performance of an obligate ram ventilator. *Conserv. Physiol.* 7:coz026. doi: 10.1093/conphys/coz026

Crear, D. P., Latour, R. J., Friedrichs, M. A. M., St-Laurent, P., and Weng, K. C. (2020). Sensitivity of a shark nursery habitat to a changing climate. *Mar. Ecol. Prog. Ser.* 652, 123–136. doi: 10.3354/meps13483

Davidson, L. N. K., and Dulvy, N. K. (2017). Global marine protected areas to prevent extinctions. *Nat. Ecol. Evol.* 1:0040. doi: 10.1038/s41559-016-0040

De Oliveira, U. D. R., Gomes, P. B., Silva Cordeiro, R. T., De Lima, G. V., and Pérez, C. D. (2019). Modeling impacts of climate change on the potential habitat of an endangered Brazilian endemic coral: discussion about deep sea refugia. *PLoS One* 14:e0211171. doi: 10.1371/journal.pone.0211171

Del Moral-Flores, L. F., Morrone, J. J., Alcocer-Durand, J., Espinosa-Pérez, H., and Pérez-Ponce de León, G. (2015). Lista patrón de los tiburones, rayas y quimeras (Chondrichthyes, Elasmobranchii, Holocephali) de México. *Arx. Misc. Zool.* 13, 47–163. doi: 10.32800/amz.2015.13.0047

Deutsch, C., Ferrel, A., Seibel, B., Portner, H. O., and Huey, R. B. (2015). Climate change tightens a metabolic constraint on marine habitats. *Science* 348, 1132–1136. doi: 10.1126/science.aaa1605

Dormann, C. F., Schymanski, S. J., Cabral, J., Chuine, I., Graham, C., Hartig, F., et al. (2012). Correlation and process in species distribution models: bridging a dichotomy. *J. Biogeogr.* 39, 2119–2131. doi: 10.1111/j.1365-2699.2011.02659.x

Drymon, J. M., Carassou, L., Powers, S. P., Grace, M., Dindo, J., and Dzwonkowski, B. (2013). Multiscale analysis of factors that affect the distribution of sharks throughout the northern Gulf of Mexico. *Fish. Bull.* 111, 370–380. doi: 10.7755/FB.111.4.6

Duffy, G. A., and Chown, S. L. (2017). Explicitly integrating a third dimension in marine species distribution modelling. *Mar. Ecol. Prog. Ser.* 564, 1–8. doi: 10.3354/meps12011

Dulvy, N. K., Fowler, S. L., Musick, J. A., Cavanagh, R. D., Kyne, P. M., Harrison, L. R., et al. (2014). Extinction risk and conservation of the world's sharks and rays. *Elife* 3:e00590. doi: 10.7554/eLife.00590

Dulvy, N. K., Rogers, S. I., Jennings, S., Stelzenmüller, V., Dye, S., and Skjoldal, H. R. (2008). Climate change and deepening of the North Sea fish assemblage: a biotic indicator of warming seas. *J. Appl. Ecol.* 45, 1029–1039. doi: 10.1111/j.1365-2664.2008.01488.x

Durack, P. J., Wijffels, S. E., and Matear, R. J. (2012). Ocean salinities reveal strong global water cycle intensification during 1950 to 2000. *Science* 336, 455–458. doi: 10.1126/science.1212222

Dwyer, R. G., Campbell, H. A., Cramp, R. L., Burk, C. L., Micheli-Campbell, M. A., Pillans, R. D., et al. (2019). Niche partitioning between river shark species is driven by seasonal fluctuations in environmental salinity. *Funct. Ecol.* 34, 2170–2185. doi: 10.1111/1365-2435.13626

Elith, J., Kearney, M., and Phillips, S. (2010). The art of modelling range-shifting species. *Methods Ecol. Evol.* 1, 330–342. doi: 10.1111/j.2041-210X.2010.00036.x

Elith, J., Phillips, S. J., Hastie, T., Dudik, M., Chee, Y. E., and Yates, C. J. (2011). A statistical explanation of Maxent for ecologist. *Divers. Distrib.* 17, 43–57. doi: 10.1111/j.1472-4642.2010.00725.x

Evans, M. R., and Moustakas, A. (2018). Plasticity in foraging behaviour as a possible response to climate change. *Ecol. Informatics.* 47, 61–66. doi: 10.1016/j.ecoinf.2017.08.001

Feary, D. A., Pratchett, M. S., Emslie, M. J., Fowler, A. M., Figueira, W. F., and Luiz, O. J. (2013). Latitudinal shifts in coral reef fishes: why some species do and others do not shift. *Fish Fish.* 15, 593–615. doi: 10.1111/faf.12036

Feitosa, L. M., Martins, L. P., Junior, L. A. S., and Lessa, R. P. (2020). Potential distribution and population trends of the smalltail shark *Carcharhinus porosus* inferred from species distribution models and historical catch data. *Aquat. Conserv.* 30, 882–891. doi: 10.1002/aqc.3293

Field, I. C., Meekan, M. G., Buckworth, R. C., and Bradshaw, C. J. A. (2009). Susceptibility of sharks, rays and chimaeras to global extinction. *Adv. Mar. Biol.* 56, 275–363. doi: 10.1016/S0065-2881(09)56004-X

Fogarty, H. E., Buroows, M. T., Pecl, G. T., Robinson, L. M., and Poloczanska, E. S. (2016). Are fish outside their usual ranges early indicators of climate-driven range shifts? *Glob. Change Biol.* 23, 2047–2057. doi: 10.1111/gcb.13635

Genner, M. J., Sims, D. W., Wearmouth, V. J., Southall, E. J., Southward, A. J., Henderson, P. A., et al. (2004). Regional climatic warming drives long-term community changes of British marine fish. *Proc. R. Soc. Lond. B Biol. Sci.* 271, 655–661. doi: 10.1098/rspb.2003.2651

Gervais, C. R., Huveneers, C., Rummer, J. L., and Brown, C. (2020). Population variation in thermal response to climate change reveals differing sensitivity in a benthic shark. *Glob. Change Biol.* 27, 108–120. doi: 10.1111/GCB.15422

Gómez-Ruiz, E. P., and Lacher, T. E. Jr. (2019). Climate change, range shifts, and the disruption of a pollinator-plant complex. *Sci. Rep.* 9:14048. doi: 10.1038/s41598-019-50059-6

Gonzalez-Pestana, A. (2018). *Habitat Suitability of Juvenile Smooth Hammerhead Shark (Sphyrna zygaena) off Northern Peru*. Ph.D. thesis, Douglas, QLD: James Cook University.

Haas, A. R., Fedler, T., and Brooks, E. J. (2017). The contemporary economic value of elasmobranchs in The Bahamas: reaping the rewards of 25 years of stewardship and conservation. *Biol. Conserv.* 207, 55–63. doi: 10.1016/j.biocon.2017.01.007

Hammerschlag, N., Schmitz, O. J., Flecker, A. S., Lafferty, K. D., Sih, A., Atwood, T. B., et al. (2019). Ecosystem function and services of aquatic predators in the Anthropocene. *Trends Ecol. Evol.* 34, 369–383. doi: 10.1016/j.tree.2019.01.005

Hare, J. A., Morrison, W. E., Nelson, M. W., Stachura, M. M., Teeters, E. J., Griffis, R. B., et al. (2016). A vulnerability assessment of fish and invertebrates to climate change on the Northeast U.S. continental shelf. *PLoS One* 11:e0146756. doi: 10.1371/journal.pone.0146756

Harris, R. M. B., Grose, M. R., Lee, G., Bindoff, N. L., Porfirio, L. L., and Fox-Hughes, P. (2014). Climate projections for ecologist. *Wires Clim. Change* 5, 621–637. doi: 10.1002/wcc.291

Hazen, E. L., Jorgensen, S., Rykaczewski, R. R., Bograd, S. J., Foley, D. G., Jonsen, I. D., et al. (2013). Predicted habitat shifts of Pacific top predators in a changing climate. *Nat. Clim. Chang.* 3, 234–238. doi: 10.1038/nclimate1686

Heard, M., Rogers, P. J., Bruce, B. D., Humphries, N. E., and Huveneers, C. (2017). Plasticity in the diel vertical movement of two pelagic predators (*Prionace glauca* and *Alopias vulpinus*) in the southeastern Indian Ocean. *Fish. Oceanogr.* 27, 199–211. doi: 10.1111/fog.12245

Heupel, M. R., Papastamatiou, Y. P., Espinoza, M., Green, M. E., Simpfendorfer, C. A., Hays, G. C., et al. (2019). Reef shark science–key questions and future directions. *Front. Mar. Sci.* 6:12. doi: 10.3389/fmars.2019.00012

Hijmans, R. J. (2012). Cross-validation of species distribution models: removing spatial sorting bias and calibration with a null model. *Ecology* 93, 679–688. doi: 10.2307/23143954

Hijmans, R. J., and Elith, J. (2013). *Dismo: Species Distribution Modeling. R package version 1.3-3*. Available online at https://CRAN.R-project.org/package=dismo. (Accessed 25 September 2019)

Hill, J. K., Griffiths, H. M., and Thomas, C. D. (2011). Climate change and evolutionary adaptations at species' range margins. *Annu. Rev. Entomol.* 56, 143–159. doi: 10.1146/annurev-ento-120709-144746

Hobday, A. J. (2010). Ensemble analysis of the future distribution of large pelagic fishes off Australia. *Prog. Oceanogr.* 86, 291–301. doi: 10.1016/j.pocean.2010.04.023

Hoegh-Guldberg, O., and Bruno, J. F. (2010). The impact of climate change on the world's marine ecosystems. *Science* 328, 1523–1528. doi: 10.1126/science.1189930

IPCC (2000). *Special Report on Emissions Scenarios: A Special Report of Working Group III of the Intergovernmental Panel on Climate Change*, eds N. Nakićenović and R. Swart (Cambridge: University Press).

IPCC (2013). "2013: Technical Summary," in *Climate Change 2013: The Physical Science Basis. Contribution of Working Group I to the Fifth Assessment Report of the Intergovernmental Panel on Climate Change*, eds T. F. Stocker, Q. Dahe, G.-K. Plattner, L. V. Alexander, S. K. Allen, N. L. Bindoff, et al. (Cambridge: Cambridge University Press), 33–115. doi: 10.1017/BO9781107415324.005

IUCN (2020). *The IUCN Red List of Threatened Species*. Available online at: www.iucnredlist.org (accessed September 25, 2020).

Jones, M. C., and Cheung, W. W. L. (2015). Multi-model ensemble projections of climate change effects on global marine biodiversity. *ICES J. Mar. Sci.* 72, 741–752. doi: 10.1093/icesjms/fsu172

Jones, M. C., Dye, S. R., Fernandes, J. A., Frolicher, T. L., Pinnegar, J. K., Warren, R., et al. (2013). Predicting the impact of climate change on threatened species in UK waters. *PLoS One* 8:e54216. doi: 10.1371/journal.pone.0054216

Kells, V. A., and Carpenter, E. (2011). *A Field Guide to Coastal Fishes*. Baltimore, MD: The John Hopkins University Press.

Kibria, G., Haroon, A. K. Y., and Nugegoda, D. (2017). *Climate Change and its Effects on Global Shark Fisheries*. doi: 10.13140/RG.2.2.15363.81441

Lezama-Ochoa, N., Murua, H., Chust, G., Van Loon, E., Ruiz, J., Hall, M., et al. (2016). Present and future potential habitat distribution of *Carcharhinus falciformis* and *Canthidermis maculata* by-catch species in the tropical tuna purse-seine fishery under climate change. *Front. Mar. Sci.* 3:34. doi: 10.3389/fmars.2016.00034

Lurgi, M., Bernat, C. L., and Montoya, J. M. (2012). Novel communities from climate change. *Philos. Trans. R. Soc. B* 367, 2913–2922. doi: 10.1098/rstb.2012.0238

Marshall, C. E., Glegg, G. A., and Howell, K. L. (2014). Species distribution modelling to support marine conservation planning: the next steps. *Mar. Policy* 45, 330–332.

Matich, P., Heithaus, M. R., and Layman, C. A. (2011). Contrasting patterns of individual specialization and trophic coupling in two marine apex predators. *J. Anim. Ecol.* 80, 294–305. doi: 10.1111/j.1365-2656.2010.01753.x

Melo-Merino, S. M., Reyes-Bonilla, H., and Lira-Noriega, A. (2020). Ecological niche models and species distribution models in marine environments: a literature review and spatial analysis of evidence. *Ecol. Model.* 415:108837. doi: 10.1016/j.ecolmodel

Mendoza-González, G., Martínez, M. L., Rojas-Soto, O., Téllez-Valdés, O., and Arias-Del Razo, I. (2016). Priority areas for conservation of beach and dune vegetation of the Mexican Atlantic coast. *J. Nat. Conserv.* 33, 25–34. doi: 10.1016/j.jnc.2016.04.007

Montgomery, D. C., and Peck, E. A. (1992). *Introduction to Linear Regression Analysis*. New York, NY: Wiley.

Morales, N. S., Fernández, I. C., and Baca-González, V. (2017). MaxEnt's parameter configuration and small samples: are we paying attention to recommendations? A systematic review. *PeerJ* 5:e3093. doi: 10.7717/peerj.3093

Motivarash, Y. B., Fofandi, D. C., Dabhi, R. M., Makrani, R. A., and Tanna, P. D. (2020). Importance of sharks in ocean ecosystem. *J. Entomol. Zool. Stud.* 8, 611–613.

Naimi, B., and Araújo, M. B. (2016). sdm: a reproducible and extensible R platform for species distribution modelling. *Ecography* 39, 368–375. doi: 10.1111/ecog.01881

Nakamura, Y., Feary, D. A., Kanda, M., and Yamaoka, K. (2013). Tropical fishes dominate temperate reef fish communities within western Japan. *PLoS One* 8:e81107. doi: 10.1371/journal.pone.0081107

Owens, H. L., Campbell, L. P., Dornak, L. L., Saupe, E. E., Barve, N., Soberón, J., et al. (2013). Constraints on interpretation of ecological niche models by limited environmental ranges on calibration areas. *Ecol. Model.* 263, 10–18. doi: 10.1016/j.ecolmodel.2013.04.011

Pacifici, M., Foden, W. B., Visconti, P., Watson, J. E. M., Butchart, S. H. M., Kovacs, K. M., et al. (2015). Assessing species vulnerability to climate change. *Nat. Clim. Change* 5, 215–224. doi: 10.1038/NCLIMATE2448

Pacoureau, N., Rigby, C. L., Kyne, P. M., Sherley, R. B., Winker, H., Carlson, J. K., et al. (2021). Half a century of global decline in oceanic sharks and rays. *Nature* 589, 567–571. doi: 10.5281/zenodo.4135325

Parmesan, C., and Yohe, G. (2003). A globally coherent fingerprint of climate change impacts across natural systems. *Nature* 421, 37–42. doi: 10.1038/nature01286

Parsons, G. R., and Hoffmayer, E. R. (2005). Seasonal changes in the distribution and relative abundance of the atlantic sharpnose shark *Rhizoprionodon terraenovae* in the North Central Gulf of Mexico. *Copeia* 4, 914–920.

Pearson, G. R., Raxworthy, C. J., Nakamura, M., and Peterson, A. T. (2007). Predicting species distributions from small numbers of occurrence records: a test case using cryptic geckos in Madagascar. *J. Biogeogr.* 34, 102–117. doi: 10.1111/j.1365-2699.2006.01594.x

Pecl, G. T., Araujo, M. B., Bell, J., Blanchard, J., Bonebrake, T. C., Chen, I., et al. (2017). Biodiversity redistribution under climate change: impacts on ecosystems and human well-being. *Science* 355:eaai9214. doi: 10.1126/science.aai9214

Perry, A., Low, P. J., Ellis, J. R., and Reynolds, J. D. (2005). Climate change and distribution shifts in marine fishes. *Science* 308:5730. doi: 10.1126/science.1111322

Peterson, A. T., Papes, M., and Soberón, J. (2008). Rethinking receiver operating characteristic analysis applications in ecological niche modeling. *Ecol. Model.* 213, 63–72. doi: 10.1016/j.ecolmodel.2007.11.008

Peterson, A. T., and Soberón, J. (2012). Species distribution modeling and ecological niche modeling: getting the concepts right. *Nat. Conserv.* 10, 102–107. doi: 10.4322/natcon.2012.019

Peterson, A. T., Sóberon, J., Pearson, R. G., Anderson, R. P., Martínez-Meyer, E., Nakamura, M., et al. (2011). *Ecological Niches and Geographic Distributions*. Princeton, NJ: Princeton University Press.

Peterson, T. A., Cobos, M. E., and Jiménez-García, D. (2018). Major challenges for correlational ecological niche model projections to future climate conditions. *Ann. N. Y. Acad. Sci.* 1429, 66–77. doi: 10.1111/nyas.13873

Phillips, S. J., Anderson, R. P., and Schapire, R. E. (2006). Maximum entropy modeling of species geographic distributions. *Ecol. Model.* 190, 231–259. doi: 10.1016/j.ecolmodel.2005.03.026

Poloczanska, E. S., Brown, C. J., Sydeman, W. J., Kiessling, W., Schoeman, D. S., Moore, P. J., et al. (2013). Global imprint of climate change on marine life. *Nat. Clim. Change* 3, 919–925. doi: 10.1038/nclimate1958

Pradhan, P. (2016). Strengthening MaxEnt modelling through screening of redundant explanatory bioclimatic variables with variance inflation factor analysis. *Researcher* 8, 29–34. doi: 10.7537/marsrsj080516.05

Qiao, H., Feng, X., Escobar, L. E., Peterson, A. T., Soberón, J., Zhu, G., et al. (2019). An evaluation of transferability of ecological niche models. *Ecography* 42, 521–534.

R Core Team (2018). *R: A Language and Environment for Statistical Computing*. Vienna: The R Foundation for Statistical Computing.

Radosavljevic, A., and Anderson, R. P. (2014). Making better MAXENT models of species distributions: complexity, overfitting and evaluation. *J. Biogeogr.* 41, 629–643. doi: 10.1111/jbi.12227

Ranintyari, M., Sunarto, M., Syamsuddin, L., and Astuty, S. (2018). Effects of oceanographic factors on spatial distribution of whale shark in Cendrawasih Bay National Park, West Papua. *Environ. Earth Sci.* 149:012050. doi: 10.1088/1755-1315/149/1/012050

Regos, A., Gangne, L., Alcaraz-Segura, D., Honrado, J. P., and Domínguez, J. (2019). Effects of species traits and environmental predictors on performance and transferability of ecological niche models. *Sci. Rep.* 9:4221. doi: 10.1038/s41598-019-40766-5

Robinson, L. M., Elith, J., Hobday, A. J., Pearson, R. G., Kendall, B. E., Possingham, H. P., et al. (2011). Pushing the limits in marine species distribution modelling: lessons from the land present challenges and opportunities. *Glob. Ecol. Biogeogr.* 20, 789–802.

Robinson, L. M., Hobday, A. J., Possingham, H. P., and Richardson, A. J. (2015). Trailing edges projected to move faster than leading edges for large pelagic fish habitats under climate change. *Deep. Res. Part II Top. Stud. Oceanogr.* 113, 225–234. doi: 10.1016/j.dsr2.2014.04.007

Rodriguez-Dominguez, A., Connell, S. D., Leung, J. Y. S., and Nagelkerken, I. (2019). Adaptive responses of fishes to climate change: feedback between physiology and behaviour. *Sci. Total Environ.* 692, 1242–1249. doi: 10.1016/j.scitotenv.2019.07.226

Rosa, R., Baptista, M., Lopes, V. M., Pegado, M. R., Paula, R., Trübenbach, K., et al. (2014). Early-life exposure to climate change impairs tropical shark survival. *Proc. R. Soc. Lond. B Biol. Sci.* 281:1738. doi: 10.1098/rspb.2014.1738

Saldaña-Ruiz, L. E., García-Rodríguez, E., Pérez-Jiménez, J. C., Tovar-Ávila, J., and Rivera-Téllez, E. (2019). Biodiversity and conservation of sharks in Pacific Mexico. *Adv. Mar. Biol.* 83, 11–60. doi: 10.1016/bs.amb.2019.08.001

Santana-Morales, O., Cartamil, D., Sosa-Nishizaki, O., Zertuche-Chanes, R., Hernández-Gutiérrez, E., and Graham, J. B. (2020). Artisanal elasmobranch fisheries of northwestern Baja California, Mexico. *Cienc. Mar.* 46, 1–18. doi: 10.7773/cm.v46i1.3023

Schlaff, A. M., Heupel, M. R., and Simpfendorfer, C. A. (2014). Influence of environmental factors on shark and ray movement, behaviour and habitat use: a review. *Rev. Fish Biol. Fish.* 24, 1089–1103. doi: 10.1007/s11160-014-9364-8

Sguotti, C., Lynam, C. P., García-Barreras, B., Ellis, J. R., and Engelhard, G. H. (2016). Distribution of skates and sharks in the North Sea: 112 years of change. *Glob. Change Biol.* 22, 2729–2743. doi: 10.1111/gcb.13316

Simões, M., Romero-Alvarez, D., Nuñez-Penichet, C., Jiménez, L., and Cobos, M. E. (2020). General theory and good practices in ecological niche modeling: a basic guide. *Biodivers. Informatics* 15, 67–68. doi: 10.17161/bi.v15i2.13376

Sirois-Delisle, C., and Kerr, J. T. (2018). Climate change-driven range losses among bumblebee species are poised to accelerate. *Sci. Rep.* 8:14464. doi: 10.1038/s41598-018-32665-y

Soberón, J., and Nakamura, M. (2009). Niches and distributional areas: concepts, methods, and assumptions. *Proc. Natl. Acad. Sci. U.S.A.* 106, 19644–19650.

Sosa-Nishizaki, O., García-Rodríguez, E., Morales-Portillo, C., Pérez-Jiménez, J. C., Rodríguez-Medrano, M. C., Bizzarro, J. J., et al. (2020). Fisheries interactions and the challenges for target and nontargeted take on shark conservation in the Mexican Pacific. *Adv. Mar. Biol.* 85, 39–69. doi: 10.1016/bs.amb.2020.03.001

Spaet, J. L. Y., Lam, C. H., Braun, C. D., and Berumen, M. L. (2017). Extensive use of mesopelagic waters by a Scalloped hammerhead shark (*Sphyrna lewini*) in the Red Sea. *Anim. Biotelemetry* 5:20. doi: 10.1186/s40317-017-0135-x

Spalding, M. D., Fox, H. E., Allen, G. R., Davidson, N., Ferdaña, Z. A., Finlayson, M., et al. (2007). Marine ecoregions of the world: a bioregionalization of coastal and shelf areas. *Bioscience* 57, 573–583. doi: 10.1641/B570707

Speed, C. W., Field, I. C., Meekan, M. G., and Bradshaw, C. J. A. (2010). Complexities of coastal shark movements and their implications for management. *Mar. Ecol. Prog. Ser.* 408, 275–293. doi: 10.3354/meps08581

Sun, C. (2018). *US DOC/NOAA/NESDIS National Centers for Environmental Information NCEI Standard Product: Global Ocean Currents Database (GOCD)*. Silver Spring, MD: NOAA.

Sunday, J. M., Pecl, G. T., Frusher, S., Hobday, A. J., Hill, N., Holbrook, N. J., et al. (2015). Species traits and climate velocity explain geographic range shifts in an ocean-warming hotspot. *Ecol. Lett.* 18, 944–953. doi: 10.1111/ele.12474

Tanaka, K. R., Van Houtan, K. S., Mailander, E., Dias, B. S., Galginaitis, C., O'Sullivan, J., et al. (2021). North Pacific warming shifts the juvenile range of a marine apex predator. *Sci. Rep.* 11:3373. doi: 10.1038/s41598-021-82424-9

Thuiller, W., Brotons, L., Araújo, M. B., and Lavorel, S. (2004). Effects of restricting environmental range of data to project current and future species distributions. *Ecography* 27, 165–172. doi: 10.1111/j.0906-7590.2004.03673.x

Thuiller, W., Lavorel, S., and Araújo, M. B. (2005). Niche properties and geographical extent as predictors of species sensitivity to climate change. *Glob. Ecol. Biogeogr.* 14, 347–357. doi: 10.1111/j.1466-822x.2005.00162.x

Tittensor, D. P., Mora, C., Jetz, W., Lotze, H. K., Ricard, D., Vanden, B. E., et al. (2010). Global patterns and predictors of marine biodiversity across taxa. *Nature* 466, 1098–1101. doi: 10.1038/nature09329

Tyberghein, L., Verbruggen, H., Pauly, K., Troupin, C., Mineur, F., and Clerck, O. D. (2011). Bio-ORACLE: a global environmental dataset for marine species. *Glob. Ecol. Biogeogr.* 21, 272–281. doi: 10.1111/j.1466-8238.2011.00656.x

Vedor, M., Queiroz, N., Mucientes, G., Couto, A., Da Costa, I., Dos Santos, A., et al. (2021). Climate-driven deoxygenation elevates fishing vulnerability for the ocean's widest ranging shak. *Elife* 10:e62508. doi: 10.7554/eLife.62508

Voda, R., Dapporto, L., Dinca, V., and Vila, R. (2015). Why do cryptic species tend not to co-occur? A Case study on two cryptic pairs of butterflies. *PLoS One* 10:e0117802. doi: 10.1371/journal.pone.0117802

Wabnitz, C. C. C., Lam, V. W. Y., Reygondeau, G., The, L. C. L., Al-Abdulrazzak, D., Khalfallah, M., et al. (2018). Climate change impacts on marine biodiversity, fisheries and society in the Arabian Gulf. *PLoS One* 13:e0194537. doi: 10.5061/dryad.mt588k1

Warren, D. L., and Seifert, S. N. (2011). Ecological niche modeling in Maxent: the importance of model complexity and the performance of model selection criteria. *Ecol. Appl.* 21, 335–342. doi: 10.1890/10-1171.1

Werkowska, W., Márquez, A. L., Real, R., and Acevedo, P. (2016). A practical overview of transferability in species distribution modelling. *Environ. Rev.* 25, 127–133. doi: 10.1139/er-2016-0045

Wessel, P., and Smith, W. H. F. (1996). A global, self-consistent, hierarchical, high-resolution shoreline database. *J. Geophys. Res. Atmos.* 101, 8741–8743. doi: 10.1029/96JB00104

Wheeler, C. R., Rummer, J. L., Bailey, B., Lockwood, J., Vance, S., and Mandelman, J. W. (2021). Future thermal regimes for epaulette sharks (*Hemiscyllium ocellatum*): growth and metabolic performance cease to be optimal. *Sci. Rep.* 11:454. doi: 10.1038/s41598-020-79953-0

Whitney, N. M., Robbins, W. D., Schultz, J. K., Bowen, B. W., and Holland, K. N. (2012). Oceanic dispersal in a sedentary reef shark (*Triaenodon obesus*): genetic evidence for extensive connectivity without a pelagic larval stage. *J. Biogeogr.* 39, 1144–1156. doi: 10.1111/j.1365-2699.2011.02660.x

Whittock, P. A., Pendoley, K. L., and Hamann, M. (2016). Using habitat suitability models in an industrial setting: the case for internesting flatback turtles. *Ecosphere* 7, 1–19. doi: 10.1002/ecs2.1551

Wiens, J. A., Stralberg, D., Jongsomjit, D., Howell, C. A., and Snyder, M. A. (2009). Niches, models, and climate change: assessing the assumptions and uncertainties. *Proc. Natl. Acad. Sci. U.S.A.* 106, 19729–19736. doi: 10.1073/pnas.0901639106

Wilkening, J., Pearson-Prestera, W., Mungi, N. A., and Bhattacharyya, S. (2019). Endangered species management and climate change: when habitat conservation becomes a moving target. *Wildl. Soc. Bull.* 43, 11–20. doi: 10.1002/wsb.944

Wong, B. B. M., and Candolin, U. (2015). Behavioral responses to changing environments. *Behav. Ecol.* 26, 665–673. doi: 10.1093/beheco/aru183

Worm, B., and Tittensor, D. P. (2011). Range contraction in large pelagic predators. *Proc. Natl. Acad. Sci. U.S.A.* 108, 11942–11947. doi: 10.1073/pnas.1102353108

Yates, P. M., Heupel, M. R., Tobin, A. J., and Simpfendorfer, C. A. (2015). Ecological drivers of shark distributions along a tropical coastline. *PLoS One* 10:e0121346. doi: 10.1371/journal.pone.0121346

Conflict of Interest: The authors declare that the research was conducted in the absence of any commercial or financial relationships that could be construed as a potential conflict of interest.

Publisher's Note: All claims expressed in this article are solely those of the authors and do not necessarily represent those of their affiliated organizations, or those of the publisher, the editors and the reviewers. Any product that may be evaluated in this article, or claim that may be made by its manufacturer, is not guaranteed or endorsed by the publisher.

frontiers in Marine Science

ORIGINAL RESEARCH
published: 22 March 2022
doi: 10.3389/fmars.2022.837259

The Risk of Multiple Anthropogenic and Climate Change Threats Must Be Considered for Continental Scale Conservation and Management of Seagrass Habitat

Kathryn McMahon[1], Kieryn Kilminster[2,3], Robert Canto[4], Chris Roelfsema[4], Mitchell Lyons[4,5], Gary A. Kendrick[6], Michelle Waycott[7,8] and James Udy[9]*

[1] Centre for Marine Ecosystems Research, School of Science, Edith Cowan University, Joondalup, WA, Australia, [2] Department of Water and Environmental Regulation, Government of Western Australia, Joondalup, WA, Australia, [3] School of Biological Sciences, University of Western Australia, Perth, WA, Australia, [4] Remote Sensing Research Centre, School of Earth and Environmental Sciences, The University of Queensland, Brisbane, QLD, Australia, [5] Centre for Ecosystem Science, School of Biological, Earth and Environmental Sciences, University of New South Wales, Sydney, NSW, Australia, [6] School of Biological Sciences, Oceans Institute, The University of Western Australia, Crawley, WA, Australia, [7] School of Biological Sciences, The University of Adelaide, Adelaide, SA, Australia, [8] Botanic Gardens and State Herbarium, Government of South Australia, Adelaide, SA, Australia, [9] School of Biology and Environmental Science, Queensland University of Technology, Brisbane, QLD, Australia

OPEN ACCESS

Edited by:
Valeria Chávez, National Autonomous University of Mexico, Mexico

Reviewed by:
W. Judson Kenworthy, Independent Researcher, Beaufort, NC, United States
Patricia González-Díaz, University of Havana, Cuba

****Correspondence:***
Kathryn McMahon
k.mcmahon@ecu.edu.au

Specialty section:
This article was submitted to Coastal Ocean Processes, a section of the journal Frontiers in Marine Science

Received: *16 December 2021*
Accepted: *02 February 2022*
Published: *22 March 2022*

Citation:
McMahon K, Kilminster K, Canto R, Roelfsema C, Lyons M, Kendrick GA, Waycott M and Udy J (2022) The Risk of Multiple Anthropogenic and Climate Change Threats Must Be Considered for Continental Scale Conservation and Management of Seagrass Habitat. Front. Mar. Sci. 9:837259. doi: 10.3389/fmars.2022.837259

Globally marine-terrestrial interfaces are highly impacted due to a range of human pressures. Seagrass habitats exist in the shallow marine waters of this interface, have significant values and are impacted by a range of pressures. Cumulative risk analysis is widely used to identify risk from multiple threats and assist in prioritizing management actions. This study conducted a cumulative risk analysis of seagrass habitat associated with the Australian continent to support management actions. We developed a spatially explicit risk model based on a database of threats to coastal aquatic habitat in Australia, spanning 35,000 km of coastline. Risk hotspots were identified using the model and reducing the risk of nutrient and sediment pollution for seagrass habitat was assessed. Incorporating future threats greatly altered the spatial-distribution of risk. High risk from multiple current threats was identified throughout all bioregions, but high risk from climate change alone manifested in only two. Improving management of nutrient and sediment loads, a common approach to conserve seagrass habitat did reduce risk, but only in temperate regions, highlighting the danger of focusing management on a single strategy. Monitoring, management and conservation actions from a national and regional perspective can be guided by these outputs.

Keywords: coastal habitat, seagrass, risk assessment, climate change, management

INTRODUCTION

Spatially-explicit risk assessment is an important tool to identify and manage habitats at a range of spatial scales from local catchments to the globe (Grech et al., 2011; Halpern et al., 2015; Turschwell et al., 2021). This requires explicit knowledge of both the focal habitat and the threats, at the same spatial scale. As the spatial extent of the focal area reduces (e.g., a region to bay), a spatially explicit approach becomes more feasible as appropriate data-sets are more readily available

(Grech et al., 2011). Increasing the size of the focal area (e.g., region to bioregion or nation) becomes challenging due to knowledge gaps relating to habitats and threats and mismatches in the spatial extent, temporal overlap and types of data (Specht et al., 2015). Broadscale assessments are possible through applying an explicit range of assumptions (Halpern and Fujita, 2013).

Coastal habitats provide valuable ecosystem services (Barbier et al., 2011) but are under increasing pressure, particularly as climate change manifests (Halpern et al., 2015). Marine spatial planning is an emerging discipline to address the piecemeal governance of these often multi-jurisdictional environments, a factor believed to have contributed to declining health of marine ecosystems worldwide (Foley et al., 2013). Spatially-explicit risk assessment at appropriate scales to complement policy, such as at the state or national level could significantly contribute to improved conservation of coastal habitats. For marine habitats, Halpern et al. (2015) provided a global assessment, while Grech et al. (2011) demonstrated the applicability of the approach in the Great Barrier Reef region, part of a state. We argue that evaluating risk at a national level is critical for both marine spatial planning and the allocation of national environmental management resources. It can also provide insight for the focus of management practices which are often at much smaller scales such as local government areas or states, while also placing it in the context of risk to climate change pressures which require management at a global scale. This national approach can also feed into blue-carbon policy and actions (Commonwealth of Australia, 2019) and contribute to international sustainable development goals for oceans where currently national environmental accounts are being developed to assess the extent, condition and threats to key ecosystems including seagrass to actively inform decision-making[1].

Seagrasses grow around the globe in nearshore coastal habitats, are one of the most highly valued ecosystems (Barbier et al., 2011) and are sensitive to anthropogenic pressures (Waycott et al., 2009; Turschwell et al., 2021). Despite increased management, research and monitoring, in many areas they continue to decline (Dunic et al., 2021). Terrestrial activities combined with runoff threaten seagrasses, as well as physical disturbance (e.g., dredging, trawling, and accidents at sea) and climate change (e.g., increased temperature and sea level rise). Globally, urban, agricultural and industrial runoff, coastal development and dredging are considered to be the greatest threat to seagrasses (Grech et al., 2012) and recent global trajectory analysis has shown poor water quality and destructive fishing practices are the best predictors of seagrass decline (Dunic et al., 2021).

The goal of our study is to perform a spatially-explicit risk assessment of current and future threats to seagrass ecosystems across the Australian continent, incorporating states and bioregions. To achieve this, three objectives were set: (1) to create the first national seagrass map; (2) generate relevant national threat maps and assign risk from these threats; (3) perform a spatially explicit cumulative risk assessment with the map and risk layers. Adopting a national approach enables risk to seagrass habitats to be presented at a spatial scale that is beyond the experience of most stakeholders. We suggest, as Landis (2003) proposed, that operating at these broad scales for risk assessment will allow informed management and conservation decisions. Resources and effort can be focused to mitigate risk to seagrass-dominated coastal habitats and inform where further targeted studies are of most benefit.

[1]https://eea.environment.gov.au/accounts/ocean-accounts

MATERIALS AND METHODS

The approach for the spatially explicit cumulative risk assessment is summarized in **Figure 1** and followed the approach of Halpern et al. (2015). This involved creating a seagrass habitat map in coastal waters of Australia (**Figure 2A**) and identifying and developing spatially explicit risk maps of threats to seagrass (**Table 1**). All layers were standardized to a 10 km × 10 km grid size, the minimum size available across all layers. The cumulative risk assessment was conducted in the online open source InVEST Habitat Risk Assessment Model (Sharp et al., 2015). Validation of the outputs (individual threat layers and cumulative risk layers) was conducted by surveying 42 seagrass experts. Scenarios were tested to demonstrate how management actions could impact cumulative risk. More details on each step are provided below.

Seagrass Map Generation

A nation-wide seagrass habitat map (10 km × 10 km grid size) was created based on the base-map of Mount and Bricher (2008) where each grid call was categorized as seagrass present or absent. Additional layers were added to the map: UNEP 2005 Seagrass Distribution Map (Green and Short, 2003) and an expert opinion layer from members of the Australian Centre for Ecological Analysis and Synthesis working group (Kilminster et al., 2015). The generated and freely available maps for each state are available at https://portal.tern.org.au/robert-franklin-c-canto/19365 and all have the acronym ACEAS at the end of the file name (Canto et al., 2014a,b,c,d,e,f,g). Then additional sources were added to this map (QDPI-F, 2009; McKenzie et al., 2014; TropWATER, 2016). The deep water seagrass map (QDPI-F, 2009) was categorized as the probability of seagrass occurrence. All cells with a probability of 25% or above were included. This final map is the maximum observed seagrass extent, as the data sources that generated the map span 1976–2014. Therefore, presence does not imply that seagrass is currently present, but there is the potential for seagrass to be present. In the north of Australia there was paucity of information, and even with the expert knowledge layer, we acknowledge that there may be areas of potential seagrass habitat that have not been identified. Additionally, due to the long timescale of observations, there may be areas that are no longer viable for seagrass habitat due to environmental change.

Threat Layer Generation

We attempted to find Australia wide, spatially explicit (10 km × 10 km grid size) datasets that represented threats to seagrass habitat identified by Grech et al. (2012) based on

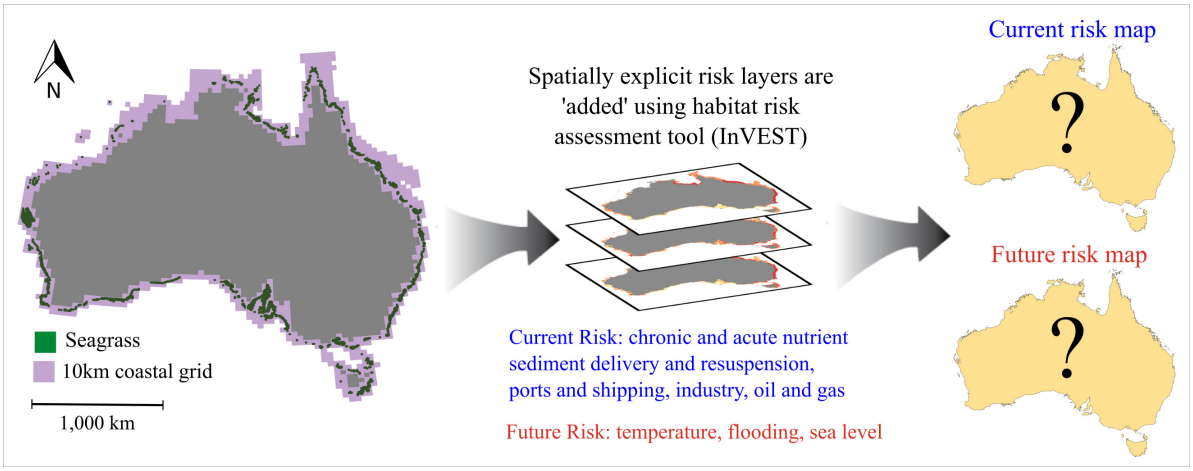

FIGURE 1 | Flow chart to demonstrate the approach for the cumulative risk assessment in this study.

two categories: current anthropogenic and climate-change threats. Data was not available for all threats identified by Grech et al. (2012) at a national scale (**Supplementary Table 1**). Seven data layers were acquired for current anthropogenic threats representing the top four ranked threats globally (Grech et al., 2012) and three climate-change threats were acquired (**Table 1**). The anthropogenic threats include: (1) acute risk of sediment and nutrient inputs; (2) chronic risk of sediment and nutrient inputs; (3) resuspension; (4) ports and dredging; (5) industrial pollution; (6) shipping accidents and (7) oil and gas production accidents. The climate change threats based on predictions in 2070 include: (8) increased temperature; (9) increased rainfall and (10) sea level rise. These are available at https://catalogue.aodn.org.au/geonetwork/srv/eng/catalog.search#/metadata/0419a746-ddc1-44d2-86e7-e5c402473956?uuid=0419a746-ddc1-44d2-86e7-e5c402473956 (Canto et al., 2016). Due to the data types available at the national scale sometimes multiple inputs were required to generate each threat layer (see **Table 1**).

Risk Assignment – Exposure and Magnitude

To assign the risk for each threat layer, the standard approach of Kaplan and Garrick (1981) was followed where risk is calculated based on the likelihood defined by exposure and magnitude, with the consequence defined as the vulnerability of seagrass habitat to that threat. Exposure was based on the spatial co-location of the seagrass grids and threat layers. Magnitude of the threat was based on the intensity of threat in that cell categorized into: no risk = no exposure to threat, Low, Moderate or High likelihood following the approaches of Sharp et al. (2015) (**Table 1**). We used two main approaches to assign a Low, Moderate and High likelihood of risk. For Port infrastructure and dredging, Shipping accidents and Oil and gas well accidents, the approach was simple, if it was present in a grid cell it was categorized High risk, cells adjacent to High were categorized Moderate, adjacent to moderate categorized as Low and all other cells were categorized as No risk. For all other threats there were quantitative values so the magnitude categories were based on these numbers. However, the quantitative relationship between the magnitude of the threat and seagrass response or condition was unknown for most threats. This uncertainty combined with the following two factors led us to incorporate a standard approach for assuming risk. Firstly, different seagrass species have different tolerances to the threats we assessed (e.g., Lee et al., 2007). Secondly, across Australia there are three bioregions with a unique suite of species (Kilminster et al., 2015) so it is likely that different species and bioregions will have different tolerances. We assumed a similar risk profile over the continental scale and based it on percentiles with grid cells <25th percentile classified as Low, 25–75th as Moderate and >75th High (**Table 1**). This approach was not followed in two of the threat layers, industrial pollution and future risk from sea level rise due to the nature of the data and our understanding of the potential risk. The detailed approach for each threat to define exposure and magnitude is detailed below and the risk map for each threat at the national scale is presented in the **Supplementary Figures 4–13**.

Urban/Agricultural Runoff

This threat was divided into two threat layers: acute sediment and nutrient inputs and chronic sediment and nutrient inputs, as the frequency and magnitude of delivery of nutrients and sediments from rivers into coastal environments is likely to have differential effects on seagrasses. We assumed that continual supply of nutrients or sediment over time would be a chronic risk to seagrasses primarily from smothering and eutrophication, whereas pulsed events would be an acute risk to seagrass primarily due to turbid plumes. Both forms of sediment and nutrient delivery have been demonstrated to have negative effects on seagrass (e.g., Cardoso et al., 2010; Lambert et al., 2021).

Acute Sediment Nutrient Risk

This threat layer was derived by considering the catchment condition moderated by the likelihood of large pulses of flow along river channels as well as the total volume of the flow.

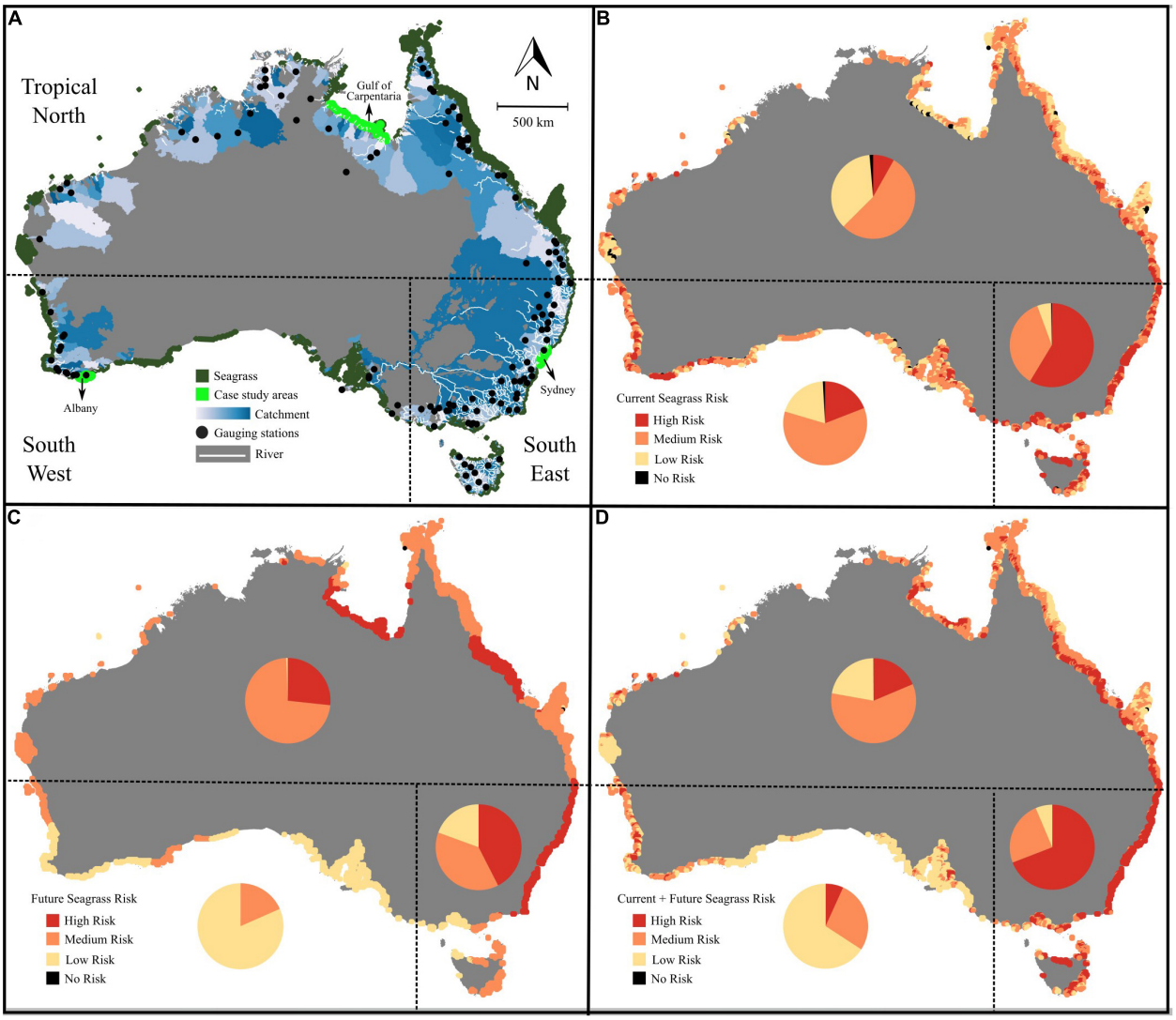

FIGURE 2 | Australia-wide map showing three seagrass bioregions with **(A)** seagrass habitat, major rivers, size of catchments and case study areas of 30 pixels (as seagrass habitat generally forms a narrow band along the coast it has been expanded to make it visible at this scale), **(B)** cumulative current risk, **(C)** cumulative future risk, and **(D)** current and future risk combined. Pie charts in each bioregion show the proportion of cells with high, moderate or low cumulative risk. Seagrass in the south-east bioregion has higher proportion of high-risk in all scenarios.

Specifically, the disturbance of the catchment (as identified in the National Estuary Audit 2000, n = 974 estuaries[2]) was used to describe catchment condition. As sediment and nutrient loads are strongly linked to catchment clearing and land use, we assumed that catchments that were near pristine and largely unmodified would pose a low risk to seagrasses in terms of sediment and nutrient loads. Similarly, the highest risk would be from catchments which are extensively modified, with a moderate risk from those moderately modified.

We considered that estuaries receiving very pulsed streamflow were more susceptible to acute nutrient and sediment loads. To determine the pulse regime, we compiled streamflow data from the Australian Bureau of Meteorology supplemented by the Western Australian Department of Water Data[3,4] () which described the daily flows from the period 1990–1999 from 241 stream gauging stations Australia-wide. Gauging stations within 250 km of the coast were 'matched' to the nearest point on the Australian coastline linked to the appropriate waterway, and estuaries matched with their nearest streamflow. We then calculated a pulse metric based on the number of days which daily streamflow was greater than 1SD above the mean daily streamflow [determined on ln(ML + 0.01) of daily data for each gauging station]. This is a generic threshold and the choice of 1SD was to capture the majority of the 'above baseline' flows. We then applied the criteria that if the pulse metric was <25th

[2]http://www.ozcoasts.gov.au/search_data/estuary_search.jsp

[3]bom.gov.au

[4]water.wa.gov.au

TABLE 1 | A summary of the threats included in the cumulative risk analysis.

		Risk categorization based on exposure and magnitude of effect			
Current threat	**Variable**	**High**	**Moderate**	**Low**	**None**
(1) Acute risk of sediment and nutrient inputs	(a) Catchment condition	Highly modified	Modified	Pristine/largely unmodified	No river enters cell
	(b) Number days daily stream flow > 1SD above mean daily stream flow	>75th	25–75th	<25th	na
	(c) Buffer: natural log of annual flow (ML)	>75th	25–75th	<25th	na
(2) Chronic risk of sediment and nutrient inputs	Ratio of mean daily flow and monthly variance with catchment condition and buffer described above	>75th	25–75th	<25th	na
(3) Resuspension	Time shields parameter exceeds 0.25 (the threshold to initiate sediment movement) (%)	>75th (>15%)	25–75th (0.9–15%)	<25th (<0.9%)	0%
(4) Ports and dredging	Presence port in cell	Present	Adjacent H	Adjacent M	All other
(5) Industrial pollution	(a) Coastal catchment adjacent coast zoned as industrial land use (% area)	>90th (>10%)	25–90th (2–10%)	<25th (<2%)	0%
	(b) Buffer		Adjacent H	Adjacent M	
(6) Shipping accidents	Presence vessel track in cell	Present	Adjacent H	Adjacent M	All other
(7) Oil and gas production accidents	Presence oil and gas production well in cell	Present	Adjacent H	Adjacent M	All other
Climate-change					
(8) Increased temperature	Predicted sea surface temperature increase for 2070 (A1B scenario)	>75th (3.2°C)	25–75th (2.8–3.2°C)	<25th (2.8°C)	<2.0°C
(9) Increased rainfall	Predicted increase in rainfall in the wet period for 2070 (A1B scenario)	>75th (>100mm)	25–75th (50,100 mm)	<25th (0–50 mm)	<0 mm
(10) Sea level rise	Predicted sea level increase for 2070 (A1B scenario)	>90th >200 mm	40–90th 50–200 mm	0.01–40th 10–50	<0.01th <10 mm

percentile, then streamflow was more constant so acute risk was assumed to be zero. If the pulse metric was within the 25–75th percentile, the acute risk was assumed to be reduced and acute risk greatest for estuaries where the pulse metric >75th percentile. The risk of acute sediment and nutrient delivery for each estuary was determined based on the catchment condition and pulse metric as summarized in **Supplementary Table 2**, where 4 is high risk, 3 moderate risk and 2 low with one indicating no risk. Different risk categories were assigned based on the combination of catchment condition and streamflow. For example, for acute nutrient and sediment delivery, if the catchment condition was pristine or largely unmodified and the pulse metric was <25th percentile indicating that likelihood of pulse events was low, then there was no overall risk from this threat. However, at the other end of the spectrum we assumed that if the pulse metric was >75th percentile, then the likelihood of pulse events was higher and the overall risk to seagrasses would increase as the catchment modification increased (**Supplementary Table 2**). Streamflow data were processed and analyzed in R (R Core Team, 2021), and the code/data used are provided as **Supplementary Material (SX)**.

Once the risk values were generated for each estuary that had been linked to the streamflow data as described above, the spatial extent of the influence of the threat, termed buffer, was considered based on annual streamflow. Areas with higher annual streamflow would have greater sediment and nutrient risks than those which received less annual streamflow. The annual flow data was derived from the same dataset as above and the metric defined as ln(annual flow, ML). Areas receiving streamflow of 20 333 ML/yr or less, were in the lowest 25th percentile, and the spatial extent of impact was considered small. A medium extent of impact was assigned for flow between 20 333 and 181 680 ML/yr (25–75th percentiles) and >181 680 ML/yr was assigned a large extent of impact. The spatial extent was estimated based on both the risk of acute sediment and nutrient risk in the estuary (1–4 above) and the streamflow category (**Supplementary Figure 1**). For estuary discharge points with a low risk of acute nutrient and sediment discharge and a small streamflow there was no buffer, so only the cell adjacent to the estuary discharge point, marked by X in **Supplementary Figure 1** was assigned the risk. For estuary discharge points with a moderate or high risk of sediment and nutrient discharge but a small streamflow, a buffer of 1 10 km × 10 km grid cell was added around the estuary discharge point. As the streamflow increased, we assumed the spatial extent of the area at risk would increase as demonstrated in **Supplementary Figure 1**. The greatest spatial extent was 5 10 km × 10 km grids from the estuary discharge point which is conservative as turbid plumes

TABLE 2 | A comparison of the vulnerability measure for each threat addressed in this study in comparison to other studies that have assessed the vulnerability of threats to seagrass habitat.

Threats assessed		**Vulnerability**	**Vulnerability**	**Threats**	**Vulnerability**	**Consequence**
This study	Grech et al., 2012	Tropical Indo-Pacific	Temperate Southern	Halpern et al., 2008	Global	**rating in this study**
Current risk						
Industrial pollution	Urban/industrial runoff	2.6	2.86	Non-point sources of pollution	1	Moderate
Acute sediment and nutrient loads	Agricultural runoff	2.6	2.86	Nutrient input	1.2	High
Chronic sediment and nutrient loads		2.6	2.86			High
Resuspension		Nd	nd			Moderate
Port infrastructure and dredging	Urban/port infrastructure development	2.5	2.78			Moderate
	Dredging	2.5	2.78			
Shipping accidents	Shipping accidents (e.g., oil spills)	1.87	2.07	Commercial activity	1.9	Low
Oil and gas production accidents		1.87	1.87	Benthic structures	1.6	Low
Future risk	Future risk					
Changes in sea surface temperature	Changes in sea surface temperature	1.9	1.89	Increase temperature	2.1	Moderate
Increases in rainfall	Increase in severity of tropical cyclones	2.21	1.16			Moderate
Sea level rise	Sea level rise	1.5	1.53			Low

during peak flood events have been measured up to 100 km from the coast (Devlin et al., 2001). Also to take into account that the risk from sediment and nutrient delivery would decline with distance from the discharge point due to dilution of sediment and nutrients (Devlin et al., 2001) we modified the risk level of the buffer with distance from the discharge point. The way the modification occurred was dependent on both the acute nutrient and sediment delivery risk level and the volume of the flow. For low acute sediment and nutrient risk there was no change in the risk level in the buffer. For moderate and high acute sediment and nutrient risk the risk declined for all cells adjacent to the discharge point by one risk level. For example with a high acute sediment and nutrient risk, all cells in the buffer dropped to moderate. But under moderate and high sediment and nutrient risk with a high streamflow, this risk was kept for one adjacent cell, and then all other cells in the buffer declined by one risk category (**Supplementary Figure 1**). The risk likelihood output is displayed in **Supplementary Figure 4**.

Chronic Sediment Nutrient Input Risk

The chronic sediment and nutrient input risk was derived following a similar approach as the acute risk, but the flow metric varied. We considered that water bodies which received their streamflow more constantly throughout the year were more susceptible to chronic nutrient and sediment load. To categorise the hydrologic regime, we calculated a hydrologic metric based on the ratio of the mean daily flow and the monthly variance. The rationale was to create a metric that reflected the constancy of the streamflow where lower values indicated a more constant flow over monthly time periods and higher values indicated more patchy flow. This captured a different timescale to acute sediment and nutrient threat. If the hydrologic metric was <25th percentile, then streamflow was more constant so chronic risk assumed to be greater. If hydrologic metric was >75th percentile, streamflow was more patchy, so chronic risk assumed to be reduced. No adjustment was made for estuaries where hydrologic metric was between 25 and 75th percentiles. Once again the final risk in the estuary was estimated based on the catchment condition and the hydrologic metric as summarized in **Supplementary Table 2** and the buffer generated based on the annual flow as described for acute sediment and nutrient risk (**Supplementary Figure 1**). The key difference between the chronic and acute risk metrics is that the acute metric is cumulative across the time period (i.e., it is an absolute value of the number of days for which flow exceeded a threshold) and the chronic metric is a relative value that integrated across the time period to categorize daily streamflow in context of how variable flow is at the monthly scale. The risk likelihood output is displayed in **Supplementary Figure 5**.

Industrial Pollution Risk

The industrial pollution layer was generated from the industrial class cover of the Australian Bureau of Agricultural and Resource Economics and Sciences (ABARES) 2005–2006 land use map derived from an AVHRR satellite image[5]. This industrial pollution layer assumes that with more industrial land use in

[5]https://data.gov.au/data/dataset/a18dbf2b-c0fe-4a26-b39a-e553bf6c39b5

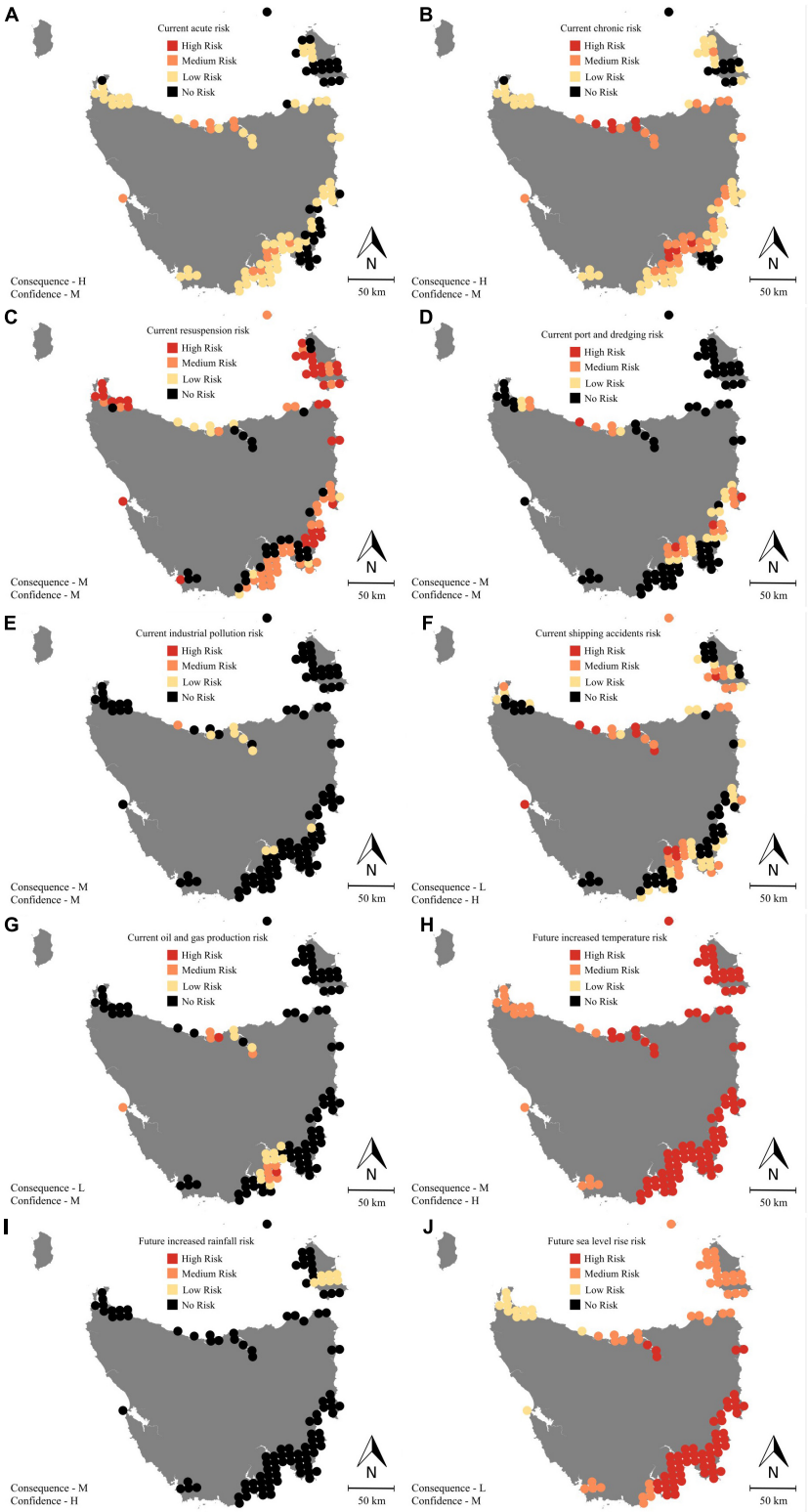

FIGURE 3 | An example of how spatially explicit current **(A–G)** and future **(H–J)** threats were applied to Tasmania (10 km × 10 km grid cells). Only cells where seagrass is present are shown. The risk of each threat was categorized as high, medium, low or no risk if there was no exposure to that threat. Each threat was weighted based on the consequence of exposure to this threat and the confidence in the threat was assessed through a survey with experts.

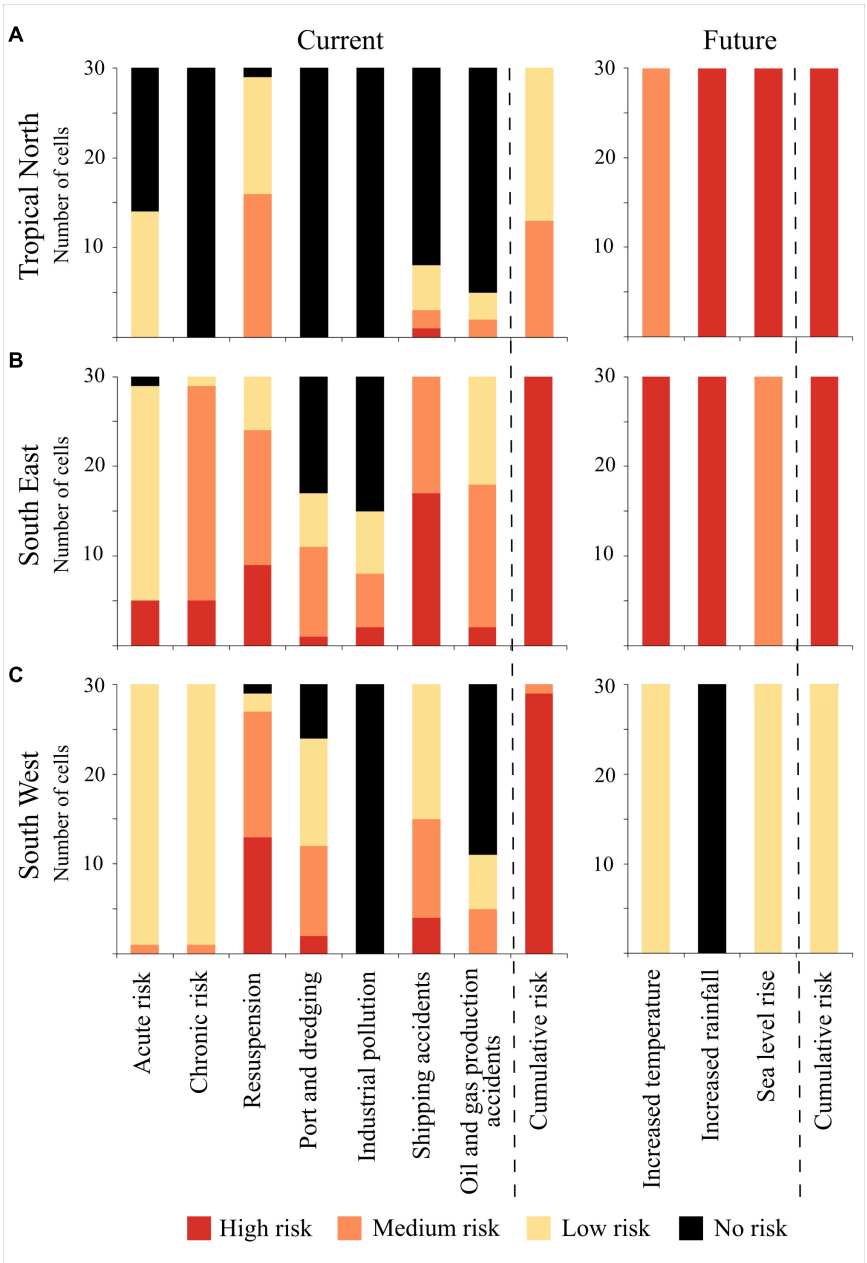

FIGURE 4 | Case study of 30 seagrass cells from each bioregion. **(A)** Tropical North (Gulf of Carpentaria), **(B)** South East (Sydney-Newcastle), and **(C)** South West (Albany) showing the breakdown of individual threats contributing to the current cumulative risk (left) and future cumulative risk (right). A similar cumulative risk (e.g., high) can be derived from different combinations of individual threats.

a 10 km × 10 km grid cell, the greater chance of industrial pollution reaching the marine environment, either through direct runoff, groundwater contamination or atmospheric deposition. In this approach, we only considered the grid cells that were adjacent to the coast, and not those further inland, hence the limitation is that we capture industrial pollution from direct run-off and groundwater contamination, but not from surface run-off from catchments further inland. The percentage of the terrestrial grid cell adjacent to the coast that contained industrial pollution was calculated, based on the number of pixels within each cell (total of 100). The categorisation of this threat was slightly modified compared to the other quantitative measures. If the terrestrial grid cells adjacent to the coastal grid cell contained no industrial land-use, then it was considered to have no exposure to industrial pollution. If less than the 25th percentile (2% of the grid cell was industrial) this was categorized as low likelihood (=low risk). The cut-off for the high risk was set at the 90th percentile (10% of the grid cell was industrial), not the 75th

percentile, as we assumed a higher level of industrial pollution was need to create a high risk. Therefore a moderate likelihood (=medium risk) was assumed to occur between the 25 and 90th percentile (2–10%) and greater than the 90th percentile (>10%) a high likelihood (=high risk). Buffers were created adjacent to any moderate or high likelihood cells to account for transport of industrial pollution in the marine environment. Any marine grid cell adjacent to a high risk cell was considered a moderate risk, and those adjacent to a moderate risk cell were considered a low risk. If any grid cell was allocated more than one risk category, then the highest category was maintained. The risk likelihood output is displayed in **Supplementary Figure 8**.

Sediment Resuspension Risk

Sediment resuspension is related to acute and chronic sediment delivery, but it represents a different pressure to seagrass ecosystems. The risk from resuspension of sediments to seagrass ecosystems is not just due to the delivery of sediment, but the sediment grain size distribution and how this interacts with waves and currents where finer sediments and greater tidal and wave energy would result in higher resuspension. The Geological and Oceanograhic Model of Australia's Continental Shelf (GEOMACS) was used and the dataset "Percentage of the time that the Shields parameter exceeded 0.25 applied to predict the risk from resuspension. The Shields parameter defines the bed shear stress required to initiate sediment movement. When it is >0.25, conditions on the seabed are highly mobile, hence there is more chance of resuspending sediments which can have a negative impact on seagrasses due to reductions in light.

We assumed that with a greater percentage of time above the Shields parameter of 0.25 there would be a greater risk due to sediment resuspension. No quantitative relationship is known for the percentage of the time the shields parameter is above 0.25 and seagrass condition so the approach of assigning a low risk below the 25th percentile (0.8% of the time), a high risk above the 75th percentile (15.8% of the time) and a moderate risk between the two. There was no exposure and hence no risk to seagrass habitat from resuspension when the Shields parameter did not exceeded 0.25 at any time (Hemer, 2006; Hughes et al., 2010; Harris and Hughes, 2012). The risk likelihood output is displayed in **Supplementary Figure 6**.

Port Infrastructure and Dredging Risk

The threat to seagrass habitat from port infrastructure and dredging was assessed based on the locations of ports in Australia provided by the Australian Customs & Border Protection Service[6]. We assumed that there was a high risk to seagrass habitat when there was a port located in a grid cell, a moderate risk in cells adjacent to a high cell, and a low risk in cells adjacent to moderate. We considered that there was no exposure to the threat of port infrastructure and development and hence no risk in all other grid cells. The risk likelihood output is displayed in **Supplementary Figure 7**.

[6]http://data.gov.au/dataset/australian-ports

Shipping Accidents Risk

The threat to seagrass habitat from shipping accidents was predicted from vessel track history in Australia sourced from the Australian Maritime Safety Authority[7] over the whole 2012 period recorded with a 3 h frequency. We assumed that there was a high risk to seagrass habitat when there was a history of vessels tracking through a grid cell, a moderate risk in cells adjacent to a high cell, and a low risk in cells adjacent to moderate adjacent cells. We considered that there was no exposure to the threat of shipping accidents and hence no risk in all other grid cells. The risk likelihood output is displayed in **Supplementary Figure 9**.

Oil and Gas Accidents Risk

The threat to seagrass habitat from oil and gas accidents was predicted from the location of oil and gas wells in the coastal environment. Gas pipelines were not considered, as this information is restricted. The location of oil and gas production wells was sourced from GeoSciences Australia[8]. We assumed that there was a high risk to seagrass habitat when an oil and gas well was in a grid cell, a moderate risk in cells adjacent to a high cell, and a low risk in cells adjacent to moderate adjacent cells. We assued that there was no exposure and hence no risk in all other grid cells. The risk likelihood output is displayed in **Supplementary Figure 10**.

Increase in Sea Surface Temperature Risk

Different seagrass species have different temperature tolerances (Lee et al., 2007) and in Australia species are distributed across locations that have a broad temperature range (Kilminster et al., 2015). Therefore some locations, such as at the range edge may be more susceptible than other locations (Jordà et al., 2012). To employ a consistent and justifiable assumption for impacts of increased temperature we used published data on short-term responses to increased temperature. This may be an overestimate of the response, as we have no understanding about adaptive capacity to changing temperatures. The majority of studies on the effects of short-term temperature increases to seagrasses have shown negative effects with increases of 2°C or more (Seddon et al., 2000; Waycott et al., 2007; Collier et al., 2011; Moore et al., 2013; Thomson et al., 2015). The OzClim Mk3.5 model 2070 predictions of sea surface temperature were used[9] and the risk assigned using a percentile approach as follow, High > 3.2°C (75th percentile), Moderate 2.8–3.2°C (25th – 75th) and Low < 2.8°C (25th percentile). The predicted temperature always increased by more than 2°C so a no risk category was not assigned. The risk likelihood output is displayed in **Supplementary Figure 11**.

Change in Rainfall Risk

We assumed that a greater rainfall would lead to more sediment and nutrient delivery, more flooding and more low light events that could impact seagrasses (Collier et al., 2012) and hence either more acute or chronic sediment and nutrient risk to seagrasses. The predicted change in rainfall in 2070 dataset by OzClim

[7]https://www.operations.amsa.gov.au/Spatial/DataServices/MapProduct

[8]http://dbforms.ga.gov.au/www/npm.well.search

[9]www.csiro.au/ozclim

TABLE 3 | Comparison of how the percentage of cells under the different current cumulative risk categories changes following a simulated nutrient reduction.

Bioregion	Scenario	Percentage of cells			
		No risk	Low risk	Moderate risk	High risk
South East	Current	0.3	5.3	35.7	58.7
	Nutrient and sediment management	0.3	6.4	44.2	49.1
Tropical North	Current	1.4	36.1	54.4	8.1
	Nutrient and sediment management	1.4	36.1	54.5	8.1
South West	Current	0.9	19.5	60.5	19.1
	Nutrient and sediment management	0.9	19.6	61.4	18.1

High risk is reduced in the south-east bioregion with nutrient reduction, but not in the other two bioregions, indicating other threats are contributing significantly to the cumulative risk.

GFDL-CM2.1 model (see Text Footnote 9) was used and we focused on the period of the year that was considered the wet period, as the OzClim predictions provided predictions based on wet and dry periods. For this threat the standard percentile risk approach was applied. We classified this data as no risk if the rainfall was not predicted to increase, low risk if it increased up to 50 mm per year (<25th percentile), moderate if it increased 50–100 mm and a high risk if it increased more than 100 mm (>75th percentile). The risk likelihood output is displayed in **Supplementary Figure 12**.

Sea Level Rise Risk

An increase in sea level can have a negative effect on seagrasses if the shoreline is hardened and they cannot colonize new habitats, also seagrasses can be lost on the deeper edge if light becomes limiting to growth (Waycott et al., 2007; Saunders et al., 2013). Saunders et al. (2013) modeled the impact of sea level rise on a large embayment in Queensland and found that the area of seagrass declined by 17% with a 1.1 m rise in sea level. Obviously these predictions are location specific but we used these as a guide to categorize the likelihood of the risk. Dataset on the projected departure from global mean (A1B scenario) at 2070 (mm) from 17 model simulations was used[10] to quantify sea level increase. For this threat the standard percentile approach was not used as it did not align well with the predictions of seagrass loss with a 1.1 m rise as a 1 m increase in sea level was equivalent to the 75th percentile and we considered a 17% loss moderate. Therefore the percentile values used were 40th percentile (0.5 m rise) for the low – moderate cutoff, 90th percentile (2.0 m rise) for the moderate to high cutoff. If no increases were predicted, then no risk was assumed, less than 50 mm was low, 50–200 was moderate as this spanned the level predicted by Saunders et al. (2013) to have an impact, and >200 mm a high likelihood. The risk likelihood output is displayed in **Supplementary Figure 13**.

Vulnerability or Consequence of the Threat

The consequence of the threat was based on the vulnerability rating of Grech et al. (2012) and Halpern et al. (2015), incorporating the frequency, functional impact, ability to resist, ability to recover and certainty of the impact of that threat (**Table 2**). Similar but not identical threats were assessed in these studies so to develop the consequence ratings, the threats in each study were grouped into similar categories, the consequence rating ranked, and then the consequence measure grouped into high, moderate and low consequence (**Table 2**).

Spatially Explicit Cumulative Risk Analysis

The cumulative risk assessment was conducted in the online open source InVEST Habitat Risk Assessment Model (Sharp et al., 2015). The final seagrass map was overlayed with the likelihood of each threat layer defined as either 1- no exposure, 2- low, 3- moderate and 4- high likelihood. The consequence layer in Invest was kept the same as the likelihood layer but the consequence of the threat was simulated by replicating the layer. If the consequence was low, one layer was used, moderate, two replicate layers and high, three replicate layers. In InVEST the cumulative risk (R) of multiple threats layers (J) is calculated based on the euclidean distance as

$$R(i) = \sum_{j=1}^{J} R(ij)$$

The euclidean distance provides a conservative, additive approach due to the uncertainty of the response to interactions between threats (Halpern and Fujita, 2013). The cumulative risk output was scaled into four categories, No cumulative risk, <25th percentile low cumulative risk, 25–75th percentile moderate risk and >75th percentile high cumulative risk.

A cumulative risk assessment was conducted for three sets: (1) current threats only (n = 7), (2) climate change threats based on 2,070 predictions (n = 3) and (3) combining current and climate change threats that simulate 2070 scenarios. When combining the current and climate change sets, no changes were made to the current risk assessment, we assumed no changes on the threat and no changes in the vulnerability due to adaptation occurred. Therefore this provides a tool to identify hotspots of risk under current conditions and into the future, helping to prioritize management actions. To demonstrate how risk varies spatially and under these cumulative risk calculations the data was summarized by each bioregion, the South West, South East and Tropical North (**Figure 2**). In addition, an area within bioregion containing 30 10 km × 10 km grid cells was selected

[10]http://www.cmar.csiro.au/sealevel/sl_proj_regional.html

to demonstrate in a higher resolution the spatial variability in current and future threats and cumulative risk.

Validation of Individual Threat Layers and Cumulative Risk Assessment

The outputs from the nation-wide risk assessment for each threat layer (n = 10) and for the cumulative risk layers from two sets, current and climate change based on 2,070, were assessed by 42 seagrass experts at the Australian Marine Science Association Conference in 2015 (**Supplementary Figure 2**). These experts self-selected and had experience working in seagrass research or management from particular regions in Australia and only provided validation data from the areas they had experience in. Two approaches were used: a quantitative assessment to assess how the risk assignment for each threat based on exposure, magnitude and consequence of the threat and the cumulative risk assessment model output deviated from the expert opinion; and a qualitative assessment to measure the confidence of the experts in the same outputs. For each approach, the experts were asked to assess three areas in their region of expertise (**Supplementary Table 3**). The qualitative assessment was carried out first on one grid cell in a particular region, then the experts were shown the model outputs and asked to give a confidence rating across all cells in that region, following the methods of Hoque et al. (2018). For the quantitative assessment experts were asked to provide their opinion of whether it was 0 = no risk, 1 = low risk, 2 = moderate risk and 3 = high risk for each threat input layer and cumulative risk assessment output layer. For the qualitative assessment experts were asked to provide a ranking of 0 = no confidence, 1 = low, 2 = moderate and 3 = high confidence in the information provided.

Testing Management Scenarios

To test how nutrient and sediment management strategies impact the overall cumulative risk under current conditions the risk rating for chronic and acute sediment and nutrient risk were modified and cumulative risk model re-run. Cells with high or moderate risk from nutrient and sediment load were dropped down one risk level, but cells already with low risk remained at low. This data was summarized by bioregion.

RESULTS

Cumulative Risk Assessment

Individual threat layers showed different spatial patterns of risk as demonstrated by the examples from Tasmania (**Figure 3**) and compared to the cumulative risk results (**Figure 2**), reinforcing the value of assessing multiple threats cumulatively (**Supplementary Figures 4–9**). For example, the Tropical North case-study (Gulf of Carpentaria) has very low current risk levels and the South East case-study (Sydney) has much higher current risk levels, yet similar future cumulative risk categories were derived for both of these regions (**Figure 4**). In the Tropical North case-study the high cumulative risk from future climate change threats was driven by the combination of high risk from increased temperature and sea-level rise, whereas in the South East case-study it was driven by the combination of high risk from temperature and increased rainfall (**Figure 4**). This again highlights the need to consider a range of threats for management decision-making and recognizing different regions may require different strategies.

There was much more spatial variation in the cumulative risk of current threats compared to future climate change threats, which were generally consistent across bioregional scales, the scale at which climate operates (**Figure 2**). When combining current and future pressures, some high risk hotspots and low risk 'cold-spots' changed. For example cumulative risk from current threats was lowest in the Tropical North (greatest proportion of low risk, **Figure 2B**), with a cold-spot in the Gulf of Carpentaria. However, when adding the high threat future pressures, this area became moderate to high risk. On the other hand, isolated hotspots of high risk that were distributed along the eastern coast of Australia under current pressures expanded into a widespread band of high risk when combined with future pressures, especially in the South East bioregion and the Great Barrier Reef World Heritage Area (GBRWHA, east coast of Australia in the Tropical North bioregion).

When simulating nutrient and sediment management strategies by reducing the areas with high or moderate risk for chronic and acute sediment risk by one category, cumulative risk in the South East bioregion reduced (**Table 3**). In other bioregions this did not result in the cumulative risk to seagrass habitat being reduced.

Validation of Individual Threat Layers

We generated ten spatially explicit threat layers specific for seagrass habitat across the Australian continent using a range of data sources (**Table 1**). When summarized across all of Australia, experts had the highest confidence in the risk assigned to climate change threats (increased temperature and changes in rainfall) as well as localized shipping accidents. There was a moderate confidence for all other layers (**Supplementary Figure 3**). For the quantitative assessment the experts matched quite closely the model predictions for all climate change threats as well as the risk from resuspension and shipping. For the remaining threats there was a slight overestimate of the model for threats from oil and gas wells, industry and ports and dredging, on average 0.5–0.8 units, with an overestimate of ∼1 category (1.2 units) for threat from sediment and nutrients (**Supplementary Figure 3**). This overestimate was mostly driven by respondents that were experts from Western Australia and Queensland indicating that their perceived threats are higher than model predictions. This is likely because most evidence for seagrass decline historically is due to eutrophication.

DISCUSSION

One of the challenges for environmental management is having information at the appropriate spatial and temporal resolution and extent to aid decision making (Specht et al., 2015). This is very apparent at national levels and across bioregions because

information is disparate and is derived from local stakeholders with different types of information. We have begun to address some of the challenges by developing a set of publicly available, national, spatial threat maps representing ten pressures for seagrass ecosystems along the 35,000 km coastline of the Australian continent. It is a data resource that can be used for future work, adapted to assess other habitats or also be used as a local-scale or nation-wide tool to aid decision making in the face of multiple threats and limited resources (Pressey et al., 2007). In addition, the approach can be applied to other regions around the globe to assess risk to seagrass habitats.

This resource was then used for a spatially explicit cumulative risk analysis based on the ten threat layers, identifying hotspots of high and low risk for coastal seagrass habitat based on the exposure and vulnerability to a range of relevant pressures. This standardized approach provides a tool to enable informed decision making at a national level (Tulloch et al., 2015). Currently the Australian Federal government is developing national environmental accounts for blue-carbon habitats including seagrasses. To do this habitat maps, condition of the habitat and potential threats to these habitats is required and these are assessed over time (see Text Footnote 1). This resource can be used to support these activities. Although, many of the major identified threats to seagrass habitat were sourced (Grech et al., 2012; Turschwell et al., 2021), information at the national scale for some key threats are still missing such as trawling or aquaculture (Turschwell et al., 2021). There is still effort needed to improve the representation of threats at a national level and this aligns with the priority to address the challenges for improving ocean health, where Claudet et al. (2020) indicated more integration of information is needed to support decision-making.

High cumulative risk areas were identified based on exposure to threats from current practices. These were generally associated with population, agricultural and/or industrial centers and were distributed around Australia, although the greatest proportion was in the most densely populated South East bioregion (**Figure 2B**). Globally loss of seagrass habitat has been attributed to deterioration of water quality from increased nutrient and sediment loads (Waycott et al., 2009; Turschwell et al., 2021) so load reduction is a management strategy commonly used to protect seagrass habitat, although not always successful due to the complex nature of the systems (Unsworth et al., 2015). It is a current management focus in all bioregions in Australia (Jackson et al., 2016; Brodie et al., 2017). Interestingly, the high cumulative risk predicted in this study could be reduced somewhat through simulating reductions in nutrient and sediment loads, but only in the South East. In the Tropical North, around the Great Barrier Reef World Heritage Area, reducing nutrients and sediments, did not reduce the cumulative risk from current threats. The environmental protection policy for seagrass habitat in the GBRWHA, part of the Tropical North, focuses on improving water quality and managing the impacts of dredging (Anon., 2015). Grech et al. (2011) also recommended focusing management on agricultural inputs (nutrient and sediments) due to the large catchment areas. However, our analysis indicates that focusing on this alone will not reduce the risk of impact to seagrass habitat. Threats with the greatest individual risks for the Great Barrier Reef example based on our analysis, includes resuspension, ports and shipping as well as risk from increased rainfall (**Supplementary Figures 6**, **7**, **9**, **12**). So reducing sediment loads may contribute somewhat to resuspension risk by reducing the pool of sediments that could be resuspended. But increased risk from rainfall requires global action to reduce the rate of greenhouse gas emissions and the changes in weather patterns. To manage for this scenario actions to increase resilience of seagrass habitats to these cumulative threats combined with interventions to facilitate recovery and or restore habitats is needed.

This study highlighted that when managing habitat based on risk at a national level; taking into account future risk from climate change altered the spatial pattern of risk. The 2,070 model projections used can be considered conservative as climate change effects may manifest at a faster rate than these predictions (IPCC, 2019). Similar to current threats, other climate change threats have also not been included such as heat waves, so further effort is needed to create these threat layers and develop a process to assign risk. Despite this, the incorporation of climate change risk into the future was valuable as it provided further insights to inform management decisions. For example, if high risk to seagrass habitat is predicted mostly from a set of current threats, reducing these specific threats could be the focus for management. But if high risk is predicted mostly from climate change threats then management actions for resilience building, facilitated recovery and restoration would be important to consider. When both current and future threats generate high risk an approach combining both sets of actions is needed. By assessing the cumulative risk from both current practices and future threats, the footprint of high risk increased, particularly in the South East and Tropical North bioregion. For example, in the globally significant GBRWHA, high risk has been identified from current threats in six hot-spots (**Figure 2B**) but when this is combined with threats from climate change (**Figure 2C**), this expands into a much larger, almost continuous band in the central and southern GBRWHA. Our approach re-affirms the importance of managing risk as a cumulative challenge (Grech et al., 2016) and the value of projecting future scenarios to guide where resilience building and restoration actions are most needed.

Cumulative risk assessment does not imply impact or predict response in a habitat. It is used as a tool to identify where multiple threats occur and assists decision-making based on a number of assumptions: that risk of multiple threats is additive; and the vulnerability of the seagrass habitats to these threats is known (Halpern and Fujita, 2013). We know that this is a simplification of the real world as the suite of seagrass species changes across bioregions and different species vary in their life-history strategy influencing their ability to resist and recover from disturbance, hence influencing their vulnerability (Kilminster et al., 2015). This has been highlighted recently where life-history was a strong predictor of the trajectory of seagrass change over time (Turschwell et al., 2021). Assemblage-specific vulnerabilities based on life-history could be integrated into this risk assessment framework, though this is presently limited to

smaller site-specific areas where more detailed habitat mapping is available. This tiered approach from using national maps with predicted extent down to assemblage or species composition at the bioregional level could be used to generate more confidence in predicting risk and prioritizing management actions for local-scale management. To improve confidence, further work is also needed to understand the interaction of these multiple threats to seagrass habitats (e.g., Ontorio et al., 2019).

Priority areas for conservation were identified based on the cumulative risk assessment, as those that had no or low cumulative risk under current conditions and included locations in the Tropical North. However, when climate threats were considered the risk rating of some of these areas increased (e.g., Gulf of Carpentaria) and new areas of low risk were identified (southern coast of the South West bioregion). Some of these locations align with World Heritage Areas and Commonwealth or State managed marine parks (Anon, 2016). We recommend taking action to assess whether management plans are in place to conserve this habitat and if feasible actions are in place to manage the multiple threats by either reducing the risk of the threats or actions to build resilience, facilitate recovery and restore seagrass habitats.

Our analysis has highlighted hotspots of risk which correspond with known areas of seagrass loss (e.g., Kendrick et al., 2002; Bryars and Neverauskas, 2004) but there are areas that were identified as low risk where in recent years seagrass 1,000 km^2 losses have occurred associated with a marine heat-wave event (Thomson et al., 2015; Strydom et al., 2020). This reiterates the need for additional threat layers to incorporate the risk of marine heat-wave events. Our approach is designed as a tool for guiding broad-scale conservation and management action with a range of assumptions, and does not account for rare events in a stochastic model of risk. Areas categorized as low risk should not be considered 'safe', in fact management strategies should be developed for threat mitigation and management, although the approach may vary compared to the high risk areas. By taking a national approach to our risk assessment we enable identification of regions with similar risk profiles where regional evaluations can be refined and a tiered approach as described above, implemented.

Monitoring, management and conservation actions can be focused based on the outputs of this research, such as tailoring monitoring programs to incorporate indicators of known current and future high risk threats and seagrass habitat response and prioritizing management actions locally on threats that have a high risk. For climate-change mitigation planning actions to build resilience, facilitate recovery and restore seagrass habitats could be implemented in areas of high risk from future pressures. By incorporating the cumulative risk outputs with a decision making framework (e.g., Tulloch et al., 2015) investments can be prioritized to management actions from a national perspective and contribute to national environmental accounting which requires assessment of habitat extent, condition and threats to the habitat over time.

DATA AVAILABILITY STATEMENT

The datasets presented in this study can be found in online repositories. The names of the repository/repositories and accession number(s) can be found below: the seagrass map datasets generated for this study can be found in the TERN portal: https://portal.tern.org.au/robert-franklin-c-canto/19365.

The threat layers generated for this study can be found on the AODN portal https://catalogue.aodn.org.au/geonetwork/srv/eng/catalog.search#/metadata/0419a746-ddc1-44d2-86e7-e5c402473956?uuid=0419a746-ddc1-44d2-86e7-e5c402473956.

The streamflow dataset and R code used to calculate the acute and chronic sediment and nutrient risk can be found on Cloudstor: https://cloudstor.aarnet.edu.au/plus/s/bo0toZtMVTtiBSC.

AUTHOR CONTRIBUTIONS

RC and CR led the seagrass map generation. KM, CR, KK, and ML led the threat layer development. RC conducted the spatial rick analysis. CR and KM led the expert validation. KM and KK led the writing. All authors conceived the idea and provided feedback on all stages of the project.

FUNDING

The Australian Centre for Ecological Analysis and Synthesis (ACEAS) was the primary funder catalyzing this work and further support was provided by each authors affiliated institution.

ACKNOWLEDGMENTS

We acknowledge the CSIRO Coastal Carbon Cluster, University of Queensland Remote Sensing Centre and Global Change Institute and Nicholas Murray from Global Ecology Lab, James Cook University for supporting some of RC's contributions. We thank other members from the ACEAS Australian Seagrass Habitats working group for stimulating discussion associated with this work. The ACEAS project was conceived and initially formulated through consultation within the National Estuaries Network (NEN). Feedback through the review process helped to improve this manuscript.

SUPPLEMENTARY MATERIAL

The Supplementary Material for this article can be found online at: https://www.frontiersin.org/articles/10.3389/fmars.2022.837259/full#supplementary-material

REFERENCES

Anon. (2015). *Reef 2050 Long-Term Sustainability Plan*. Australia: Commonwealth of Australia.

Anon. (2016). *Commonwealth Marine Reserves Review*. Australian: Recommended zoning for Australia's nsetwork of Commonwealth marine reserves. Australian Government Department of the Environment and Energy.

Barbier, E. B., Hacker, S. D., Kennedy, C., Koch, E. W., Stier, A. C., and Silliman, B. R. (2011). The value of estuarine and coastal ecosystem services. *Ecol. Monogr.* 81, 169–193.

Brodie, J. E., Lewis, S. E., Collier, C. J., Wooldridge, S., Bainbridge, Z., Waterhouse, J., et al. (2017). Setting ecologically relevant targets for river pollutant loads to meet marine water quality requirements for the great barrier reef, australia: a preliminary methodology and analysis. *Ocean Coast. Man.* 143, 136–147.

Bryars, S., and Neverauskas, V. (2004). Natural recolonisation of seagrasses at a disused sewage sludge outfall. *Aquat. Bot.* 80, 283–289.

Canto, R., Kilminster, K., Lyons, M., Roelfsema, C., and McMahon, K. (2016). Spatially explicit current and future threats to seagrass habitats in Australia. *GeoNetwork Open. Source Data Sharing Portal.* doi: 10.4227/05/58b7902525db5

Canto, R., Udy, J., McMahon, K., Waycott, M., Kilminster, K., Kendrick, G., et al. (2014a). Australia seagrass habitat map. *GeoNetwork Open Source Data Sharing Portal* doi: 10.4227/05/54F7CFDDAB949

Canto, R., Udy, J., McMahon, K., Waycott, M., Kilminster, K., Kendrick, G., et al. (2014b). New south wales seagrass habitat map. *GeoNetwork Open Source Data Sharing Portal* doi: 10.4227/05/54F7CBFAEAB85

Canto, R., Udy, J., McMahon, K., Waycott, M., Kilminster, K., Kendrick, G., et al. (2014c). queensland seagrass habitat map. *GeoNetwork Open Source Data Sharing Portal* doi: 10.4227/05/54F7D01E367A6

Canto, R., Udy, J., McMahon, K., Waycott, M., Kilminster, K., Kendrick, G., et al. (2014d). South australia seagrass habitat map. *GeoNetwork Open Source Data Sharing Portal* doi: 10.4227/05/54F7D008C8A9F

Canto, R., Udy, J., McMahon, K., Waycott, M., Kilminster, K., Kendrick, G., et al. (2014e). Tasmania seagrass habitat map. *GeoNetwork Open Source Data Sharing Portal* doi: 10.4227/05/54F7CFC62C221

Canto, R., Udy, J., McMahon, K., Waycott, M., Kilminster, K., Kendrick, G., et al. (2014f). Victoria seagrass habitat map. *GeoNetwork Open Source Data Sharing Portal* doi: 10.4227/05/54F7CFF4A9547

Canto, R., Udy, J., McMahon, K., Waycott, M., Kilminster, K., Kendrick, G., et al. (2014g). Western australia seagrass habitat map. *GeoNetwork Open Source Data Sharing Portal* doi: 10.4227/05/54F8F99CC756E

Cardoso, P. G., Leston, S., Grilo, T. F., Bordalo, M. D., Crespo, D., Raffaelli, D., et al. (2010). Implications of nutrient decline in the seagrass ecosystem success. *Mar. Pollut. Bull.* 60, 601–608. doi: 10.1016/j.marpolbul.2009.11.004

Claudet, J., Bopp, L., Cheung, W. W. L., Devillers, R., Escobar-Briones, E., Haugan, P., et al. (2020). A Roadmap for using the UN decade of ocean science for sustainable development in support of science, policy, and action. *One Earth* 2, 34–42. doi: 10.1016/j.oneear.2019.10.012

Collier, C. J., Uthicke, S., and Waycott, M. (2011). Thermal tolerance of two seagrass species at contrasting light levels: implications for future distribution in the Great barrier reef. *Limnand Ocean* 56, 2200–2210.

Collier, C. J., Waycott, M., and McKenzie, L. J. (2012). Light thresholds derived from seagrass loss in the coastal zone of the northern great barrier reef, australia. *Ecol. Ind.* 23, 211–219.

Commonwealth of Australia (2019). *Towards an Emissions Reduction Fund Method of Blue Carbon*. Australian: Australian Government, Department of Energy and Environment.

Devlin, M., Waterhouse, J., Taylor, J., and Brodie, J. (2001). *Flood Plumes in the Great Barrier Reef: Spatial and Temporal Patterns in Composition and Distribution*. Marine Park: Great Barrier Reef Marine Park Authority.

Dunic, J. C., Brown, C. J., Connolly, R. M., Turschwell, M. P., and Côté, I. M. (2021). Long-term declines and recovery of meadow area across the world's seagrass bioregions. *Glob. Change Biol.* 27, 4096–4109. doi: 10.1111/gcb.15684

Foley, M. M., Armsby, M. H., Prahler, E. E., Caldwell, M. R., Erickson, A. L., Kittinger, J. N., et al. (2013). Improving ocean management through the use of ecological principles and integrated ecosystem assessments. *Bioscience* 63, 619–631.

Grech, A., Chartrand-Miller, K., Erftemeijer, P., Fonseca, M., McKenzie, L., Rasheed, M., et al. (2012). A comparison of threats, vulnerabilities and management approaches in global seagrass bioregions. *Environ. Res. Lett.* 7:8.

Grech, A., Coles, R., and Marsh, H. (2011). A broad-scale assessment of the risk to coastal seagrasses from cumulative threats. *Mar. Policy* 35, 560–567.

Grech, A., Pressey, R. L., and Day, J. C. (2016). Coal, cumulative impacts, and the great barrier reef. *Conserv. Lett.* 9, 200–207.

Green, E. P., and Short, F. T. (2003). *World Atlas of Seagrasses*. Berkley: University of California Press.

Halpern, B. S., and Fujita, R. (2013). Assumptions, challenges, and future directions in cumulative impact analysis. *Ecosphere* 4:131.

Halpern, B. S., Walbridge, S., Selkoe, K. A., Kappel, C. V., Micheli, F., and D'Agrosa, C. (2008). A global map of human impact on marine ecosystems. *Sci. Total Environ.* 319, 948–952.

Halpern, B., Frazier, M., Potapenko, J., Casey, K., Koenig, K., Longo, C., et al. (2015). Spatial and temporal changes in cumulative human impacts on the world's ocean. *Nat. Commun.* 6:7615. doi: 10.1038/ncomms8615

Harris, P. T., and Hughes, M. G. (2012). Predicted benthic disturbance regimes on the australian continental shelf: a modelling approach. *Mar. Ecol. Prog. Ser.* 449, 13–25.

Hemer, M. (2006). The magnitude and frequency of combined flow bed shear stress as a measure of exposure on the australian continental shelf. *Cont. She Res.* 26, 1258–1280.

Hoque, M. A.-A., Phinn, S., Roelfsema, C., and Childs, I. (2018). Assessing tropical cyclone risks using geospatial techniques. *Appl. Geog.* 98, 22–33. doi: 10.1016/j.apgeog.2018.07.004

Hughes, M., Harris, P., and Brooke, B. (2010). Seabed exposure and ecological disturbance on australia's continental shelf: potential surrogates for marine biodiversity. *Geosci. Austr. Record* 2010:43.

IPCC (2019). *Climate Change and Land: an IPCC Special Report on Climate Change, Desertification, Land Degradation, Sustainable Land Management, Food Security, and Greenhouse gas Fluxes in Terrestrial Ecosystems*.

Jackson, W. J., Argent, R. M., Bax, N. J., Bui, E., Clark, G. F., Coleman, S., et al. (2016). "Overview of state and trends of coasts," in *Australia State of The Environment 2016, Australian Government Department of the Environment and Energy*, (Canberra). Available online at: https://soe.environment.gov.au/theme/overview/coasts/topic/overview-state-and-trends-coasts (accessed January 30, 2020).

Jordà, G., Marbà, N., and Duarte, C. (2012). Mediterranean seagrass vulnerable to regional climate warming. *Nat. Climate Change* 2, 821–824.

Kaplan, S., and Garrick, B. J. (1981). On the quantitative definition of risk. *Risk Anal.* 1, 11–27.

Kendrick, G., Aylward, M., Hegge, B., Cambridge, M., Hillman, K., Wyllie, A., et al. (2002). Changes in seagrass coverage in cockburn sound, western australia between 1967 and 1999. *Aquat. Bot.* 73, 75–87.

Kilminster, K., McMahon, K., Waycott, M., Kendrick, G. A., Scanes, P., McKenzie, L., et al. (2015). Unravelling complexity in seagrass systems for management: australia as a microcosm. *Sci. Total Environ.* 534, 97–109. doi: 10.1016/j.scitotenv.2015.04.061

Lambert, V., Bainbridge, Z., Collier, C., Lewis, S., Adams, M., Carter, A., et al. (2021). Connecting targets for catchment sediment loads to ecological outcomes for seagrass using multiple lines of evidence. *Mar. Poll. Bull.* 169:112494. doi: 10.1016/j.marpolbul.2021.112494

Landis, W. G. (2003). The frontiers in ecological risk assessment at expanding spatial and temporal scales. *Hum. Ecol. Risk Assess.* 9, 1415–1424. doi: 10.1080/10807030390250912

Lee, K. S., Park, S. R., and Kim, Y. K. (2007). Effects of irradiance, temperature, and nutrients on growth dynamics of seagrasses: a review. *J. Exp. Mar. Biol. Ecol.* 350, 144–175. doi: 10.1016/j.jembe.2007.06.016

McKenzie, L., Yoshida, R., Grech, A., and Coles, R. (2014). *Composite of Coastal Seagrass Meadows in Queensland, Australia - November 1984 to June 2010*. Cairns, QLD: Publisher Fisheries Queensland. doi: 10.1594/PANGAEA.826368

Moore, K., Shields, E., and Parrish, D. (2013). Impacts of varying estuarine temperature and light conditions on *Zostera marina* (eelgrass) and its interactions with *Ruppia maritima* (widgeongrass). *Est Coast.* 37, S20–S30.

Mount, R., and Bricher, P. (2008). *Estuarine, Coastal and Marine (ECM) National Habitat Map Series Project Report February 2008*. Canberra: Report to the

Department of Climate Change and the National Land and Water Resources Audit.

Ontorio, Y., Cuesta-Gracia, A., Ruiz, J. M., Romero, J., and Pérez, M. (2019). The negative effects of short-term extreme thermal events on the seagrass *Posidonia oceanica* are exacerbated by ammonium additions. *PLoS One* 14:e0222798. doi: 10.1371/journal.pone.0222798

Pressey, R., Cabeza, M., Watts, M., Cowling, R., and Wilson, K. (2007). Conservation planning in a changing world. *Trends Ecol. Evol.* 22, 583–592.

QDPI-F (2009). *Subtidal SeagrassDistribution, 1994 – 1995*. Cairns, QLD: MTSRF-1-1-5, AIMS, Source: QDPI-F.

R Core Team (2021). *R: A Language and Environment for Statistical Computing*. Vienna, Austria: R Foundation for Statistical Computing.

Saunders, M., Leon, J., Phinn, S., Callaghan, D., O'Brien, K., Roelfsema, C., et al. (2013). Coastal retreat and improved water quality mitigate losses of seagrass from sea level rise. *Glob Chan. Biol.* 19, 2569–2583. doi: 10.1111/gcb.12218

Seddon, S., Connolly, R., and Edyvane, K. (2000). Large-scale seagrass dieback in northern spencer gulf, south australia. *Aquat. Bot.* 66, 297–310.

Sharp, R., Tallis, H., Ricketts, T., Guerry, A., Wood, S., Chaplin-Kramer, R., et al. (2015). *InVEST +VERSION+ User's Guide*. Stanford: The Natural Capital Project, Stanford University, University of Minnesota, The Nature Conservancy, and World Wildlife Fund.

Specht, A., Guru, S., Houghton, L., Keniger, L., Driver, P., Ritchie, E. G., et al. (2015). Data management challenges in analysis and synthesis in the ecosystem sciences. *Sci. Total Environ.* 534, 144–158. doi: 10.1016/j.scitotenv.2015.03.092

Strydom, S., Murray, K., Wilson, S. K., Huntley, B., Rule, M. J., Heithus, M. R., et al. (2020). Too hot to handle: unprecedented seagrass death driven by marine heatwave in a world heritage area. *Glob Chan. Biol.* 26, 3525–3538. doi: 10.1111/gcb.15065

Thomson, J. A., Burkholder, D. A., Heithaus, M. R., Fourqurean, J. W., Fraser, M. W., Statton, J., et al. (2015). Extreme temperatures, foundation species, and abrupt ecosystem change: an example from an iconic seagrass ecosystem. *Glob. Chan. Biol.* 21, 1463–1474. doi: 10.1111/gcb.12694

TropWATER (2016). *Collation of Spatial Seagrass Data From 1984 - 2014 for The Great Barrier Reef World Heritage Area*. Available online at: http://eatlas.org.au/data/uuid/77998615-bbab-4270-bcb1-96c46f56f85a (accessed February 1, 2017).

Tulloch, V., Tulloch, A., Visconti, P., Halpern, B., Watson, J., Evans, M., et al. (2015). Why do we map threats? Linking threat mapping with actions to make better conservation decisions. *Front. Ecol. Environ.* 13:91–99.

Turschwell, M. P., Connolly, R. M., Dunic, J. C., Sievers, M., Buelow, C. A., Pearson, R. M., et al. (2021). Anthropogenic pressures and life history predict trajectories of seagrass meadow extent at a global scale. *PNAS* 118, e2110802118. doi: 10.1073/pnas.2110802118

Unsworth, R. K. F., Collier, C. J., Waycott, M., McKenzie, L. J., and Cullen-Unsworth, L. C. (2015). A framework for the resilience of seagrass ecosystems. *Mar. Pollut. Bull.* 100, 34–46. doi: 10.1016/j.marpolbul.2015.08.016

Waycott, M., Collier, C. J., McMahon, K., Ralph, P. J., McKenzie, L. J., Udy, J., et al. (2007). "Vulnerability of seagrasses in the great barrier reef to climate change," in *Climate Change and the Great Barrier Reef: A Vulnerability Assessment Great Barrier Reef Marine Park Authority and Australian Greenhouse Office*, eds J. E. Johnson and P. Marshall (Australia).

Waycott, M., Duarte, C. M., Carruthers, T. J. B., Orth, R. J., Dennison, W. C., Olyarnik, S., et al. (2009). Accelerating loss of seagrasses across the globe threatens coastal ecosystems. *Proc. Natl. Acad. Sci. U.S.A.* 106, 12377–11238. doi: 10.1073/pnas.0905620106

Conflict of Interest: The authors declare that the research was conducted in the absence of any commercial or financial relationships that could be construed as a potential conflict of interest.

frontiers | Frontiers in Marine Science

ORIGINAL RESEARCH
published: 01 April 2022
doi: 10.3389/fmars.2022.838967

Differential Responses of Eelgrass and Macroalgae in Pacific Northwest Estuaries Following an Unprecedented NE Pacific Ocean Marine Heatwave

Caitlin L. Magel[1*†], *Francis Chan*[1], *Margot Hessing-Lewis*[2,3] *and Sally D. Hacker*[1]

[1] Department of Integrative Biology, Oregon State University, Corvallis, OR, United States, [2] Hakai Institute, Campbell River, BC, Canada, [3] Institute for the Oceans and Fisheries,University of British Columbia, Vancouver, BC, Canada

OPEN ACCESS

Edited by:
Itxaso Odériz, National Autonomous University of Mexico, Mexico

Reviewed by:
Francisca C. García, King Abdullah University of Science and Technology, Saudi Arabia
Laura K. Reynolds, University of Florida, United States

***Correspondence:**
Caitlin L. Magel
magelcai@uw.edu

†Present address:
Caitlin L. Magel, Puget Sound Institute, University of Washington Tacoma, Tacoma, WA, United States

Specialty section:
This article was submitted to Coastal Ocean Processes, a section of the journal Frontiers in Marine Science

Received: *18 December 2021*
Accepted: *09 March 2022*
Published: *01 April 2022*

Citation:
Magel CL, Chan F, Hessing-Lewis M and Hacker SD (2022) Differential Responses of Eelgrass and Macroalgae in Pacific Northwest Estuaries Following an Unprecedented NE Pacific Ocean Marine Heatwave. Front. Mar. Sci. 9:838967. doi: 10.3389/fmars.2022.838967

The 2013-2016 northeast Pacific Ocean marine heatwave (MHW) had myriad impacts on marine communities, but little is known about how this event affected coastal estuaries. We examined the extent to which elevated temperatures associated with the offshore MHW were observed in four estuaries (Willapa Bay, Washington and Netarts Bay, Yaquina Bay, and Coos Bay, Oregon) and the responses of macrophytes at marine dominated sites within these estuaries. Records of eelgrass (*Zostera marina*), ulvoid macroalgae (*Ulva* and *Enteromorpha* spp.), and environmental characteristics, including water temperature, were analyzed over three periods: before (2006-2010), during (2015-2016), and after (2017-2019) the MHW. During the MHW, all four estuaries experienced "estuarine heatwaves" (anomalous warm water events) at monitoring stations and there was an associated decline in macroalgae biomass. In northern estuaries (Willapa and Netarts bays) where water temperatures are normally higher and estuaries are shallower, aboveground eelgrass biomass declined and did not recover for at least three years after the MHW. In southern estuaries (Yaquina and Coos bays), where water temperatures are normally colder and estuaries are deeper, the MHW was associated with a neutral, or temporarily positive, change in aboveground eelgrass biomass. Our analysis supports the hypothesis that upwelling intensity and estuarine depth determined the severity of MHW impacts on macrophytes at marine dominated sites, and that the colder and deeper estuaries in the south may serve as refuges for eelgrass but not macroalgae. We suggest that estuary-specific responses were predictable given the drivers of macrophyte abundance at marine dominated sites, and that baseline ocean upwelling and estuarine temperature can be used to anticipate macrophyte responses at marine dominated sites to MHWs in the future.

Keywords: marine heatwave, estuaries, eelgrass *Zostera marina*, ulvoid macroalgae, ocean upwelling, climate change

INTRODUCTION

Over the past century, climate change has led to longer and more frequent extremes in ocean temperatures that can have dramatic effects on marine and coastal ecosystems (Oliver et al., 2018). Marine heatwaves (MHWs) are defined as prolonged periods of anomalously high sea surface temperature (Hobday et al., 2016) and are superimposed on the existing anthropogenic warming trend of the global ocean (Domingues et al., 2008; Wijffels et al., 2016). However, the impacts of MHW events likely differ from those caused by gradual ocean warming, and there has been increased interest in how these acute thermal events affect biophysical and biogeochemical processes (Cavole et al., 2016; Benthuysen et al., 2020). A number of significant MHWs have occurred in the last 20 years, including a 2003 event in the Mediterranean Sea (Olita et al., 2006), several events between 2011 and 2016 around the continent of Australia (Pearce and Feng, 2013; Oliver et al., 2017; Benthuysen et al., 2018), a 2012 event in the northwest Atlantic Ocean (Chen et al., 2014), and the most extreme MHW on record known as "The Blob" in the northeast (NE) Pacific Ocean, which persisted from 2013-2016 (Di Lorenzo and Mantua, 2016).

Following the offshore formation of the NE Pacific Ocean MHW in 2013, coastal sea surface temperature anomalies were observed along the US west coast beginning in January 2014 and extending through August 2016 (Gentemann et al., 2017). Documented changes from this large event included decreases in primary production, geographical shifts of species ranging from copepods to sharks, mass strandings of marine mammals and seabirds, and closures of economically important fisheries from harmful algal blooms (reviewed in Cavole et al., 2016). In addition, offshore foundational marine macrophytes, including giant kelp and bull kelp, were strongly affected (Cavanaugh et al., 2019; Rogers-Bennett and Catton, 2019). However, the extent to which this MHW propagated into Pacific coastal estuaries triggering "estuarine heatwaves," with subsequent effects on estuarine macrophytes (including seagrass and macroalgae), has not been considered. Furthermore, little is generally known about how MHWs interact with local-scale physiographic characteristics of estuaries to amplify or diminish their impacts.

Seagrasses and macroalgae are the foundation of highly productive estuaries by providing habitat for commercially important fish species, coastal protection *via* wave attenuation, and nutrient cycling (Barbier et al., 2011; Smale et al., 2013; Nordlund et al., 2016). Moreover, there is growing interest in conservation and restoration of marine macrophytes for their important role in the carbon cycle (Howard et al., 2017) and their potential to mitigate ocean acidification (Hendriks et al., 2014; Magel, 2020). However, it is estimated that roughly 30% of the global seagrass distribution has been lost, prompting concern over the future of this critical habitat (Orth et al., 2006; Waycott et al., 2009). Negative impacts of MHWs on seagrasses have been documented in Australia (Thomson et al., 2015; Kendrick et al., 2019) and seagrasses are known to be sensitive to elevated water temperature, particularly for populations near their thermal limits (Marbà and Duarte, 2010; Koch et al., 2013; Kaldy et al., 2017; Lefcheck et al., 2017; Aoki et al., 2020). Less is known, however, about the causes of estuarine macroalgae loss, with most attention focused on macroalgal blooms and eutrophication (except see Sfriso and Marcomini, 1996). In addition, seagrasses and macroalgae exhibit a range of interactions with one another depending on estuarine conditions (Burkholder et al., 1992; Hauxwell et al., 2001; McGlathery, 2001; Armitage et al., 2005; Burkholder et al., 2007; Hessing-Lewis et al., 2011). Thus, it is important to understand the resilience of both seagrasses and macroalgae to MHWs in order to anticipate the consequences of these events and guide conservation and management (Unsworth et al., 2018).

Shallow mudflat habitats in estuaries can transition between seagrass dominated, macroalgae dominated, or unvegetated mud in response to environmental conditions (Nyström et al., 2012), indicating a range of community states in these ecosystems. The dynamics that produce these states can be non-linear, driven by biophysical feedbacks between vegetation, sediment, and the water column (e.g., McGlathery et al., 2013; Maxwell et al., 2017; O'Brien et al., 2018), and differences in the physiological tolerances of seagrasses and macroalgae to variable light intensity, water temperature, and nutrients (Roca et al., 2016). These nonlinearities present significant challenges for estuarine conservation and restoration if they result in further declines, or lags in system recovery, after the removal of the original perturbation (Nyström et al., 2012; Roca et al., 2016; Maxwell et al., 2017; O'Brien et al., 2018).

Here we explore the response and recovery dynamics of native eelgrass (*Zostera marina*) and ulvoid macroalgae (*Ulva* spp. and *Enteromorpha* spp.) in estuaries along the US Pacific Northwest coast that were exposed to the recent NE Pacific Ocean MHW. In these estuaries, macrophytes experience a range of water temperatures (Thom et al., 2003), urbanization and eutrophication (Shelton et al., 2017), and disturbance from aquaculture practices (Tallis et al., 2009). Most studies have shown US Pacific Northwest eelgrass to be relatively resilient to these perturbations as indicated by their high production and wide distributional range (Thom et al., 2003; Hessing-Lewis and Hacker, 2013). For instance, a recent study of the long-term dynamics of *Z. marina* in Puget Sound showed that, at the ecosystem scale of a large coastal basin, eelgrass abundance remained stable despite both anthropogenic and environmental change over the last 40 years (Shelton et al., 2017). Against thermal stress, *Z. marina* is thought to be "protected" in this region because eelgrass currently exists well within its reported temperature tolerance (up to about 30°C) (Lee et al., 2007). Coastal upwelling likely contributes to this high productivity and apparent resilience (Kaldy and Lee, 2007; Hessing-Lewis and Hacker, 2013). However, declines have also been observed along the US west coast, including small bays of the San Juan Islands, Washington in 2003 (Wyllie-Echeverria et al., 2003), Morro Bay, California from 2007-2013 (Walter et al., 2018), and the upper reaches of Coos Bay, Oregon starting in 2016 (Magel, 2020). In addition, studies of *Z. marina* in the US Pacific Northwest have shown decreased growth at water temperatures above 15°C

(Thom et al., 2001; Kaldy et al., 2017), which is lower than those considered stressful at other locations within the species' worldwide distribution (Kaldy and Lee, 2007).

In this study, we combine data from eelgrass and macroalgae surveys in four US Pacific Northwest estuaries (from north to south: Willapa Bay, Netarts Bay, Yaquina Bay, and Coos Bay; **Figure 1**) spanning 400 km of coastline and 14 years that covered the periods before, during, and after the NE Pacific Ocean MHW. These estuaries experience differences in oceanographic conditions that influence macrophyte production (Hessing-Lewis and Hacker, 2013). Along the coast, upwelling strength and the duration of the upwelling season increases from north to south (Hickey and Banas, 2003). This spatial variation in upwelling, combined with coastal topography (Hickey and Banas, 2008) and watershed drivers (Howarth et al., 2011), creates a latitudinal gradient in estuarine water temperature and nutrient concentrations (Brown et al., 2007; Brown and Ozretich, 2009). Estuaries in central and southern Oregon, such as Yaquina Bay and Coos Bay, tend to be colder and have higher nutrient concentrations compared to estuaries in the north such as Netarts Bay and Willapa Bay, resulting in differences in macrophyte biomass and community structure (Thom et al., 2003; Hessing-Lewis and Hacker, 2013). Previous research by Hessing-Lewis and Hacker (2013) showed that southern estuaries (i.e., Coos Bay and Yaquina Bay) had high total macrophyte biomass dominated by ulvoid macroalgae, whereas northern estuaries (i.e., Netarts Bay and Willapa Bay) had lower macrophyte biomass that was dominated by native eelgrass. The dominance of ulvoid macroalgae in southern estuaries was associated with cold and nutrient-rich, ocean-derived water while eelgrass production was negatively correlated with these conditions (Hessing-Lewis and Hacker, 2013; Kaldy, 2014). With high epiphyte and ulvoid macroalgae biomass, competition for nutrients and light between primary producers could also limit eelgrass, although previous research in the US Pacific Northwest has found little evidence of competition between eelgrass and ulvoid macroalgae (Hessing-Lewis et al., 2011; Hessing-Lewis and Hacker, 2013; Hessing-Lewis et al., 2015). Instead, eelgrass and ulvoid macroalgae in US Pacific Northwest estuaries appear to be responding to different drivers.

Given the differences in the chemical, physical, and ecological structure of US Pacific Northwest estuaries, we asked three questions to explore the resilience of estuarine macrophytes to a strong MHW event: 1) Did spatiotemporal patterns in eelgrass and ulvoid macroalgae biomass change before, during, or after the 2013-2016 NE Pacific Ocean MHW? 2) If biomass did change, was recovery observed in the post MHW period and were responses coherent across estuaries and macrophyte taxa? Finally, 3) if there was variability in the response and recovery of macrophytes, was it influenced by differences in estuary-specific oceanographic and estuarine conditions, including the extent to which elevated temperatures associated with the MHW were observed in these estuaries?

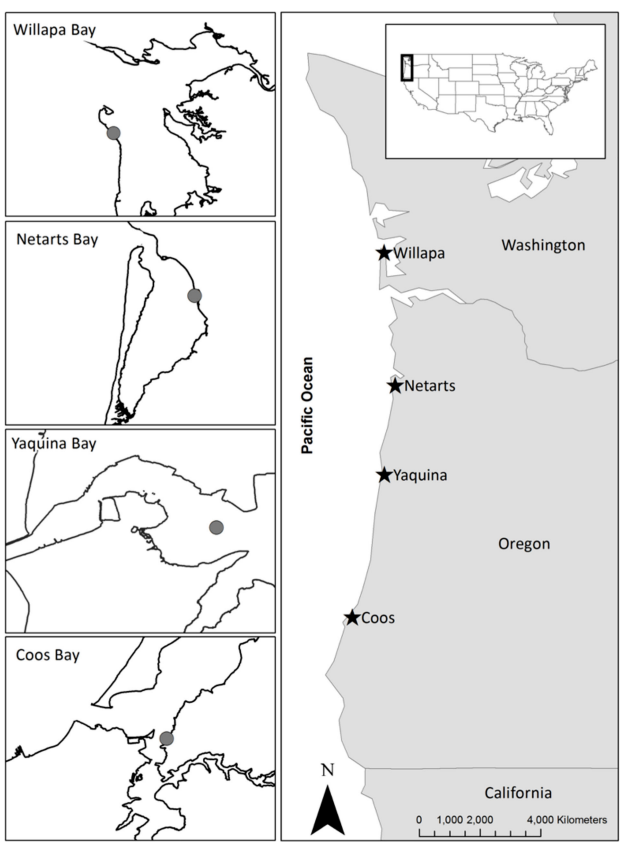

FIGURE 1 | Map of the study sites in four estuaries of the US Pacific Northwest coast, including Willapa Bay, Washington and Netarts Bay, Yaquina Bay, and Coos Bay, Oregon. Gray circles on each inset map indicate the location of macrophyte sampling. Site locations and characteristics are given in **Appendix A**: **Tables S1**, **S3**.

METHODS

Study Sites and Macrophyte Surveys

We considered the change in aboveground eelgrass (native *Zostera marina*) and ulvoid macroalgae (*Ulva* and *Enteromorpha* spp.) biomass and environmental characteristics, including water temperature, before (2006-2010), during (2015-2016), and after (2017-2019) the NE Pacific Ocean MHW in four estuaries (Willapa Bay, Washington, and Netarts Bay, Yaquina Bay, and Coos Bay, Oregon, US; **Figure 1**). These estuaries vary in oceanographic, estuarine, and watershed conditions (**Appendix A**: **Tables S1** and **S2**). Willapa Bay and Netarts Bay are shallower with more intertidal area (relative to estuary size) compared to Yaquina Bay and Coos Bay (Lee and Brown, 2009). Yaquina Bay and Coos Bay have larger catchment sizes, greater population density, and higher freshwater nutrient loads compared to Willapa Bay and Netarts Bay (**Appendix A**: **Table S1**).

Within each estuary, we conducted annual surveys during peak macrophyte biomass at a single contiguous intertidal eelgrass bed from 2016–2019 (**Figure 1**). Past studies have found that the biomass of macrophytes in these estuaries is highest in July and August and does not vary much over the

summer (Hessing-Lewis et al., 2011; Magel, 2020). Hayduk et al. (2019) performed multiple surveys at marine dominated beds and found similar biomass of eelgrass and ulvoid macroalgae among sites within each estuary, whereas differences among estuaries were significant. Therefore, we utilized individual sites to characterize annual variation within estuaries and differences among estuaries. The beds were located close (< 6 km) to the mouth of each estuary (**Figure 1**) and within ± 0.1 m of mean lower low water, where they experienced marine dominated conditions, including high salinities, high nutrients, and cold waters associated with ocean upwelling (Brown and Ozretich, 2009; Hessing-Lewis and Hacker, 2013). These surveys were combined with previous annual surveys conducted in 2006-2010 (Hessing-Lewis and Hacker, 2013) and 2015 (Hayduk et al., 2019) that used the same sampling methods at many of the same sites. Unpublished data for our Willapa site were obtained from M. Hessing-Lewis for 2007-2010, which differed from the site reported in Hessing-Lewis and Hacker (2013). Data were not collected in Willapa Bay in 2015 nor in Netarts Bay in 2007 and 2009.

The annual surveys consisted of haphazard placement of 15–20 0.5-meter x 0.5-meter (or 0.25 m^2) quadrats within the eelgrass bed at each site during low tide. Percent cover of eelgrass and ulvoid macroalgae, number of eelgrass shoots, and the wet volume of ulvoid macroalgae were recorded. Field samples of at least 20 randomly collected eelgrass shoots and volumes of ulvoid macroalgae were collected, frozen, and returned to the lab for processing. In the lab, epiphytes were gently scraped from each eelgrass shoot using a microscope slide, and each shoot was dried (60°C for 48-72 hr) and weighed. Epiphyte samples were similarly dried and weighed for samples collected from 2016–2019 but not for the prior years. To estimate the annual aboveground biomass of eelgrass per 0.25 m^2 at each site, we multiplied the mean eelgrass per shoot biomass by the average shoot density from the field surveys. Annual epiphyte load was calculated as the average epiphyte biomass per average eelgrass shoot biomass.

To determine macroalgae biomass per 0.25 m^2, this study and Hessing-Lewis et al. (2011) established relationships to convert field measurements of either percent cover or wet volume (mL) to dry weight biomass (grams). For the Hessing-Lewis et al. (2011); Hessing-Lewis and Hacker (2013), and Hayduk et al. (2019) studies, the dry weight biomass was converted from macroalgae percent cover using the relationship: Macroalgae Dry Weight = Log (1.61 × Percent Cover – 3.83) (R^2 = 0.85, p < 0.001, n = 199 field samples). For this study, dry weight biomass was converted from macroalgae wet volume using the relationship: Macroalgae Dry Weight = –0.67 × Wet Volume + 29.04 (R^2 = 0.90, p < 0.001, n = 97 field samples).

Water Temperature Climatologies and Estuarine Heatwaves

Estuarine water temperature (°C) records were obtained from monitoring locations nearest to macrophyte survey sites in each estuary (see **Appendix A**: **Table S3** for data sources). Data were combined from two sources in each estuary: the Northwest Association of Networked Ocean Observing Systems (NANOOS) and another local source (see **Appendix A**: **Table S3** for additional sources). These additional datasets helped to fill in gaps in the NANOOS time series to create a more complete temperature record in each estuary, particularly during the focal years of our study (2006-2019). Overlapping daily average water temperature records from NANOOS were regressed with the local dataset for each estuary to ensure close agreement (see **Appendix B** for additional detail on the water temperature dataset comparisons). In addition, sea surface temperature records from 1979-2019 were obtained from an offshore mooring buoy located near Cape Blanco, Oregon (**Appendix A**: **Table S3**).

From the compiled datasets, daily average water temperature was calculated for each estuary and the coastal ocean. Water temperature climatologies and categorization of heatwaves for each estuary and the coastal ocean were determined using the R package 'heatwaveR' (Schlegel and Smit, 2018). This program determines MHWs based on the Hobday et al. (2016) definition and categories established by Hobday et al. (2018). Briefly, Hobday et al. (2016) consider a warm water occurrence to be a MHW if the event lasts for 5+ days, with temperatures above the 90th percentile based on a historical baseline. Graphs of the long-term climatology overlaid with MHW events were produced for each estuary and the coastal ocean. A cumulative intensity metric (°C above average x number of days elevated) was also used to capture the severity and the duration of heatwave events that occurred during the specified time period of the study [see the 'heatwaveR' documentation (Schlegel and Smit, 2018) for additional information on this metric]. For each estuary, cumulative intensity of all heatwaves was summed from November 2013 through January 2016, the duration of the NE Pacific MHW (Schmeisser et al., 2019), in order to compare the relative severity of heatwaves experienced by the four estuaries.

Environmental Factors Dataset

We compiled a dataset of average ocean upwelling, surface current strengths, and estuarine water temperature and salinity during June and July for each year (2006-2010 and 2015-2019) and estuary (see sources and data in **Appendix A**: **Tables S3** and **S2**, respectively). Mean Ekman transport (referred to here as upwelling index, $m^3\ s^{-1}\ 100\ m^{-1}$ of coastline) was calculated from sea level pressure maps and were averaged for a 0.5 degree latitude radius around the geographic coordinates of the mouth of each estuary following the method of Gouhier et al. (2010). Mean offshore (cm s^{-1} west) and alongshore (cm s^{-1} south) currents were obtained from Oregon State University's CODAR dataset and were averaged for a 0.6 degree latitude/longitude radius around the geographic coordinates of the mouth of each estuary. Current data were filtered for values with at least 50% coverage. Ekman transport (upwelling index) and current strengths measure different aspects of upwelling along the coast. Records of salinity were also compiled from monitoring locations nearest to macrophyte survey sites in each estuary (**Appendix A**: **Table S3**). Watershed size, normalized by estuary area [catchment area (km^2) per estuary area (km^2)], was obtained for each estuary from Hessing-Lewis and Hacker (2013)

(**Appendix A**: **Table S1**). Average tidal exchange volume (m^3 d^{-1}) and freshwater inflow normalized to estuary volume ($year^{-1}$) were obtained for each estuary from Lee and Brown (2009) (**Appendix A**: **Table S1**). Tidal exchange volume and freshwater inflow measurements were not available over time, thus we used non-temporal, fixed values in our dataset.

Data and Statistical Analyses

All statistical analyses were performed using R (v. 4.0.2, R Development Core Team 2020). Generalized least squares regressions, including first-order autoregressive terms to account for the potential autocorrelation in time series data, were used to determine whether eelgrass and macroalgae biomass (g dry weight per 0.25 m^2) changed over time at each site (2006-2019). Additionally, we used analysis of variance ['Anova' function of the 'car' R package (Fox and Weisberg, 2019)] and Tukey HSD comparisons of means ['lsmeans' R package (Lenth, 2016)] to test whether there were differences among sites, MHW time periods [before (2006-2010), during (2015-2016), and after (2017-2019) the NE Pacific Ocean MHW], or an interaction between site and time period for eelgrass metrics (shoot density per 0.25 m^2, per shoot biomass, and eelgrass biomass) and macroalgae biomass. Eelgrass and macroalgae biomass values were log-transformed prior to analysis to improve normality.

We used partial least squares regression [PLSR; Carrascal et al. (2009)] analysis to assess the relationship between macrophyte biomass in the four estuaries with respect to the watershed, estuary, and ocean condition factors described above (**Appendix A**: **Tables S1**, **S2**). We conducted separate analyses for three time periods: all years (2006-2019), before the MHW (2006-2010), and during and after MHW (2015-2019). Given data limitations and lack of statistical power, we were unable to perform separate PLSR analyses using data from before, during, and after the MHW. PLSR is well suited to deal with multicollinearity in explanatory and response variables, which was evident in our data and is common in ecological datasets (Mevik and Wehrens, 2007). Using the PLSR technique, we defined blocks of response and explanatory variables. The response block (Y block) contained eelgrass biomass (log transformed), macroalgae biomass (log transformed), and epiphyte load. Each observation of eelgrass and macroalgae biomass and epiphyte load were paired with corresponding environmental factors for that estuary and/or year. The block of explanatory variables (X block) included 8 environmental parameters for each estuary [**Appendix A**: **Tables S1**, **S2**; i.e., mean estuary water temperature, salinity, upwelling index, offshore ocean current, and alongshore ocean current in June for each year; summed estuary heatwave cumulative intensity (°C x days; Schlegel and Smit [2018]) for the months preceding our sampling (January and July) for each year; tidal exchange volume (m^3 d^{-1}) and volume normalized freshwater inflow ($year^{-1}$)]. If explanatory variable observations were missing for one year, we imputed the estuary-specific averages because PLSR analysis necessitates complete observations. Using the compiled data, the response variables (Y block) were modelled through the analysis of linear combinations among predictor variables (X block).

We then used squared weight (weight^2), cross-correlation, and variable importance for projection (VIP) metrics to describe the importance of individual environmental factors as predictors of eelgrass and macroalgae biomass and epiphyte load. Explanatory variables with VIP greater than 1 are most relevant for explaining the variation observed in the block of response variables. The Stone-Geisser's cross-validation metric (Q^2) was used to determine significance of the PLSR axes. Axes are significant if Q^2 is greater than or equal to 0.0975 (Carrascal et al., 2009). Radar plots with two axes for all years (2006-2019), before the MHW (2006-2010), and during and after the MHW (2015-2019) were used to explore the correlations between explanatory and response variables depending on time period. The R package 'plsdepot' (Sanchez, 2012) was used to develop and visualize the PLSR outputs.

RESULTS

NE Pacific Ocean MHW and Estuarine Heatwaves

During the period of the NE Pacific Ocean MHW, there was evidence of corresponding heatwaves (water temperatures that exceed the local climatological threshold) in all four estuaries and the coastal ocean (**Figure 2** and **Table 1**). At the coastal ocean buoy near Cape Blanco, Oregon, the MHW event was first detected in late winter or early spring 2014 and then was amplified in summer 2014 through fall 2015 (**Figure 2A**). Beginning around the same time, estuarine heatwave events were also detected and tended to be strongest during the fall and winter and dissipate during spring and summer (**Figures 2B**–**E**). In estuaries, the heatwaves amplified starting in fall 2014 and remained elevated through spring 2015 (**Figures 2B**–**E**). Smaller heatwave events were present in the summer and fall 2015 and well into winter 2016. Yaquina Bay experienced a particularly strong heatwave in winter and spring 2016, however the duration and magnitude of this event was not observed in the other estuaries (**Figure 2D**).

On average, Willapa Bay and Netarts Bay daily water temperatures were frequently above 15°C during summer 2014 and summer 2015 (**Figures 2B, C**), whereas summer water temperatures in Yaquina Bay and Coos Bay were comparatively lower (at or below 15°C) (**Figures 2D**, **E**). Willapa Bay (6-16°C) and Netarts Bay (8-14°C) water temperature climatologies showed greater seasonal variation, compared to Yaquina Bay (9-12°C) and Coos Bay (10-13°C) (**Figures 2B–E**).

Although the occurrence of estuarine heatwaves was variable between estuaries and years, the time period corresponding to the NE Pacific Ocean MHW event coincided with greater regularity of estuarine warming (**Figure 2**, **Table 1** and **Appendix A**: **Figure S1**). Total cumulative intensity (°C x days) of estuarine heatwaves between November 2013 and January 2016 was highest in Netarts Bay (625.2), followed by Yaquina Bay (493.8) and Coos Bay (391.3), and lowest in Willapa Bay (369.9). However, missing water temperature data in Willapa Bay (late 2014) and Coos Bay (early 2015) precluded a

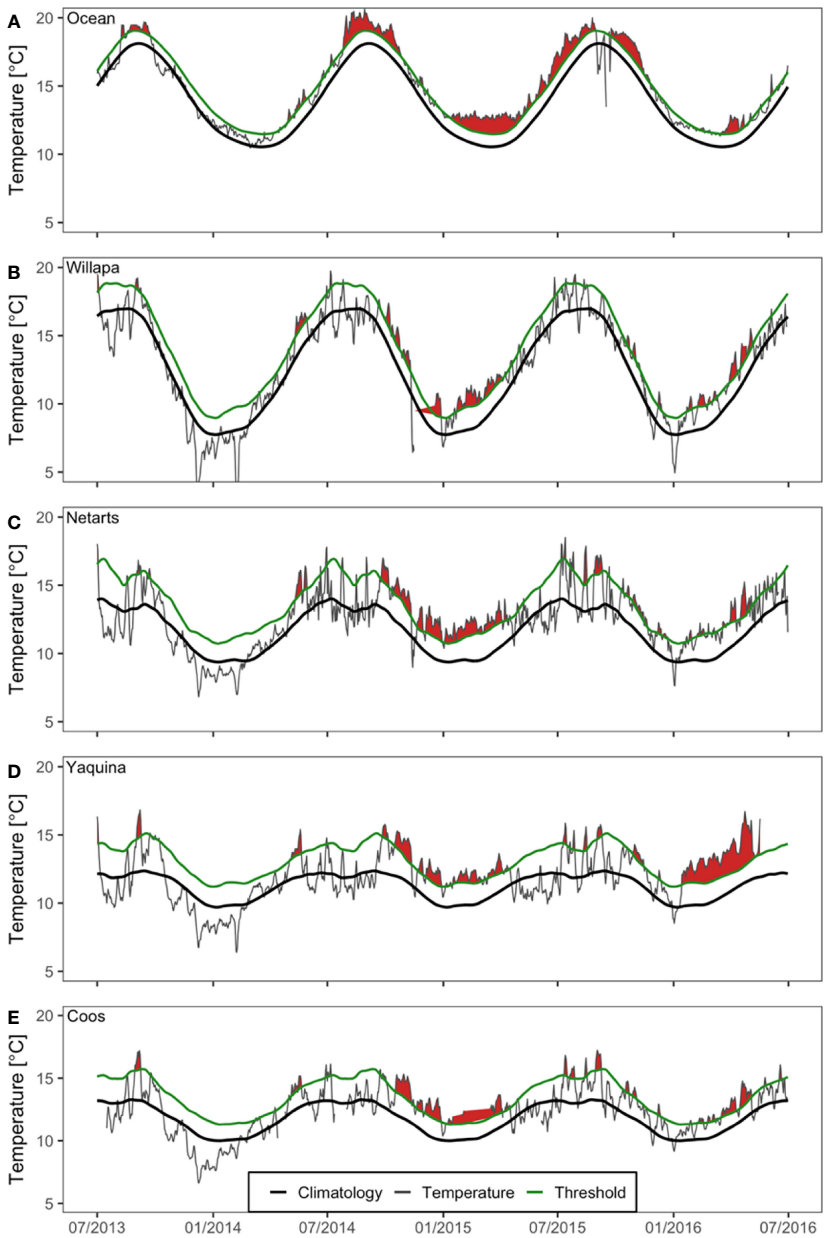

FIGURE 2 | Water temperature (gray) and detected heatwave events (red fill) at monitoring stations in the northeast Pacific Ocean **(A)** and four US Pacific Northwest estuaries (**Figure 1**): Willapa Bay **(B)**, Netarts Bay **(C)**, Yaquina Bay **(D)**, and Coos Bay **(E)** during July 2013 – July 2016. Seasonal climatologies (black) and heatwave thresholds (green) are based on the available historical data from each estuary. Graphs were produced using definitions and functions contained in the 'heatwaveR' R package (Schlegel and Smit, 2018). Occasional data gaps exist during this time period, indicated by the absence of the gray line, and heatwave condition is interpolated across missing data.

complete understanding of the differences in the severity and duration of estuarine heatwaves (**Figure 2**).

Spatial and Temporal Patterns of Macrophytes

Regression analysis revealed that eelgrass at marine dominated sites in Willapa Bay and Netarts Bay declined across years (Willapa: slope = -3.7, p = 0.014; Netarts: slope = -2.8, p = 0.002), whereas no change was observed in Yaquina Bay or Coos Bay (**Figure 3**). Eelgrass biomass differed among estuaries (two-way ANOVA, F = 151.3, df = 3, $p < 0.001$), MHW time periods (i.e., before, during, after) (F = 58.8, df = 2, $p < 0.001$), and there was an estuary by time period interaction (F = 37.2, df = 6, $p < 0.001$) (**Figure 4A** and **Appendix A**: **Table S4**). Tukey *post-hoc* tests for each estuary revealed that, in Willapa Bay and Netarts Bay, eelgrass biomass declined during the MHW and

TABLE 1 | Interannual average (standard error) summer (July or August) macrophyte (eelgrass, macroalgae, and epiphyte) biomass, estuary water temperature (January–July), and the estuarine heat wave (EHW) cumulative intensity from January to July (number of heat wave events lasting at least five days, when present) for Willapa Bay, WA, Netarts Bay, OR, Yaquina Bay, OR, and Coos Bay, OR from 2006-2010 and 2015-2019.

	Year	Willapa Bay	Netarts Bay	Yaquina Bay	Coos Bay
Eelgrass biomass (SE) (g dry wt 0.25 m^{-2})	2006	*n/a*	58.7 (2.00)	22.9 (2.30)	22.5 (2.30)
	2007	61.19 (2.39)	*n/a*	21.7 (3.00)	17.2 (1.20)
	2008	51.54 (1.94)	53.3 (2.50)	16.8 (1.60)	15.1 (2.60)
	2009	41.57 (2.28)	*n/a*	12.9 (1.00)	8.5 (1.70)
	2010	42.10 (3.13)	40.1 (3.00)	15.7 (1.50)	13.7 (1.60)
	2015	*n/a*	42.37 (1.94)	20.13 (1.43)	42.59 (2.91)
	2016	31.48 (1.61)	28.86 (1.05)	15.25 (2.71)	45.32 (2.94)
	2017	27.57 (1.60)	18.32 (1.33)	19.29 (1.99)	21.31 (1.64)
	2018	18.65 (1.30)	24.05 (1.57)	11.50 (1.22)	23.77 (2.78)
	2019	16.12 (2.37)	22.13 (1.56)	11.15 (1.86)	18.51 (1.96)
Macroalgae biomass (SE) (g dry wt 0.25 m^{-2})	2006	*n/a*	1.7 (0.70)	24.4 (3.60)	24.5 (3.10)
	2007	0.41 (0.17)	*n/a*	29.2 (4.80)	45.2 (4.00)
	2008	1.96 (0.72)	0.7 (0.50)	65.8 (3.50)	62.6 (5.00)
	2009	7.49 (2.04)	*n/a*	46.4 (4.70)	42.7 (4.10)
	2010	4.30 (1.73)	1.1 (0.30)	49.4 (3.30)	12.3 (2.20)
	2015	*n/a*	0.79 (0.20)	10.1 (0.49)	7.77 (0.48)
	2016	0.11 (0.06)	0.11 (0.06)	29.26 (2.77)	6.75 (0.80)
	2017	0.20 (0.08)	0.43 (0.09)	15.46 (3.35)	7.53 (0.85)
	2018	6.54 (2.21)	0.35 (0.09)	37.43 (4.43)	3.61 (0.64)
	2019	3.43 (1.30)	3.25 (1.88)	39.60 (3.66)	5.78 (0.96)
Epiphyte load (SE) (g dry wt per g eelgrass)	2016	0.01 (0.01)	0.04 (0.01)	0.16 (0.02)	0.04 (0.01)
	2017	0.06 (0.01)	0.10 (0.01)	0.25 (0.03)	0.15 (0.03)
	2018	0.01 (0.01)	0.34 (0.06)	0.45 (0.06)	0.30 (0.04)
	2019	0.03 (0.01)	0.27 (0.06)	0.52 (0.08)	0.44 (0.05)
Water Temperature (SE) (°C)	2006	10.6 (0.22)	11.3 (0.13)	13.2 (0.66)*	11.8 (0.12)
	2007	14.6 (0.28)	11.4 (0.19)	11.3 (0.13)	11.7 (0.16)
	2008	10.9 (0.20)	9.7 (0.14)	9.7 (0.08)	10.5 (0.12)
	2009	10.8 (0.26)	11 (0.16)	10.2 (0.10)	10.9 (0.13)
	2010	11.7 (0.17)	11.2 (0.08)	11.2 (0.07)	11.7 (0.08)
	2015	13.0 (0.21)	12.8 (0.10)	11.9 (0.08)	12.7 (0.11)
	2016	12.7 (0.23)	12.7 (0.13)	13.3 (0.14)	12.6 (0.10)
	2017	12.3 (0.24)	12.5 (0.15)	11.9 (0.09)	11.8 (0.12)
	2018	11.8 (0.23)	11.7 (0.17)	*n/a*	11.7 (0.11)
	2019	12.3 (0.28)	11.9 (0.16)	11.3 (0.10)	11.8 (0.12)
EHW Cumulative Intensity (°C x days) **(# of events)**	2006	0	0	116.5 (1)	21.2 (1)
	2007	103.0 (2)	46.3 (1)	59.3 (2)	58.8 (2)
	2008	0	0	0	0
	2009	0	0	0	0
	2010	0	0	17.6 (1)	0
	2015	*n/a*	233.5 (2)	185.3 (3)	111.4 (6)
	2016	116.8 (6)	102.2 (4)	376.2 (1)	113.6 (4)
	2017	0	0	14.6 (1)	13.0 (1)
	2018	0	28.1 (1)	0	0
	2019	23.3 (1)	34.2 (1)	28.7 (1)	28.3 (1)

**Value based on limited data.*

*n/a, data not available. The dataset for the partial least squares regression (PLSR) analysis, including imputed values, can be found in **Appendix A**: **Table S2** and data sources are given in **Appendix A**: **Table S3**.*

continued to decline afterward (Before > During > After), whereas in Yaquina Bay there were no differences through time (Before = During = After). In Coos Bay, eelgrass biomass was highest during the MHW and lowest preceding the MHW (During > After > Before).

Eelgrass shoot density and per shoot biomass also differed among the marine dominated site in each estuary (density: $F = 69.0$, $df = 3$, $p < 0.001$; shoot biomass: $F = 54.7$, $df = 3$, $p < 0.001$), MHW time periods ($F = 12.6$, $df = 2$, $p < 0.001$; $F = 24.2$, $df = 2$, $p < 0.001$), and there was an estuary by time period interaction ($F = 26.6$, $df = 6$, $p < 0.001$; $F = 14.0$, $df = 6$, $p < 0.001$) (**Appendix A**: **Figure S2** and **Table S4**). Tukey *post-hoc* tests revealed that eelgrass density continued to decline after the MHW in Willapa Bay (Before = During > After) and Netarts Bay (Before > During > After), returned to its original density after the MHW (Before = After > During) in Yaquina Bay, but increased in density during and after the MHW (After > Before > During) in Coos Bay. Eelgrass shoot biomass showed similar patterns with declines after the MHW in Willapa Bay (Before = During > After) and Netarts Bay (Before = During > After), little change in Yaquina

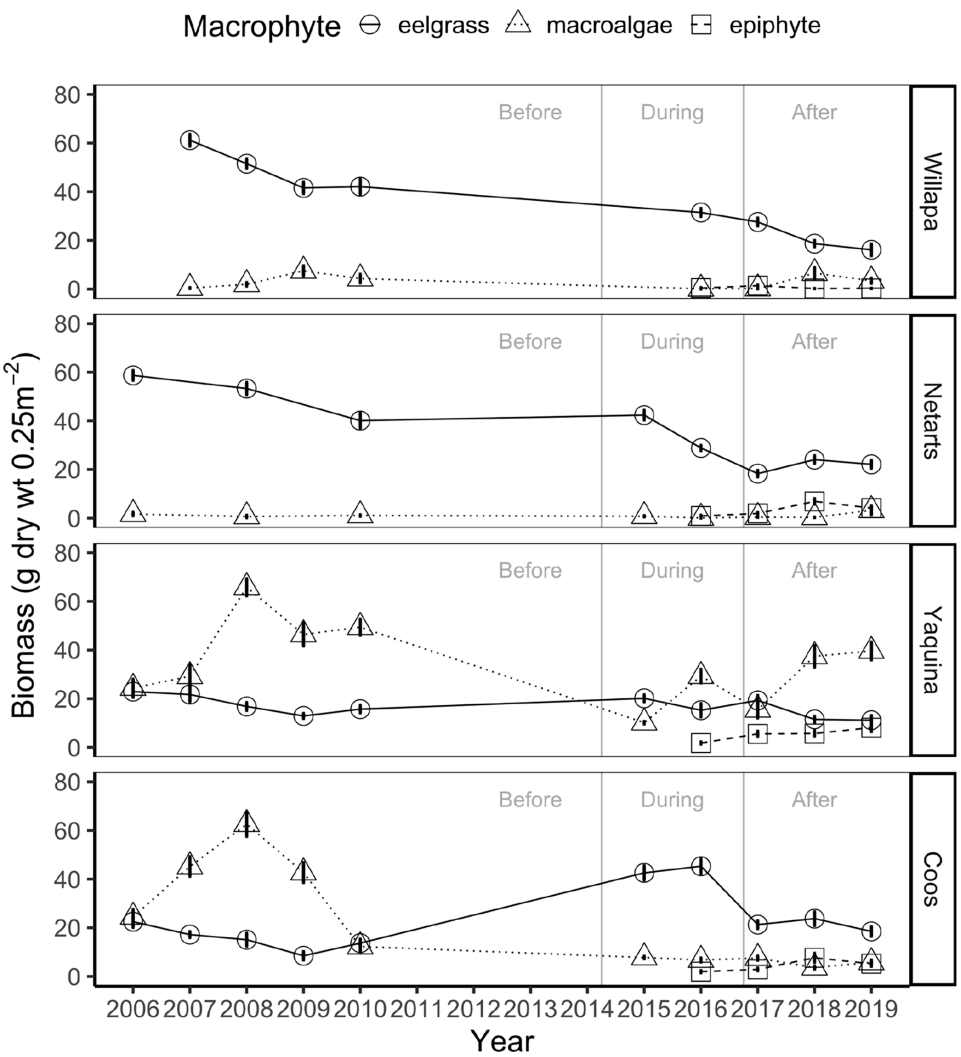

FIGURE 3 | Mean interannual biomass ± standard error (g dry wt 0.25 m^{-2}) of eelgrass (circles, solid lines), ulvoid macroalgae (triangles, dotted lines), and epiphytes (squares, dashed lines) at marine dominated sites in four US Pacific Northwest estuaries (**Figure 1**) between 2006-2019 over three time periods: before, during, and after the NE Pacific Ocean marine heatwave.

Bay (During > After, but neither differ from Before), and a temporary increase in Coos Bay during the MHW (During > Before = After).

Regression analysis showed no change in macroalgae biomass between 2006-2019 across estuaries at the marine dominated sites (**Figure 3**). Macroalgae biomass differed among estuaries (two-way ANOVA, F = 404.4, df = 3, $p < 0.001$), MHW time periods (F = 6.3, df = 2, $p < 0.01$), and there was an estuary by time period interaction (F = 22.7, df = 6, $p < 0.001$) (**Figure 4B** and **Appendix A**: **Table S4**). Tukey *post-hoc* tests for each estuary showed that macroalgae biomass declined during the MHW in Willapa Bay (Before = After > During) and Netarts Bay (Before > During, but neither differ from After). In both Yaquina Bay and Coos Bay, macroalgae biomass declined during the MHW but there was some recovery in Yaquina Bay (Before > After > During) but not in Coos Bay (Before > During = After).

Finally, total macrophyte biomass (eelgrass + macroalgae) differed among marine dominated sites in these estuaries (F = 2.6, df = 3, $p = 0.05$), MHW time periods (F = 91.7, df = 2, $p < 0.001$), and there was an estuary by time period interaction (F = 18.3, df = 6, $p < 0.001$) (**Figure 4C** and **Appendix A**: **Table S4**). Tukey *post-hoc* tests showed that total biomass in Willapa Bay and Netarts Bay decreased across the time periods (Before > During > After). For Yaquina Bay, total biomass was lowest during the MHW and highest before (Before > After > During) whereas in Coos Bay, total biomass was lowest after the MHW (Before = During > After).

Epiphyte load from 2016–2019 differed among estuaries at our sites (one-way ANOVA, F = 5.29, df = 3, $p < 0.05$), with the

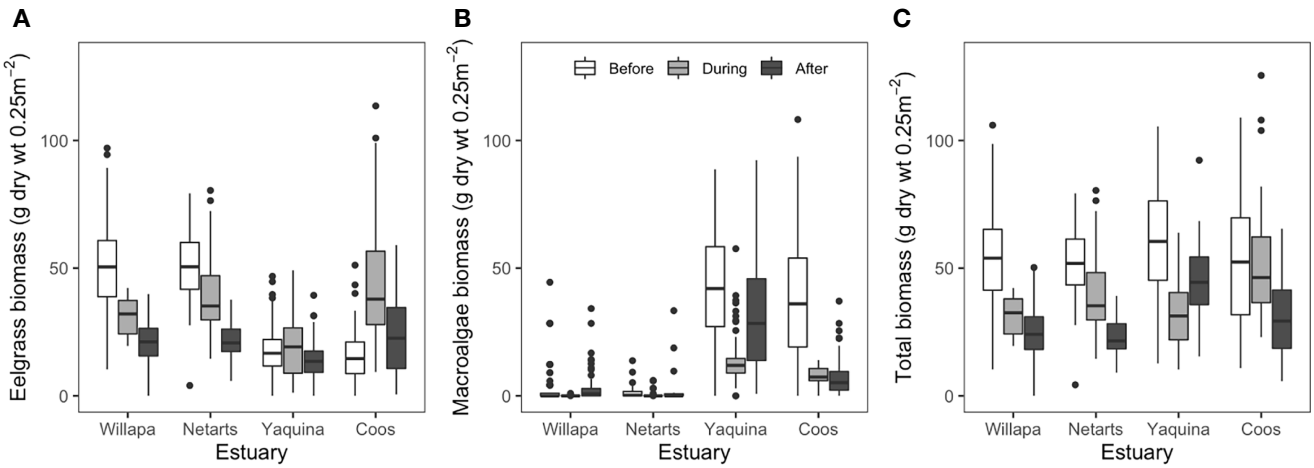

FIGURE 4 | Comparison of eelgrass biomass **(A)**, ulvoid macroalgae biomass **(B)**, and total macrophyte (eelgrass plus macroalgae) biomass **(C)** at marine dominated sites in four US Pacific Northwest estuaries (**Figure 1**) before (2006-2010, white fill), during (2015-2016, light gray fill), and after (2017-2019, dark gray fill) the NE Pacific Ocean marine heatwave (2013-2016). Boxes (with median centerline) encompass the interquartile range (25th-75th percentile) of the data for each estuary and period. Whiskers extend to the most extreme data point that is no more than 1.5 times the length of the box and values falling beyond that range are shown as points. For clarity, ANOVA comparisons are not shown but are discussed in text.

highest loads in Yaquina Bay compared to Willapa Bay (Tukey-adjusted comparison: t-ratio = -3.2, df = 12, $p < 0.05$) (**Figure 3** and **Appendix A**: **Figure S3**). Netarts Bay and Coos Bay both had moderate epiphyte loads.

Estuarine Heatwaves and Other Environmental Effects on Macrophyte Biomass

The relationships between the eelgrass and macroalgae biomass, epiphyte load, and environmental drivers from 2006-2019 are shown in a radar plot (**Figure 5**). Overall, the PLSR analysis showed that 56.7% of the observed variability in macrophyte biomass was explained by the two PLSR axes. In addition, 75.8% of the variability in the block of environmental drivers, consisting of 8 metrics of watershed, estuary, and ocean conditions, was explained by the two PLSR axes. In terms of each axis separately, Axis 1 was significant ($Q^2_{axis\ 1} = 0.37$), explained the majority of the observed variability in the macrophyte biomass block (52%), and was positively correlated with the vector for eelgrass biomass ("eelgrass") and negatively correlated with vectors for macroalgae biomass ("macroalgae") and epiphyte load ("epiphytes") (**Figure 5**). Axis 2 was also significant ($Q^2_{axis\ 2} = 0.13$) but explained only 14% of the variation in the macrophyte biomass block.

For each taxon separately, we found that, of the proportion of variability in eelgrass biomass that was statistically explained in the PLSR, 48% was positively correlated with the block of environmental drivers, according to the PLSR cross-correlation value (**Table 2**). In particular, summer eelgrass biomass was positively related to water temperature ("Temp") and tidal exchange volume ("VolExch") across years, indicated by

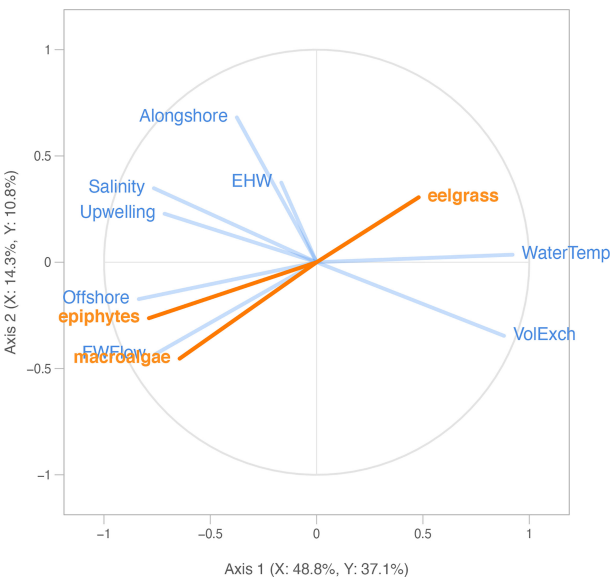

FIGURE 5 | Partial least squares correlation radar plot of 8 explanatory environmental variables (blue; see **Appendix A**: **Tables S1**, **S2** for abbreviations) and response macrophyte variables (orange; **Figures 2**, **3**), including eelgrass biomass ("eelgrass"), ulvoid macroalgae biomass ("macroalgae"), and epiphyte load ("epiphytes"), across all years (2006-2019) and four US Pacific Northwest estuaries (**Figure 1**). Eelgrass and macroalgae biomass were log-transformed for the analysis, epiphyte load was not transformed. Each segment represents a model variable. Longer segments (closer to the circle perimeter) indicate that the variable is better represented. Segments close together are highly and positively correlated variables. Segments in opposite directions are negatively correlated. Orthogonal segments indicate no correlation.

TABLE 2 | Summary of the partial least squares regression (PLSR) analysis between the response block (Y), including three response variables, and the explanatory block (X), including 8 explanatory variables (see **Appendix A**: **Tables S1** and **S2** for variable abbreviations) for four US Pacific Northwest estuaries (**Figure 1**) across all years (2006-2019).

PLSR Component	Variable	Load	Weight^2	VIP	Cross-Correlation	Correlation
X	**Tidal Exch. Volume**	+	0.14	1.07	0.58	0.88
	Freshwater Flow	−	0.25	1.40	-0.76	-0.76
	Water Temperature	+	0.21	1.30	0.71	0.92
	Offshore Current	−	0.20	1.25	-0.68	-0.84
	Estuarine Heat Wave	−	0.00	0.16	0.08	-0.17
	Salinity	−	0.11	0.95	-0.52	-0.77
	Upwelling Index	−	0.09	0.85	-0.46	-0.72
	Alongshore Current	−	0.00	0.05	-0.03	-0.38
Y	Eelgrass	+	*n/a*	*n/a*	0.48	0.80
	Macroalgae	−	*n/a*	*n/a*	-0.64	-0.85
	Epiphytes	−	*n/a*	*n/a*	-0.79	-0.87

Load indicates the sign of the relationship of each variable with Axis 1 and weight^2 indicates the proportion of Axis 1 explained by each variable. Variable importance (VIP) measures the explanatory power of each variable for the Y block. VIP > 1 are considered most important (indicated with bold text). Cross-correlation is the coefficient between each variable and the opposing block. Correlation is the coefficient between each variable and its own block. n/a = metric not applicable to variable.

vectors that are aligned with one another in the PLSR plot (**Figure 5**). For the proportion of variability in macroalgae biomass that was statistically explained in the PLSR, 64% was negatively correlated with the block of environmental drivers (**Table 2**). Annual summer macroalgae biomass was positively related to freshwater flow ("FWFlow") and offshore current strength ("Offshore") indicated by vectors that are aligned with one another in the PLSR plot (**Figure 5**). In addition, macroalgae was negatively correlated with water temperature ("Temp") indicated by vectors that are opposite one another. Macroalgae biomass was negatively correlated with eelgrass biomass, but positively related to epiphyte load. Finally, similar to macroalgae, 79% of the statistically explained variability in epiphyte load was negatively correlated with the block of environmental drivers according to the cross-correlation value (**Table 2**). Epiphyte load was also positively related to offshore current ("Offshore") and freshwater flow ("FWFlow"), somewhat positively related to salinity ("Salinity") and upwelling index ("Upwelling), and negatively related to water temperature ("Temp") (**Figure 5**). Alongshore current strength ("Alongshore") and estuarine heatwave cumulative intensity ("EWH") were generally unrelated to the response variables, indicated by the orthogonal vectors.

Given that Axis 1 was significant and strongly related to all three response variables, we focused on the relative contribution of each environmental driver in explaining this axis (**Figure 5**). Environmental variables contributing (weight^2) greater than a value of 1 divided by the total number of variables (in this case 1/8 or about 12%) were considered important. According to the weight^2 values, normalized freshwater flow ("FWFlow": 25%), water temperature ("Temp": 21%), offshore current ("Offshore": 20%), and tidal exchange volume ("VolExch": 14%) contributed significantly to Axis 1 (**Table 2**). The remaining four environmental drivers, including estuarine heatwaves ("EHW": 0%), all contributed less than 12% to Axis 1 (**Table 2**).

We also performed separate PLSR analyses for before the MHW (2006-2010) and during and after the MHW (2015-2019) relative to the NE Pacific Ocean MHW. Relationships between macrophyte biomass and environmental drivers before and after the MHW remained relatively similar and thus are well represented by the PLSR containing all years (**Appendix A**: **Figures S4**, **S5** and **Appendix A**: **Tables S5**, **S6**). However, one notable difference is the eelgrass vector, which is positively associated with water temperature ("Temp") and tidal exchange ("VolExch") in the overall and early years models (**Figure 5** and **Appendix A**: **Figure S4**), changed orientation to become orthogonal (unrelated) to those environmental driver vectors and became positively aligned with alongshore current strength ("Alongshore") in the later years model (**Appendix A**: **Figure S5**).

DISCUSSION

Responses to the MHW Differed by Estuary and Macrophyte Taxa

Marine dominated sites in four US Pacific Northwest estuaries experienced abnormally elevated water temperature events ("estuarine heatwaves") between 2014-2016, coinciding with the timing of the NE Pacific Ocean marine heatwave (MHW) along the US west coast (**Figure 2** and **Table 1**) (Gentemann et al., 2017). Changes in macrophyte abundance at the four marine dominated sites were associated with the MHW, however these changes were not coherent across estuaries or macrophyte taxa (**Figures 3**, **4**). The lack of coherence observed, combined with our partial least square regression (PLSR) analysis, indicates that underlying physiographic differences in these estuaries, primarily ocean upwelling exposure and freshwater flow, likely altered the response of macrophytes to the MHW and associated estuarine heatwaves.

Total macrophyte biomass at our marine dominated sites generally declined in all estuaries during the MHW, in part because of universal declines in ulvoid macroalgae (**Figures 3**, **4**). However, eelgrass varied in response to the MHW; there were declines in eelgrass biomass in northern estuaries (Willapa Bay and Netarts Bay) but either no change or an increase in eelgrass

biomass in southern estuaries (Yaquina Bay and Coos Bay) (**Figure 4** and **Appendix A**: **Figure S2**). After the MHW, ulvoid macroalgae returned to its original biomass in all estuaries except Coos Bay, remaining low through the end of our study (2019). Moreover, even though eelgrass in Coos Bay and Yaquina Bay returned to its pre-MHW biomass after the MHW abated, it continued to decline in Willapa Bay and Netarts Bay suggesting a lag in recovery of eelgrass in northern estuaries.

What might explain the differences in macrophyte response to the MHW across the four estuaries? Our analysis suggests that the differing responses of eelgrass in Willapa Bay and Netarts Bay (declining biomass and no subsequent recovery) compared to Coos Bay and Yaquina Bay (stable or increasing) are likely a consequence of differences in upwelling intensity and water depth among the estuaries (**Figure 5** and **Table 2**). Although all sites in our study were located at approximately the same tidal elevation (within 0.1 m of mean lower low water), the overall depth of these estuaries and the proximity of the macrophyte beds to the main estuary channel differed. For example, Willapa Bay and Netarts Bay are shallower with less upwelling influence compared to Yaquina Bay and Coos Bay, which are deeper and experience stronger upwelling conditions. In addition, the sites in Willapa Bay and Netarts Bay were located further from the main estuary channel compared to the sites in Yaquina Bay and Coos Bay, which may have influenced macrophyte response to the MHW. Water depth, in particular, was identified as an important mitigating factor for eelgrass experiencing a MHW in the coastal bays of Virginia, US (Aoki et al., 2020). In that study, all water depths experienced elevated temperatures, but deeper eelgrass beds had a shorter total duration of warm water exposure and thus greater resilience (Aoki et al., 2020). It is important to note that eelgrass in the US Pacific Northwest occurs both in the intertidal and subtidal zones, but we lacked survey data to characterize the response of subtidal eelgrass to the MHW for this study.

Although eelgrass (*Z. marina*) is known to tolerate water temperatures up to 30°C (Orth and Moore, 1986; Lee et al., 2007), it has been shown to display acclimation to local environments (Kaldy and Lee, 2007; Kaldy, 2014; Reynolds et al., 2016) and, regionally, eelgrass in the US Pacific Northwest is thought to be most productive at 5–8°C with signs of physiological stress above 15°C (Thom et al., 2003). Because estuary water temperatures already commonly reach 15°C in Willapa Bay and Netarts Bay during the summer, the additional thermal stress of the MHW event likely exceeded a performance threshold for eelgrass at the marine dominated sites that resulted in reduced biomass and recovery. On the other hand, as a consequence of normally more intense upwelling and colder waters in the south, the eelgrass population at marine dominated sites in Yaquina Bay and Coos Bay appeared to be unaffected or to benefit from the MHW. Support for this hypothesis can be found in the comparison of the PLSR analyses for "all years" versus "during and after the MHW." The factor that had the most positive effect on eelgrass biomass during the MHW was alongshore upwelling intensity, suggesting that the warm water associated with the MHW was mitigated by colder upwelled waters, creating a thermal regime in the marine dominated zone of southern estuaries that was conducive to eelgrass growth (**Appendix A**: **Figure S5** and **Table S6**). The long-term trends in eelgrass biomass among the estuaries suggest that aboveground eelgrass biomass in southern estuaries, which was a third of that in northern estuaries prior to the MHW, is typically constrained by the cold, nutrient rich water delivered to these estuaries during non-MHW conditions (**Figures 2**, **4**; Hessing-Lewis and Hacker, 2013).

The relationship between ulvoid macroalgae biomass and water temperature is not well defined, with previous studies reporting a negative relationship (Rivers and Peckol, 1995), positive relationship (Nelson et al., 2003), or no relationship (Kentula and DeWitt, 2003). However, similar to epiphytes (Kaldy et al., 2017) and kelp (Arafeh-Dalmau et al., 2019; Cavanaugh et al., 2019; Rogers-Bennett and Catton, 2019), we found that ulvoid macroalgae at marine dominated sites appeared to be sensitive to elevated temperatures with dramatic declines in the southern estuaries where ulvoid macroalgae dominated prior to the MHW (**Figures 3**, **4**). Thus, even estuaries that experience more intense upwelling failed to provide a thermal refuge for macroalgae at marine dominated sites during the MHW.

Coincident with water temperature changes, altered nutrient delivery to estuaries due to oceanographic changes in stratification and upwelling during the MHW (Brodeur et al., 2019) may have influenced macrophyte production. Although macroalgae are traditionally considered nutrient-limited (Wheeler and Björnsäter, 1992), previous research in US Pacific Northwest estuaries suggests that, under most conditions, neither ulvoid macroalgae nor eelgrass experience nutrient limitation given the persistent exposure to nutrient rich upwelled waters during the growing season (Williams and Ruckelshaus, 1993; Hessing-Lewis and Hacker, 2013; Kaldy, 2014; Hessing-Lewis et al., 2015; Kaldy et al., 2017). Instead, macrophyte production in this region is primarily limited by light and temperature. However, although water temperature appears to be the main driver of macrophyte dynamics in this study, nutrients cannot be ruled out as a factor, particularly given the dramatic declines in ulvoid macroalgae that we observed. Therefore, future studies should characterize freshwater and marine nutrient loads and the nutrient ratio in macrophyte tissues to further tease apart the combined effects of temperature and nutrients during climatic events.

Other Factors Contributing to Variable Macrophyte Responses

The effect of the MHW may have been exacerbated by other differences among the estuaries, particularly in the timing of summer tides and the local climatic conditions. For example, summer spring low tides in northern estuaries are later in the morning compared to southern estuaries (roughly an hour difference between Willapa Bay and Coos Bay). This difference could expose intertidal macrophytes in Willapa Bay and Netarts Bay to additional heat stress, similar to what has been observed for rocky intertidal organisms along the US west coast (Helmuth et al., 2006). Additional local climate differences could play a

mitigating role in macrophyte responses to MHWs, as well. Strong summer upwelling off Yaquina Bay and Coos Bay can lead to more frequent, dense coastal fog in the south compared to the north (Thom et al., 2003), which keeps summer air temperatures cooler and could reduce desiccation of intertidal macrophytes during aerial exposure at low tide (Boese et al., 2003). Moreover, the joint occurrence of the MHW with an atmospheric El Niño event, which increased both ocean and air temperatures across the US Pacific Northwest (Schmeisser et al., 2019), may accentuate the differences in the local tide- and climate-related thermal exposure of macrophytes among the estuaries.

There may have been indirect effects of the MHW on eelgrass through the reduction of negative species interactions with macroalgae and epiphytes. In particular, algal blooms (including macroalgae and epiphytes) can negatively affect seagrasses *via* reduced light availability and altered biogeochemical conditions (e.g., Burkholder et al., 1992; Hauxwell et al., 2001; McGlathery, 2001; Armitage et al., 2005; Burkholder et al., 2007; Hessing-Lewis et al., 2011; Nelson, 2017). However, for macroalgae, previous research in the same estuaries considered in this study did not find evidence of competition with eelgrass, even at very high macroalgae biomass in the marine dominated sites within the estuary (Hessing-Lewis et al., 2011; Hessing-Lewis and Hacker, 2013; Hessing-Lewis et al., 2015). In fact, in our study, eelgrass declines associated with the MHW were most pronounced in northern estuaries where ulvoid macroalgae biomass was already low prior to the MHW (**Figures 3**, **4**). In Coos Bay, where ulvoid macroalgae biomass can be high, eelgrass did increase as macroalgae decreased during the MHW, but eelgrass returned to pre-MHW biomass despite macroalgae biomass remaining low (**Figures 3**, **4**). Therefore, it does not appear that the possible indirect effects of macroalgae decline from the MHW contributed to the observed responses in eelgrass in any of the estuaries.

For epiphytes, the lack of survey data prior to the MHW prevents us from determining epiphyte response to the MHW or possible subsequent indirect effects to eelgrass. However, comparing our data to that of a synthesis by Nelson (2018) on eelgrass epiphyte loads in our study estuaries prior to the MHW, we find that average epiphyte load likely declined in all four estuaries during the MHW but then recovered afterward (see **Appendix A**: **Table S4**). Three previous studies concluded that eelgrass in US Pacific Northwest estuaries can tolerate high seasonal epiphyte loads because light availability at intertidal sites is sufficient during the summer when epiphytes are most dense (Ruesink, 2016; Nelson, 2018; Hayduk et al., 2019). In addition, our data (**Figure 2** and **Appendix A**: **Figure S3**) and that of others (Nelson, 2018) show that epiphyte loads were already low in Willapa Bay and Netarts Bay where eelgrass declines were most pronounced, potentially a result of the underlying warmer water temperatures in these estuaries (Kaldy et al., 2017). Therefore, it is unlikely that changing epiphyte load was the primary driver of the eelgrass responses we observed. However, if epiphytes did decline in Yaquina Bay and Coos Bay in response to the MHW, this may have contributed to the stimulated eelgrass growth we observed in those locations during and after the MHW.

Variable Recovery of Eelgrass After the MHW Event

Eelgrass responses following the end of the MHW indicate differences in resilience among these sites to warm water events. At the Coos Bay site, eelgrass returned to pre-MHW biomass by 2019 but the continued decline of eelgrass (in total biomass, shoot density, and per shoot biomass) in Willapa Bay and Netarts Bay after the end of MHW indicates a substantial lag in recovery despite a reversal of adverse conditions in those estuaries. Lagged recovery in seagrass systems can be indicative of the presence of strong biophysical, physiological, and/or demographic feedbacks that maintain the system in the unrecovered state even after the perturbation has been removed (e.g., Roca et al., 2016; Maxwell et al., 2017; O'Brien et al., 2018). Change in eelgrass morphology as a consequence of a warming event, such as those identified by DuBois et al. (2020) in mesocosm studies of *Zostera marina*, could contribute to such feedbacks. Typically, positive feedbacks buffer seagrass from environmental stress (especially for larger and longer-lived seagrasses, such as *Zostera marina*), but once a threshold is exceeded, degradation can occur rapidly and recovery time scales can be protracted (Roca et al., 2016; O'Brien et al., 2018). The importance of specific feedbacks in preventing recovery can vary greatly between seagrass communities (Maxwell et al., 2017; O'Brien et al., 2018) and structural and demographic parameters such as those measured in our study (e.g., biomass and shoot density) are likely to respond more slowly during degradation and recovery compared to physiological indicators (Roca et al., 2016). Furthermore, previous experimental research in mesocosms found genotypic variation in *Zostera marina* sensitivity to warming (Reynolds et al., 2016; DuBois et al., 2019) and that the relative performance of genotypes shifts following a warming event (DuBois et al., 2019). In the case of our study, we lacked sufficient information about the biophysical condition and genetic makeup of the beds to explore the possible causes of differential recovery of eelgrass in the four estuaries, or the role of feedbacks in the lack of eelgrass recovery observed in the northern estuaries. Moreover, it is unclear why ulvoid macroalgae responded positively to the cessation of the MHW in all the estuaries except Coos Bay where it is normally abundant.

Understanding Resilience of Estuarine Macrophytes to Climate Change

Future climate predictions for the US Pacific Northwest coast include warming air and sea surface temperatures, decreased precipitation, and the potential for increased upwelling and MHW events (Sydeman et al., 2014; Joh and Di Lorenzo, 2017; USGCRP, 2017). If MHW events increase in frequency and magnitude in the NE Pacific Ocean (Joh and Di Lorenzo, 2017), eelgrass and ulvoid macroalgae in at marine dominated sites in northern estuaries are likely to be negatively affected, whereas

eelgrass at marine dominated sites in southern estuaries may respond positively, up to a point. On the other hand, future increases in upwelling intensity (Sydeman et al., 2014) may offset MHW effects, favoring eelgrass over ulvoid macroalgae and epiphytes in northern estuaries, and the opposite in southern estuaries. Emerging research suggests the potential for acclimation and adaptation of macrophytes due to phenotypic variation (reviewed in Duarte et al., 2018), which could shape the resilience of these species over time. For example, DuBois et al. (2020) found that sublethal effects of warming resulted in phenotypic plasticity of *Zostera marina* that could confer either resilience or susceptibility to future exposure. Given the unique combinations of ocean and climate conditions experienced in US Pacific Northwest estuaries, our study provides a framework for understanding the differential consequences of marine heatwaves to estuarine macrophyte communities. We suggest that indicators of baseline ocean upwelling and estuarine temperature can be used to anticipate macrophyte response to future MHWs, but additional studies are needed to predict the resilience of macrophytes across the full spectrum of estuarine conditions.

DATA AVAILABILITY STATEMENT

The original contributions presented in the study are included in the article/**Supplementary Material**. Further inquiries can be directed to the corresponding author.

AUTHOR CONTRIBUTIONS

This study was conceived of and designed by CM, FC, and SH. CM, MH-L, and SH performed the field and lab work. CM performed the statistical analyses. CM wrote the manuscript and all authors provided edits for the final version. All authors contributed to the article and approved the submitted version.

FUNDING

Research in Willapa Bay from 2006–2010 was funded by a Western Regional Aquaculture Center (USDA) grant to SH. Research in Coos Bay from 2006-2010 was funded by the National Estuarine Reserve System (NOAA) to MH-L. Additional financial support to the authors came from OSU Department of Integrative Biology.

ACKNOWLEDGMENTS

We thank NANOOS for data access and the many individuals who collected long term records of water temperature. Additional data were provided by A. Helms and A. DeMarzo for Coos Bay, T. C. Mochon-Collura for Yaquina Bay, B. Hales for Netarts Bay, and A. Suhrbier for Willapa Bay. J. Hayduk provided 2015 macrophyte data. Many Oregon State University undergraduate students also contributed to field and lab work, including M. McGuire, C. Lozano, F. Hubbard, M. Hertford, C. Norman, and J. Moon. Thanks to several reviewers whose comments improved our manuscript.

SUPPLEMENTARY MATERIAL

The Supplementary Material for this article can be found online at: https://www.frontiersin.org/articles/10.3389/fmars.2022.838967/full#supplementary-material

REFERENCES

Aoki, L. R., McGlathery, K. J., Wiberg, P. L., and Al-Haj, A. (2020). Depth Affects Seagrass Restoration Success and Resilience to Marine Heat Wave Disturbance. *Estuaries Coasts* 43, 316–328. doi: 10.1007/s12237-019-00685-0

Arafeh-Dalmau, N., Montaño-Moctezuma, G., Martínez, J. A., Beas-Luna, R., Schoeman, D. S., and Torres-Moye, G. (2019). Extreme Marine Heatwaves Alter Kelp Forest Community Near its Equatorward Distribution Limit. *Front. Marine Sci.* 6. doi: 10.3389/fmars.2019.00499

Armitage, A. R., Frankovich, T. A., Heck, K. L., and Fourqurean, J. W. (2005). Experimental Nutrient Enrichment Causes Complex Changes in Seagrass, Microalgae, and Macroalgae Community Structure in Florida Bay. *Estuaries* 28, 422–434. doi: 10.1007/BF02693924

Barbier, E. B., Hacker, S. D., Kennedy, C., Koch, E. W., Stier, A. C., and Silliman, B. R. (2011). The Value of Estuarine and Coastal Ecosystem Services. *Ecol. Monogr.* 81, 169–193. doi: 10.1890/10-1510.1

Benthuysen, J. A., Oliver, E. C. J., Chen, K., and Wernberg, T. (2020). Editorial: Advances in Understanding Marine Heatwaves and Their Impacts. *Front. Marine Sci.* 7. doi: 10.3389/fmars.2020.00147

Benthuysen, J. A., Oliver, E. C. J., Feng, M., and Marshall, A. G. (2018). Extreme Marine Warming Across Tropical Australia During Austral Summer 2015–2016. *J. Geophysical Res.: Oceans* 123, 1301–1326. doi: 10.1002/2017JC013326

Boese, B. L., Alayan, K. E., Gooch, E. F., and Robbins, B. D. (2003). Desiccation Index: A Measure of Damage Caused by Adverse Aerial Exposure on Intertidal Eelgrass (*Zostera Marina*) in an Oregon (USA) Estuary. *Aquat. Bot.* 76, 329–337. doi: 10.1016/S0304-3770(03)00068-8

Brodeur, R. D., Auth, T. D., and Phillips, A. J. (2019). Major Shifts in Pelagic Micronekton and Macrozooplankton Community Structure in an Upwelling Ecosystem Related to an Unprecedented Marine Heatwave. *Front. Marine Sci.* 6. doi: 10.3389/fmars.2019.00212

Brown, C. A., Nelson, W. G., Boese, B. L., DeWitt, T. H., Eldridge, P. M., Kaldy, J. E., et al. (2007). An Approach to Developing Nutrient Criteria for Pacific Northwest Estuaries: A Case Study of Yaquina Estuary, Oregon. EPA/600/R-07/046. U.S. EPA. *Office Res. Development Natl. Health Environ. Effects Res. Lab. Western Ecol. Division*. pp. 169.

Brown, C. A., and Ozretich, R. J. (2009). Coupling Between the Coastal Ocean and Yaquina Bay, Oregon: Importance of Oceanic Inputs Relative to Other Nitrogen Sources. *Estuaries Coasts* 32, 219–237. doi: 10.1007/s12237-008-9128-6

Burkholder, J. M., Mason, K. M., and Glasgow, H. B. (1992). Water-Column Nitrate Enrichment Promotes Decline of Eelgrass *Zostera Marina*: Evidence From Seasonal Mesocosm Experiments. *Marine Ecol. Prog. Ser.* 81, 163–178. doi: 10.3354/meps081163

Burkholder, J. M., Tomasko, D. A., and Touchette, B. W. (2007). Seagrasses and Eutrophication. *J. Exp. Marine Biol. Ecol.* 350, 46–72. doi: 10.1016/j.jembe.2007.06.024

Carrascal, L. M., Galván, I., and Gordo, O. (2009). Partial Least Squares Regression as an Alternative to Current Regression Methods Used in Ecology. *Oikos* 118, 681–690. doi: 10.1111/j.1600-0706.2008.16881.x

Cavanaugh, K. C., Reed, D. C., Bell, R. W., Castorani, M. C. N., and Beas-Luna, R. (2019). Spatial Variability in the Resistance and Resilience of Giant Kelp in Southern and Baja California to a Multiyear Heatwave. *Front. Marine Sci.* 6. doi: 10.3389/fmars.2019.00413

Cavole, L. M., Demko, A. M., Diner, R. E., Giddings, A., Koester, I., Pagniello, C. M. L. S., et al. (2016). Biological Impacts of the 2013–2015 Warm-Water Anomaly in the Northeast Pacific: Winners, Losers, and the Future. *Oceanography* 29, 273–285. doi: 10.5670/oceanog.2016.32

Chen, K., Gawarkiewicz, G. G., Lentz, S. J., and Bane, J. M. (2014). Diagnosing the Warming of the Northeastern U.S. Coastal Ocean in 2012: A Linkage Between the Atmospheric Jet Stream Variability and Ocean Response. *J. Geophysical Res.: Oceans* 119, 218–227. doi: 10.1002/2013JC009393

Di Lorenzo, E., and Mantua, N. (2016). Multi-Year Persistence of the 2014/15 North Pacific Marine Heatwave. *Nat. Climate Change* 6, 1042–1047. doi: 10.1038/nclimate3082

Domingues, C. M., Church, J. A., White, N. J., Gleckler, P. J., Wijffels, S. E., Barker, P. M., et al. (2008). Improved Estimates of Upper-Ocean Warming and Multi-Decadal Sea-Level Rise. *Nature* 453, 1090–1093. doi: 10.1038/nature07080

Duarte, B., Martins, I., Rosa, R., Matos, A. R., Roleda, M. Y., Reusch, T. B. H., et al. (2018). Climate Change Impacts on Seagrass Meadows and Macroalgal Forests: An Integrative Perspective on Acclimation and Adaptation Potential. *Front. Marine Sci.* 5. doi: 10.3389/fmars.2018.00190

DuBois, K., Abbott, J. M., Williams, S. L., and Stachowicz, J. J. (2019). Relative Performance of Eelgrass Genotypes Shifts During an Extreme Warming Event: Disentangling the Roles of Multiple Traits. *Marine Ecol. Prog. Ser.* 615, 67–77. doi: 10.3354/meps12914

DuBois, K., Williams, S. L., and Stachowicz, J. J. (2020). Previous Exposure Mediates the Response of Eelgrass to Future Warming *via* Clonal Trans-Generational Plasticity. *Ecology* 101 (12), e03169. doi: 10.1002/ecy.3169

Fox, J., and Weisberg, S. (2019). *An R Companion to Applied Regression* (Third. Thousand Oaks, CA: Sage).

Gentemann, C. L., Fewings, M. R., and García-Reyes, M. (2017). Satellite Sea Surface Temperatures Along the West Coast of the United States During the 2014–2016 Northeast Pacific Marine Heat Wave. *Geophysical Res. Lett.* 44, 312–319. doi: 10.1002/2016GL071039

Gouhier, T. C., Guichard, F., and Menge, B. A. (2010). Ecological Processes can Synchronize Marine Population Dynamics Over Continental Scales. *Proc. Natl. Acad. Sci.* 107, 8281–8286. doi: 10.1073/pnas.0914588107

Hauxwell, J., Cebrián, J., Furlong, C., and Valiela, I. (2001). Macroalgal Canopies Contribute to Eelgrass (*Zostera Marina*) Decline in Temperate Estuarine Ecosystems. *Ecology* 82, 1007–1022. doi: 10.1890/0012-9658(2001)082[1007:MCCTEZ]2.0.CO;2

Hayduk, J. L., Hacker, S. D., Henderson, J. S., and Tomas, F. (2019). Evidence for Regional-Scale Controls on Eelgrass (*Zostera Marina*) and Mesograzer Community Structure in Upwelling-Influenced Estuaries. *Limnol. Oceanography* 64, 1120–1134. doi: 10.1002/lno.11102

Helmuth, B., Broitman, B. R., Blanchette, C. A., Gilman, S., Halpin, P., Harley, C. D. G., et al. (2006). Mosaic Patterns of Thermal Stress in the Rocky Intertidal Zone: Implications for Climate Change. *Ecol. Monogr.* 76, 461–479. doi: 10.1890/0012-9615(2006)076[0461:MPOTSI]2.0.CO;2

Hendriks, I. E., Olsen, Y. S., Ramajo, L., Basso, L., Steckbauer, A., Moore, T. S., et al. (2014). Photosynthetic Activity Buffers Ocean Acidification in Seagrass Meadows. *Biogeosciences* 11, 333–346. doi: 10.5194/bg-11-333-2014

Hessing-Lewis, M. L., and Hacker, S. D. (2013). Upwelling-Influence, Macroalgal Blooms, and Seagrass Production; Temporal Trends From Latitudinal and Local Scales in Northeast Pacific Estuaries. *Limnol. Oceanography* 58, 1103–1112. doi: 10.4319/lo.2013.58.3.1103

Hessing-Lewis, M. L., Hacker, S. D., Menge, B. A., McConville, S., and Henderson, J. (2015). Are Large Macroalgal Blooms Necessarily Bad? Nutrient Impacts on Seagrass in Upwelling-Influenced Estuaries. *Ecol. Appl.* 25, 1330–1347. doi: 10.1890/14-0548.1

Hessing-Lewis, M. L., Hacker, S. D., Menge, B. A., and Rumrill, S. S. (2011). Context-Dependent Eelgrass–Macroalgae Interactions Along an Estuarine Gradient in the Pacific Northwest, USA. *Estuaries Coasts* 34, 1169–1181. doi: 10.1007/s12237-011-9412-8

Hickey, B. M., and Banas, N. S. (2003). Oceanography of the US Pacific Northwest Coastal Ocean and Estuaries With Application to Coastal Ecology. *Estuaries* 26, 1010–1031. doi: 10.1007/BF02803360

Hickey, B. M., and Banas, N. S. (2008). Why is the Northern End of the California Current System So Productive? *Oceanography* 21, 90–107. doi: 10.5670/oceanog.2008.07

Hobday, A. J., Alexander, L. V., Perkins, S. E., Smale, D. A., Straub, S. C., Oliver, E. C. J., et al. (2016). A Hierarchical Approach to Defining Marine Heatwaves. *Prog. Oceanography* 141, 227–238. doi: 10.1016/j.pocean.2015.12.014

Hobday, A. J., Oliver, E. C. J., Gupta, A. S., Benthuysen, J. A., Burrows, M. T., Donat, M. G., et al. (2018). Categorizing and Naming Marine Heatwaves. *Oceanography* 31, 162–173. doi: 10.5670/oceanog.2018.205

Howard, J., Sutton-Grier, A., Herr, D., Kleypas, J., Landis, E., Mcleod, E., et al. (2017). Clarifying the Role of Coastal and Marine Systems in Climate Mitigation. *Front. Ecol. Environ.* 15, 42–50. doi: 10.1002/fee.1451

Howarth, R., Chan, F., Conley, D. J., Garnier, J., Doney, S. C., Marino, R., et al. (2011). Coupled Biogeochemical Cycles: Eutrophication and Hypoxia in Temperate Estuaries and Coastal Marine Ecosystems. *Front. Ecol. Environ.* 9, 18–26. doi: 10.1890/100008

Joh, Y., and Di Lorenzo, E. (2017). Increasing Coupling Between NPGO and PDO Leads to Prolonged Marine Heatwaves in the Northeast Pacific. *Geophysical Res. Lett.* 44, 11663–11671. doi: 10.1002/2017GL075930

Kaldy, J. E. (2014). Effect of Temperature and Nutrient Manipulations on Eelgrass *Zostera Marina* L. From the Pacific Northwest, USA. *J. Exp. Marine Biol. Ecol.* 453, 108–115. doi: 10.1016/j.jembe.2013.12.020

Kaldy, J. E., Brown, C. A., Nelson, W. G., and Frazier, M. (2017). Macrophyte Community Response to Nitrogen Loading and Thermal Stressors in Rapidly Flushed Mesocosm Systems. *J. Exp. Marine Biol. Ecol.* 497, 107–119. doi: 10.1016/j.jembe.2017.09.022

Kaldy, J. E., and Lee, K. (2007). Factors Controlling *Zostera Marina* L. Growth in the Eastern and Western Pacific Ocean: Comparisons Between Korea and Oregon, USA. *Aquat. Bot.* 87, 116–126. doi: 10.1016/j.aquabot.2007.03.008

Kendrick, G. A., Nowicki, R. J., Olsen, Y. S., Strydom, S., Fraser, M. W., Sinclair, E. A., et al. (2019). A Systematic Review of How Multiple Stressors From an Extreme Event Drove Ecosystem-Wide Loss of Resilience in an Iconic Seagrass Community. *Front. Marine Sci.* 6. doi: 10.3389/fmars.2019.00455

Kentula, M. E., and DeWitt, T. H. (2003). Abundance of Seagrass (*Zostera Marina* L.) and Macroalgae in Relation to the Salinity-Temperature Gradient in Yaquina Bay, Oregon, USA. *Estuaries* 26, 1130–1141. doi: 10.1007/BF02803369

Koch, M., Bowes, G., Ross, C., and Zhang, X. (2013). Climate Change and Ocean Acidification Effects on Seagrasses and Marine Macroalgae. *Global Change Biol.* 19, 103–132. doi: 10.1111/j.1365-2486.2012.02791.x

Lee, H., and Brown, C. A. (2009). Classification of Regional Patterns of Environmental Drivers and Benthic Habitats in Pacific Northwest Estuaries. *EPA/600/R-09/140. U.S. EPA Office Res. Development Natl. Health Environ. Effects Res. Lab. Western Ecol. Division*. pp. 298.

Lee, K., Park, S. R., and Kim, Y. K. (2007). Effects of Irradiance, Temperature, and Nutrients on Growth Dynamics of Seagrasses: A Review. *J. Exp. Marine Biol. Ecol.* 350, 144–175. doi: 10.1016/j.jembe.2007.06.016

Lefcheck, J. S., Wilcox, D. J., Murphy, R. R., Marion, S. R., and Orth, R. J. (2017). Multiple Stressors Threaten the Imperiled Coastal Foundation Species Eelgrass (*Zostera Marina*) in Chesapeake Bay, USA. *Global Change Biol.* 23, 3474–3483. doi: 10.1111/gcb.13623

Lenth, R. V. (2016). Least-Squares Means: The R Package Lsmeans. *J. Stat. Software* 69, 1–33. doi: 10.18637/jss.v069.i01

Magel, C. L. (2020). *Ecosystem Functions of Pacific Northwest Estuaries: The Role of Ocean and Watershed Drivers in Eelgrass and Coho Salmon Dynamics* (PhD Dissertation, Corvallis, Oregon, USA: Oregon State University).

Marbà, N., and Duarte, C. M. (2010). Mediterranean Warming Triggers Seagrass (*Posidonia Oceanica*) Shoot Mortality. *Global Change Biol.* 16, 2366–2375. doi: 10.1111/j.1365-2486.2009.02130.x

Maxwell, P. S., Eklöf, J. S., van Katwijk, M. M., O'Brien, K. R., de la Torre-Castro, M., Boström, C., et al. (2017). The Fundamental Role of Ecological Feedback Mechanisms for the Adaptive Management of Seagrass Ecosystems – a Review. *Biol. Rev.* 92, 1521–1538. doi: 10.1111/brv.12294

McGlathery, K. J. (2001). Macroalgal Blooms Contribute to the Decline of Seagrass in Nutrient-Enriched Coastal Waters. *J. Phycol.* 37, 453–456. doi: 10.1046/j.1529-8817.2001.037004453.x

McGlathery, K. J., Reidenbach, M. A., D'Odorico, P., Fagherazzi, S., Pace, M. L., and Porter, J. H. (2013). Nonlinear Dynamics and Alternative Stable States in

Shallow Coastal Systems. *Oceanography* 26, 220–231. doi: 10.5670/oceanog.2013.66

Mevik, B., and Wehrens, R. (2007). The Pls Package: Principal Component and Partial Least Squares Regression in R. *J. Stat. Software* 18, 1–23. doi: 10.18637/jss.v018.i02

Nelson, W. G. (2017). Development of an Epiphyte Indicator of Nutrient Enrichment: Threshold Values for Seagrass Epiphyte Load. *Ecol. Indic.* 74, 343–356. doi: 10.1016/j.ecolind.2016.11.035

Nelson, W. G. (2018). An Evaluation of Factors Controlling the Abundance of Epiphytes on *Zostera Marina* Along an Estuarine Gradient in Yaquina Bay, Oregon, USA. *Aquat. Bot.* 148, 53–63. doi: 10.1016/j.aquabot.2018.04.010

Nelson, T., Nelson, A., and Tjoelker, M. (2003). Seasonal and Spatial Patterns of "Green Tides" (ulvoid algal blooms) and related water quality parameters in the coastal waters of Washington state, USA. *Botanica Marina* 46, 263–275. doi: 10.1515/BOT.2003.024

Nordlund, L. M., Koch, E. W., Barbier, E. B., and Creed, J. C. (2016). Seagrass Ecosystem Services and Their Variability Across Genera and Geographical Regions. *PloS One* 11, e0163091. doi: 10.1371/journal.pone.0163091

Nyström, M., Norström, A. V., Blenckner, T., de la Torre-Castro, M., Eklöf, J. S., Folke, C., et al. (2012). Confronting Feedbacks of Degraded Marine Ecosystems. *Ecosystems* 15, 695–710. doi: 10.1007/s10021-012-9530-6

O'Brien, K. R., Waycott, M., Maxwell, P., Kendrick, G. A., Udy, J. W., Ferguson, A. J. P., et al. (2018). Seagrass Ecosystem Trajectory Depends on the Relative Timescales of Resistance, Recovery and Disturbance. *Marine Pollution Bull.* 134, 166–176. doi: 10.1016/j.marpolbul.2017.09.006

Olita, A., Sorgente, R., Ribotti, A., Natale, S., and Gabersek, S. (2006). Effects of the 2003 European Heatwave on the Central Mediterranean Sea Surface Layer: A Numerical Simulation. *Ocean Sci. Discussions* 3, 85–125. doi: 10.5194/osd-3-85-2006

Oliver, E. C. J., Benthuysen, J. A., Bindoff, N. L., Hobday, A. J., Holbrook, N. J., Mundy, C. N., et al. (2017). The Unprecedented 2015/16 Tasman Sea Marine Heatwave. *Nat. Commun.* 8, 16101. doi: 10.1038/ncomms16101

Oliver, E. C. J., Donat, M. G., Burrows, M. T., Moore, P. J., Smale, D. A., Alexander, L. V., et al. (2018). Longer and More Frequent Marine Heatwaves Over the Past Century. *Nat. Commun.* 9, 1324. doi: 10.1038/s41467-018-03732-9

Orth, R. J., Carruthers, T. J. B., Dennison, W. C., Duarte, C. M., Fourqurean, J. W., Heck, K. L., et al. (2006). A Global Crisis for Seagrass Ecosystems. *BioScience* 56, 987–996. doi: 10.1641/0006-3568(2006)56[987:AGCFSE]2.0.CO;2

Orth, R. J., and Moore, K. A. (1986). Seasonal and Year-to-Year Variations in the Growth of *Zostera Marina* L. (Eelgrass) in the Lower Chesapeake Bay. *Aquat. Bot.* 24 (4), 335–341. doi: 10.1016/0304-3770(86)90100-2

Pearce, A. F., and Feng, M. (2013). The Rise and Fall of the "Marine Heat Wave" Off Western Australia During the Summer of 2010/2011. *J. Marine Syst.* 111–112:139–56. doi: 10.1016/j.jmarsys.2012.10.009

Reynolds, L. K., DuBois, K., Abbott, J. M., Williams, S. L., and Stachowicz, J. J. (2016). Response of a Habitat-Forming Marine Plant to a Simulated Warming Event is Delayed, Genotype Specific, and Varies With Phenology. *PloS One* 11 (6), e0154532. doi: 10.1371/journal.pone.0154532

Rivers, J. S., and Peckol, P. (1995). Summer Decline of *Ulva Lactuca* (Chlorophyta) in a Eutrophic Embayment: Interactive Effects of Temperature and Nitrogen Availability? *J. Phycol.* 31, 223–228. doi: 10.1111/j.0022-3646.1995.00223.x

Roca, G., Alcoverro, T., Krause-Jensen, D., Balsby, T. J. S., van Katwijk, M. M., Marbà, N., et al. (2016). Response of Seagrass Indicators to Shifts in Environmental Stressors: A Global Review and Management Synthesis. *Ecol. Indic.* 63, 310–323. doi: 10.1016/j.ecolind.2015.12.007

Rogers-Bennett, L., and Catton, C. A. (2019). Marine Heat Wave and Multiple Stressors Tip Bull Kelp Forest to Sea Urchin Barrens. *Sci. Rep.* 9, 15050. doi: 10.1038/s41598-019-51114-y

Ruesink, J. L. (2016). Epiphyte Load and Seagrass Performance are Decoupled in an Estuary With Low Eutrophication Risk. *J. Exp. Marine Biol. Ecol.* 481, 1–8. doi: 10.1016/j.jembe.2016.03.022

Sanchez, G. (2012). *Plsdepot: Partial Least Squares (PLS) Data Analysis Methods*. Available at: https://cran.r-project.org/package=plsdepot.

Schlegel, R. W., and Smit, A. J. (2018). Heatwaver: A Central Algorithm for the Detection of Heatwaves and Cold-Spells. *J. Open Source Software* 3, 821. doi: 10.21105/joss.00821

Schmeisser, L., Bond, N. A., Siedlecki, S. A., and Ackerman, T. P. (2019). The Role of Clouds and Surface Heat Fluxes in the Maintenance of the 2013–2016 Northeast Pacific Marine Heatwave. *J. Geophysical Res.: Atmospheres* 124, 10772–10783. doi: 10.1029/2019JD030780

Sfriso, A., and Marcomini, A. (1996). Decline of *Ulva* Growth in the Lagoon of Venice. *Bioresource Technol.* 58, 299–307. doi: 10.1016/S0960-8524(96)00120-4

Shelton, A. O., Francis, T. B., Feist, B. E., Williams, G. D., Lindquist, A., and Levin, P. S. (2017). Forty Years of Seagrass Population Stability and Resilience in an Urbanizing Estuary. *J. Ecol.* 105, 458–470. doi: 10.1111/1365-2745.12682

Smale, D. A., Burrows, M. T., Moore, P., O'Connor, N., and Hawkins, S. J. (2013). Threats and Knowledge Gaps for Ecosystem Services Provided by Kelp Forests: A Northeast Atlantic Perspective. *Ecol. Evol.* 3, 4016–4038. doi: 10.1002/ece3.774

Sydeman, W. J., García-Reyes, M., Schoeman, D. S., Rykaczewski, R. R., Thompson, S. A., Black, B. A., et al. (2014). Climate Change and Wind Intensification in Coastal Upwelling Ecosystems. *Science* 345, 77–80. doi: 10.1126/science.1251635

Tallis, H. M., Ruesink, J. L., Dumbauld, B., Hacker, S., and Wisehart, L. M. (2009). Oysters and Aquaculture Practices Affect Eelgrass Density and Productivity in a Pacific Northwest Estuary. *J. Shellfish Res.* 28, 251–261. doi: 10.2983/035.028.0207

Thom, R. M., Borde, A. B., Blanton, S. L., Woodruff, D. L., and Williams, G. D. (2001). "The Influence of Climate Variation and Change on Structure and Processes in Nearshore Vegetated Communities of Puget Sound and Other Northwest Estuaries," in *In Proceedings of the 2001 Puget Sound Research Conference*. Ed. T. Droscher (Olympia, Washington: Puget Sound Water Quality Action Team).

Thom, R. M., Borde, A. B., Rumrill, S., Woodruff, D. L., Williams, G. D., Southard, J. A., et al. (2003). Factors Influencing Spatial and Annual Variability in Eelgrass (*Zostera Marina* L.) Meadows in Willapa Bay, Washington, and Coos Bay, Oregon, Estuaries. *Estuaries* 26, 1117–1129. doi: 10.1007/BF02803368

Thomson, J. A., Burkholder, D. A., Heithaus, M. R., Fourqurean, J. W., Fraser, M. W., Statton, J., et al. (2015). Extreme Temperatures, Foundation Species, and Abrupt Ecosystem Change: An Example From an Iconic Seagrass Ecosystem. *Global Change Biol.* 21, 1463–1474. doi: 10.1111/gcb.12694

Unsworth, R. K. F., McKenzie, L. J., Nordlund, L. M., and Cullen-Unsworth, L. C. (2018). A Changing Climate for Seagrass Conservation? *Curr. Biol.* 28, R1229–R1232. doi: 10.1016/j.cub.2018.09.027

USGCRP. (2017). Climate Science Special Report: Fourth National Climate Assessment, Volume I. D. J. Wuebbles, D. W. Fahey, K. A. Hibbard, D. J. Dokken, B. C. Stewart and T. K. Maycock (eds.). (Washington, DC, USA: U.S. Global Change Research Program) pp, 470. doi: 10.7930/J0J964J6

Walter, R. K., Rainville, E. J., and O'Leary, J. K. (2018). Hydrodynamics in a Shallow Seasonally Low-Inflow Estuary Following Eelgrass Collapse. *Estuarine Coastal Shelf Sci.* 213, 160–175. doi: 10.1016/j.ecss.2018.08.026

Waycott, M., Duarte, C. M., Carruthers, T. J. B., Orth, R. J., Dennison, W. C., Olyarnik, S., et al. (2009). Accelerating Loss of Seagrasses Across the Globe Threatens Coastal Ecosystems. *Proc. Natl. Acad. Sci.* 106, 12377–12381. doi: 10.1073/pnas.0905620106

Wheeler, P. A., and Björnsäter, B. R. (1992). Seasonal Fluctuations in Tissue Nitrogen, Phosphorus, and N:P for Five Macroalgal Species Common to the Pacific Northwest Coast. *J. Phycol.* 28, 1–6. doi: 10.1111/j.0022-3646.1992.00001.x

Wijffels, S., Roemmich, D., Monselesan, D., Church, J., and Gilson, J. (2016). Ocean Temperatures Chronicle the Ongoing Warming of Earth. *Nat. Climate Change* 6 (2),116–118. doi: 10.1038/nclimate2924

Williams, S. L., and Ruckelshaus, M. H. (1993). Effects of Nitrogen Availability and Herbivory on Eelgrass (*Zostera Marina*) and Epiphytes. *Ecology* 74, 904–918. doi: 10.2307/1940815

Wyllie-Echeverria, S., Mumford, T. E., Gaydos, J. K., and Buffum, S. (2003). *Z. Marina* Declines in San Juan County, WA: Westcott Bay Taskforce Mini-Workshop: 26 July 2003. *SeaDocs Soc.* pp. 18.

Conflict of Interest: The authors declare that the research was conducted in the absence of any commercial or financial relationships that could be construed as a potential conflict of interest.

this article, or claim that may be made by its manufacturer, is not guaranteed or endorsed by the publisher.

frontiers | Frontiers in Marine Science

ORIGINAL RESEARCH
published: 04 April 2022
doi: 10.3389/fmars.2022.856110

Bacterial Community in Cold Surge-Caused Sea Ice Differs From Seawater in Mid-Latitude Region: A Case Study in Aoshan Bay, Southern Yellow Sea

Hongwei Ren[1,2], *Jihua Liu*[1,2,3]*, *Gang Li*[4] *and Yubin Hu*[1,2]*

[1] Institute of Marine Science and Technology, Shandong University, Qingdao, China, [2] Joint Laboratory for Ocean Research and Education at Dalhousie University, Shandong University and Xiamen University, Qingdao, China, [3] Southern Marine Science and Engineering Guangdong Laboratory, Zhuhai, China, [4] Key Laboratory of Tropical Marine Bio-resources and Ecology, South China Sea Institute of Oceanology, Chinese Academy of Sciences, Guangzhou, China

OPEN ACCESS

Edited by:
Valeria Chávez,
National Autonomous University of Mexico, Mexico

Reviewed by:
Dolors Vaque,
Spanish National Research Council (CSIC), Spain
Yuqiu Wei,
Chinese Academy of Fishery Sciences (CAFS), China

***Correspondence:**
Jihua Liu
liujihua1982@sdu.edu.cn
Yubin Hu
yubinhu@sdu.edu.cn

Specialty section:
This article was submitted to Coastal Ocean Processes, a section of the journal Frontiers in Marine Science

Received: 16 January 2022
Accepted: 28 February 2022
Published: 04 April 2022

Citation:
Ren H, Liu J, Li G and Hu Y (2022) Bacterial Community in Cold Surge-Caused Sea Ice Differs From Seawater in Mid-Latitude Region: A Case Study in Aoshan Bay, Southern Yellow Sea. Front. Mar. Sci. 9:856110. doi: 10.3389/fmars.2022.856110

Cold surges result in a rapid drop in air temperature and freezing of seawater, which was likely to impact bacterial communities. We examined the differences in bacteria abundance and bacterial community composition in the sea ice and seawater during a cold surge along Aoshan Bay, southern Yellow Sea in January 2021. Results showed that the differences in bacteria abundance between sea ice and seawater likely resulted from the physical impact of ice formation. The parent water played a key role in bacterial community composition in the early phase of ice formation, in which bacterial community compositions at class level were similar, but the relative abundances were different between sea ice and seawater. The *Gammaproteobacteria* dominated in sea ice, and the relative abundances of *Verrucomicrobiae* were also significantly higher, possibly due to the high concentration of algal-derived DOM in coastal areas. The predicted functional profiles suggested the lower abundance of functional genes related to ATP-binding cassette transporters in sea ice than in seawater, which might be due to the bacteria not requiring varieties of functional genes of ATP-binding cassette transporters in restricted sea ice brine.

Keywords: cold surge, bacterial community, bacteria abundance, mid-latitude, sea ice

INTRODUCTION

Human activities have caused a dramatic increase in atmospheric carbon dioxide (CO_2) concentration. Rising levels of atmospheric CO_2, in turn, have led to global temperature rise and climate change (Alexander et al., 2006; Hansen et al., 2006). Previous studies have indicated that the frequent cold surges in Eurasia are closely associated with the decreases in autumn-winter Arctic Sea ice resulting from rising temperature (Takaya and Nakamura, 2005; Petoukhov and Semenov, 2010; Park et al., 2011; Kug et al., 2015; Johnson et al., 2018). The outbreak of cold surges will be accompanied by cooling, strong winds, rain, snow, and other extreme weather phenomena, causing frost, rime, and other disasters (Liu et al., 2012). Temperature is one of the most important factors affecting microbial microorganism growth, and the suitable temperature is within a certain range

for bacteria (Ewert and Deming, 2014). The occurrence of cold surges is coupled with a sharp drop in temperature, which may have an inevitable impact on microorganisms, due to the inability to adapt quickly to sustain their regular metabolic functions (Shivaji and Prakash, 2010; Subramanian et al., 2011). Low temperature also creates favorable conditions for the formation of sea ice. In high-latitude regions, it was found that both bacteria and algae experienced a strong metabolic inhibition during the ice formation (Grossmann and Gleitz, 1993), and the ice formation and growth reshaped bacterial community structure in drift ice (Eronen-Rasimus et al., 2015). However, few studies were conducted in mid-latitude regions (Xu et al., 2012). During the formation and growth of sea ice, organic and inorganic components dissolved in seawater are concentrated into the brine (Duprat et al., 2020). Internal channels with highly saline brine establish and create distinct habitats for microbial communities, encompassing members such as algae, bacteria, and viruses from seawater (Lund-Hansen et al., 2020). The activity of microbes in sea ice is greatly affected by environmental variables such as temperature, brine salinity, nutrients, and organic matter, which are different from seawater (Torstensson et al., 2018; Piontek et al., 2020). As the most abundant cellular lives in the ocean, bacteria play an essential role in the marine microbial loop (Azam et al., 1983). The transformation of various forms of carbon by bacterial activities is an important regulator of global carbon fluxes in marine environments and is of profound importance for marine ecosystems (Azam et al., 1983; Jiao et al., 2010, 2014; Zhao et al., 2019). Bacteria are carried from seawater into the formed sea ice matrix, and succession and development of bacterial communities were found along with ice-type changes (Eronen-Rasimus et al., 2015). Compared to the bacteria in high-latitude regions which may have adapted to the low temperature and the formation of sea ice, the bacterial community in mid-latitude regions where sea ice barely happened may have different strategies to the formation of sea ice, especially when the ice formation happened in a very short period.

In the context of global climate change, how bacterial communities vary from seawater to sea ice during the abrupt temperature drop and icing caused by cold surges in mid-latitude regions, where sea ice formation was seldom observed in the past, is poorly known. In this study, we examined the differences in bacterial community between the sea ice and seawater directly after the cold surge in January 2021 to understand the impact of ice formation on bacteria abundance (BA) and community composition.

MATERIALS AND METHODS

Site Description and Sample Collection

Aoshan Bay is a semi-enclosed coastal inlet located in southern Yellow Sea, China. Given its geographical location and climatic conditions, the minimum air temperature in winter around the bay is typically above −5°C (Guo et al., 2014), and the sea fluidity and the sunlight radiation during the day merely meet the conditions for ice formation. However, a cold surge occurred in East Asia on January 6th, 2021 and lasted for 3 days, during which the minimum air temperature in this bay reached −14°C and massive sea ice appeared on the shore and lasted for 7 days. On January 11th, the ice and seawater samples around Aoshan Bay were collected to investigate the change of bacterial community. Samples were taken from three sites, among which two sites (S1 and S2) were located in the inner bay and one (S3) in the outer bay (**Figure 1**). Ice thickness ranged from 30 to 50 mm, and the *in situ* temperature of ice was measured by inserting a needle temperature probe (TP101) into ice core, with a precision of ± 0.1°C. The sea ice was collected using a stainless-steel saw to cut chunks from the thin ice and placed into polypropylene bags. Air was gently removed from the bag using a vacuum pump (H1, Reelanx). In addition, under-ice seawater samples were directly collected using 1-L HDPE bottles.

Sample Processing and Analysis

After returning to laboratory, the sea ice was melted in the dark at room temperature and processed immediately after melting completely. The salinity of the melted sea ice and seawater was measured with a salinity meter (Orion star A212, Thermo Scientific, United States). Brine salinity (S_{brine}) was calculated from ice temperature using the equation: S_{brine} = 1,000/[1-(54.11/T)] (Cox and Weeks, 1983). After this, the melted ice and seawater samples were separately filtered through 0.2-μm-pore-size polycarbonate membrane filters (25 mm diameter; Millipore), and the filters were then stored in cryotubes at −80°C for later DNA extraction. At the same time, 30 mL of melted sea ice and seawater were separately filtered through 0.45-μm-pore-size membrane filters (Millipore), and the filtrates were stored at −20°C for nutrients analysis. Nutrient concentrations including nitrite, nitrate, ammonium, silicate and phosphate, were measured using a segmented flow analyzer (SEAL Analytical Ltd., AA3 HR Autoanalyzer) according to

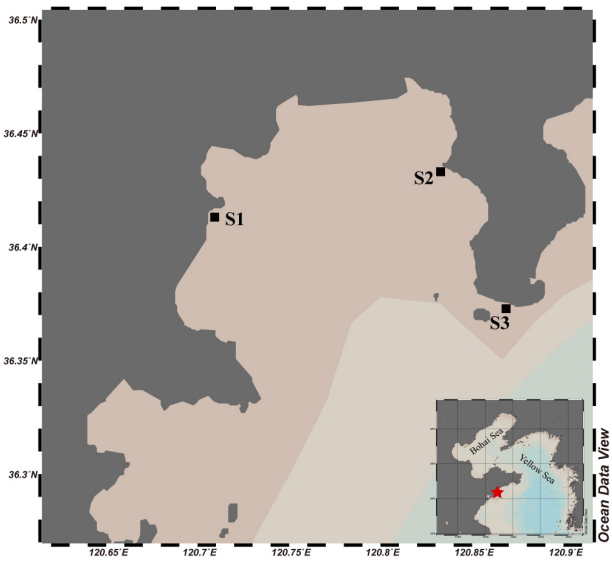

FIGURE 1 | Map of Aoshan Bay with the squares showing the sampling stations. The water color indicates the relative depth of the water column.

the classical colorimetric methods (Grasshoff et al., 1999). The detection limits for all channels were 0.1 μmol kg^{-1}. 500 mL of melted sea ice or seawater was filtered on a pre-combusted glass fiber filter (25-mm, Whatman GF/F), and the filter and aliquots of 30 mL of filtration were stored at −20°C for chlorophyll a (Chl-a) and dissolved organic carbon (DOC) analysis, respectively. Chl-a was extracted overnight by immersing the GF/F filter into 90% acetone solution and was measured with a Cary Eclipse spectrofluorometer (Agilent Technologies, Santa Clara, CA) (Pinhassi et al., 2004). DOC was measured using the high-temperature combustion method with a TOC-L analyzer (Shimadzu, Japan) (Liu et al., 2020). Samples of seawater and melted sea ice were pre-filtrated through a 20-μm nylon mesh, then fixed with glutaraldehyde at 1% final concentration and stored at −80°C for BA analysis. After staining with SYBR Green I Nucleic Acid Gel Stain (Invitrogen) for 10 min in the dark, the bacteria cell counting was performed with a flow cytometer (Accuri C6, Becton-Dickinson, United States), according to side scattering light (SSC) and green fluorescence (FL1) (Li et al., 2018). Nutrients, Chl-a, DOC, and BA data of sea ice were normalized to brine concentration to correct for dilution during melting, and normalized salinity (C_{brine}) were calculated following the equation of $C_{brine} = C_{bulk}$ (S_{brine}/S_{bulk}), where C_{bulk} was the measured concentration in bulk sea ice; S_{brine} was the brine salinity and S_{bulk} was the measured salinity of the melted ice (Cox and Weeks, 1983). The sample at site S3 for nitrate determination in sea ice was contaminated, so the data was discarded.

DNA Extraction Amplification and Sequencing

DNA was extracted from 0.2-μm-pore-size membrane filters (Millipore) using DNeasy PowerSoil Kit (Qiagen, Germany) (Zhao et al., 2021). The V3–V4 region of 16S rRNA genes was amplified using primer pairs 341F (5′-CCTAYGGGRBGCASCAG-3′) and 806R (5′-GGACTACNNGGGTATCTAAT-3′) (Liu et al., 2019), and the amplicons were sequenced using the Illumina MiSeq platform.

Bioinformatic and Statistical Analysis

Demultiplexing and quality filtering of raw sequences were conducted in QIIME2 (Bolyen et al., 2019), where amplicon sequencing variants (ASVs) were generated with DADA2 and classified against the SILVA 138 database (Robeson et al., 2020). Sequences assigned to archaea, chloroplast and mitochondrion were removed from the dataset. Sequencing data from each sample were normalized based on the smallest sample size to avoid potential bias caused by sequencing depth. All sequence data were rarefied to 66,141 sequences per sample for bacterial diversity analyses. To determine whether alpha diversity differs across samples, a variety of alpha diversity indices were calculated, including Shannon (diversity) and Pielou (evenness) index (Shannon, 1948). To estimate similarity among samples, hierarchical cluster analysis was also conducted based on a matrix of different ASVs and their abundance in each sample using Bray-Curtis dissimilarity calculated using vegan (R package) and a dendrogram inferred with the unweighted pair-group average algorithm (UPGMA) (Ortega-Retuerta et al., 2013). The BAs of sea ice and seawater were compared using a two-group White's non-parametric *t*-test in STAMP (Parks et al., 2014). To compare the differences in the bacterial community composition between sea ice and seawater, Bray-Curtis distance-based principal coordinate analysis (PCoA) was conducted in the R package "vegan" (Oksanen et al., 2019). The correlation matrix among different environment parameters was obtained using the function "cor," and the plot was obtained using the function "corrplot" of the "corrplot" package on R4.1.1. The predicted functional analysis was performed by Tax4Fun2 v. 1.1.5 software to explore the functional gene content in the bacterial community based on the 16S rRNA sequencing data (Wemheuer et al., 2020). The differences of functional genes or pathways between sea ice and seawater were compared using *t*-test in STAMP (Parks et al., 2014).

RESULTS

Biochemical Environmental Parameters

The brine salinity of sea ice varied between 35.64 and 55.84, and the salinity in seawater ranged from 32.23 to 40.37 (**Table 1**). The temperature in seawater was around −1.1°C, while the temperature in sea ice varied from −3.2 to −2.0°C. Salinity between the seawater and sea ice (brine salinity) were similar at site S1, while the brine salinity of sea ice was higher than that of seawater at site S2 and S3. Nitrate concentrations in seawater were different among the three sampling sites, whereas the nitrite, ammonium, silicate, and phosphorus were more homogenous. The nutrient concentration of sea ice was higher, particularly at site S2. The DOC concentrations of seawater and sea ice ranged from 168.1 to 219.0 and from 211.7 to 552.2 μmol kg^{-1}, respectively. Higher DOC concentrations in seawater and ice were found at sites S1 and S2, individually. Seawater at sites S2 and S3 showed a high concentration of Chl-a. The Chl-a concentration in sea ice was lower than that in seawater, and that at site S1 was the lowest among the three sites. The BA in seawater varied from 1.4×10^6 to 1.6×10^6 cells mL^{-1}, and the maximum abundance was observed at site S2 (**Figure 2**). Brine-scaled sea-ice BA distribution was similar to bacteria in seawater and the abundance of bacteria at site S2 was the highest, and BA in seawater was lower than that observed in sea ice.

Bacterial Diversity and Community Composition

Community diversity based on Shannon diversity index and evenness of the community reflected by the Pielou's index showed that diversity and evenness of the sea ice bacterial assemblages were similar to those of corresponding seawater assemblages (**Figure 3**). A total of nine bacterial phyla were identified in all samples. *Proteobacteria* were the dominant phylum existed in both sea ice and seawater samples, accounting for more than 70% of the whole bacterial community (**Figure 4A**). Phyla of *Bacteroidota*, *Actinobacteriota,* and *Verrucomicrobiota* were also detected in each sample, but their relative abundances

TABLE 1 | Salinity (S), temperature (T), nutrients (μmol kg^{-1}), dissolved organic carbon (DOC), and Chl-a concentrations in seawater and sea ice.

Samples	Sample type	S	T (°C)	NO_2^- (μmol kg^{-1})	NO_3^- (μmol kg^{-1})	NH_4^+ (μmol kg^{-1})	SiO_3^{2-} (μmol kg^{-1})	PO_4^{3-} (μmol kg^{-1})	DOC (μmol kg^{-1})	Chl-a (μg L^{-1})
S1	Seawater	40.37	−1.0	0.45	3.78	2.81	5.10	0.08	219.0	0.68
	Sea ice	39.07	−2.2	0.82	4.74	16.68	5.73	0.18	211.7	0.05
S2	Seawater	33.05	−1.2	0.22	16.37	1.44	5.79	0.07	201.1	2.37
	Sea ice	55.84	−3.2	2.88	14.97	33.20	20.36	0.89	552.2	1.97
S3	Seawater	32.23	−1.0	0.24	12.05	0.57	4.78	0.02	168.1	1.64
	Sea ice	35.64	−2.0	1.15	–	6.50	11.84	0.15	218.2	1.33

All parameters in sea ice are scaled to brine volume.

were much lower. *Actinobacteriota* were more abundant in seawater, while *Verrucomicrobiota* were more abundant in sea ice. *Alphaproteobacteria* (31.7–60.0%), *Gammaproteobacteria* (20.6–48.9%), *Bacteroidia* (7.2–10.6%), *Verrucomicrobiae* (1.8–7.0%), *Acidimicrobiia* (1.1–7.3%), and *Actinobacteria* (0.7–2.4%) were determined as six major classes of bacteria among six samples (**Figure 4B**). The relative abundance of *Alphaproteobacteria* in seawater (45.0–60%) was higher than that in sea ice (31.7–38.9%), as well as *Acidimicrobiia*. While *Gammaproteobacteria* were more abundant in sea ice. *Verrucomicrobiae* followed the same pattern as *Gammaproteobacteria*. *Bacteroidia* and *Actinobacteria* showed variable abundance patterns in the samples. PCoA was used to evaluate the overall differences between sea ice and seawater bacterial communities based on Bray-Curtis distance (**Figure 5A**). PCo1 and PCo2 explained 52 and 33%, respectively, of the variance among the 6 samples, giving a total of 85% of the variance (**Figure 5A**). PCo1 grouped the samples into two major components: the samples of sea ice with negative PCo1 values and the samples of seawater ($S2_{sw}$ and $S3_{sw}$) with positive PCo1 values, except for the sample of $S1_{sw}$ with a negative PCo1 value. On the PCo2 axis, $S1_{ice}$ and $S1_{sw}$ (with high positive PCo2 values) and $S2_{ice}$ and $S3_{ice}$ (with high negative PCo2 values) samples were mainly responsible for the variance. Seawater samples were clustered together but separated from ice samples, indicating high similarity among the bacterial communities in sea ice or seawater. In addition, UPGMA clustering dendrogram supported the result of the PCoA analysis by revealing the distinctiveness of bacterial communities in sea ice and seawater, except for the samples at site S1, where the seawater sample was clustered with sea ice (**Figure 5B**). The most significant differences ($p < 0.05$) between seawater and sea ice at class level were related to *Alphaproteobacteria* and *Gammaproteobacteria*. *Alphaproteobacteria* were significantly more abundant in seawater, whereas *Gammaproteobacteria*, *Verrucomicrobiae*, *Bacilli*, and *Desulfobulbia* were significantly more abundant in sea ice (**Figure 5C**).

The predicted functional analyses of 6 samples were carried out by Tax4Fun2 tools. A total of 46 KEGG subsystems presented at level 2 were found in samples, of which a total of 359 pathways were included in the subsystems. The pathways of the top 20 relative abundance were shown in **Supplementary Figure 1**, and the pathways with relatively high abundance obtained in different samples include: metabolic pathways, biosynthesis of secondary metabolites, biosynthesis of antibiotics, membrane transport, and ATP-binding cassette (ABC) transporters. Stamp analysis and *t*-test revealed the pathway of ABC transporters was significantly different between seawater and sea ice. Further analysis of the functional genes involved in ABC transporters indicated that genes encoding for oligopeptide transport system ATP-binding protein (*oppF*), oligopeptide transport system ATP-binding protein (*malK*), dipeptide transport system permease protein (*dppB*), raffinose/stachyose/melibiose transport system permease protein (*msmF*), and putative aldouronate transport system permease protein (*lplB*) were more abundant in seawater (**Figure 6**).

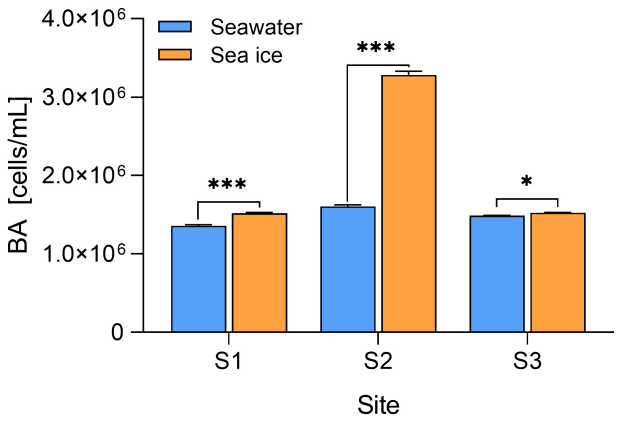

FIGURE 2 | Bacteria abundance (BA) in seawater and sea ice. The BA in sea ice is scaled to brine volume. Error bars are SDs ($n = 3$). Level of significance: $^*p < 0.05$; $^{***}p < 0.001$.

DISCUSSION

Seawater and sea ice exhibited differences in terms of chemical properties and bacterial community. The decline of temperature reduced the fraction of the liquid remaining in sea ice with the result that the salinity and nutrients became increasingly concentrated in the brine, as well as dissolved organic components (**Table 1**). The high salinity of seawater at S1 might be due to the shallow water depth, where salt expulsion during sea ice formation caused an increase in salinity in the under-ice seawater column. The concentration of DOC in sea ice at site S2 was higher than that at the other two sites,

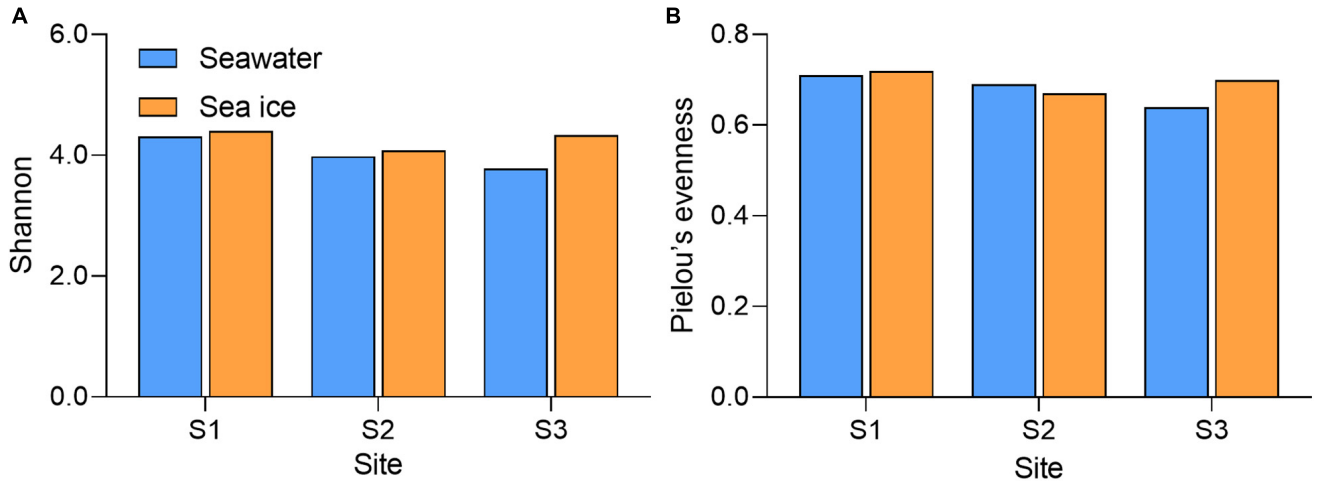

FIGURE 3 | Bacterial community diversity **(A)** and evenness **(B)** in the seawater and sea ice.

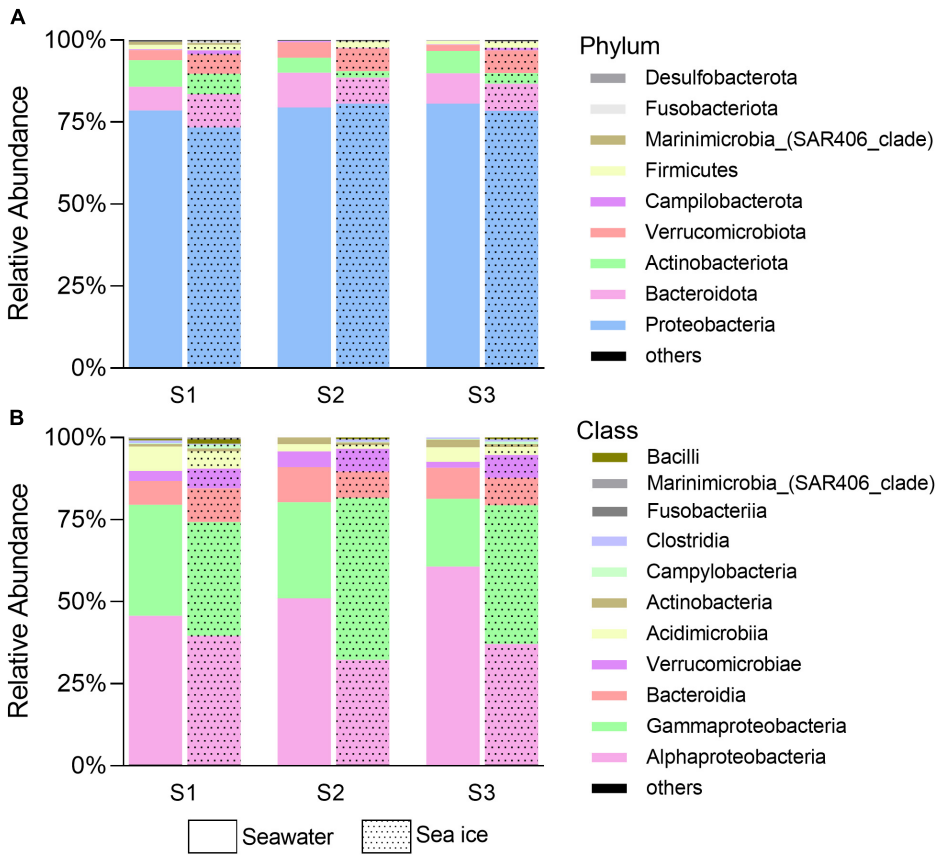

FIGURE 4 | Bacterial community in phylum **(A)** and class **(B)** level in seawater and sea ice. Others denote the sum of rare bacteria arbitrarily defined as having a frequency of < 0.5% of total sequences.

which might be explained by the high concentration of Chl-a in sea ice (Eronen-Rasimus et al., 2014). Cold surges caused nearshore seawater to change from liquid to ice, where changes in physical conditions drove bacterial communities to adapt to the lifestyle in sea ice, and the community variations were consistent with previous studies in the Arctic (Grossmann and Gleitz, 1993; Eronen-Rasimus et al., 2015; Hatam et al., 2016). The BA in the sea ice was higher ($p < 0.05$) than that in the

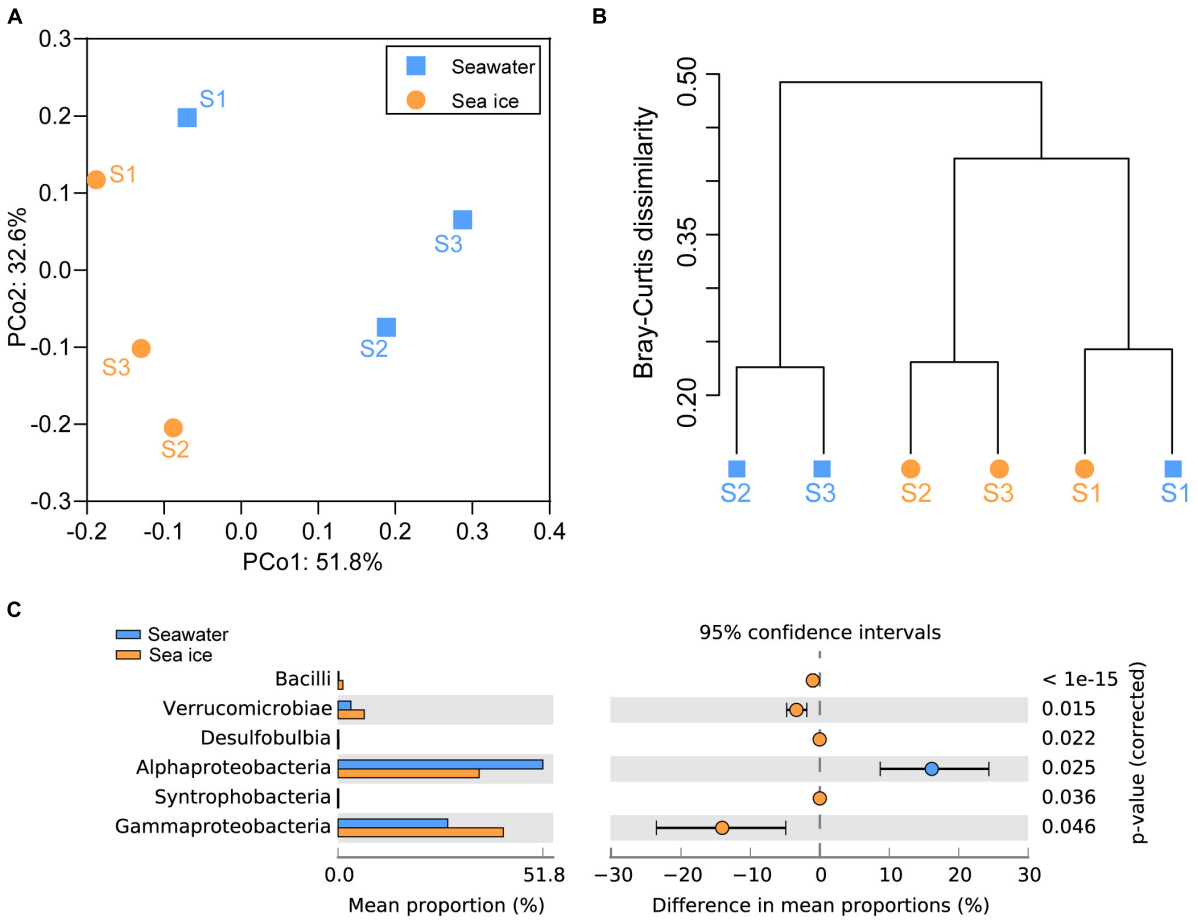

FIGURE 5 | Relationships between the bacterial communities in seawater and sea ice. **(A)** Principal coordinates analysis (PCoA) plot of Bray–Curtis distances for bacterial communities in seawater and sea ice. **(B)** Dendrogram from the cluster analysis of the relationship between bacterial communities in seawater and sea ice samples. **(C)** Comparison (White's non-parametric *t*-test in STAMP) of the bacterial classes between seawater and sea ice. Plots compare the bacteria in seawater (blue) to that in sea ice (orange). Only differences with a *p*-value less than 0.05 are shown.

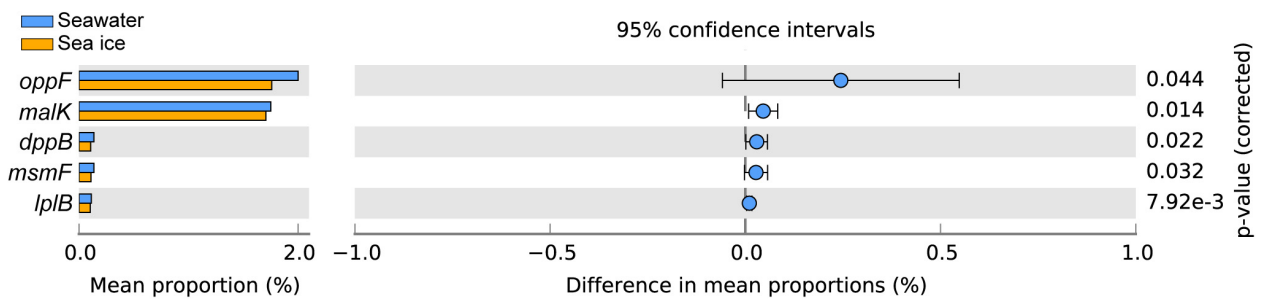

FIGURE 6 | Statistical analysis of functional genes in pathway of ATP-binding cassette transporters in seawater and sea ice. Differences between samples are shown at 95% confidence intervals.

seawater at each site, which might be due to that the bacteria were concentrated in the brine inclusions during the ice formation (Eronen-Rasimus et al., 2014). In addition, the high BA of S2 may be related to the high DOC concentration in sea ice, suggesting that bacterial metabolism might be regulated by the DOC availability (Lu et al., 2015). Differences in the bacterial community composition were observed both at phylum and class levels between seawater and sea ice. The result suggested that bacterial community similarity within sea ice or seawater was higher than geographic distance. Pressure caused by ice formation was a stronger factor to shape the community compared to geographical

distance (Eronen-Rasimus et al., 2015). However, the difference in community composition was not apparent as a result of the short time of ice formation. The same bacterial classes were found in both seawater and sea ice, while the difference between seawater and sea ice was mainly reflected in the relative abundance of different classes, indicating that the early stage of sea-ice bacterial communities was determined by seawater under the ice (Eronen-Rasimus et al., 2015). Due to the versatile metabolism, *Proteobacteria* were dominant in both sea ice and seawater in all locations, and formation of sea ice did not alter the proportion of *Proteobacteria* in entire bacterial community. However, due to the change of the condition, it is clear that the relative abundance at class level within *Proteobacteria* changed during the formation of sea ice. The classes *Alphaproteobacteria* and *Gammaproteobacteria* dominated the bacterial communities, consistent with the previous study of the seawater bacterial communities in the Yellow Sea (Guo et al., 2011; Liu et al., 2013). *Gammaproteobacteria* were the most abundant class in the sea ice, and *Gammaproteobacteria* dominance in the initial phases of ice formation was also found in an experimental study where the cultivation was enriched with algal-derived DOM (Eronen-Rasimus et al., 2014). Mid-latitude regions with high abundance of algae might stimulate the growth of *Gammaproteobacteria*. In addition to the dominant bacterial classes, a high relative abundance of *Verrucomicrobiae* was found in the sea ice compared with that in seawater ($p < 0.05$) (**Figure 5C**), and it could be found in sea ice in the polar regions (Bowman et al., 2012; Freitas et al., 2012; Hatam et al., 2014). Previous study indicated that class *Verrucomicrobiae* preferred a particle-attached life style (Chiang et al., 2018), and the phytoplankton concentrated in the brine during the formation of sea ice might stimulate bacterial growth. The sequences affiliated with the class *Bacilli* were in very low levels in both environments but more abundant in sea ice, probably due to the ability to survive in sea ice, which was also found in Arctic Sea ice (Han et al., 2014). The class *Acidimicrobiia* and *Actinobacteria*, of the phylum *Actinobacteriota*, were the other two major bacterial groups inhabiting sea ice and seawater, and the relative abundances in seawater were higher than in sea ice. Previous reports indicated that *Actinobacteriota* was not only commonly seen in seawater (Lu et al., 2015; Yu et al., 2018), but also present in sea ice (Brinkmeyer et al., 2004; Eronen-Rasimus et al., 2015). It was found that *Actinobacteria* favored a low salinity habitat, and the abundance of *Actinobacteriota* decreased in ice with high brine salinity (Eronen-Rasimus et al., 2015). The phenomenon of higher abundance of ABC transporters in seawater might be explained by that diverse substrates could be utilized in seawater and bacteria may therefore require various ABC systems (Garmory and Titball, 2004), while the substrates are more specific in the restricted young sea ice brine.

CONCLUSION

This study investigated the bacterial community in seawater and sea ice after a cold surge in the coastal area of the mid-latitude. The differences in bacteria abundance (BA) between sea ice and seawater might be associated with the physical impact of ice formation, and BA in sea ice was higher than in seawater, which was consistent with the findings in Arctic. The bacterial community composition in sea ice was similar to that in seawater, while the relative abundances were significantly different. The sea-ice bacterial community was dominated by *Gammaproteobacteria*, which could be capable of opportunistic growth in sea ice with high concentration of algal-derived DOM in coastal areas, and the high relative abundance of *Verrucomicrobiae* in sea ice might also be that. The relatively lower abundance of functional genes of ATP-binding cassette transporters in sea ice might result from the restricted environment in sea ice brine. More works need be done to investigate the impact of cold surges on microbial communities in mid-latitudes along with global climate change.

DATA AVAILABILITY STATEMENT

The datasets presented in this study can be found in online repositories. The names of the repository/repositories and accession number(s) can be found below: NCBI (accession: PRJNA797534).

AUTHOR CONTRIBUTIONS

YH designed the research. HR analyzed the data and drafted the manuscript. YH, JL, GL, and HR discussed the interpretation of the results. All authors agreed to authorship and approved the manuscript submission.

FUNDING

This work was financially supported by the Key Research and Development Program of Shandong Province (2020ZLYS04), the National Natural Science Foundation of China (41806094), the National Key Research and Development Program of China (2020YFA0608300), the Joint Funds of the National Natural Science Foundation of China (U1906216), and the Young Scholars Program of Shandong University (2018WLJH43).

ACKNOWLEDGMENTS

We would like to especially thank Xianzhe Gong for the internal review of this manuscript.

SUPPLEMENTARY MATERIAL

The Supplementary Material for this article can be found online at: https://www.frontiersin.org/articles/10.3389/fmars.2022.856110/full#supplementary-material

REFERENCES

Alexander, L. V., Zhang, X., Peterson, T. C., Caesar, J., Gleason, B., Tank, A. M. G. K., et al. (2006). Global observed changes in daily climate extremes of temperature and precipitation. *J. Geophys. Res. Atmos.* 111:D05109. doi: 10.1029/2005jd006290

Azam, F., Fenchel, T., Field, J. G., Gray, J. S., Meyerreil, L. A., and Thingstad, F. (1983). The ecological role of water-column microbes in the sea. *Mar. Ecol. Prog. Ser.* 10, 257–263. doi: 10.3354/meps010257

Bolyen, E., Rideout, J. R., Dillon, M. R., Bokulich, N. A., Abnet, C. C., Al-Ghalith, G. A., et al. (2019). Reproducible, interactive, scalable and extensible microbiome data science using QIIME 2. *Nat. Biotechnol.* 37, 852–857. doi: 10.1038/s41587-019-0209-9

Bowman, J. S., Rasmussen, S., Blom, N., Deming, J. W., Rysgaard, S., and Sicheritz-Ponten, T. (2012). Microbial community structure of Arctic multiyear sea ice and surface seawater by 454 sequencing of the 16S RNA gene. *ISME J.* 6, 11–20. doi: 10.1038/ismej.2011.76

Brinkmeyer, R., Glockner, F. O., Helmke, E., and Amann, R. (2004). Predominance of beta-*proteobacteria* in summer melt pools on Arctic pack ice. *Limnol. Oceanogr.* 49, 1013–1021. doi: 10.4319/lo.2004.49.4.1013

Chiang, E., Schmidt, M. L., Berry, M. A., Biddanda, B. A., Burtner, A., Johengen, T. H., et al. (2018). Verrucomicrobia are prevalent in north-temperate freshwater lakes and display class-level preferences between lake habitats. *PLoS One* 13:e0195112. doi: 10.1371/journal.pone.0195112

Cox, G. F. N., and Weeks, W. F. (1983). Equations for determining the gas and brine volumes in sea-ice samples. *J. Glaciol.* 29, 306–316. doi: 10.3189/S0022143000008364

Duprat, L., Corkill, M., Genovese, C., Townsend, A. T., Moreau, S., Meiners, K. M., et al. (2020). Nutrient distribution in East Antarctic summer sea ice: a potential iron contribution from glacial basal melt. *J. Geophys. Res. Oceans* 125:e16130. doi: 10.1029/2020JC016130

Eronen-Rasimus, E., Kaartokallio, H., Lyra, C., Autio, R., Kuosa, H., Dieckmann, G. S., et al. (2014). Bacterial community dynamics and activity in relation to dissolved organic matter availability during sea-ice formation in a mesocosm experiment. *Microbiologyopen* 3, 139–156. doi: 10.1002/mbo3.157

Eronen-Rasimus, E., Lyra, C., Rintala, J. M., Jurgens, K., Ikonen, V., and Kaartokallio, H. (2015). Ice formation and growth shape bacterial community structure in Baltic Sea drift ice. *FEMS Microbiol. Ecol.* 91, 1–13. doi: 10.1093/femsec/fiu022

Ewert, M., and Deming, J. W. (2014). Bacterial responses to fluctuations and extremes in temperature and brine salinity at the surface of Arctic winter sea ice. *FEMS Microbiol. Ecol.* 89, 476–489. doi: 10.1111/1574-6941.12363

Freitas, S., Hatosy, S., Fuhrman, J. A., Huse, S. M., Welch, D. B., Sogin, M. L., et al. (2012). Global distribution and diversity of marine Verrucomicrobia. *ISME J.* 6, 1499–1505. doi: 10.1038/ismej.2012.3

Garmory, H. S., and Titball, R. W. (2004). ATP-binding cassette transporters are targets for the development of antibacterial vaccines and therapies. *Infect. Immun.* 72, 6757–6763. doi: 10.1128/IAI.72.12.6757-6763.2004

Grasshoff, K., Kremling, K., and Ehrhardt, M. (1999). *Methods of Seawater Analysis*. Hoboken, NJ: John Wiley & Sons.

Grossmann, S., and Gleitz, M. (1993). Microbial responses to experimental sea-ice formation: implications for the establishment of Antarctic sea-ice communities. *J. Exp. Mar. Biol. Ecol.* 173, 273–289. doi: 10.1016/0022-0981(93)90058-v

Guo, C., Li, F. C., Jiang, P., Liu, Z. P., and Qin, S. (2011). Bacterial diversity in surface water of the Yellow Sea during and after a green alga tide in 2008. *Chin. J. Oceanol. Limnol.* 29, 1147–1154. doi: 10.1007/s00343-011-0264-7

Guo, Y. L., Xiong, X. J., Chen, C., Yu, L., and Guo, Y. Q. (2014). Hydro-meteorological interpretation and cause analysis on Qingdao's warmer winter. *Coast. Eng.* 33, 1–11.

Han, D., Kang, I., Ha, H. K., Kim, H. C., Kim, O. S., Lee, B. Y., et al. (2014). Bacterial communities of surface mixed layer in the Pacific sector of the western Arctic Ocean during sea-ice melting. *PLoS One* 9:e86887. doi: 10.1371/journal.pone.0086887

Hansen, J., Sato, M., Ruedy, R., Lo, K., Lea, D. W., and Medina-Elizade, M. (2006). Global temperature change. *Proc. Natl. Acad. Sci. U.S.A.* 103, 14288–14293. doi: 10.1073/pnas.0606291103

Hatam, I., Charchuk, R., Lange, B., Beckers, J., Haas, C., and Lanoil, B. (2014). Distinct bacterial assemblages reside at different depths in Arctic multiyear sea ice. *FEMS Microbiol. Ecol.* 90, 115–125. doi: 10.1111/1574-6941.12377

Hatam, I., Lange, B., Beckers, J., Haas, C., and Lanoil, B. (2016). Bacterial communities from Arctic seasonal sea ice are more compositionally variable than those from multi-year sea ice. *ISME J.* 10, 2543–2552. doi: 10.1038/ismej.2016.4

Jiao, N., Herndl, G. J., Hansell, D. A., Benner, R., Kattner, G., Wilhelm, S. W., et al. (2010). Microbial production of recalcitrant dissolved organic matter: long-term carbon storage in the global ocean. *Nat. Rev. Microbiol.* 8, 593–599. doi: 10.1038/nrmicro2386

Jiao, N., Robinson, C., Azam, F., Thomas, H., Baltar, F., Dang, H., et al. (2014). Mechanisms of microbial carbon sequestration in the ocean – future research directions. *Biogeosciences* 11, 5285–5306. doi: 10.5194/bg-11-5285-2014

Johnson, N. C., Xie, S. P., Kosaka, Y., and Li, X. (2018). Increasing occurrence of cold and warm extremes during the recent global warming slowdown. *Nat. Commun.* 9:1724. doi: 10.1038/s41467-018-04040-y

Kug, J. S., Jeong, J. H., Jang, Y. S., Kim, B. M., Folland, C. K., Min, S. K., et al. (2015). Two distinct influences of Arctic warming on cold winters over North America and East Asia. *Nat. Geosci.* 8, 759–762. doi: 10.1038/Ngeo2517

Li, G., Liu, J., Diao, Z., Jiang, X., Li, J., Ke, Z., et al. (2018). Subsurface low dissolved oxygen occurred at fresh- and saline-water intersection of the Pearl River estuary during the summer period. *Mar. Pollut. Bull.* 126, 585–591. doi: 10.1016/j.marpolbul.2017.09.061

Liu, J., Curry, J. A., Wang, H., Song, M., and Horton, R. M. (2012). Impact of declining Arctic sea ice on winter snowfall. *Proc. Natl. Acad. Sci. U.S.A.* 109, 4074–4079. doi: 10.1073/pnas.1114910109

Liu, M., Liu, L., Chen, H., Yu, Z., Yang, J. R., Xue, Y., et al. (2019). Community dynamics of free-living and particle-attached bacteria following a reservoir *Microcystis* bloom. *Sci. Total Environ.* 660, 501–511. doi: 10.1016/j.scitotenv.2018.12.414

Liu, M., Xiao, T., Sun, J., Wei, H., Wu, Y., Zhao, Y., et al. (2013). Bacterial community structures associated with a natural spring phytoplankton bloom in the Yellow Sea, China. *Deep Sea Res. II Top. Stud. Oceanogr.* 97, 85–92. doi: 10.1016/j.dsr2.2013.05.016

Liu, S., Baetge, N., Comstock, J., Opalk, K., Parsons, R., Halewood, E., et al. (2020). Stable isotope probing identifies bacterioplankton lineages capable of utilizing dissolved organic matter across a range of bioavailability. *Front. Microbiol.* 11:580397. doi: 10.3389/fmicb.2020.580397

Lu, X., Sun, S., Zhang, Y. Q., Hollibaugh, J. T., and Mou, X. (2015). Temporal and vertical distributions of bacterioplankton at the Gray's reef national marine sanctuary. *Appl. Environ. Microbiol.* 81, 910–917. doi: 10.1128/AEM.02802-14

Lund-Hansen, L. C., Sgaard, D. H., Sorrell, B. K., Gradinger, R., and Meiners, K. M. (2020). *Arctic Sea Ice Ecology: Seasonal Dynamics in Algal and Bacterial Productivity*. Berlin: Springer.

Oksanen, J., Blanchet, F. G., Kindt, R., Legendre, P., Minchin, P. R., O'Hara, R. B., et al. (2019). Vegan: community ecology package.

Ortega-Retuerta, E., Joux, F., Jeffrey, W. H., and Ghiglione, J. F. (2013). Spatial variability of particle-attached and free-living bacterial diversity in surface waters from the Mackenzie River to the Beaufort Sea (Canadian Arctic). *Biogeosciences* 10, 2747–2759. doi: 10.5194/bg-10-2747-2013

Park, T. W., Ho, C. H., Jeong, S. J., Choi, Y. S., Park, S. K., and Song, C. K. (2011). Different characteristics of cold day and cold surge frequency over East Asia in a global warming situation. *J. Geophys. Res. Atmos.* 116:D12118. doi: 10.1029/2010jd015369

Parks, D. H., Tyson, G. W., Hugenholtz, P., and Beiko, R. G. (2014). STAMP: statistical analysis of taxonomic and functional profiles. *Bioinformatics* 30, 3123–3124. doi: 10.1093/bioinformatics/btu494

Petoukhov, V., and Semenov, V. A. (2010). A link between reduced Barents-Kara sea ice and cold winter extremes over northern continents. *J. Geophys. Res. Atmos.* 115:D21111. doi: 10.1029/2009jd013568

Pinhassi, J., Sala, M. M., Havskum, H., Peters, F., Guadayol, O., Malits, A., et al. (2004). Changes in bacterioplankton composition under different phytoplankton regimens. *Appl. Environ. Microbiol.* 70, 6753–6766. doi: 10.1128/AEM.70.11.6753-6766.2004

Piontek, J., Galgani, L., Nöthig, E. M., Peeken, I., and Engel, A. (2020). Organic matter composition and heterotrophic bacterial activity at declining summer

sea ice in the central Arctic Ocean. *Limnol. Oceanogr.* 66, S343–S362. doi: 10.1002/lno.11639

Robeson, M. S., O'Rourke, D. R., Kaehler, B. D., Ziemski, M., Dillon, M. R., Foster, J. T., et al. (2020). RESCRIPt: reproducible sequence taxonomy reference database management for the masses. *bioRxiv [Preprint]* doi: 10.1101/2020.10.05.326504

Shannon, C. E. (1948). A mathematical theory of communication. *Bell Syst. Tech. J.* 27, 379–423. doi: 10.1002/j.1538-7305.1948.tb01338.x

Shivaji, S., and Prakash, J. S. (2010). How do bacteria sense and respond to low temperature? *Arch. Microbiol.* 192, 85–95. doi: 10.1007/s00203-009-0539-y

Subramanian, P., Joe, M. M., Yim, W.-J., Hong, B.-H., Tipayno, S. C., Saravanan, V. S., et al. (2011). Psychrotolerance mechanisms in cold-adapted bacteria and their perspectives as plant growth-promoting bacteria in temperate agriculture. *Korean J. Soil Sci. Fert.* 44, 625–636. doi: 10.7745/kjssf.2011.44.4.625

Takaya, K., and Nakamura, H. (2005). Mechanisms of intraseasonal amplification of the cold Siberian high. *J. Atmos. Sci.* 62, 4423–4440. doi: 10.1175/Jas3629.1

Torstensson, A., Fransson, A., Currie, K., Wulff, A., and Chierici, M. (2018). Microalgal photophysiology and macronutrient distribution in summer sea ice in the Amundsen and Ross Seas, Antarctica. *PLoS One* 13:e0195587. doi: 10.1371/journal.pone.0195587

Wemheuer, F., Taylor, J. A., Daniel, R., Johnston, E., Meinicke, P., Thomas, T., et al. (2020). Tax4Fun2: prediction of habitat-specific functional profiles and functional redundancy based on 16S rRNA gene sequences. *Environ. Microbiome* 15:11. doi: 10.1186/s40793-020-00358-7

Xu, Z. Y., Yang, Y. Z., Wang, G. F., Cao, W. X., Li, Z. J., and Sun, Z. H. (2012). Optical properties of sea ice in Liaodong Bay, China. *J. Geophys. Res. Oceans* 117:C03007. doi: 10.1029/2010jc006756

Yu, S. X., Pang, Y. L., Wang, Y. C., Li, J. L., and Qin, S. (2018). Distribution of bacterial communities along the spatial and environmental gradients from Bohai Sea to northern Yellow Sea. *PeerJ* 6:e4272. doi: 10.7717/peerj.4272

Zhao, D., Gao, P., Xu, L., Qu, L., Han, Y., Zheng, L., et al. (2021). Disproportionate responses between free-living and particle-attached bacteria during the transition to oxygen-deficient zones in the Bohai Seawater. *Sci. Total Environ.* 791:148097. doi: 10.1016/j.scitotenv.2021.148097

Zhao, Z., Gonsior, M., Schmitt-Kopplin, P., Zhan, Y., Zhang, R., Jiao, N., et al. (2019). Microbial transformation of virus-induced dissolved organic matter from picocyanobacteria: coupling of bacterial diversity and DOM chemodiversity. *ISME J.* 13, 2551–2565. doi: 10.1038/s41396-019-0449-1

Conflict of Interest: The authors declare that the research was conducted in the absence of any commercial or financial relationships that could be construed as a potential conflict of interest.

Publisher's Note: All claims expressed in this article are solely those of the authors and do not necessarily represent those of their affiliated organizations, or those of the publisher, the editors and the reviewers. Any product that may be evaluated in this article, or claim that may be made by its manufacturer, is not guaranteed or endorsed by the publisher.

frontiers | Frontiers in Marine Science

TYPE Original Research
PUBLISHED 22 July 2022
DOI 10.3389/fmars.2022.898904

OPEN ACCESS

EDITED BY
Rodolfo Silva,
Institute of Engineering, National Autonomous University of Mexico, Mexico

REVIEWED BY
Pedro Diaz-Simal,
Environmental Hydraulics Institute (IHCantabria), Spain
Jose A. Jimenez,
Universitat Politecnica de Catalunya, Spain

*CORRESPONDENCE
Román A. Canul Turriza
roacanul@uacam.mx

SPECIALTY SECTION
This article was submitted to Coastal Ocean Processes, a section of the journal Frontiers in Marine Science

RECEIVED 18 March 2022
ACCEPTED 30 June 2022
PUBLISHED 22 July 2022

CITATION
Fernández-Díaz VZ, Canul Turriza RA, Kuc Castilla A and Hinojosa-Huerta O (2022) Loss of coastal ecosystem services in Mexico: An approach to economic valuation in the face of sea level rise.
Front. Mar. Sci. 9:898904.
doi: 10.3389/fmars.2022.898904

Loss of coastal ecosystem services in Mexico: An approach to economic valuation in the face of sea level rise

Violeta Z. Fernández-Díaz[1], Román A. Canul Turriza[2,3]*, Angel Kuc Castilla[4] and Osvel Hinojosa-Huerta[2]

[1]Facultad de Ciencias Marinas, Universidad Autónoma de Baja California, Ensenada, Mexico, [2]Cornell Lab of Ornithology, Cornell University, Ithaca, NY, United States, [3]Facultad de Ingeniería, Universidad de Campeche, Campeche, Mexico, [4]Área académica de Ingeniería Civil, Universidad Internacional Iberoamericana, Campeche, Mexico

The economic valuation of coastal ecosystem services is a critical step for the design of sound public policies that support the preservation of the services that nature provides to society in the context of climate change. Using the value transfer method, we obtained the economic valuation that represents the loss of coastal ecosystem services caused by sea level rise in Mexico. Using the Bathtub method, digital elevation models and sea level data, we identified the areas in the country prone to flooding and the associated ecosystem impacts. In Mexico, the annual economic loss caused by the disappearance of coastal ecosystem services is estimated at $6,476,402,405 USD, where wetlands represent the greatest economic losses, since they represent the largest affected ecosystem by area. However, beaches and dunes are the most valued ecosystem due to the economic activities that occur in these areas. In the mangroves, the service as habitat, refuge and nursery is the most valued for its positive relationship with fisheries. The states with the most economic losses are Baja California Sur, Sinaloa and Campeche. The protection of the coastal zone in Mexico should be a priority in the development strategies in the country because its loss and/or rehabilitation imply high economic costs and compromises the wellbeing of society.

KEYWORDS

ecosystem services, economic valuation, sea level rise, flooding, Mexico

Introduction

The importance of coastal ecosystems and the services they provided to society are widely recognized (Costanza et al., 1997a; Daily, 1997; Liu et al., 2011; de Groot et al., 2012; Barbier, 2015). People obtain benefits from these ecosystems (Nicholls et al., 2011;

Weiss et al., 2011)through the environmental services they provide to society, divided in four main categories: provisioning, regulating, cultural and supporting services (Reid et al., 2005; Aktürk and Güneroğlu, 2021). Coastal ecosystems, such as sandy beaches, dunes, mangroves, and other wetlands, provide protection against storms and coastal flooding, through their capacity as natural barriers to reduce the energy of the waves and retain sediment, they also provide refuge and nursing habitat for a diversity of species, and support recreational, aesthetic and cultural values for people (Shepard et al., 2011; Arkema et al., 2013; Barbier, 2015). In this sense, coastal ecosystems have been recently proposed as measures of adaptation and mitigation against climate change under the concept of Nature-based Solutions, as long as they remain in a healthy condition (Baustian et al., 2020; Ruckelshaus et al., 2020; Hagedoorn et al., 2021).

The provision of ecosystem services directly depends on the functionality of these ecosystems and on the natural and anthropic impacts that affect them (Mendoza-González et al., 2012); especially in the context of climate change and the continuous and accelerated sea level rise, which represents a threat for coastal ecosystems worldwide (Kopp et al., 2016). The incidence of hydro-meteorological extreme events (such as hurricanes and strong storms) could intensify (Kirezci et al., 2020), exposing coastal ecosystems to flooding and erosion, leading to their degradation and the potential loss of their services, increasing the vulnerability of coastal communities and habitats.

Therefore, the economic valuation of ecosystem services shows that coastal ecosystems are finite and that their depreciation or degradation has associated costs that negatively impact social wellbeing (Instituto Nacional de Ecología y Cambio Climático, 2021). The economic valuation of ecosystem services is the evaluation of compensations (de Groot et al., 2012), that is, the value of these services reflects the value that society is willing to exchange to conserve these natural resources. However, these valuations are not trivial, since most of the ecosystems, especially the coastal ones, do not have established prices from which their value could be derived. For this reason, different economic valuation methods are used, that allow the allocation of a monetary value for ecosystems. The benefit transfer method, also known as value transfer, has been widely used to value ecosystem services in different places and at different scales, because it allows transferring the results of existing valuation studies to other sites with similar ecosystems and beneficiaries, reducing time and costs (Reid et al., 2005; Bishop, 2010; Liu et al., 2011; Mendoza-González et al., 2012; Brander, 2013).

Mexico is a country rich in ecosystems, a reason that has led to the development of diverse studies for the identification, description, prioritization, and economic valuation of its services (Margulis, 1992; Loa, 1994; Barbier Strand Ivar, 1998; Sanjurjo, 2001; Mendoza-González et al., 2012; Camacho-Valdéz et al., 2013; Lithgow et al., 2017; Instituto Nacional de Ecología y Cambio Climático, 2021). However, the valuation of ecosystem services losses that might result from sea level rise in Mexico is practically non-existent. Therefore, in this paper we present an approach to the economic valuation of the loss of ecosystem services provided by mangroves, sandy beaches and dunes, and wetlands in Mexico, in the face of sea level rise by the end of the 21st century. In the results we identify the areas of the Mexican coast prone to flooding associated with sea level rise and an approximation to the economic valuation of this potential loss. We also identify the states most affected by the loss of coastal ecosystems and their services, considering that this information can be used for decision-making in coastal management and for the implementation of actions that could lead to improving their resilience and can in the long term serve as protection options against sea level rise in Mexico.

Materials and methods

Study area

Mexico has a privileged geographic location, with access to the Pacific Ocean, the Gulf of California, the Gulf of Mexico and the Caribbean Sea. The coastal extent in the country is 11,122 km, with 3,149,920 km of Territorial Sea and Exclusive Economic Zone, in addition to a wide continental shelf and insular territory that together provide diverse coastal ecosystems and resources (Instituto Nacional de Ecología y Cambio Climático, 2021). Due to the heterogeneity of the Mexican coast (Silva et al., 2011), we divided the country in four marine regions, hosting 70 coastal and marine priority areas for their high biodiversity, the importance of their resources and the level of threats they face. These regions are: 1) Region I Northern Pacific and Gulf of California, a marginal sea characterized by having a diversity of coastal environments and interior islands, with natural landscapes and conservation status valued worldwide. The Pacific is characterized by the presence of large systems of coastal sand dunes, as well as numerous bays that provide refuge, breeding and nursing habitats for whales. 2) Region II Central Pacific and 3) Region III Southern Pacific harbor an important number of coastal lagoons, estuarine systems, bays, sand bars and sandy beaches. The spatial orientation of the coastline made this region vulnerable to the impact of extreme wave effects and sea level rise. 4) Region IV Gulf of Mexico and Caribbean Sea, some of the largest and most productive coastal lagoons of the country are located in this region, as well as estuarine zones, coastal marshes, mangroves, coral reefs and rocky shoals that provide habitat for priority species (Figure 1).

Of all the coastal ecosystems in these regions, the sandy beaches, coastal dunes, mangroves, and other wetlands are of particular relevance due the ecosystem services they provide,

FIGURE 1
Coastal and marine priority regions in Mexico. Modified from Arriaga Cabrera et al. (1998).

including natural protection against extreme wave action, erosion control, refuge and nursery habitat, aesthetic and recreation values (Reid et al., 2005; Ramsar, 2013). Mexico is one of the countries in Latin America with highest proportion of exposed low coastal zones, which makes it especially vulnerable to sea level rise and degradation of its coastal ecosystems (Romero et al., 2012; Silva et al., 2014; Lithgow et al., 2017). The sea level data measured in tidal stations in Mexico are limited and not very robust, which impairs their reliability to develop future projections for the country. This has led to using scenarios presented by international institutions such as the IPCC, to implement research to assess the adverse effects of sea level rise in the country, as is the case of coastal flooding (Zavala-Hidalgo et al., 2010).

Identifying coastal areas prone to flooding by sea level rise

In the absence of an accepted universal model, we applied the Bathtub or "bucket-fill" method, which is relatively simple and efficient to identify areas prone to flooding (Hansen, 2016; Williams and Lück-Vogel, 2020; de Lima et al., 2021). This method assumes a uniform water level increase over a specific topography, and areas are identified as "prone to flooding" where the elevation is equal or lower than the defined sea level.

Although the Bathtub has a degree of uncertainty because it is a static model and does not consider hydrodynamic effects related to wave propagation and its transformations, it is neither practical nor advisable to use detailed numerical models. given their complexity, high computational cost, and the detailed input data required for the spatial scale of this study (the entire coastal zone of Mexico). In this sense, the Bathtub method provides a good approximation for the identification of flood-prone areas when it comes to large spatial scales (Hansen, 2016). We followed the spatial analysis described by Afanador and Ruíz (2009). We used the USGS 30 m spatial resolution Shuttle Radar Topography Mission (SRTM) Digital Elevation Model (DEM) as a topographic base of the entire coastal territory of Mexico. As a flood scenario, we established seawater levels that resulted from the sum of sea level rise of +0.84 m from the long-period SSP5-8.5 (2081-2100), established by the IPCC in its Sixth Assessment Report (IPCC, 2021) and the maximum high tide recorded for 25 coastal regions of Mexico based on their meteorological and oceanographic characteristics (Dirección General de Puertos, 2001). With the results obtained from this analysis, we generated a flood map using geoprocessing tools, thus allowing the identification of areas prone to flooding along the coast of Mexico.

Area of coastal ecosystems flooded by sea level rise

Based on the land use and vegetation maps of the coasts of Mexico (SEDENA, 2015.), we identified that mangroves, wetlands, and beaches and dunes are the ecosystems that have the greatest presence throughout the country. We classified this database into three groups considering the ecosystems mentioned above, where we categorized beaches and dunes in the same group, we categorized mangroves in a group independent of wetlands due to the variety of environmental services they provide, and we

categorized all classes related to water bodies, marshes, swamps, and flood zones in the group of wetlands. For the latter we used as a reference the definition of wetland established by the Ramsar Convention (Ramsar, 2013). Finally, based on the results of the flood extent analysis obtained with the Bathtub method, and using geoprocessing tools, we determined the flood areas for each of the three coastal ecosystems in the 17 coastal Mexican states. In this way, we estimated the area of mangroves, beaches and dunes, and wetlands that could be affected by sea level rise. It is important to emphasize that due to the scale of the analysis and the diversity of ecosystems present on the coast of Mexico, we did not consider the dynamism and adaptive capacity to flooding that these ecosystems may initially show in the face of sea level rise.

Economic valuation of coastal ecosystem services loss

We obtained the approximation to the economic valuation of ecosystem loss using the value transfer methodology, taking as a basis standardized economic values of ecosystem services and quantifying the monetary cost per hectare of ecosystems located in flooded areas. We selected the ecosystem services for the assessment based on the environmental and social characteristics of the Mexican coasts and considering what would be the impact of losing these services as a consequence of degradation and/or loss of coastal ecosystems, being of greater importance those that provide protection against storms, erosion control, habitat, refuge and nursery, water supply, aesthetics and recreation (Table 1). The information needed to complete a benefit transfer valuation is available in various environmental valuation databases, including "Environmental Valuation Reference Inventory" (EVRI) and "The Economics of Ecosystems and Biodiversity" (TEEB) (McComb et al., 2006).

We use these databases and previous published research (Mendoza-González et al., 2012; Pérez-Maqueo et al., 2013a) to perform our value transfer. Overall, we found 25 valuation studies of the ecosystem services provided by the beach and coastal dunes, mangroves and wetlands, were performed in countries of Latin America like Mexico, USA, Canada, Costa Rica, Belize, as well as in countries in the European and Asian region, such as Spain, Malaysia, Thailand, Philippines, Sri Lanka, and China (Bennett and Reynolds, 1993; Barbier Strand Ivar, 1998; Lara-Domínguez et al., 1998; Sathirathai, 1998; Bann, 1999; Barbier et al., 2002; Gunawardena and Rowan, 2005; Barbier, 2007; Dissanayake and Smakhtin, 2007; Samonte-Tan et al., 2007; Tong et al., 2007; Aburto-Oropeza et al., 2008; Cooper et al., 2008; Batker et al., 2010; Brenner et al., 2010; Economics Earth, 2010; Janekarnkij, 2010; Liu et al., 2010; Tianhong et al., 2010; Kauffman, 2011; Mendoza-González et al., 2012; Molnar et al., 2012; Camacho-Valdéz et al., 2013; Pérez-Maqueo et al., 2013a; Ballard et al., 2015) (see **Tables 4–6** of **Supplementary Material**). The economic values of ecosystem services correspond to different years and methodologies, so it was necessary to standardize by adjusting them to United States dollars (US$) using the Consumer Price Index (CPI) and the Purchasing Power Parity (PPP) for the year 2020. These indicators were obtained from the World Bank (2021). Finally, we made the adjustment using the following formula (Envalue, 2007; Mendoza-González et al., 2012):

$$ESV = \frac{(value/CPI) \times 100}{PPP} \times USA\ \ PPP$$

Where:

ESV: ecosystem services value

Value: is the value in the original year in the original currency.

CPI: is an index of inflation of the source data, with a base year in 2020.

PPP: is the Purchasing Power Parity between the original currency and US$ in 2020.

The proposed methodology for the monetary quantification of environmental loss is illustrated in Figure 2, it mainly consists of 3 steps. First, the terrain heights and ecosystems available in

TABLE 1 Average yearly valuation of coastal ecosystem services for the year 2020.

Coastal ecosystem	Ecosystem services	Average valuation (2020)US$ ha^{-1} year^{-1}
Mangrove	Refuge and nursery habitat	630.75
	Erosion control	83.07
	Storm buffering	335.41
	Aesthetic and recreation	107.82
Wetland	Refuge and nursery habitat	229.04
	Water supply	550.04
	Storm buffering	715.78
	Aesthetic and recreation	155.76
Beach and dune	Storm buffering	27,429.73
	Aesthetic and recreation	9,088.38

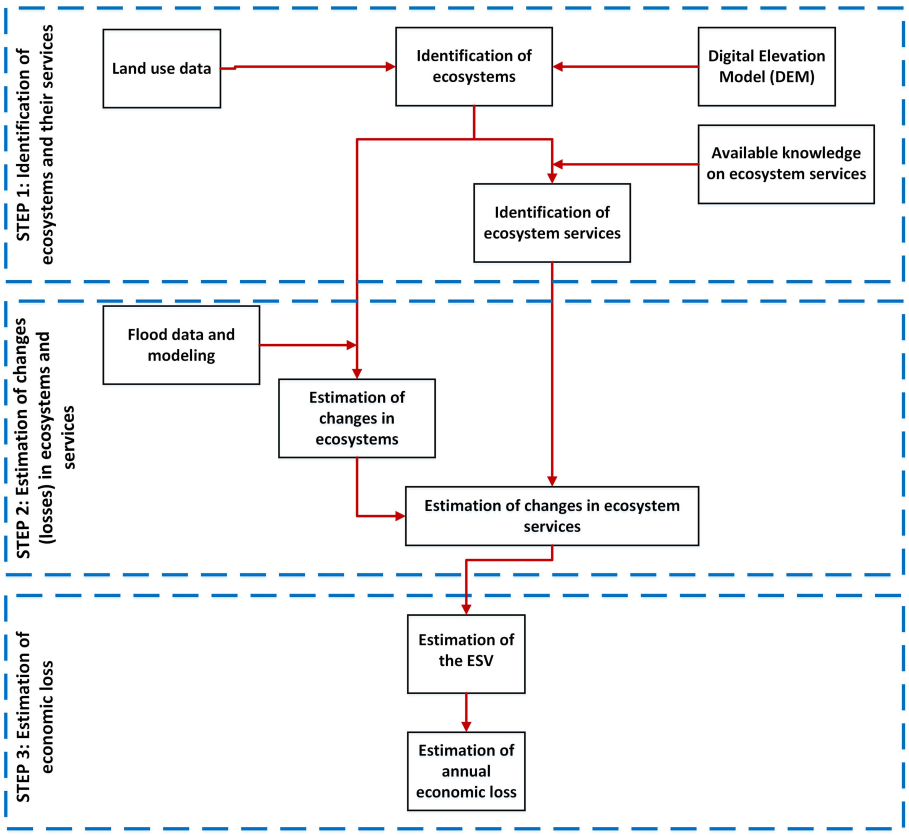

FIGURE 2
Steps of the proposed method for the estimation of economic loss for the ecosystem services losses.

the study area are identified using land and ecosystem data, the main services of each ecosystem are algo identified. Second, the changes for each ecosystem are evaluated incorporating flood data (model). Based on the estimated changes, the areas of flooded ecosystems are identified. Third, estimation of the ESV and the annual economic loss caused by the disappearance of ecosystem services in relation to sea level rise.

Results

A total of 2,715,023 ha on the Mexican coast is prone to flooding under the predicted scenario of sea level rise by the end of the century. The Gulf of California (R-I) and the Gulf of Mexico and the Caribbean Sea (R-IV) represent 46% and 45% of the total area prone to flooding, respectively. The states of Baja California, Baja California Sur, Sonora, Sinaloa, Nayarit, Tamaulipas, Veracruz, Tabasco, Campeche, Yucatán and Quintana Roo are located in these regions and present the largest potential flood extensions (Figure 3 and Table 2). The coasts of the states located in the R-II and R-III have the smallest extensions of potential flooding, with 1% and 8% of the total respectively.

Of the three ecosystems, the largest predicted loss area at the national level corresponds to wetlands, with 2,479,767 ha, which represents 91% of the total potentially affected coastal ecosystems; followed by the loss of 175,099 ha of mangroves, which represents 7%, and the loss of 60,157 ha of beaches and dunes, corresponding to 2%. Campeche, Sinaloa, Baja California Sur, Yucatán and Tabasco are the states that would lose the most mangrove area. Baja California Sur, Sinaloa, Campeche and Tamaulipas are the states that would lose the most wetland area, and Baja California Sur, Sinaloa, Sonora and Baja California would lose more beaches and dunes. On the other hand, Michoacán, Jalisco and Colima are the states with less predicted impacts on these ecosystems (Figure 3).

At the national level, we estimate that the annual economic loss caused by the disappearance of ecosystem services in relation to sea level rise would amount to $6,492,551,964 USD. The loss of mangrove services is estimated at $202,588,949 USD per year, which corresponds to 3% of the national total, where its most valued service, and therefore the one that represents the

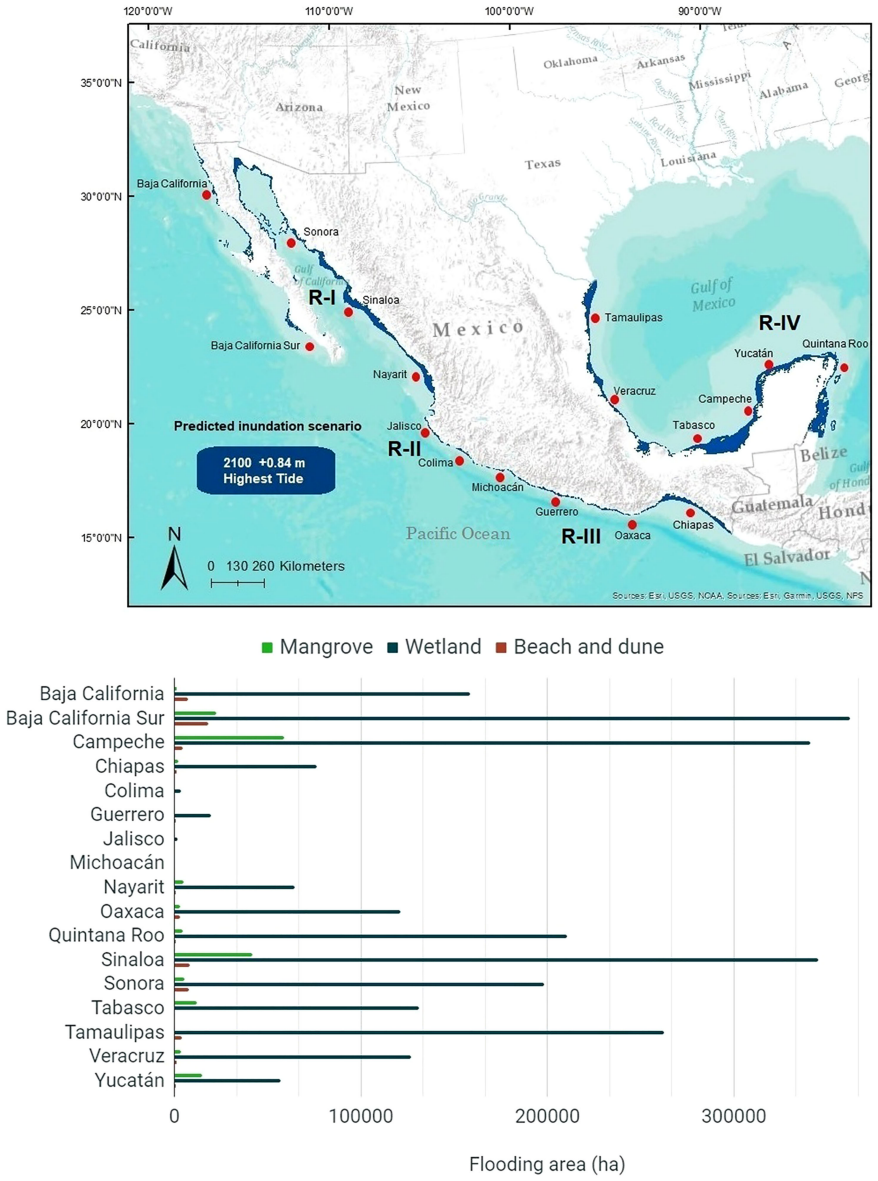

FIGURE 3
Predicted coastal flooding areas resulting from sea level rise in Mexico.

greatest economic loss, is that of shelter and nursery habitat for important commercial species. Erosion control is the least valued service (see the Supplementary Material). Campeche, Sinaloa, Baja California Sur, Yucatán and Tabasco are the states that have the greatest potential economic losses due to the effects of sea level rise on this ecosystem.

Regarding wetlands, the loss of their services represents $4,093,153,701 USD per year, corresponding to 63% of the total nationally. Baja California Sur, Sinaloa, Campeche, Tamaulipas, and Quintana Roo are the states with the greatest potential economic losses due to service decreases in this ecosystem. In the case of beaches and dunes, the loss of their services amounts to $2,196,809,314 USD per year, corresponding to 34% of the national total, where Baja California Sur, Sinaloa, Sonora, Baja California, and Campeche are the states with the greatest potential economic repercussions (Figure 4 and Table 3). For wetlands, and beaches and dunes, the most valued service is protection against storms, while the aesthetic and recreation service are less valued (see the Supplementary Material).

TABLE 2 Total area and area by ecosystem prone to flooding for the Mexican coast.

		Mangrove	Wetland	Beach and dune	Area prone to flooding (ha)
R-I	Baja California	1,394	158,772	7,226	167,392
	Baja California Sur	22,362	362,113	17,984	402,459
	Sonora	5,606	198,085	7,969	211,660
	Sinaloa	41,904	345,456	8,310	395,671
	Nayarit	4,721	64,278	781	69,781
R-II	Jalisco	29	1,832	323	2,185
	Colima	64	3,518	315	3,897
	Michoacán	39	71	54	164
	Guerrero	282	19,459	635	20,376
R-III	Oaxaca	3,016	121,258	2,999	127,273
	Chiapas	2,282	76,087	1,386	79,755
R-IV	Tamaulipas	120	262,399	4,197	266,717
	Veracruz	3,403	126,816	1,338	131,557
	Tabasco	11,997	131,256	312	143,566
	Campeche	58,820	340,934	4,607	404,361
	Yucatán	14,795	56,728	916	72,439
	Quintana Roo	4,264	210,704	802	215,770
	Total	**175,098**	**2,479,767**	**60,157**	**2,715,023**

Discussion

Ecosystems provide a large and important range of free services on which we depend. The degradation of coastal ecosystems in Mexico and the potential loss of its services due to sea level rise represents an estimated annual economic cost of $6,492,551,964 USD, corresponding to 0.6% of the country's Gross Domestic Product (GDP) for 2020. This estimated cost has a non-homogeneous distribution among the coastal ecosystems in the country, based on the valuation of their services and the area prone to flooding. Although the projections of sea level rise in Mexico are similar to global estimates, they vary regionally, showing a lower increase in the coasts of regions II and III, and higher effects in the coasts of regions I and IV (Palacio-Aponte et al., 2005; Zavala-Hidalgo et al., 2010).

Our results corroborate these observations, since the states located in regions I and IV present the largest potential flood areas in comparison with the states in regions II and III. One of the main reasons is the heterogeneous morphology of the

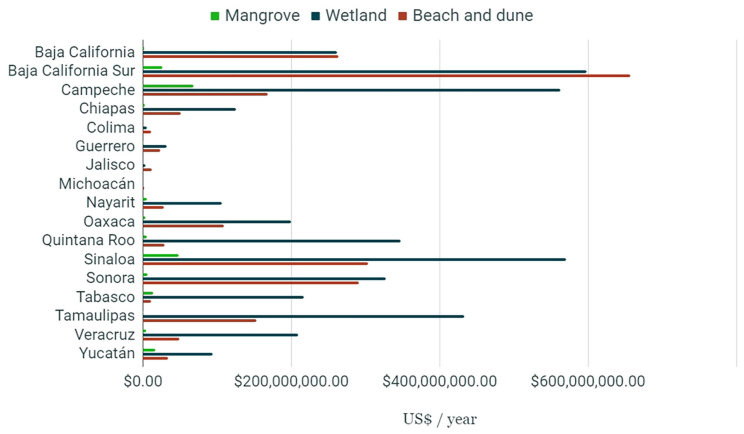

FIGURE 4
Annual economic losses by state due to the disappearance of ecosystem services in Mexico.

TABLE 3 Estimated monetary cost from the loss of services for each coastal ecosystem in Mexico.

	Ecosystem services	Total value for the loss of ecosystem servicesUS$ year^{-1}	Total national value for the loss of ecosystem servicesUS$ year^{-1}
Mangrove	Refuge and nursery habitat	110,443,370	202,588,949
	Erosion control	14,536,676	
	Storm buffering	58,729,783	
	Aesthetic and recreation	18,879,119	
Wetland	Refuge and nursery habitat	567,965,930	4,093,153,701
	Water supply	1,363,971,272	
	Storm buffering	1,774,967,925	
	Aesthetic and recreation	386,248,574	
Beach and dune	Storm buffering	1,650,082,283	2,196,809,314
	Aesthetic and recreation	546,727,031	
	Total		**6,492,551,964**

Mexican coast (Silva et al., 2014), as a result of the influence of a diversity of processes, including tectonic activity that cause vertical uprising of the earth's crust in the active regions along the Pacific (R-II and R-III) (Zavala-Hidalgo et al., 2010). This represents a critical factor in the potential degradation of ecosystems and the loss of their services.

In this sense, states such as Jalisco, Colima, Michoacán and Guerrero had lower areas prone to flooding, which means a lower probability of ecosystem degradation and lower economic losses. This was not the case of states such as Baja California Sur, Sinaloa and Campeche, located in R-I and R-IV, where vast coastal plains are common and the potential for ecosystem degradation is larger, hence the loss of services is more likely, resulting in higher potential economic costs (**Tables 2**, **4**). Studies focused on assessing the sea level rise vulnerability in Mexico at the end of this century identify severe flooding impacts in all the states along the Gulf of Mexico, as well as for Sinaloa, Baja California Sur and Sonora in the Pacific coast and Gulf of California (Ivanova and Gámez, 2012). This coincides with our results in this study. However, sea level rise maps using the bathtub method are generally only used as a communication tool to assist in illustrating the general risks of sea level rise and should not be relied on solely for decision-making purposes. This is because the maps are simple and do not consider many of the complex processes of coastal inundation. For example, the bathtub approach does not consider existing seawalls, storm surge, erosion or other local factors, which can all influence the extent of erosion from sea-level rise (Geoscience Australia, 2015).

Sandy beaches and dunes are widely distributed along the Mexican coasts. Approximately 70% of the coasts along the Pacific and the Gulf of California are sandy beaches, as is the case of 92% along the Gulf of Mexico and the Caribbean (Silva et al., 2014; CONABIO, 2022). The permanent and intense interaction between dunes and beaches is conducive to consider them as a management functional unit. In this sense, their total extension in the Mexican coasts is 808,711 hama (Martínez et al., 2014). Taking this into account and the results we obtained, the potential loss of this ecosystem due to sea level rise represents 7.5% of the national extent. Even though this ecosystem has the lower estimates of affected area by sea level rise (2%) in comparison with mangroves and wetlands (**Table 2**), their value is very significant, because the loss of their services is estimated at $2,196,809,314 USD annually, which corresponds to 54% of the economic losses of wetlands, with a much larger potential flooded area (91%) (**Table 4**).

This is due to the valuation of the services of beaches and dunes in comparison with the value assigned to other ecosystems. Beaches and dunes are very economically very important for Mexico, since the services of this ecosystem have allowed the development of economic activities associated with tourism and recreation. The arrival of international tourists has increased continuously during the last 60 years, as has the economic income related to this activity, significantly boosting the growth of some regions of the country (Martínez et al., 2014). The coasts of states located in regions I and IV, such as Quintana Roo and Baja California Sur, are the locations that have had the greatest economic growth thanks to tourism (Llamosas-Rosas et al., 2021). In this sense, there are large economic investments that would be affected by the degradation of beaches and dunes and the loss of their valuable services. The potential loss of this ecosystem and its services due to sea level rise should be of particular relevance for Mexico, due to the great economic impact that it can cause

TABLE 4 Estimated total cost caused by potential ecosystem services losses for each coastal state in Mexico.

	Mangrove ecosystem services total lossUS$ year^{-1}	Wetland ecosystem services total lossUS$ year^{-1}	Beach and dune ecosystem servicestotal lossUS$ year^{-1}	Ecosystem servicestotal lossUS$ year^{-1}
Baja California	1,612,838	262,071,490	263,885,146	527,569,474
Baja California Sur	25,872,711	597,710,708	656,748,187	1,280,331,606
Campeche	68,054,441	562,753,261	168,227,430	799,035,132
Chiapas	2,640,522	125,590,338	50,613,417	178,844,277
Colima	73,598	5,806,120	11,520,886	17,400,604
Guerrero	326,207	32,119,392	23,191,947	55,637,546
Jalisco	33,664	3,024,684	11,829,316	14,887,665
Michoacán	44,950	117,909	1,973,885	2,136,744
Nayarit	5,462,728	106,099,297	28,538,008	140,100,033
Oaxaca	3,489,403	200,150,755	109,506,896	313,147,054
Quintana Roo	4,933,325	347,792,324	29,277,467	382,003,116
Sinaloa	48,483,472	570,217,099	303,477,822	922,178,393
Sonora	6,486,229	326,962,733	291,007,124	624,456,086
Tabasco	13,880,951	216,654,438	11,398,861	241,934,250
Tamaulipas	138,912	433,121,385	153,278,162	586,538,459
Veracruz	3,936,907	209,325,422	48,877,021	262,139,350
Yucatán	17,118,091	93,636,344	33,457,740	144,212,175
	202,588,949	**4,093,153,701**	**2,196,809,314**	**6,492,551,964**

derived from the possible limitation of tourist activities and/or the need to invest in conservation measures. protection and adaptation.

However, this ecosystem is highly dynamic and has the potential to respond to changes in sea level, i.e., an upward and landward translation of the active profile in pace with rising sea level and maintaining the shape of the equilibrium profile, which decreases the protection service loss, as long as the beach has enough space to move and is not restricted by coastal infrastructure. In this regard, a sandy beach-dune system can migrate landwards, while maintaining its relative elevation and thus protective function service under sea level rise provided accommodation space and sand are available (López-Dóriga and Jiménez, 2020). Therefore, the magnitude of the physical changes and the impacts on beaches and dunes that could be caused by sea level rise will vary regionally, depending on the type of existing threats and the levels of degradation at each location. A serious and widespread problem that this ecosystem is already facing is that its physical space is becoming smaller, due to human development and other productive activities on the Mexican coastal zone, which seriously compromises its ecological integrity and makes it more vulnerable to sea level rise, increasing consequently the potential economic costs due to the loss of its services.

It is necessary to consider that we do not include shoreline changes other than sea level rise induced, and this should be equivalent to "isolating" the sea level rise component in the long-term behavior of these coastal areas. Other factors such as fluvial sediments and longshore and cross-shore sediment transport patterns would also contribute to their long-term evolution. Thus, our results provide a first approximation of the effects of sea level rise on the beaches and dunes of the Mexican coast.

The magnitude of the physical changes and the impacts on beaches and dunes that could be caused by sea level rise will vary regionally, depending on the type of existing threats and the levels of degradation at each location. However, a serious and widespread problem that this ecosystem is already facing is that its physical space is becoming smaller, due to human development and other productive activities on the coastal zone, which seriously compromises its ecological integrity and makes it more vulnerable to sea level rise, increasing consequently the potential economic costs due to the loss of its services.

Regarding wetlands, the estimated costs for the loss of their services ($4,093,153,701 USD) represent 63% of the total cost at the national level, again placing regions I and IV as the most affected, and highlighting states such as Baja California Sur, Sinaloa and Campeche with the greatest economic losses

(Table 4). Lagoons such as Ojo de Liebre and San Ignacio in Baja California Sur, have a high value as refuge and nursery habitat for the gray whale. The wetlands of Sonora and Sinaloa provide critical habitat to millions of migratory birds, a diversity of fish and endemic vegetation of high ecological value. The loss of services of this ecosystem, in addition to the high revenue related to activities such as fishing, aquaculture and tourism, would imply migration to other economic activities or adaptation by implementing protection and/or recovery programs.

The permanence and migration of coastal wetlands in Mexico will depend on the new conditions of salinity, depth and permanence of the water, as well as the conditions of anoxia that this entails in the coastal spaces that will be invaded by the increase in sea level. The anthropic pressure that has been exerted on this ecosystem is a key factor to consider, which might have already impacted its resiliency and might add to its degradation and loss. In states such as Baja California Sur, Sonora and Sinaloa, due to their arid to semi-arid climatic characteristics, wetlands are critical ecosystems for migratory birds and a diversity of species that use them to complete their annual cycles. In this sense, it is essential to generate conservation strategies for these ecosystems in the face of rising sea levels.

As well as beaches and dunes, wetlands have the ability to build up vertically by sediment accretion and the accommodation space, namely the vertical and lateral space available for fine sediments to accumulate and to be colonized by wetland vegetation. The wetlands resilience to sea level rise is primarily driven by the availability of accommodation space, which is strongly influenced by the building of anthropogenic infrastructure in the coastal zone (Schuerch et al., 2018). It has to be noted that we do not include in this approach any adaptive factors that make wetlands respond dynamically to sea level rise. Despite this, our results show an approximation of the Mexican wetland areas that would be most affected by sea level rise and where more specific analyses should be performed leading to actions to enhance resilience. The permanence and migration of coastal wetlands in Mexico will depend on the new conditions of salinity, sediment availability, depth and permanence of the water, as well as the conditions of anoxia that this entails in the coastal spaces that will be invaded by the increase in sea level. The anthropic pressure that has been exerted on this ecosystem is a key factor to consider, which might have already impacted its resiliency and might add to its degradation and loss.

Mangroves are present in all the coastal states of the country, with a coverage of 905,086 ha (CONABIO, 2022). Based on this, the loss of mangroves caused by sea level rise would represent 19% of the national coverage, generating high economic impacts in the states of Campeche, Sinaloa, Baja California Sur, Tabasco, and Yucatan (Table 4). In the Mexican Pacific, the most important mangrove forest is located in Marismas Nacionales (southern Sinaloa and northern Nayarit), a site recognized as Wetland of International Importance by the Ramsar Convention (Villanueva-Fragoso et al., 2010). Sinaloa, being the second state with the highest economic losses due to the disappearance of its mangrove services, will face an annual loss of $48,483,472 USD (Table 4). Although Nayarit is not listed among the states with the greatest losses, it is important to mention that practically the whole mangrove forest in Marismas Nacionales would be degraded.

In general, the economic loss represented by the degradation of mangroves acquires greater relevance for the refuge and nursery habitat service, due to the close relationship that exists between this ecosystem and the fishing landings of various commercial species, a well-documented phenomenon along region (Aburto-Oropeza et al., 2008). However, mangroves not only benefit commercial species. For example, throughout Mexico, mangroves are critical breeding habitat for the Reddish Egret (*Egretta rufescens*), an endangered species in Mexico and a priority bird at the continental level, and for the Bare-throated Tiger Heron (*Tigrisoma mexicanum*), a species subject to special protection in Mexico (SEMARNAT, 2010). These coastal forests also provide habitat for protected waterbirds, including the Ridgway's Rail (*Rallus obsoletus*, protected as threatened) along Baja California Sur, Sonora Sinaloa and Nayarit, and the Clapper Rail (*Rallus crepitans*, protected as endangered) in the Gulf of Mexico and the Yucatán Peninsula (SEMARNAT, 2010). Similarly, the mangroves of Yucatan are a refuge for various species of resident and migratory waterbirds, and fish and invertebrate species of great commercial value. Local communities in Tabasco use the mangrove as raw material, an activity regulated through extraction programs controlled by the Ministry of the Environment and Natural Resources (SEMARNAT) of Mexico, which allows them to have an economic income.

The estimation of the economic loss of ecosystem services allows us to discuss the importance of valuing ecosystems as first approximation for decision making, as well as allowing us to infer the economic importance for a region or state. The value of this economic loss can be compared to the GDP for each state (Table 5).

Regardless of the ecosystem type and the potential area to be lost to flooding, each of these three ecosystems has a unique ecological importance and, as a whole, their health determines the economic development potential and the social well-being of the coastal and marine zones of Mexico. The information presented here allows the identification of the coastal areas of Mexico prone to flooding due to sea level rise and the identification of coastal ecosystems at risk, as well as the economic loss that the degradation of these environmental services would represent. This information is especially relevant in the face of climate change, since the economic valuation of ecosystem services is an essential tool required to guarantee that the services that nature provides to society are quantified and considered in the formulation of sound public policies in the country (Instituto Nacional de Ecología y Cambio Climático, 2021), which will then guide conservation efforts and promote the resilience of these

TABLE 5 Comparison between the GDP of Mexico's coastal states in 2020 (in millions of GDP) and the monetary cost for the loss of ecosystem services.

State	National GDP (%)	GDP nominal (million USD)	Ecosystem servicestotal lossUS$ year^{-1}
Jalisco	7.22	77,591	14,887,665
Veracruz de Ignacio	4.51	48,412	262,139,350
Baja California	3.64	39,117	527,569,474
Sonora	3.46	37,155	624,456,086
Tamaulipas	3.09	33,180	586,538,459
Campeche	2.75	29,573	799,035,132
Tabasco	2.54	27,325	241,934,250
Michoacán de Ocampo	2.51	26,988	2,136,744
Sinaloa	2.27	24,345	922,178,393
Oaxaca	1.56	16,809	313,147,054
Yucatán	1.51	16,259	144,212,175
Chiapas	1.5	16,138	178,844,277
Guerrero	1.35	14,518	55,637,546
Quintana Roo	1.34	14,414	382,003,116
Baja California Sur	0.8	8,581	1,280,331,606
Nayarit	0.69	7,361	140,100,033
Colima	0.64	6,903	17,400,604

ecosystems over time. However, we emphasize the need to consider in similar local and regional scale studies, the dynamism of these ecosystems to respond to sea level rise, as well as socioeconomic and socioecological aspects.

Conclusions

This article provides an approximation to the economic valuation of the loss of ecosystem services caused by sea level rise by the end of the century in Mexico. At the national level, the estimated annual economic cost of the potential loss of coastal ecosystem services is $6,476,402,405 USD, distributed non-homogeneously and based on the valuation of different services in the three main ecosystem types: mangroves, wetlands, and beaches and dunes. The impacts on wetlands represent 63% of the estimated loss, mainly driven by the extent and vulnerability of this ecosystem type in the country. Beaches and dunes are extremely valued for their protection services against extreme weather events and as the basis for important economic activities. Mangroves represent a smaller proportion of the national estimate, but it is the ecosystem type that provides the most services as habitat for protected species and for commercially important fisheries. Overall, the states with highest potential economic losses are Baja California Sur, Sinaloa, Campeche, and Tamaulipas.

Although sea level rise represents a greater threat for regions I and IV and to a lesser extent for regions II and III, a broad perspective must be used to guide research and management efforts in the immediate future, to increase the relevance of science in the design of public policies and conservation strategies that can address these threats. It is critical to use a multi-disciplinary approach to define mitigation and adaptation actions to reduce the potential economic losses that are expected by sea level rise. Coastal ecosystems in Mexico should be a national priority in terms of research, protection, management, and restoration, since their loss and/or rehabilitation entails very high economic costs and compromises the well-being of society.

Quantifying the dynamic effects of sea level rise is a great challenge due to the complexity of interactions between coastal processes acting at different scales and over different time periods. In this sense, the main limitation in our analysis is sea level rise as a stable component and the lack of ecosystem dynamism to respond to sea level rise with some degree of adaptation. In this sense, the results presented here should be taken with caution, as they could represent an overestimation of the cost of the loss of the ecosystem services analyzed. Nevertheless, our results provide a first approximation for Mexico and a baseline that should be refined and compared with integrative assessments. Because each state in Mexico has physical variability in its coasts and has different degrees of ecological disturbance and presence of anthropogenic activities, specific integrative studies should be performed considering local physical characteristics, as well as the capacity of the ecosystem to respond dynamically to sea level rise.

Data availability statement

The original contributions presented in the study are included in the article/**Supplementary Material**. Further inquiries can be directed to the corresponding author.

Author contributions

VF wrote the first draft, performed analyses and performed, reviewed, and edited the manuscript. RC conceived the manuscript, collected data, performed the analyses, reviewed, and edited the manuscript. AK performed the analyses, reviewed, and edited the manuscript. OH reviewed and edited the manuscript. All authors contributed to the article and approved the submitted version.

Conflict of interest

The authors declare that the research was conducted in the absence of any commercial or financial relationships that could be construed as a potential conflict of interest.

Publisher's note

Supplementary material

The Supplementary Material for this article can be found online at: https://www.frontiersin.org/articles/10.3389/fmars.2022.898904/full#supplementary-material

References

Aburto-Oropeza, O., Ezcurra, E., Danemann, G., Valdez, V., Murray, J., and Sala, E. (2008). Mangroves in the gulf of California increase fishery yields. *Proc. Natl. Acad. Sci.* 105 (30), 10456–10459. doi: 10.1073/pnas.0804601105

Afanador, F., and RuÍz, A. (2009). "Inundación por ascenso del nivel medio del mar mediante fotografía aérea y datos lidar," in *Métodos en teledetección aplicada a la prevención de riesgos naturales en el litoral*. Eds. I. D. C. A. J. Alcántara Carrió, F. I. Isla Mendy, M. Alvarado Ortega, A. H. F. Klein, A. Cabrera Hernández and R. Sandoval (Servicio de Publicaciones del Programa Iberoamericano de Ciencia y Tecnología para el Desarrollo: España), 79–99.

Aktürk, E., and Güneroğlu, N. (2021). Degradation of coastal ecosystem services in southern black Sea: A case study of trabzon city. *Ocean Coast. Manage.* 213, 105837. doi: 10.1016/j.ocecoaman.2021.105837

Arkema, K. K., Guannel, G., Verutes, G., Wood, S. A., Guerry, A., Ruckelshaus, M., et al. (2013). Coastal habitats shield people and property from sea-level rise and storms. *Nat. Climate Change* 3 (10), 913–918. doi: 10.1038/nclimate1944

Arriaga Cabrera, L., Vázquez Domínguez, E., González Cano, J., Jiménez Rosenberg, R., Muñoz López, E., and Aguilar Sierra, V. (coordinadores). (1998). *Regiones marinas prioritarias de México*. Comisión Nacional para el Conocimiento y uso de la Biodiversidad. México.

Ballard, J., Pezda, J., and Spencer, D. (2015). *An economic valuation of southern California coastal wetlands*. Bren School of Environmental Science and Management, Santa Barbara, CA.

Bann, C. (1999). *A contigent valuation of the mangroves of benut, Johor State, Malaysia* (Report for Johor State Forestry Department/DANCED/Darudec. Johor State, Malaysia).

Barbier, E. B. (2007). Valuing ecosystem services as productive inputs. *Economic Policy* 22 (49), 177–229. doi: 10.1111/j.1468-0327.2007.00174.x

Barbier, E. B. (2015). Valuing the storm protection service of estuarine and coastal ecosystems. *Ecosystem Serv.* 11, 32–38. doi: 10.1016/j.ecoser.2014.06.010

Barbier Strand Ivar, E. (1998). Valuing mangrove-fishery linkages a case study of campeche, Mexico. *Environ. Resource Economics* 12, 151–166. doi: 10.1023/A:1008248003520

Barbier, E. B., Strand, I., and Sathirathai, S. (2002). Do open access conditions affect the valuation of an externality? estimating the welfare effects of mangrove-fishery linkages in Thailand. *Environ. Resource Economics* 21 (4), 343–365. doi: 10.1023/A:1015129502284

Batker, D., de la Torre, I., Costanza, R., Swedeen, P., Day, J. W., Boumans, R., et al. (2010). *Gaining ground: Wetlands, hurricanes and the economy: The value of restoring the Mississippi river delta (Part 1/2)*. Earth Economics, Washington, USA.

Baustian, M. M., Jung, H., Bienn, H. C., Barra, M., Hemmerling, S. A., Wang, Y., et al. (2020). Engaging coastal community members about natural and nature-based solutions to assess their ecosystem function. *Ecol. Eng.* 143, 100015. doi: 10.1016/j.ecoena.2019.100015

Bennett, E. L., and Reynolds, C. J. (1993). The value of a mangrove area in Sarawak. *Biodiversity Conserv.* 2 (4), 359–375. doi: 10.1007/BF00114040

Bishop, J. (2010). *TEEB : The economics of ecosystems and biodiversity report for business: executive summary*. Earthscan, UK.

Brander, L. (2013). "Guidance manual on value transfer methods for ecosystem services," in *Regional assessment report with focus on asia. united nations environment program* (Nairobi, Kenya: UN Environment Programme (UNEP). doi: 10.13140/2.1.4203.8569

Brenner, J., Jiménez, J. A., Sardá, R., and Garola, A. (2010). An assessment of the non-market value of the ecosystem services provided by the Catalan coastal zone, Spain. *Ocean Coast. Manage.* 53 (1), 27–38. doi: 10.1016/j.ocecoaman.2009.10.008

Camacho-Valdéz, V., Ruiz-luna, A., Ghermandi, A., and Nunes, P. A. L. D. (2013). Valuation of ecosystem services provided by coastal wetlands in northwest Mexico. *Ocean Coast. Manage.* 78, 1–11. doi: 10.1016/j.ocecoaman.2013.02.017

CONABIO (2022) *Extensión y distribución de manglares*. Available at: https://www.biodiversidad.gob.mx/monitoreo/smmm/extensionDist.

Cooper, E., Burke, L., and Bood, N. (2008). *Coastal capital: Economic contribution of coral reefs and mangroves to Belize* (Washington, DC: World Resources Institute).

Costanza, R., D'Arge, R., de Groot, R., Farber, S., Grasso, M., Hannon, B., et al. (1997a). The value of the world's ecosystem services and natural capital. *Nature* 387 (6630), 253–260. doi: 10.1038/387253a0

Daily, G. (1997). Introduction: What are ecosystem services? In: G.C. Daily, Ed., *Nature's Services: Societal Dependence on Natural Ecosystems*, Island Press, Washington DC, 1–10.

de Groot, R., Brander, L., van der Ploeg, S., Costanza, R., Bernard, F., Braat, L., et al. (2012). Global estimates of the value of ecosystems and their services in monetary units. *Ecosystem Serv.* 1 (1), 50–61. doi: 10.1016/j.ecoser.2012.07.005

de Lima, L. T., Fernández-Fernández, S., Weiss, C. V. C., Bitencourt, V., and Bernardes, C. (2021). Free and open-source software for geographic information system on coastal management: A study case of sea-level rise in southern Brazil. *Regional Stud. Mar. Sci.* 48, 102025. doi: 10.1016/j.rsma.2021.102025

Dirección General de Puertos (2001). *Programa maestro de desarrollo portuario y programa operativo anual* (SCT: Coordinación General de Puertos y Marina Mercante).

Dissanayake, P., and Smakhtin, V. (2007) *Environmental and social values of river water: Examples from the menik ganga, Sri Lanka (IWMI working paper, no. 121)*. Available at: http://hdl.handle.net/10535/4740.

Economics E. (2010). "Nature's value in the térraba-sierpe national wetlands," in *The essential of ecosystem services*. Economics Earth, Washington, USA

Envalue (2007) *). new south Wales environment protection Authority.".*

Geoscience australia (2015). *Sea-level rise maps* Available at: http://www.ozcoasts.gov.au/climate/sd_visual.jsp.

Gunawardena, M., and Rowan, J. S. (2005). Economic valuation of a mangrove ecosystem threatened by shrimp aquaculture in Sri Lanka. *Environ. Manage.* 36 (4), 535–550. doi: 10.1007/s00267-003-0286-9

Hagedoorn, L. C., Appeaning, K., Koetse, M. J., Kinney, K., Pieter, J., and van Beukering, H. (2021). Angry waves that eat the coast : An economic analysis of nature-based and engineering solutions to coastal erosion. *Ocean Coast. Manage.* 214, 105945. doi: 10.1016/j.ocecoaman.2021.105945

Hansen, J. E. (2016). *The use of modelling tools to assess local scale inundation and erosion risk* (CoastAdapt, National Climate Change Adaptation Research Facility, Gold Coast: University of Western Australia). Available at: https://coastadapt.com.au/use-modelling-tools-assess-local-scale-inundation-and-erosion-risk#:~:text=Models.

Instituto Nacional de Ecología y Cambio Climático (2021) *Recursos marinos y ecosistemas costeros*. Available at: http://www2.inecc.gob.mx/publicaciones2/libros/100/cap3_2.html.

IPCC (2021). Summary for Policymakers. In: *Climate Change 2021: The Physical Science Basis. Contribution of Working Group I to the Sixth Assessment Report of the Intergovernmental Panel on Climate Change*. [V. Masson-Delmotte and P. A.S.L.C.S.N. Zhai Pirani Connors Péan Berger (eds.)] Cambridge University Press, Cambridge, United Kingdom and New York, NY, USA, pp. 3–32, doi: 10.1017/9781009157896.001.

Ivanova, A., and Gámez, A. E. (2012). *Plan estatal de acción ante el cambio climático para Baja California sur (PEACC-BCS)* (CONACYT, SEMARNAT, INE, UABCS: México).

Janekarnkij, P. (2010). *Assessing the value of krabi river estuary ramsar site: Conservation and development*. Department of Agricultural and Resource Economics, Faculty of Economics, Kasetsart University, Bangkok.

Kauffman, G. J. (2011). *Economic value of stormwater in Delaware*. Water Resources Agency, Institute for Public Administration School of Public Policy and Administration College of Arts and Sciences University of Delaware

Kirezci, E., Young, I. R., Ranasinghe, R., Muis, S., Nicholls, R. J., Lincke, D., et al. (2020). Projections of global-scale extreme sea levels and resulting episodic coastal flooding over the 21st century. *Sci. Rep.* 10 (1), 11629. doi: 10.1038/s41598-020-67736-6

Kopp, R. E., Kemp, A. C., Bittermann, K., Horton, B. P., Donnelly, J. P., Gehrels, W. R., et al. (2016). Temperature-driven global sea-level variability in the common era. *Proc. Natl. Acad. Sci. United States America* 113 (11), E1434–E1441. doi: 10.1073/pnas.1517056113

Lara-Domínguez, A. L., Yañez Arancibia, A., and Seijo, J. C. (1998). "Valuación económica de los ecosistemas. estudio de caso de los manglares en campeche," in *Aspectos económicos sobre la biodiversidad de méxico*. Eds. H. Benítez, E. Vega, A. Peña Jimenez and S. Ávila Foucat (CONABIO, Instituto Nacional de Ecología: México), 199.

Lithgow, D., Martínez, M. L., Silva, R., Geneletti, D., Gallego-, J. B., Cerdán, C. R., et al. (2017). Ecosystem services to enhance coastal resilience in Mexico : The gap between the perceptions of decision-makers and academics. *Journal of Coastal Research*. 77 (sp1), 116–126. doi: 10.2112/SI77-012.1

Liu, S., Costanza, R., Troy, A., D'Aagostino, J., and Mates, W. (2010). Valuing new jersey's ecosystem services and natural capital: A spatially explicit benefit transfer approach. *Environ. Manage.* 45 (6), 1271–1285. doi: 10.1007/s00267-010-9483-5

Liu, S., Portela, R., Rao, N., Ghermandi, A., and Wang, X. (2011). "12.04 - environmental benefit transfers of ecosystem service valuation," in *Treatise on estuarine and coastal science*. Eds. E. Wolanski and D. McLusky (Academic Press: Netherlands), 55–77. doi: 10.1016/B978-0-12-374711-2.01204-3

Llamosas-Rosas, I., Rangel González, E., and Sandoval Bustos, M. (2021). Medición de la actividad económica en las principales zonas turísticas de playa en méxico a través imágenes satelitales. *Ensayos. Rev. Economía* 40, 115–136. doi: 10.29105/ensayos40.2-1

Loa, L. E. (1994). "Los Manglares de méxico. sinopsis general para su manejo," in *El Ecosistema de manglar en américa latina y la cuenca del caribe: Su manejo y conservación*. Ed. D. Suman (Rosenstiel School of Marine and Atmospheric Science. Univ. de Miami. The Tinker Foundation: United States of America), 144–151.

López-Dóriga, U., and Jiménez, J. A. (2020). Impact of relative sea-level rise on low-lying coastal areas of catalonia, nw mediterranean, spain. *Water* 12 (11), 3252. doi: 10.3390/w12113252

Margulis, S. (1992). *Back of the envelope estimates of environmental damage costs in Mexico*, Vol. 824. Work Bank, Washington, DC.

Martínez, M. L., Moreno-Casasola, P., Espejel, I., Jiménez-Orocio, O., Infante-Mata, D., and Rodríguez-Revelo, N. (2014). *Diagnóstico de las dunas costeras de México*. CONAFOR. México. 350 pp.

McComb, G., Lantz, V., Nash, K., and Rittmaster, R. (2006). International valuation databases: Overview, methods and operational issues. *Ecol. Economics* 60 (2), 461–472. doi: 10.1016/j.ecolecon.2006.05.009

Mendoza-González, G., Martínez, M. L., Lithgow, D., Pérez-Maqueo, O., and Simonin, P. (2012). Land use change and its effects on the value of ecosystem services along the coast of the gulf of Mexico. *Ecol. Economics* 82, 23–32. doi: 10.1016/j.ecolecon.2012.07.018

Molnar, M., Kocian, M., and Batker, D. (2012). *Valuing the aquatic benefits of British columbia's lower mainland: Nearshore natural capital valuation*. Earth Economics, Washington, USA.

Nicholls, R. J., Marinova, N., Lowe, J. A., Brown, S., Vellinga, P., de Gusmão, D., et al. (2011). Sea-Level rise and its possible impacts given a "beyond 4°C world" in the twenty-first century. *Philos. Trans. R. Soc. A: Mathematical Phys. Eng. Sci.* 369 (1934), 161–181. doi: 10.1098/rsta.2010.0291

Palacio-Aponte, A. G., Medina-Media, V., and Bautista, F. (2005). "Diagnóstico ambiental de la costa del estado de campeche: enfoques geomorfológico, pedológico y geopedológico," in *Caracterización y manejo de los suelos de la península de yucatán: Implicaciones agropecuarias, forestales y ambientales*. Eds. F. Bautista and G. Palacio (Universidad Autónoma de Campeche, Universidad Autónoma de Yucatán, Instituto Nacional de Ecología: México), 282.

Pérez-Maqueo, O., Martínez, M. L., Lithgow, D., Mendoza-González, G., Feagin, R. A., and Gallego-Fernández, J. B. (2013a). "The coasts and their costs," in *Restoration of coastal dunes*. Eds. M. L. Martínez, P. A. Hesp and J. B. Gallego-Fernández (Springer-Verlag: Berlin, Germany), 347. doi: 10.1007/978-3-642-33445-0_18

Ramsar (2013). *Manual de la convención de ramsar: Guía a la convención de humedales (Ramsar, irán 1971)* (Secretaría de la Convención de Ramsar: Iran). Available at: http://www.ramsar.org.

Reid, W., Mooney, H., Cropper, A., Capistrano, D., Carpenter, S., and Chopra, K. (2005). "Millennium ecosystem assessment," in *Ecosystems and human well-being: synthesis*. Island Press, Washington, DC.

Romero, C., Athayde, S., Collomb, J. G. E., DiGiano, M., Schmink, M., Schramski, S., et al. (2012). Conservation and development in Latin America and southern Africa: Setting the stage. *Ecol. Soc.* 17 (2), 17. doi: 10.5751/ES-04863-170217

Ruckelshaus, M., Reguero, B. G., Arkema, K., Guerrero, R., Weekes, K., Bailey, A., et al. (2020). Harnessing new data technologies for nature-based solutions in assessing and managing risk in coastal zones. *Int. J. Disaster Risk Reduction* 51, 101795. doi: 10.1016/j.ijdrr.2020.101795

Samonte-Tan, G. P. B., White, A. T., Tercero, M. A., Diviva, J., Tabara, E., and Caballes, C. (2007). Economic valuation of coastal and marine resources: Bohol marine triangle, Philippines. *Coast. Manage.* 35 (2–3), 319–338. doi: 10.1080/08920750601169634

Sanjurjo, E. (2001). *Valoración económica de servicios ambientales prestados por Ecosistemas : Humedales en méxico*. Instituto Nacional de Ecología, México

Sathirathai, S. (1998). *Economic valuation of mangroves and the roles of local communities in the conservation of natural resources: Case study of Surat thani, south of Thailand*. The Economy and Environment Program for South East Asia (EEPSEA), Singapore.

Schuerch, M., Spencer, T., Temmerman, S., Kirwan, M. L., Wolff, C., Lincke, D., et al. (2018). Future response of global coastal wetlands to sea-level rise. *Nature* 561 (7722), 231–234. doi: 10.1038/s41586-018-0476-5

Secretaría de la Defensa Nacional (SEDENA). (2015). "Vegetación," Available at: www.sedena.gob.mx/dgcart.html.

SEMARNAT (2010). *Norma Oficial Mexicana NOM-059-ECOL-2010, Protección ambiental-Especies nativas de México de flora y fauna silvestres-Categorías de riesgo y especificaciones para su inclusión, exclusión o cambio-Lista de especies en riesgo*. Available at: https://www.gob.mx/profepa/documentos/norma-oficial-mexicana-nom-059-semarnat-2010.

Shepard, C. C., Crain, C. M., and Beck, M. W. (2011). The protective role of coastal marshes: A systematic review and meta-analysis. *PLS One* 6 (11), e27374. doi: 10.1371/journal.pone.0027374

Silva, R., Lacouture, M. M. V., Durón, F. J. R., Paez, D. P., Pérez, M. A. O., Baldwin, E. G. M., et al. (2011). *Caracterización de la zona costera y planteamiento de elementos técnicos para la elaboración de criterios de regulación y manejo sustentable*. Instituto de Ingeniería UNAM, México.

Silva, R., Martínez, M. L., Hesp, P. A., Catalan, P., Osorio, A. F., Martell, R., et al. (2014). Present and future challenges of coastal erosion in Latin America. *J. Coast. Res.*, 71, 1–16. doi: 10.2112/SI71-001.1

Tianhong, L., Wenkai, L., and Zhenghan, Q. (2010). Variations in ecosystem service value in response to land use changes in shenzhen. *Ecol. Economics* 69 (7), 1427–1435. doi: 10.1016/j.ecolecon.2008.05.018

Tong, C., Feagin, R. A., Lu, J., Zhang, X., Zhu, X., Wang, W., et al. (2007). Ecosystem service values and restoration in the urban sanyang wetland of wenzhou, China. *Ecol. Eng.* 29 (3), 249–258. doi: 10.1016/j.ecoleng.2006.03.002

Villanueva-Fragoso, S., Ponce-Vélez, G., García, C., and Presa, J. (2010). "Vulnerabilidad de la zona costera . ecosistemas costeros," in *Vulneravilidad de las zonas costeras mexicanas ante el cambio climático*. Eds. A. V. Botello, S.

Villanueva-Fragoso, J. Gutiérrez and J. Rojas (Semarnat-INE, UNAM-ICMyL, Universidad Autónoma de Campeche: México), 37–72.

Weiss, J. L., Overpeck, J. T., and Strauss, B. (2011). Implications of recent sea level rise science for low-elevation areas in coastal cities of the conterminous U.S.A: A letter. *Climatic Change* 105 (3–4), 635–645. doi: 10.1007/s10584-011-0024-x

Williams, L. L., and Lück-Vogel, M. (2020). Comparative assessment of the GIS based bathtub model and an enhanced bathtub model for coastal inundation. *J. Coast. Conserv.* 24 (2), 23. doi: 10.1007/s11852-020-00735-x

World Bank (2021) *PPP Conversion factor, GDP (LCU per international $)*. Available at: https://data.worldbank.org/indicator/PA.NUS.PPP.

Zavala-Hidalgo, J., de Buen Kalman, R., Hernández-Maguey, F., and Romero-Centeno, R. (2010). "Tendencias del nivel del mar en las costas mexicanas," in *Vulnerabilidad de las zonas costeras mexicanas ante el cambio climático*. Eds. A. V. Botello, S. Villanueva-Fragoso, J. Gutiérrez and Rojas-Galaviz,, 514, 249–267. Semarnat-ine, unam-icmyl, Universidad Autónoma de Campeche, México.

frontiers | Frontiers in Marine Science

TYPE Original Research
PUBLISHED 02 September 2022
DOI 10.3389/fmars.2022.930440

OPEN ACCESS

EDITED BY
Valeria Chávez,
Institute of Engineering, National Autonomous University of Mexico, Mexico City, Mexico

REVIEWED BY
Wenfei Ni,
Pacific Northwest National Laboratory, United States
Cheryl A Brown,
United States Environmental Protection Agency (EPA), United States

*CORRESPONDENCE
Maria Jose Marin Jarrin
mjmarin@espol.edu.ec

SPECIALTY SECTION
This article was submitted to Coastal Ocean Processes, a section of the journal Frontiers in Marine Science

RECEIVED 28 April 2022
ACCEPTED 28 July 2022
PUBLISHED 02 September 2022

CITATION
Marin Jarrin MJ, Sutherland DA and Helms AR (2022) Water temperature variability in the Coos Estuary and its potential link to eelgrass loss. *Front. Mar. Sci.* 9:930440. doi: 10.3389/fmars.2022.930440

Water temperature variability in the Coos Estuary and its potential link to eelgrass loss

Maria Jose Marin Jarrin[1]*, David A. Sutherland[1] and Alicia R. Helms[2]

[1]Department of Earth Sciences, University of Oregon, Eugene, OR, United States, [2]South Slough National Estuarine Research Reserve, Charleston, OR, United States

Subtidal water temperatures in estuaries influence where organisms can survive and are determined by oceanic, atmospheric and riverine heat fluxes, modulated by the distinct geometry and bathymetry of the system. Here, we use 14 years of data from the Coos Estuary, in southwest Oregon, USA, to explore the impact of anomalously warm oceanic and atmospheric conditions during 2014-2016 on the estuary temperature. The arrival of a marine heatwave in September 2014 increased water temperature in the greater Pacific Northwest region until March 2015, and again from July to August 2015. Additionally, in 2014-2016, the Equatorial Pacific showed increased temperatures due to El Niño events. In the Coos Estuary, this warming was observed at all the water quality stations, producing more than 100 days with temperatures at least 1.5°C warmer than normal, and notably, a higher prevalence during Fall and Winter seasons. Larger temperature variations occurred at shallower stations located further away from the mouth of the estuary, changing the along-estuary temperature gradient and potentially the advection of heat through the estuary. After the onset of these increased temperatures, eelgrass declined sharply, but only in certain stations in the shallow estuary South Slough and has not yet returned to long term average values. As global temperatures continue rising due to climate change, increased numbers of marine heatwaves and El Niño events are expected, leading to higher temperature stress on the marine ecosystem within estuaries.

KEYWORDS

temperature, estuary, bathymetry, marine heatwave, El Niño, Eelgrass (*Zostera marina*)

Introduction

Estuaries act as mixing zones between oceanic and riverine waters, providing many ecosystem and cultural services (Milcu et al., 2013; Sherman and DeBruyckere, 2018; Zapata et al., 2018), and motivating numerous studies to examine the links between environmental conditions and ecosystem health (Costanza et al., 1997; Seppelt et al.,

2011). In the Pacific Northwest (PNW; Figure 1), estuaries are influenced on the ocean side by the primarily wind-driven California Current System (CCS; Hickey and Banas, 2003). These winds driving the CCS along the west coast of North America are forced by atmospheric circulation related to the North Pacific High and the Aleutian Low, which vary seasonally. In the winter the Aleutian Low migrates southward, producing downwelling-favorable winds along the PNW, while in summer the North Pacific High migrates northward producing southward-directed upwelling-favorable winds (e.g., Huyer, 1983; Hickey and Banas, 2003; Davis et al., 2014). Upwelled waters on the PNW continental shelf are typically colder (Figure 1B), with higher salinity, higher nutrients and lower oxygen levels. During winter, storms produce episodic river discharge events that result in lower salinity, lower temperature and higher turbidity along the coast (Hickey and Banas, 2003; Huyer et al., 2007).

The CCS exhibits significant interannual variability on top of its seasonal hydrographic changes (Figure 1C). These interannual variations are dominated by the El Niño Southern Oscillation (ENSO), where positive values of the Ocean Niño Index (ONI) are related to higher temperatures and sea level at the mouth of PNW estuaries (Wyrtki, 1984; Huyer et al., 2002). The triad of Sep-Oct-Nov 2014 ONI index registered SST anomalies greater than 0.5 °C in the Niño 3.4 region (5°N-5°S, 120°-170°W), which led to an officially declared El Niño in the Equatorial Pacific (https://origin.cpc.ncep.noaa.gov/). Though this first El Niño warm pulse was weak (0.5 °C in May-2014), another El Niño event produced SST anomalies of 4 °C in 2015, with maximum anomalies between Nov-2015 and Jan-2016. Positive anomalies were observed in this ENSO area until March-April-May 2016, with a peak of anomalies of 2.6 °C at the end of 2015. On decadal time scales, variations can be related to the Pacific Decadal Oscillation (PDO) and the North Pacific Gyre Oscillation (NPGO), which emerge as the first and second principal components of sea surface temperature and sea surface height, respectively (Di Lorenzo et al., 2008; Capotondi et al., 2019). The NPGO correlates with wind stress in the North Pacific, with weakened wind-driven upwelling occurring when the index is negative (Di Lorenzo et al., 2008). A positive PDO pattern, which is associated with a strengthened Alaskan gyre, is correlated to increased coastal upwelling between 38°N and 48° N (Chhak and Di Lorenzo, 2007; Di Lorenzo et al., 2008).

On top of these basin-scale patterns, marine heatwaves (MHWs) in the Eastern Pacific Ocean also contribute to interannual variations. MHWs are a result of decreased surface cooling in the Gulf of Alaska and decreased equatorward Ekman transport due to an atmospheric ridge (Di Lorenzo and Mantua, 2016; Capotondi et al., 2019). For example, during the winter of 2013, the MHW termed the "Blob" (Bond et al., 2015) was observed in the North Pacific and moved onto the shelf from Sep-2014 until Mar-2015, increasing SST more than 1.5 °C at the

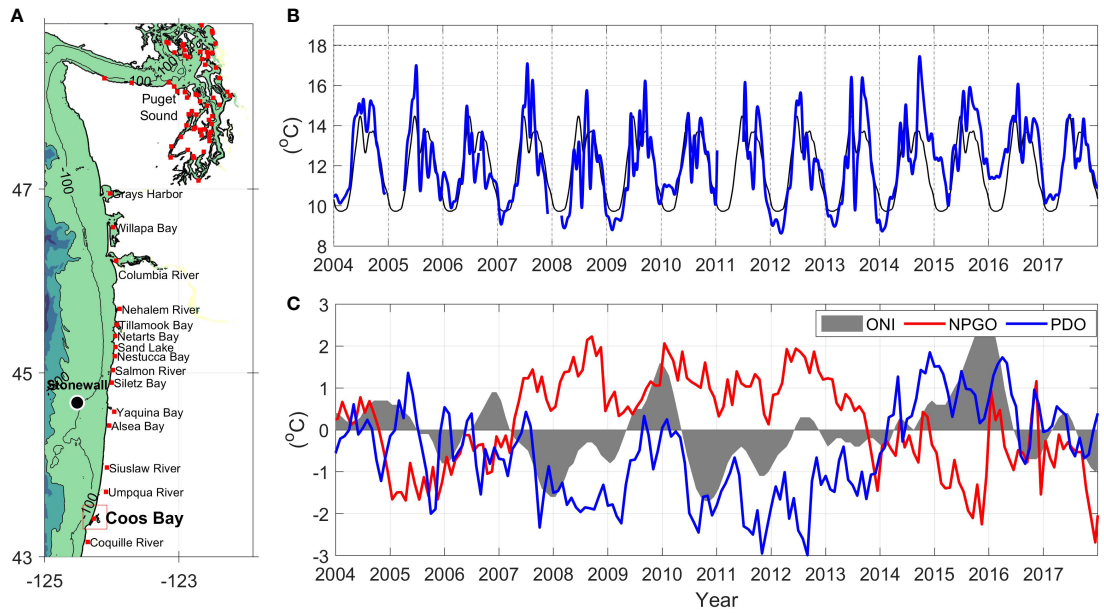

FIGURE 1
(A) Estuaries in the PNW where eelgrass (*Zostera marina)* is present, including our study area (Coos Bay). The Stonewall buoy is also shown as a black circle. **(B)** Water temperature at the Stonewall buoy with the climatological mean calculated for 2004-2014 (black) and the daily averaged values with a 30-day low pass filter (blue). **(C)** Basin scale indices (water temperature anomaly): Oceanic Niño Index (ONI; gray area), North Pacific Gyre Oscillation (NPGO; red line), and Pacific Decadal Oscillation (PDO; blue line).

Stonewall buoy (Figure 1B). Positive anomalies (>1.5 °C) were observed at Stonewall again from Jul-2015 to May-2016 related to a second marine heatwave (Di Lorenzo and Mantua, 2016; Gentemann et al., 2017). Anthropogenic global warming is resulting in increased temperatures as well, which are predicted to increase stratification and reduce availability of nutrients higher in the water column, akin to the variations observed during El Niño years (Schneider, 1993; Di Lorenzo et al., 2009; Barnard et al., 2017). During 2014–2016, when the Coos Estuary showed anomalously warm waters (Shanks et al., 2020), the Equatorial Pacific was anomalously warm due to an El Niño event (Jacox et al., 2016), while MHWs were present on the PNW continental shelf.

The seasonal patterns in the continental shelf hydrodynamics influence the ecology of the PNW ocean and estuaries. For example, many local fish and invertebrates spawn in the winter to ensure the retention of pelagic eggs and larvae nearshore (Logerwell et al., 2003; Bi et al., 2011; Shanks et al., 2020). Plants are also influenced by the seasonal patterns in temperature. For example, eelgrass (*Zostera marina*) carries fewer leaves in the winter, while in the summer, they present a greater number of longer and thicker shoots (Phillips et al., 1983). This marine flowering plant forms broad meadows in intertidal and shallow subtidal flats, as well as fringe meadows on steeper shorelines, hence specific genotypes are selectively adapted to different habitats and environmental stressors (Phillips, 1984; Hessing-Lewis et al., 2011). Thom et al. (2003) showed the greatest densities of eelgrass in the Coos Estuary, OR, were found in the most marine-influenced sites. These sites had a smaller seasonal temperature range, while the stations further away from the mouth of the estuary were subjected to broader temperature ranges, higher turbidity, and lower salinity.

Many environmental parameters, outside a specific species-dependent range, can cause stress on the fauna and flora of estuaries, including salinity, water temperature, turbidity, light availability, air temperature, water velocity, and nutrient levels (Thom et al., 2003; Echavarria-Heras et al., 2006; Lee et al., 2007; Nejrup and Pedersen, 2008; Kaldy, 2012; Kaldy, 2014; Salo and Pedersen, 2014; Basilio et al., 2017; Daly et al., 2017; Magel et al., 2022). For example, declines in eelgrass populations have been observed in the PNW and were related to increased water temperatures after the 1997-1998 El Niño event (Thom et al., 2003). Water temperatures above 25°C can significantly reduce photosynthetic and respiration rates (Nejrup and Pedersen, 2008; Gao et al., 2017; Beca-Carretero et al., 2018), inhibit leaf growth (Zimmerman et al., 1989), as well as increase susceptibility to eelgrass wasting disease (Kaldy, 2014; Groner et al., 2021). As a response to warm seasons, *Z. marina* may respond by reproducing sexually through the production of flowers and seeds (Lee et al., 2007). These seeds can also be affected by temperature by changing the size and chemical composition (Jarvis et al., 2012; Delefosse et al., 2016), and if the temperature stress is perennial, the eelgrass beds may not be able to survive (Jarvis et al., 2012).

Here, we study the seasonal and interannual variability of water temperature within the Coos Estuary to explore its links with a recently observed decrease in eelgrass abundance. Using long-term observations, we evaluate the impact of the ambient ocean conditions, river discharge and atmospheric heat flux on the water temperature in the estuary. Our observations show that temperature varies locally and seasonally across specific regions of the estuary, much like the observed eelgrass declines, and is driven by a combination of basin scale variability and local conditions dictated by the strongly-forced estuary.

Study area

The Coos Estuary is located inshore of a narrow continental shelf south of Stonewall Bank (Hickey and Banas, 2003) and is the second largest estuary in Oregon in terms of area and volume (Figure 1). Water temperatures inside the Coos Estuary are significantly correlated with continental shelf values as measured by the Stonewall buoy (Strub et al., 1987; Miller and Shanks, 2004; Huyer et al., 2007). At the Stonewall buoy, temperature shows a seasonality related to the CCS: equatorward winds drive cold upwelled waters towards the coast during the summer, while during the winter southward winds produce downwelling accompanied with warmer waters. On top of this seasonality, several warm-water events have been registered at the Stonewall buoy, including El Niño events which produce 1-2°C anomalies (Huyer et al., 2002; Peterson et al., 2017) and MHWs, which in 2014 produced an anomaly of 7°C in 1 hour at the Stonewall buoy (Gentemann et al., 2017; Shanks et al., 2020). These ocean conditions set the boundary conditions at the mouth of PNW estuaries and can travel up-estuary at a rate on the order of 10 km d^{-1}, at least in the case of Willapa Bay (Hickey and Banas, 2003).

The propagation of oceanic signals into an estuary is produced by a combination of baroclinic, barotropic and diffusive processes, which depend on the geometry, depth, and forcing of each system. The main channel of the Coos Estuary (Figure 2) is annually dredged from the mouth to 24 km up-estuary near the Coos River entrance, to maintain 11 m of depth and 91 m of width (Eidam et al., 2020). Adjacent tidal flats, inlets and sloughs branch out of the main channel; these shallow areas range between 0.5 m above MLLW to 1.0 bellow MLLW of depth, extend approximately 15 km^2 and provide the primary habitat for *Zostera marina* (Emmett et al., 2000; Groth and Rumrill, 2009; Eidam et al., 2020). The main source of freshwater is the South Fork Coos River in the eastern portion of the estuary (Figure 2), which has a total discharge that ranges from 2 to 800 m^3 s^{-1}, with maximum peaks related to winter storm events. Additionally, there are numerous other sources of freshwater,

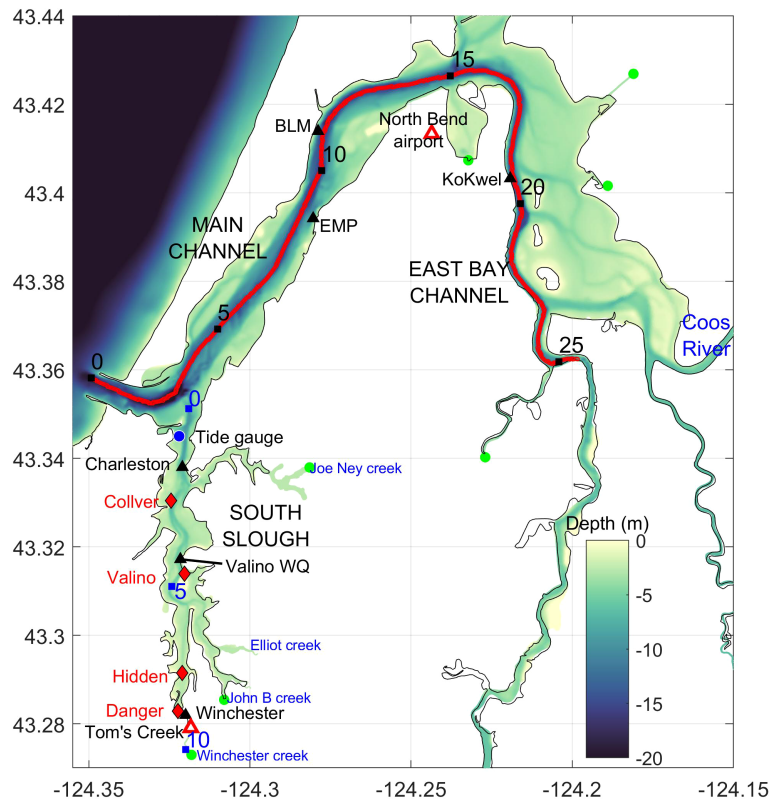

FIGURE 2
The Coos Estuary, showing bathymetry in meters below mean sea level (colored contours) and the location of water quality monitoring stations (black triangles), meteorological stations (red triangle), tide gauge (blue circle), freshwater sources (green circles), and eelgrass stations (red diamonds). Black numbers refer to distance (in km) from the mouth along the thalweg; blue numbers show distance (in km) from the intersection of South Slough with the main estuary.

including the Winchester, Elliot and Joe Ney Creeks that feed into South Slough. South Slough is a shallow sub-estuary that trends southward about 3 km from the mouth of the main estuary, has a natural depth of 5 m in its un-dredged sinuous channel, and is home to the South Slough National Estuarine Research Reserve (SSNERR), which collects water quality and eelgrass data throughout the entire estuary.

The subtidal estuarine exchange flow in the Coos Estuary is relatively constant throughout the year as it is dominated by tides, with a small secondary increase in winter as river discharge ramps up (Conroy et al., 2020). The main semidiurnal tidal constituent, M_2, height amplitude is 0.8 m, with mean tidal currents of 1 m s^{-1} resulting in a tidal excursion of 14 km (Baptista, 1989). Sutherland and O'Neill (2016) showed that the Coos Estuary has characteristics of a salt-wedge during high river discharges, a well-mixed estuary during low discharges, and a partially-mixed estuary during moderate discharge times. They also found that, as in other estuaries in the PNW, Ekman-driven upwelling moves high-salinity, low-temperature, low-oxygen waters into the estuary (Sutherland and O'Neill, 2016). Though estuaries are expected to be exporters of nutrients (e.g., Roegner et al., 2002; Roegner et al., 2011), Roegner and Shanks (2001) found that the Coos Estuary, specifically the seaward portion of South Slough, is an importer of nutrients in the summer, due to the close proximity of the coastal ocean.

Eelgrass, which plays a key role in the coastal zone worldwide (Phillips, 1984; Hosack et al., 2006; Lee and Brown, 2009), has decreased in abundance in PNW estuaries (Magel et al., 2022), including the Coos at one annually-sampled site. In the Coos, eelgrass is spatially variable, and estuary-wide eelgrass presence has been obtained through aerial photography and high density lidar intensity images from 2005 and 2016 with the aid of the US Environmental Protection Agency (EPA) and the Pacific Marine and Estuarine Fish Habitat Partnership (PMEP), respectively (Clinton et al., 2007; Sherman and DeBruyckere, 2018). In May 2005, false color, near-infrared aerial photography (Supplementary Figure 1A) revealed high eelgrass density in the Coos Estuary covering 24x10^6 m^2 of total area. Higher density is

observed in locations closer to the mouth of the estuary, where colder more saline oceanic waters flood the tidal flats (Thom et al., 2003). In July 2016, airborne, multispectral imagery was collected over Coos Bay that led to map of presence/absence of eelgrass beds (Supplementary Figure 1B). This 2016 survey revealed a decrease of eelgrass-covered area in the Coos Estuary, with higher presence in the main channel than in South Slough (Supplementary Figure 1B), despite the proximity of the sub-estuary to the mouth of the estuary and influence of coastal waters (Raimonet and Cloern, 2017). Previously, Thom et al. (2003) showed that stations in the Coos Estuary closer to the mouth had higher values of eelgrass density (100–200 shoots per m^2) related to the influence of oceanic, low-turbidity waters, while stations farther away from the mouth of the estuary had smaller density, related to increased turbidity due to the input of freshwater. A similar result was found across multiple PNW estuaries by Magel et al. (2022). Thom et al. (2003) also suggested that eelgrass decline was correlated with anomalously warm waters during the 1997–1998 El Niño; the degree to which this happens again between 2014-2016 is the subject of this study (Figure 1). However, despite the proximity of South Slough to the mouth of the estuary, the spatial signature of eelgrass declines between 2005 and 2016 reveals that a simple picture of proximity to the ocean leading to loss does not hold, i.e., other factors influencing temperature along and across the estuary must play a role.

Methods

Environmental conditions

We obtain water property, sea level, river discharge and meteorological conditions from several monitoring stations located in the estuary (Figure 2 and Table 1). Inside South Slough, the Charleston Bridge, Valino Island and Winchester Arm stations are telemetered to provide near real-time data access by SSNERR (http://nvs.nanoos.org). Temperature, salinity and various other parameters, are measured automatically every 15 minutes at all stations (Figure 3). The instruments are maintained monthly to limit biofouling by SSNERR (NOAA National Estuarine Research Reserve System (NERRS), 2020).

Meteorological data were obtained from stations both offshore and on land. Offshore wind data, taken to be representative of upwelling or downwelling conditions at the coast, are from the NOAA Stonewall Bank buoy (Figure 1), approximately 120 km north of the estuary. We use hourly wind data to calculate the along-shore north-south component of wind stress (Large and Pond 1981), given the wind speed at the height above ground from each station (Table 1). Surface water temperatures were also obtained from the Stonewall buoy at hourly intervals. On land, wind velocity data were extracted from a meteorological station at the North Bend Southwest Oregon Regional Airport (Table 1,

TABLE 1 Information on oceanographic and meteorological stations analyzed in this study.

Station	Institution	Date range	*Water depth/height (m)*	*Distance from mouth (km)*
Eelgrass sampling stations				
Collver Point	SSNERR	2004–present	Intertidal	4.5
Valino Island	SSNERR	2004–present	Intertidal	6.3
Hidden Creek	SSNERR	2010–present	Intertidal	8.8
Danger Point	SSNERR	2004–present	Intertidal	9.9
Water quality stations (water temperature, salinity)				
Charleston Bridge (CH)	SSNERR	2002–present	4.0 / 0.5	3.0
Valino Island (VA)	SSNERR	1999–present	2.4 / 0.5	5.6
Winchester Creek (WI)	SSNERR	1995–present	1.1 / 0.5	7.1
Empire Docks (EMP)	CTCLUSI	2011–2014	6.0 / 0.5	6.9
North Spit BLM	CTCLUSI	2008–2016	10.5/0.5	8.2
KoKwel Wharf (Coquille)	Coquille Indian Tribe	2013–2017	19	18.6
Sea level from tide gauge				
Charleston #9432780	NOAA	1991–present	3.0 / –	3.0
Meteorological stations (wind, air temperature)				
North Bend airportWBAN #24284	NOAA	1949–present	5.1 (elev.)	12.5
Stonewall buoyNDBC #46050	NOAA - NDBC	1991–present	3.8 (elev.)	147.5
River gauge station				
South Fork of Coos River. St.#14323600	Coos Watershed Association	2003–present	44 (elev.)	49
Winchester Creek	Coos Watershed Association	2010–2011; 2015–present	3.5 m (depth of channel)	10.8

Locations shown in Figure 1. Instrument height above bottom is shown, as depths change tidally.

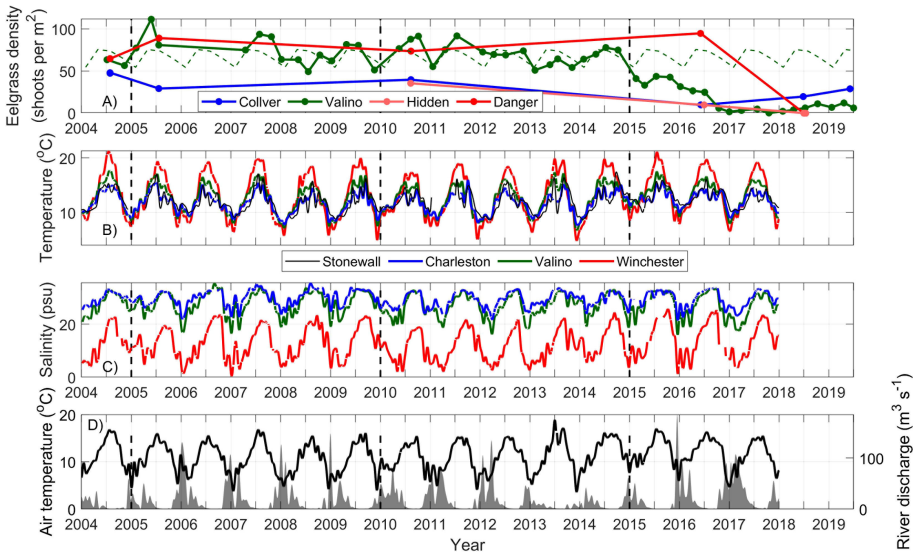

FIGURE 3
(A) Eelgrass density at 4 stations in South Slough. The 2004-2014 climatology for Valino is shown in broken green line. **(B)** Long-term hydrographic characteristics at 4 SSNERR stations, Charleston WQ (blue), Valino WQ (thick green), Winchester WQ (red) and the Stonewall buoy (black), showing low-pass filtered water temperature over 2014–2018. **(C)** same as in **(B)** but for salinity. **(D)** Air temperature at the North Bend Airport meteorological station (black) and South Fork of the Coos River discharge (gray). For locations, see Figure 2.

location shown in Figure 2). The North Bend airport also provides air temperature, relative humidity, barometric pressure, total solar radiation and precipitation.

River discharge data from the South Fork Coos River gauge (Figure 2 and Table 1) from 2003 to present were used as a proxy for the variation in freshwater input to the estuary. Additionally, there are river discharge and water temperature data at Winchester Creek, the main source of freshwater entering the landward end in South Slough, available from 2011 and 2013-2016 (Figure 2 and Table 1). Hourly tidal height time series were obtained from a NOAA tide gauge in Charleston (Figure 2 and Table 1).

Heat budget

We use a heat budget approach to determine the total heat content of the volume of water of the estuary, from heat fluxes through the volume boundaries (Smith, 1983; Stevenson and Niiler, 1983). Here, we explore the heat budget of the Coos Estuary qualitatively, using a simplified heat budget for a shallow and vertically well mixed estuary,

$$\frac{\partial T_{av}}{\partial t} + u_{av}\frac{\partial T_{av}}{\partial x} + Residual = \frac{Q_0}{\rho C_p h} \quad (1)$$

where T_{av} and u_{av}. are depth-averaged temperature and along-estuary horizontal current, respectively. We neglect several terms in the full heat budget, which are contained in the "Residual" term in Eq. 1 and are described next. Since surface to bottom differences in temperature in the Coos Estuary are out of phase with sea level differences, as well as with velocity (Roegner and Shanks, 2001; Conroy et al., 2020), we can assume heat divergence and entrainment are small. We also neglect the vertical heat flux through the sediment at the bottom, given the turbidity in the estuary as well as the amount of vegetation that both reduce the exchange of heat between the sediment and the water (Evans et al., 1998; McKay and Iorio, 2008).

This simplified heat budget, then, contains four terms: the heat storage, the along-estuary advective heat flux divergence, the residual term which includes the neglected terms, and on the right-hand side (RHS), the atmospheric heat flux. The storage of heat in the water column (first term in Eq. 1), is a partially measurable variable, since the measurements are obtained at a single depth (0.5 m). However, Sutherland and O'Neill (2016) show that in most of the profiles along the estuary, temperature isolines are nearly vertical, indicating well-mixed conditions. Hence, we assume that the point measurements represent the water column, though this assumption is most uncertain during high discharge (Sutherland and O'Neill, 2016).

The heat flux term is Q_0 which is the net surface heat flux, ρ is density averaged over the water column and C_p is the specific heat of sea water, both calculated as a function of temperature and salinity, and h is the time-varying water depth. Q_0 may be decomposed into the incoming solar short-wave radiation, outgoing longwave radiation, latent heat exchange due to

evaporation or condensation, sensible heat exchange at the surface and heat exchange due to precipitation (assumed here to be negligible). Shortwave and longwave radiation, were obtained from the NCEP-NCAR Reanalysis (Kalnay et al., 1996) at the land location closest to the Coos Estuary (123.75° W, 44.7611°N). Sensible and latent heat fluxes are estimated using bulk formulae from the MATLAB Air-Sea toolbox (https://github.com/sea-mat/air-sea), using the water quality parameters at Valino WQ and the meteorological observations at the North Bend airport.

The second term in Eq. 1 represents the horizontal advective flux divergence of heat past a point in the along-estuary direction. We assume the across-estuary advective heat flux divergence is small, since the across-channel velocity is 2 magnitudes smaller than the along-estuary component (Roegner and Shanks, 2001; Conroy et al., 2020). Hence, it is included in the "Residual" term of Eq. 1. We calculate the along-estuary advective component of the heat budget by assuming that the heat storage (first term in Eq. 1) minus atmospheric heat flux (RHS in Eq. 1), is dominated by the along-estuary advective heat fluxes plus the residual. These horizontal heat flux divergences depend on the temperature gradient and velocity, which change due to the influence of the oceanic and riverine end-members.

Eelgrass (*Zostera marina*) in the Coos Estuary

Changes in the environmental conditions of an estuary have been observed to modify the seasonal trends of *Zostera marina* (Table 2). Due to the observed response of *Z. marina* to temperature, salinity and turbidity (Table 2), we use eelgrass as a proxy of response to environmental stressors in the Coos Estuary. The availability of observations and the importance of eelgrass to the ecosystem here and worldwide (e.g., Short and Coles, 2001) make it a critical species to examine. Table 2 synthesizes the current literature on temperature, salinity and turbidity on eelgrass density in estuaries in the PNW. Generally, warmer waters and waters with salinity outside an optimal range stress the eelgrass along the west coast. Although sediment also plays a role in eelgrass health, it is beyond the scope of variables we explore here.

SSNERR surveys eelgrass in the Coos Estuary, including quarterly to annual monitoring of percent cover, shoot density, canopy height and flowering shoot counts at 4 locations in South Slough (Table 1). Collver Point, Valino Island, Hidden Creek, and Danger Point, are sampled using SeagrassNet and NERRS biomonitoring protocols (Short et al., 2006). Eelgrass characteristics are sampled at 0.25 m^2 quadrats along permanent transects during low tides (Supplementary Figure 2). From 2004 to 2015, Valino Island transects contained 12 plots, and from 2016 to present 6 plots were added to the low and mid transects for a total of 18 plots.

Climatology and statistics

In order to compare the oceanographic and meteorological conditions of the Coos Estuary between 2014-2016 with the years before the observed eelgrass decline, we used the available data from 2004-2014 to calculate daily averages and standard deviations. Once the daily climatology was calculated, event-driven variability was filtered out by using a low-pass 30-day filter. Correlations between time series were calculated at different time lags, with significance level of 95%, using the large N (number of observations) approximation $\hat{\rho}_{crit}(\alpha, N) = \frac{q_t(\frac{\alpha}{2}, N-2)}{\sqrt{N}}$, where q_t refers to the Student's-t distribution with N-2

TABLE 2 Temperature, salinity and turbidity optimal physiological values and thresholds for the survival of *Zostera marina* in the Pacific Northwest.

Parameter	Optimal values	Threshold	Location	Season/ Month	Source
Temperature	10–20 °C	>18 °C	Coos Bay, OR	July-August (1998-2001)	(Thom et al., 2003)
	16–19.1 °C	>18 °C	Willapa Bay, WA	July-August (1998-2001)	(Thom et al., 2003)
	15–23 °C	>25 °C (stressful) >30 °C (lethal)	Yaquina Bay, OR (collected)	In lab	(Kaldy, 2014)
	15.4–24.2 °C	>32 °C	Puget Sound, WA		(Phillips, 1984; Thom et al., 2018; Thom & Albright, 1990)
		1.5 – 2.5 °C above normal	San Diego, CA		(Johnson et al., 2003)
Salinity	24.5–32.1 psu		Coos Bay, OR	July-August (1998-2001)	(Thom et al., 2003)
	13.3–29.2 psu		Willapa Bay, WA	July-August (1998-2001)	(Thom et al., 2003)
Turbidity or Irradiance		limited to substrates where at least 1% of the incident light remains	South Oyster Bay, Long Island Sound, New York		(Phillips, 1984)

degrees of freedom, and α s the lower-tail confidence region, in our case 0.05. The water-year climatological cumulative river discharge was calculated from October 1st to September 30th, from 2004 to 2014. We define dry conditions in the estuary to be values below 95% of the climatological cumulative discharge value.

Results

Climatological environmental conditions in the Coos Estuary

Water temperature and salinity levels in the Coos Estuary are influenced by the atmosphere (wind and heat fluxes), ambient ocean conditions, and river discharge (Figure 3). During the winter, storms produce enhanced northward winds locally over the estuary (Figure 4). These same storms bring rain, increasing river discharge into the estuary episodically (Figure 4). Over the climatological period examined here (2004-2014), river discharge between November and May reached an average of 32 m^3 s^{-1} (although peaks in distinct years show much higher individual event magnitudes), after which is a dry period between June and October, where the average discharge decreased by an order of magnitude to 3.2 m^3 s^{-1} (Figure 4D). The average water-year cumulative discharge calculated for the South Fork Coos River is 6330 m^3 s^{-1}. In a typical year, 90% of this cumulative discharge is accumulated between November and April.

During the dry summer, air temperature reached maximum values of 15.2°C at the North Bend airport station, while in winter, values below 7 °C were recorded (Figure 4C). Outside the estuary, water temperatures at the Stonewall buoy location (Figure 4B) showed a similar pattern of seasonal variability: during the summer, temperatures increased, averaging 13 °C, albeit with event-driven decreases in temperature between July and September when upwelling brings colder waters to the coast. During the winter, colder water temperatures were observed at Stonewall, averaging 10 °C, and related to wintertime atmospheric heat loss.

Subtidal data from the Coos show that estuarine temperature is strongly correlated to the temperature variability on the nearby continental shelf (ocean end-member), but the correlation weakens with distance from the mouth (Supplementary Figure 3). Additional spatial variability is induced by the heterogenous input of freshwater: the main

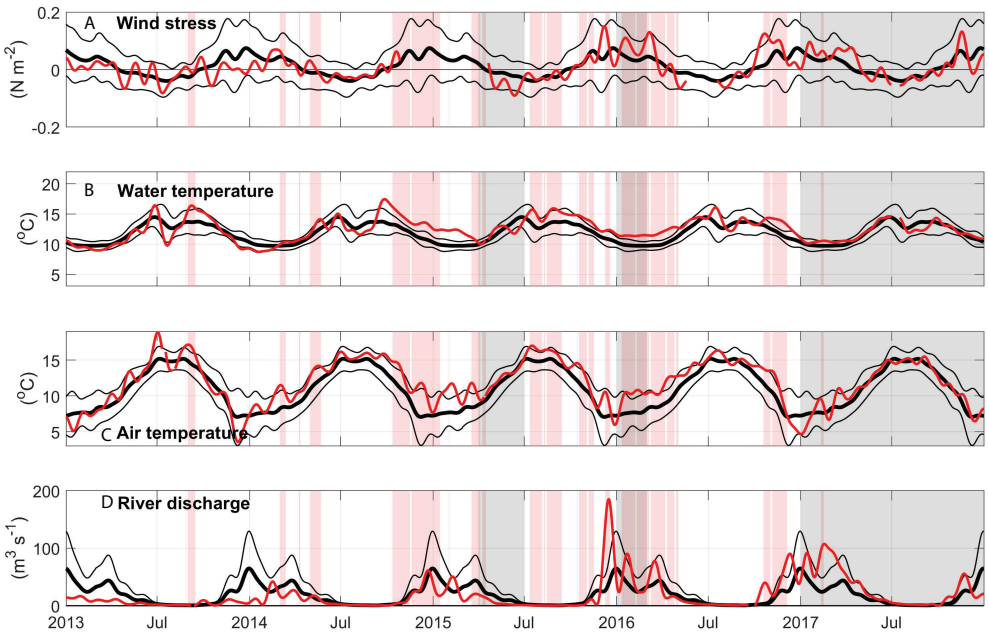

FIGURE 4
Environmental conditions outside the estuary during 2013-2017. **(A)** Daily averages with a 30-day low pass filter of North-South wind stress (N m^{-2}) from the North Bend Airport meteorological station (red lines) showing 2004-2014 climatological mean calculated for 2004-2014 (thick black lines), thin black lines show ±1 standard deviation. Vertical red bands show periods in which water temperature at Charleston WQ is 1 standard deviation above the 2004-2014 climatology (Figure 6). Vertical gray bands show periods in which eelgrass density at Valino is at least 1 standard deviation below the 2004-2014 climatology. **(B)** same as **(A)** but for surface water temperature (°C) at the Stonewall buoy, **(C)** same as **(A)** but for air temperature (°C) at the North Bend Airport meteorological station, **(D)** same as **(A)** but for South Fork Coos River discharge (m^3 s^{-1}).

estuary receives the largest magnitude sources of river water (>10 freshwater sources) while South Slough has fewer sources with relatively smaller magnitudes (374 m^3 s^{-1} for the entire estuary, 8.8 m^3 s^{-1} for South Slough).

Inside the estuary, the 2004-2014 temperature climatology shows maximum values between July and October (Figure 5), which coincides with the highest air temperature values (Figure 4C) and reduced freshwater input (Figure 4D). The highest water temperatures were observed in stations further away from the mouth (KoKwel, 18 °C; and Winchester, 18.4 °C) during this season (Figure 5). Salinity was also high during the dry summer period with maximum values at the station closest to the mouth (Charleston, 29.2 psu). Winchester Creek data (Figure 6) showed that river temperature increases during the summer, yet remains ~2 °C cooler than both the Valino and Winchester locations in the estuary. At the end of the dry period, before freshwater increases, Charleston WQ (station closest to the mouth of the estuary) registered temperatures up to 3.5 °C colder and 9.6 psu saltier than Winchester WQ (station furthest up-estuary in South Slough), due to the influence of upwelling on the coastal ocean. Valino WQ (station located mid-estuary in South Slough) also registered the influence of cold salty upwelled waters, while Winchester WQ and Winchester Creek temperature continued to increase (Figure 5).

The rainy period, from November to March, was characterized by colder waters in Winchester Creek (Figure 6F). During this season all stations had similar temperatures (Figure 5), with even lower peaks during increases in discharge (Figure 4B). Due to the increase in freshwater input, salinity decreases, with lowest values in the stations closest to the river mouths (Winchester and KoKwel Wharf, and the eelgrass stations of Danger and Hidden). Despite KoKwel Wharf being closer to the input of freshwater from Coos River, temperature is slightly higher than BLM (10.2 °C, Figure 5). Long time series for the EMP, BLM, and KoKwel Wharf WQ stations are not available. However, existing data from 2013-2016 (Figures 6A–C) shows the strong seasonal pattern of temperature and salinity in these stations within the main channel. Salinity is highest at EMP, the station closest to the mouth, while KoKwel Wharf (closer to the main freshwater source) responds with greater amplitude variations to storm events (i.e., much fresher during February).

A few stressful years

A combination of anomalous atmospheric and oceanic processes occurred in the PNW from late 2013 until 2017: during the winter of 2013, "The Blob" was observed in the North Pacific due to a high-pressure system, moving onto the shelf from Sep-2014 until Mar-2015, increasing sea surface temperature more than 1.5 °C, i.e., the eelgrass threshold (Figure 1B). At the end of 2014, a strong El Niño event was registered in the Equatorial Pacific (up to 2.6 °C anomalies by the end of 2015, Figure 1C), influencing the PNW with warm anomalies of more than 1.5°C from Jul-2015 to May-2016, with additional input of heat due to another marine heatwave (Figure 1B). These anomalies would exceed the temperature stress threshold for eelgrass in the PNW (Table 2).

The persistent high-pressure also impeded the arrival of winter storms in 2013-2014, reducing river discharge and

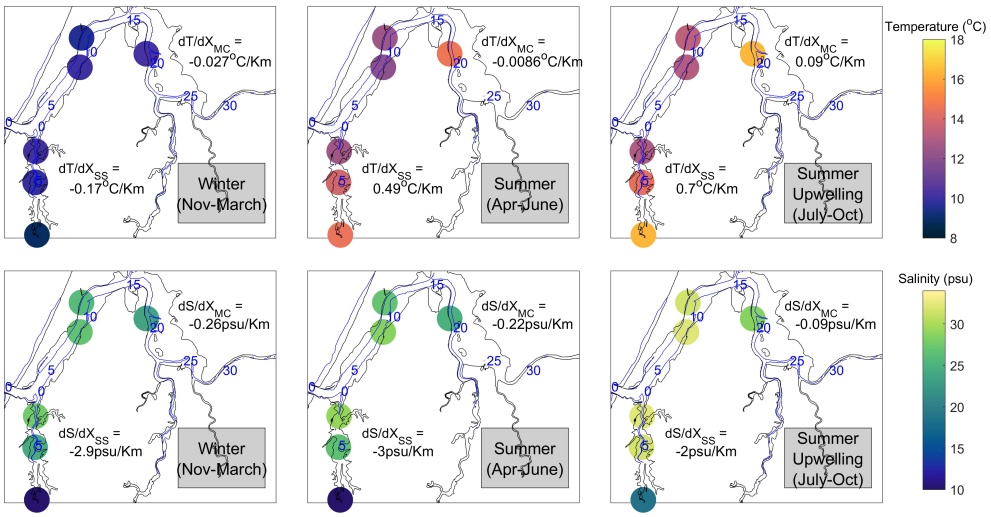

FIGURE 5
Spatial distribution of temperature (top plots) and salinity (bottom plots) 2004-2014 climatology derived at stations inside the Coos Estuary during Winter (left), Summer (middle) and Upwelling (right) time periods. Blue numbers refer to distance (km) from the mouth along the thalweg in the main channel and along the channel in South Slough.

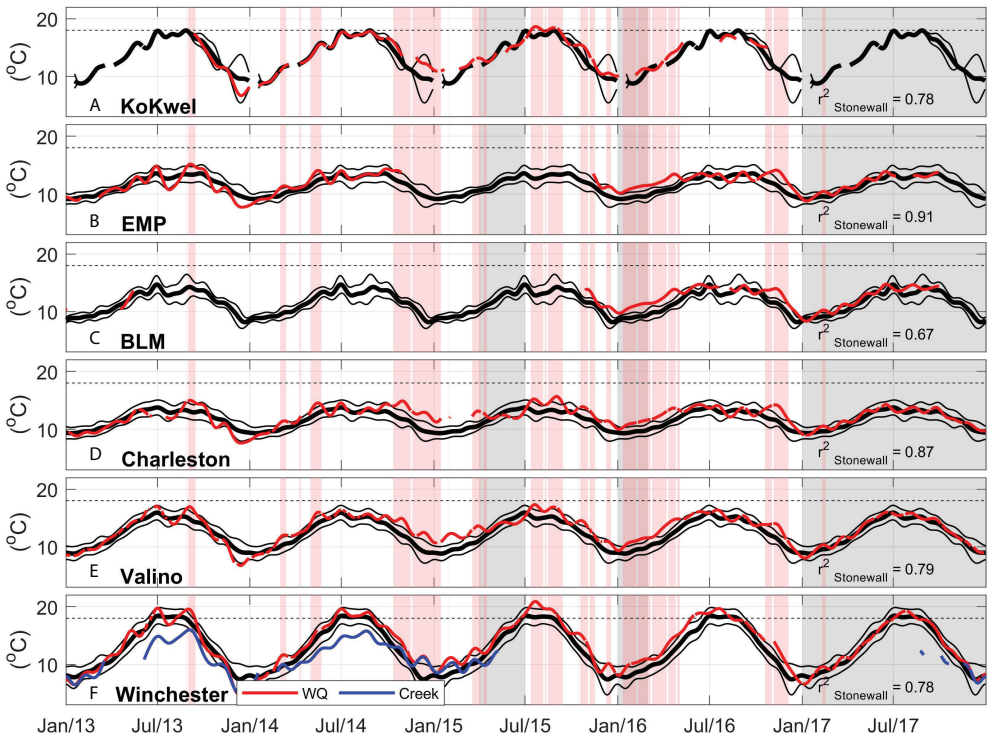

FIGURE 6
Coos Estuary water temperature during 2013-2017, thick black lines show 2004-2014 climatological mean, thin black lines show +/- 1 standard deviation, thin red line shows daily averages with a 30-day low pass filter. Red bands show periods in which water temperature at Charleston WQ is 1 standard deviation above the 2004-2014 climatology (black line in Figure 6D). Gray bands show periods in which eelgrass density at Valino is below the 2004-2014 climatology by one standard deviation. Correlation between Charleston WQ and the Stonewall buoy shown in text (significance level = 0.04). **(A)** KoKwel Wharf, **(B)** EMP, **(C)** BLM, **(D)** Charleston, **(E)** Valino and **(F)** Winchester WQ and Winchester Creek (blue). 18 °C eelgrass temperature threshold in broken black line for reference.

increasing air temperature at the estuaries in the PNW (Wang et al., 2014). During the winter of 2013-2014, the PNW experienced drought conditions reflected in the below-average water-year cumulative discharge at the South Fork Coos River location: 3240 m^3 s^{-1} during 2013, and 4750 m^3 s^{-1} during 2014, only 50% and 71% of the 2004-2014 climatological cumulative of 6330 m^3 s^{-1}, respectively (Figure 4D). Lower river discharge is also related to the higher-than-average salinity during 2013 and 2014 (Figure 7). During this warm period, the Coos Estuary experienced extended time periods with water temperature ≥1.5° C than the mean: Charleston WQ registered 107 of the anomalously warm days during 2014, 116 days in 2015 and 146 days in 2016 (Supplementary Figure 4, calculated using the low-pass filtered data). The intrusion of anomalously warmer water in the Coos Estuary is especially noticeable during the Fall and Winter of 2014–2016 (Figure 6). In fact, of the days ≥1.5 °C the mean, 80% occurred during the winter months of October to December. In Oct-2014, water temperature registered 1 standard deviation above the mean at KoKwel Wharf, Charleston, Valino and Winchester, until the following Apr-2015. From Jul-2015 until May-2016, anomalously warm waters were again observed, with only short periods within 1 standard deviation of the mean. Despite the proximity of Valino WQ and Winchester WQ to the ocean boundary (5.6 and 7.1 km respectively, Figure 2), these stations showed a greater number of days with temperature anomalies above 1.5 °C in 2013-2016 compared to other water quality stations at similar or greater distance (Supplementary Figure 4), suggesting local estuarine dynamics are important. Winchester Creek also showed waters 2°C warmer than its 2004-2014 climatology in 2015, when discharge values were close to normal (Figure 6F). These temperatures were close to the estuarine water quality station at Winchester, during the rainy winter season of 2015 (Figure 6F).

Heat budget in the Coos Estuary

The heat budget decomposition shows that heat storage (Figure 8A) is very small with no seasonal pattern. The net surface heat flux (Figure 8B), Q_0 , decomposed into the incoming solar short-wave radiation, outgoing longwave radiation, latent and sensible heat exchange at the surface, is highest in the

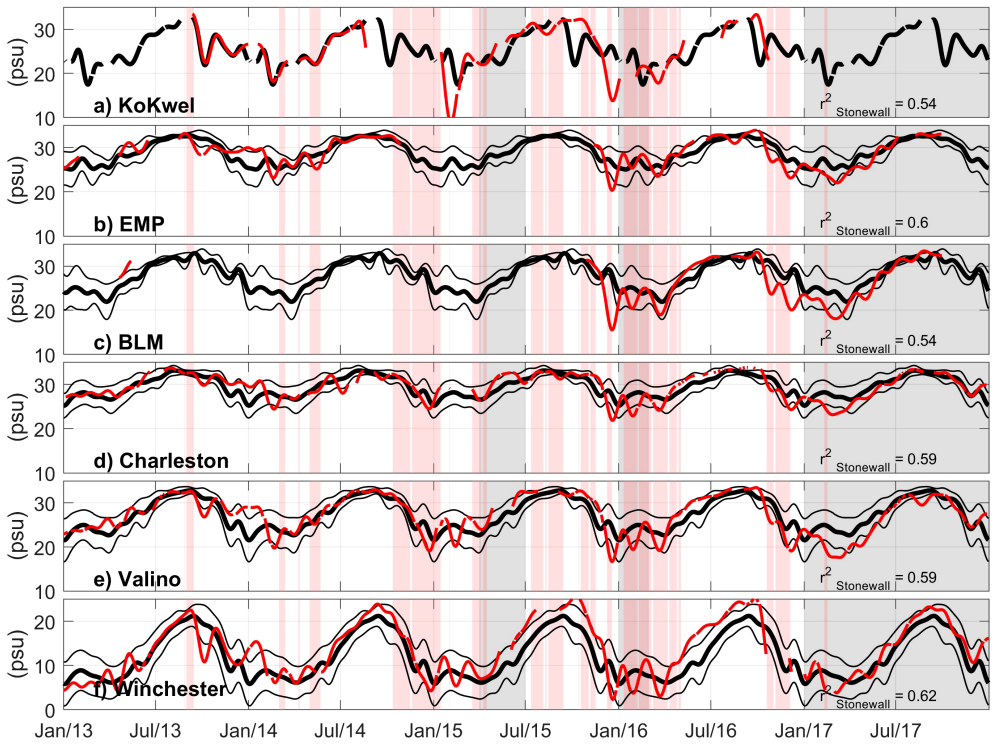

FIGURE 7
Coos Estuary salinity during 2013-2017, thick black lines show 2004-2014 climatological mean, thin black lines show ±1 standard deviation, thin red line shows daily averages with a 30-day low pass filter. Red bands show periods in which water temperature at Charleston WQ is 1 standard deviation above the 2004-2014 climatology (black line in Figure 6D). Gray bands show periods in which eelgrass density at Valino is below the 2004-2014 climatology by one standard deviation. Correlation between Charleston WQ and the Stonewall buoy shown in text. **(A)** KoKwel Wharf, **(B)** EMP, **(C)** BLM, **(D)** Charleston, **(E)** Valino and **(F)** Winchester WQ.

summer and becomes negative in the winter, representing heat loss. Shortwave and longwave radiation have the greatest magnitudes, with values that fluctuate seasonally between 250 and 50 W m^{-2} (shortwave) and -90 and -50 W m^{-2} (longwave). Sensible and latent heat, though smaller, also show a seasonal pattern with positive values in July and August, related to wind and the air-sea temperature difference. Compared to the 2004-2014 climatology, Q_0 during 2014–2016 was anomalously positive (when data are available), mainly due to the shortwave radiation from March to July in those years, and parallels the anomalously high air temperature (Figure 4C).

The 2004-2014 climatology of along-estuary advective heat flux divergence, which depends on the temperature gradient and velocity, shows a strong seasonal pattern mostly in South Slough (between Charleston and Winchester WQ stations, 4.1 km apart), while the main channel (between Charleston and BLM WQ stations, 7.3 km apart) shows a smaller seasonal gradient (Figure 8). Stronger differences between Charleston and Winchester are observed during the dry season (up to -7 °C in late July), due to minimal river discharge and cooler upwelled waters on the oceanic side. In the winter, positive values of $\frac{\partial T_{av}}{\partial x}$, are observed in South Slough, when cooler river discharge closer to Winchester WQ reduces temperature there (Figure 6D) while the oceanic values vary relatively little. Water temperatures at Valino are significantly correlated (r^2 = 0.62) to the along-estuary temperature gradient calculated here, with a change in sign of $\frac{\partial T_{av}}{\partial x}$ at 11.6 °C. Our data shows that during the dry seasons of 2014–2016 (Figure 8D), the temperature gradient was stronger (more negative, especially in 2015–2016), due to warmer waters in the oceanic end member. This is observed in both South Slough (r^2=0.6, Stonewall warmer 43 days before South Slough $\frac{\partial T_{av}}{\partial x}$) and in the main channel. During the rainy season, the temperature gradient is usually driven by increased discharge due to storm events. In the estuary, discharge from the Coos River increases 18 days before the along-estuary temperature gradient changes sign to positive values at South Slough ($\frac{\partial T_{av}}{\partial x}$ r^2=0.6; Figure 4D). In 2013-2014, drought-induced reduced river discharge (Figure 4) would have decreased the advective export of water, while in 2014–2016 closer-to-normal river discharge would have exported relatively warmer riverine waters toward the mouth of the estuary (see winter of 2015 in Figure 6).

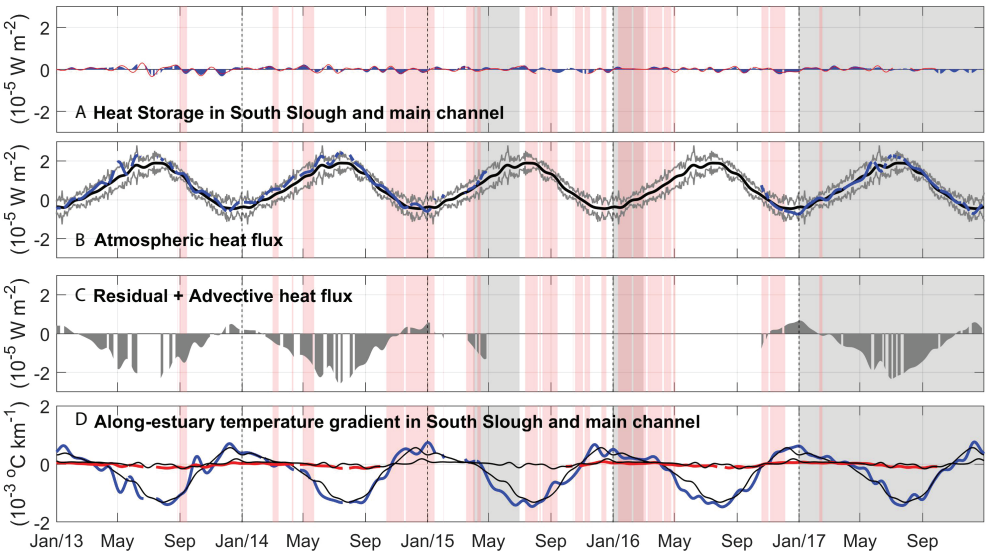

FIGURE 8
Heat budget components in the Coos Estuary during 2013-2017. **(A)** Heat storage in South Slough (blue) and the main channel (red). **(B)** Atmospheric heat flux using data from the Valino water quality station. **(C)** Residual + Advective heat flux (Heat storage minus Atmospheric heat flux), and **(D)** Along-estuary temperature gradient in South Slough (Charleston to Winchester) in blue and in the main channel (Charleston to KoKwel Wharf) in red. Positive $\partial T_{av}/\partial x$ indicates that the station closest to the ocean is warmer than the station furthest up-estuary. Red bands show periods in which water temperature at Charleston WQ is above the 2004-2014 climatology +1 standard deviation (Figure 6). Gray bands show periods in which eelgrass density at Valino is below the 2004-2014 climatology by one standard deviation.

Quarterly variability of eelgrass in South Slough

Quarterly eelgrass surveys at Valino Island since 2004 give an unprecedented long-term view of eelgrass health in South Slough (Figure 9). Valino Island showed mean (μ) densities of 50 shoots per m^2 (with standard deviations, σ = 31), where temperature ranged from 15.9 to 8.8 °C, and can be considered the optimal range. Data from the Danger Point site, furthest away from the mouth and surveyed much less frequently, showed similar values (μ = 54, σ = 43). The closest water quality station to Danger showed a broader temperature (18.4 – 7.4 °C) and salinity range (21 – 6 psu at Winchester). Two other sites at Collver Point and Hidden Creek, showed lower eelgrass densities (μ= 32, σ= 14; μ= 11, σ= 17) throughout the available years. Due to the timing of sampling only once per quarter, assessing the seasonal trend is impossible statistically. Nonetheless, eelgrass in South Slough, as represented by the Valino Island site, shows a robust seasonal pattern in mean shoot density that typically increases in summer, and declines in the fall/winter (Figure 3). Canopy height, number of flowering shoots and percent cover displayed a similar seasonality (not shown). Other eelgrass data collected by the Oregon Department of Fish and Wildlife (ODFW SEACOR) and Oregon State University, provide assessment of eelgrass in the Coos Estuary in scattered locations throughout the estuary during 2015–2018. These stations show higher values of eelgrass density (60-326 eelgrass shoots per m^2) compared to the South Slough stations (Figure 9), through most of the surveys. These ocean-dominated stations do not show a strong decline in eelgrass density during the anomalous years, as that observed in the more estuarine-dominated South Slough.

During 2013–2014, *Z. marina* phenology at Valino Island followed the expected seasonal pattern (Figure 3A): low percent cover and density in the winter months, with density of 54 shoots per m^2 during the Nov-2013 survey. In summer 2014, high productivity was registered at Valino Island, with a value of 78 shoots per m^2. By Apr-2015, however, eelgrass density decreased to significantly lower than the long-term mean (33 shoots per m^2), after the warming of estuarine waters during the previous fall and winter (Figure 6). Beyond the seasonal high of Jul-2015 (44 shoots per m^2), density remained very low with values around 5 shoots per m^2 through to present day. This decay was not only observed in the density, but in the height of the canopy and the total percent cover. The other eelgrass survey sites at Collver Point, Danger Point, and Hidden Creek, also show low density, canopy height, number of flowering shoots and percent cover in the annual survey during this period (June-July 2016). Of these stations, only Collver, the most marine station, seems to recover with densities of 20 shoots per m^2 (Jun-2021). Surveys from stations outside of South Slough, show a small decrease yet not as large in magnitude or as long-lasting as

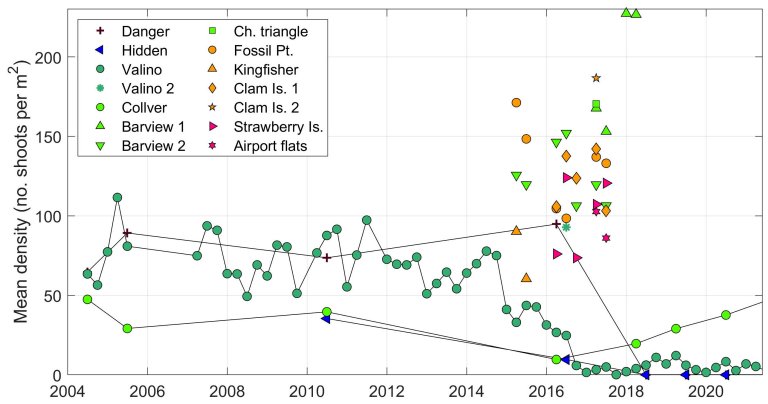

FIGURE 9
Density of eelgrass (number of shoots m^2) until present for all eelgrass measurements from stations shown in Figure 2B and Supplemental Figure 1B. Stations are colored by general areas: purple to green = South Slough, yellow to pink = main channel. Connected symbols correspond to the stations shown in Figure 3A.

at Valino Island, where a decay from 170 to 90 eelgrass shoots per m^2 was observed from Feb-2015 to Jul-2016 (Figure 9).

Discussion

Water quality, river discharge, air temperature, and wind stress data all demonstrate the strong seasonality in the Coos Estuary that mimics the larger scale CCS patterns (Figure 3). Warmer, saltier estuarine characteristics are observed between April and June, after which upwelling-favorable conditions produce cold, saltier waters at the ocean boundary, which finally transition to rainy, fresher and colder conditions in the estuary due to increased precipitation and reduced solar input. This seasonality is affected by interannual variations of the surrounding atmosphere and ocean, which modulate the estuary on all its boundaries, i.e., from the ambient ocean waters at its mouth, the river discharge input, and the atmospheric heat fluxes on its surface. However, the results do indicate that there is significant spatial variability in how the estuary responds to these larger-scale interannual variations due to local bathymetry and geometry constraints. For example, during the warmer years of 2014-2016, the up-estuary stations in South Slough (Valino, Winchester) are relatively warmer for extended periods of time compared to stations that are further away from the mouth in the main channel (e.g., BLM, KoKwel). This disparate response to environmental forcing may stress species, such as eelgrass, which occupy distinct regions of the estuary. By disentangling the impact of the temporal variations in estuarine water forcing with spatial factors (e.g., depth and distance from the mouth), we provide a framework to discuss how changing estuarine conditions might stress organisms differentially. We start by 1) examining changes outside the estuary at the basin scale, then move into 2) along-estuary gradients and spatial variability in hydrographic conditions before considering 3) long-term temporal variability due to the expected future warming under anthropogenic climate change. Finally, we examine the dramatic eelgrass decrease observed within the Coos Estuary in the context of the temperature variability described above.

Basin scale variability

Though many organisms grow in wide temperature ranges, a persistent anomaly may stress species such as eelgrass beyond recovery (e.g., >1.5 °C above normal, Table 2). During the winter of 2013–2014, the PNW experienced drought conditions, related to a persistent atmospheric high-pressure ridge linked to variability in the North Pacific Oscillation (Figure 1), a known precursor of El Niño conditions (Wang et al., 2014; Di Lorenzo and Mantua, 2016). The high-pressure also affected the arrival of winter storms in the PNW, resulting in the below-average water-year cumulative discharge in the Coos River (Figure 4D) and increased air temperature in the Coos Estuary in 2013-2014 (Figure 4C). This combination produced anomalously warm water temperatures during 2014 in the Coos Estuary. During the winter of 2013, the "Blob" was observed in the North Pacific and moved onto the shelf from Sep-2014 until Mar-2015, increasing SST more than 1.5 °C eelgrass threshold at the Stonewall buoy. Positive anomalies (>1.5°C, Figure 1B) were observed at Stonewall again from Jul-2015 to May-2016 related to a second marine heatwave (Di Lorenzo and Mantua, 2016). During the El Niño event in 2015 SST anomalies of 4 °C where registered at the Stonewall buoy, with maximum anomalies between Nov-2015 and Jan-2016. This El Niño

event increased the likelihood of storms and precipitation in the PNW, increasing river discharge at the Coos River, as registered during 2015-2016 (Alexander et al., 2002; Goodman et al., 2018). This atmospheric connection also reduces upwelling-favorable winds which would normally bring colder waters during the late summer to the Coos Estuary (Capotondi et al., 2019).

Though the El Niño conditions can have a strong impact on the PNW, observational and modelling efforts (Jacox et al., 2016) indicate that the temperature anomalies observed on the continental shelf (Figure 1B) were mostly related to the marine heatwave. At the Stonewall buoy, the combination of these basin-scale processes increased water temperature (>1.5°C warmer than the 2004-2014 climatology) during the fall and winter of 2014, 2015 and slightly during 2016 (Figure 4B). The warm anomalies slightly decreased during the upwelling seasons of each year but picked up again after the winds started to relax (Figure 4A). These anomalies were observed in estuaries from San Francisco Bay (up to 3°C, Cloern et al., 2017), to Puget Sound (up to 1 °C, Jackson et al., 2018). In the Coos Estuary, anomalies up to 2°C were observed in Charleston, 3 km from the mouth, in March-2015. Increased water temperature at the ocean boundary will increase the heat that can be advected into the estuary and alter the along-estuary temperature gradient.

Along-estuary differences in temperature

Water temperature and salinity levels in estuaries are controlled by the interaction of advective fluxes, atmospheric fluxes and exchanges with the ocean boundary at the estuary mouth and the river boundaries at each freshwater input (Smith, 1983; Stevenson and Niiler, 1983). Our subtidal data highlights the influence of the ocean end-member on temperature in the estuary, which weakens with distance from the mouth due to the impact of the river end-member. Additionally, the along and across-estuary temperature gradients vary with depth, which is set by dredging in the Coos and many other estuaries of the PNW, though not within South Slough (Eidam et al., 2020). Though tidal advection is a major factor in the Coos Estuary (Conroy et al., 2020), South Slough shows greater temporal temperature variability than the main channel, most likely due to a combination of shallower channels (~5 m) and increased areas of tidal flats (Sutherland and O'Neill, 2016). Dynamically, the main channel stations are located farther seaward than the up-estuary stations in South Slough, even though their physical distances are closer. That is, if one accounts for the length of the salinity intrusion over the main channel versus South Slough, the Valino and Winchester stations would be located up-estuary of any existing observation's locations in the main channel. As temperature increases beyond the climatology due to interannual or climate variability, the storage and flux of heat will change and affect the estuarine ecosystems.

Our qualitative approach to the heat budget in the Coos Estuary (Eq. 1) allows one to spatially and temporally fingerprint the anomalously warm water due to interannual variability during 2014-2016, and can be applied to other estuaries in the PNW (Figure 1A). The analysis for the Coos Estuary highlights the increased atmospheric heat flux in South Slough during the marine heatwave in 2014-2015, due to the inverse dependence on depth.

On top of the anomalous atmospheric heat flux during 2014–2016, the advective heat flux shows changes due to variability of the along-estuary temperature gradient as well as changes to along-estuary velocity. Our data shows that during the dry seasons of 2014–2016 (Figure 8D), the temperature gradient was stronger (more negative, especially in 2015–2016), due to warmer waters in the oceanic end member (Charleston – red bars in Figure 8). During drought years, a decreased estuarine circulation could potentially increase temperature inside the estuary. During normal river discharge years, the ocean influx is greater, so if these ocean waters are relatively warm that could also lead to an increase in temperature within the estuary. As ocean temperature increased in late 2014 on the ocean-end member, an anomalous temperature gradient is observed in South Slough (Figure 8), when Winchester Creek temperature increases (Figure 6). In 2015-2016 the water-year cumulative discharge was normal. A simple back-of-the-envelope calculation of the second term in Eq. 1 using $\frac{\partial T_{dv}}{\partial x}$ requires speeds of 0.01 m s^{-1} in South Slough. This speed can be estimated from observations by dividing the river discharge by the estuarine cross-sectional area of interest. We use available data from water-penetrating airborne lidar survey (Conroy et al., 2020), to calculate the area for a cross section near Valino, and a scaled river discharge for the watershed area in Winchester, Joe Ney Creek, Elliot Creek and John B. Creek (Figure 2). This produces maximum speeds of 0.014 m s^{-1} in the winter, confirming our advective flux calculations.

Long term variability

The combination of anomalously warm water in the PNW with anomalously warm air temperature and advection of riverine waters, produced anomalously warm estuarine waters in South Slough during 2014–2016. These potentially stressful years motivate the question if we can expect this combination to occur more or less often in a warming climate. Observations along the PNW coast (including the ones presented here) show responses related to the large-scale climatic patterns (e.g., ENSO, PDO and NPGO), where positive basin-scale temperature anomalies led to increased temperature inside estuarine systems (Johnson et al., 2003; Cloern et al., 2017; Jackson et al., 2018). Climate model simulations suggest that in the

future, an increased variance of the North Pacific Oscillation (NPO) can be expected (Wang et al., 2014; Black et al., 2018; Capotondi et al., 2019), which was the leading cause of the marine heatwave (the Blob) and also connected to the 2013-2014 drought conditions in the PNW. El Niño events, correlated to higher temperature and sea level in the PNW are also expected to occur more often in the future (Wang et al., 2014; Di Lorenzo and Mantua, 2016). El Niño events have also been correlated to a more intense downwelling and later onset of summer upwelling in the PNW both of which would produce warmer temperatures in the ocean end-member (Frischknecht et al., 2015). Additionally, it is still unclear whether river discharge will increase or decrease with climate change in the PNW, most models agree that in South Slough, Yaquina, Willapa and Coquille estuary, higher discharge is expected in October and November, while lower discharge is expected in July and August (Steele et al., 2012), moving the dry period in these estuaries earlier in the year, similar to that observed in 2014–2016.

The temperature time series here, focused on the last decade, can hint at what can be expected in the future. Traditionally, the spring and fall transitions that mark the beginning and end of upwelling season, respectively, also demarcate the arrival of distinct transport pathways across the shelf, enhanced primary and secondary production, and many other ecological processes. These transitions have been changing in time over the past century, in response to the ocean, river and atmospheric forcing dictated to some degree by basin-scale processes and climate change (Di Lorenzo et al., 2015; Black et al., 2018; Capotondi et al., 2019). Given the importance of the estuarine temperature gradient to the ecological health of South Slough and other PNW estuaries, we develop a method similar to the upwelling index produced by Pierce et al. (2006). That is, we find the day of the year when the landward and shallowest station is warmer than the most marine-influenced station (here that means the Winchester to Charleston temperature gradient in summer) and the day of the year in which this relationship reverses (Winchester is colder than Charleston in winter, Figure 10A). Figure 10B shows these "transition" days for all the years available, as well as the Spring/Fall transition from Pierce et al. (2006), calculated using daily upwelling indices, proportional to alongshore wind stress at 45°N. This transition from spring to fall index at 45°N shows a progression towards earlier upwelling, leading to a stronger influence of the ocean in PNW estuaries (Pierce et al., 2006). Due to the dependence of the temperature gradient on discharge, we also define transition dates for the Coos Estuary River discharge as greater and smaller than 3.2 $m^3 s^{-1}$ (average during dry season). Our 14-year-long time series shows a similar pattern to the Spring Transition dates that mark the beginning of upwelling season (r^2 = 0.56), while the Fall transition is delayed by 23 days in average (r^2 = 0.54). Our data also show that the end of the warming period in South Slough does not only depend on the oceanic conditions (which is correlated with the Pierce index), but also on river discharge (r^2 = 0.47) and atmospheric forcing (r^2 = 0.57). Hence, in a future of warming climate, when large-scale oscillations are expected to occur more frequently (Di Lorenzo and Mantua, 2016), an increase in the temperature in the estuaries of the PNW, as well as an extended dry, warm season can be expected, which will have large impacts on these ecosystems.

Increased estuary temperature due to climate variability is widely documented (Nixon et al., 2004; Preston, 2004; Seekell and Pace, 2011), yet the combination of intensified end-member heat sources and their impact on the hydrodynamics is not as well described. Our transition-day time series, though short and not statistically significant ($\frac{\partial T_{av}}{\partial x}$ slope $\neq$ 0, r^2 = 0.03), is significantly correlated to the Pierce transition index (r^2 = 0.55), which extends from 1995 to 2020. The Summer Pierce transition index (and by correlation, our estuarine temperature gradient) shows a shift towards an earlier beginning of the summer, and later start of the winter season (Summer transition date slope $\neq$ 0, r^2 = 0.3), as also predicted from river discharge forecasting (Steele et al., 2012). This extended earlier dry season can affect the ecosystem by changing ranges of temperature, stratification, and may produce hypoxia (Officer et al., 1984) or affect organisms such as eelgrass and oysters (Borde et al., 2003; Thom et al., 2003; Black et al., 2014). Finally, as temperature increases, the dynamic influence on water density may become significant, especially during the summer, affecting the baroclinic circulation in estuaries, by intensifying or weakening the along-channel density differences that drive estuarine circulation (Hickey et al., 2003; Raimonet and Cloern, 2017).

Effects on eelgrass (*Zostera marina*)

In-situ observations as well as remotely sensed surveys reveal that eelgrass has decreased in abundance in the up-estuary portions of South Slough and the greater Coos Estuary (Figure 2; Supplementary Figure 1). Remotely sensed data from 2005 and 2016 show a decrease of eelgrass-covered area in the Coos Estuary, with higher survival in the main channel than in South Slough (Supplementary Figure 2B), despite the proximity of the sub-estuary to the mouth of the estuary and influence of coastal waters (Raimonet and Cloern, 2017; Magel et al., 2022). Notably, stations in South Slough that were only 3-10 km from the mouth are less marine-influenced than the main channel stations that reside 5-15 km from the mouth, a result that is consistent with the structure of the salinity intrusion in the Coos Estuary (Conroy et al., 2020). Though our data show increased water and air temperature over the whole estuary (Figure 6), a stronger decline of eelgrass was also registered in *in-*

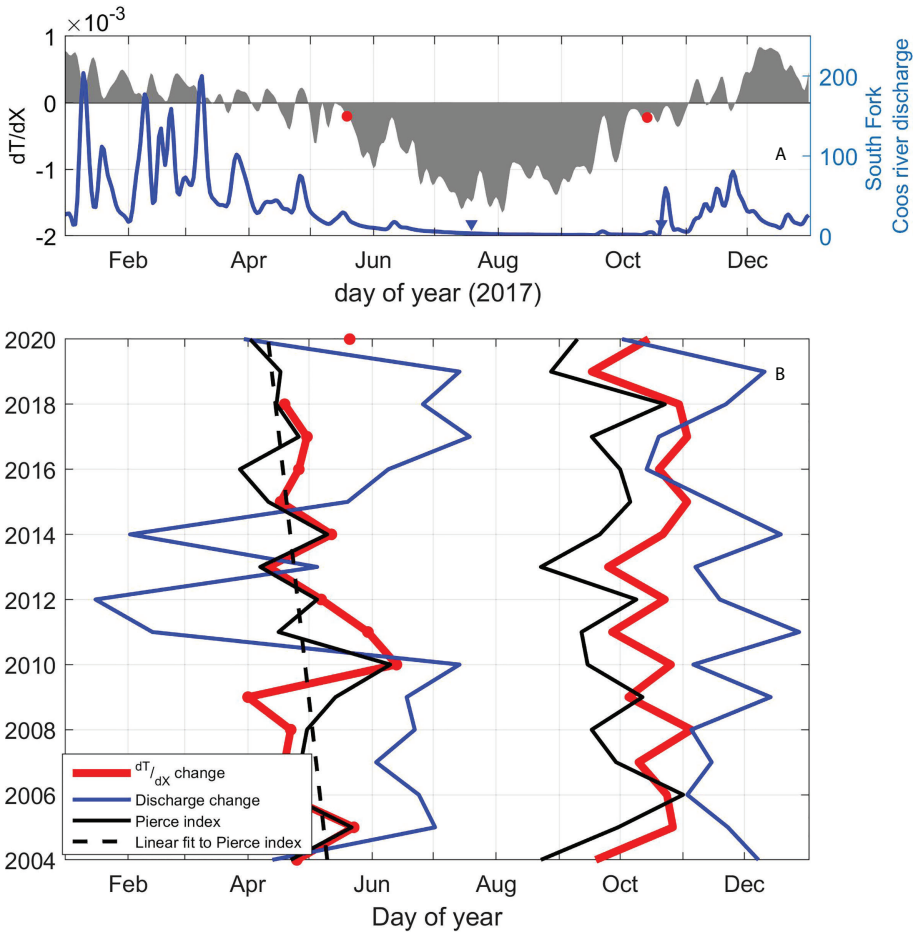

FIGURE 10
(A) Temperature gradient and discharge transition date determination example (2017) and zero-crossing of gradients before and after the dry season. **(B)** Annual variability of transition periods: in red spring and summer temperature gradient change (notice no available data for 2019); in blue South Fork of the Coos River discharge transition dates; in black Pierce index (2006) spring and fall transition dates for all years. Statistically significant linear fit to Pierce index spring transition (2006) in black broken line.

situ stations within the up-estuary portion of South Slough (Figure 3).

Eelgrass is sensitive to temperature stress, as it can increase photosynthetic and respiration rates (Beca-Carretero et al., 2018), and lead to higher susceptibility to wasting disease (Kaldy, 2014). Our results suggest that the MHWs and increased air temperature contributed to the eelgrass density decline in 2015 (Figures 3, 10, Supplementary Figure 4). In contrast, Magel et al. (2022) show an increase in eelgrass at one annually-surveyed station (Barview, see Figure 9) closer to the main channel than Valino Island. Their results show an increase in eelgrass density and biomass during the summer of 2015 and summer of 2016, followed by a decline to longer term average values. They attribute the anomalous increase during a MHW to increased upwelling. However, the annual frequency of those surveys leaves open questions about lags in response, as well as the co-occurrence of other biological interactions (epiphyte and macroalgae interaction). Our data shows that despite the short seasonal increase in eelgrass cover, the density of eelgrass at Valino Island declined again in 2016 when anomalously warm waters related to the El Niño event were again observed. Eelgrass at Valino has not fully recovered since (Figure 3). Stronger declines in eelgrass density were registered in the stations in South Slough compared to stations in the main channel (Supplementary Figure 2C) which are warmer for extended periods of time, especially during 2014-2016 (Supplementary Figure 3). This temperature anomaly can be attributed not only to the distance from the oceanic end-member and the river end-member, but also to storage of heat in shallower areas, such as those where eelgrass is found (0.5–1.0 m MLLW).

Conclusions

In the Pacific Northwest, long-term and large spatial-scale processes, such as El Niño and marine heatwaves, imprint interannual variability on top of typical seasonal trends. Here we used 14 years of data from the Coos Estuary, in southwestern Oregon, to quantify the effects of anomalous oceanic and atmospheric conditions on the estuary, which includes a dramatic die-off in eelgrass.

Superimposed on the interannual and long-term trends, PNW estuaries have a strong seasonal variability in temperature, in which lower water temperatures occur between November and March due to increased river discharge and wintertime atmospheric heat loss, producing a negative along-estuary temperature gradient. During the dry season, warmer air temperature and reduced river discharge increase water temperature, increasing the along-estuary temperature gradient. Between July and October, equatorward winds at the coast produce the upwelling of cold, saline, nutrient rich waters, increasing the temperature gradient further.

The combination of drought in 2013–2014, El Niño in 2014, the Blob marine heatwave in 2014–2015, and El Niño in 2016, produced anomalously warm waters in the coastal ocean outside of the estuary, along with warmer air temperatures and increased river discharge during the El Niño events. Inside the estuary, the warming was recorded in all the available water quality observations, with higher anomalies found in the shallower locations and those located further away from the estuary mouth. Water temperature increased landward, suggesting that river input and atmospheric heat flux may be important contributors to the anomalous conditions observed. These relatively higher temperatures found landward changed the overall along-estuary temperature gradient in the estuary with higher values in the beginning of the dry season before upwelling at the coast begins. Enhanced temperature gradients, along with relatively higher absolute temperatures in the upper estuary can cause stress on organisms, such as eelgrass, potentially explaining at least part of the die-off observed.

These temperature-related stress factors can be expected to occur more frequently in a warming climate, when more marine heatwaves and El Niño events can be expected. Our analysis shows that the temperature gradient in the Coos Estuary is correlated to an upwelling index that is proportional to alongshore wind stress. The longer upwelling index timeseries shows a shift towards earlier spring transitions, which would produce a longer summer season and possibly stronger influence of temperature on the baroclinic component of circulation.

Though time series available in the PNW are relatively short to assess long-term trends statistically, the observations analyzed here show 1) a shift to a later, shorter rainy season and 2) an increased synchrony of decadal (i.e., PDO) and interannual (i.e., MHWs) processes. As global temperatures warm due to climate change, we can expect an increased number of marine heatwaves and El Niño events, which will increase the temperature in Pacific Northwest estuaries, leading to changes in seasonal timing and potentially shifting the habitat areas in estuary ecosystems.

Data availability statement

The datasets presented in this study can be found in online repositories. The names of the repository/repositories and accession number(s) can be found below: http://nvs.nanoos.org https://www.ndbc.noaa.gov/station_page.php?station=46050, http://streamdata.cooswatershed.org/.

Author contributions

MJMJ is the lead author on the manuscript, developing the methodology, analyzing the observational data, and writing the manuscript. DS served as advisor, aiding in data interpretation and manuscript editing. AH collected and analyzed the eelgrass data, and aided in the results and discussion. All authors contributed to the article and approved the submitted version.

Funding

The Science Collaborative is funded by the National Oceanic and Atmospheric Administration and managed by the University of Michigan Water Center (NA19NOS4190058 and NA19NOS4200076). Additional funding for MJMJ was provided through Operations Award as 315-10 Davidson Fellowship and Student Development Opportunities. Funds for publication were granted through the Open Access Article Processing Charge Committee and the University of Oregon Libraries.

Acknowledgments

Eelgrass density data in locations outside of South Slough were obtained through several collaborations of SSNERR with the Oregon Department of Fish and Wildlife (ODFW SEACOR), Oregon State University (OSU) and the Pacific Marine Environmental Laboratory. This work was sponsored by the National Estuarine Research Reserve System Science Collaborative, which supports collaborative research that addresses coastal management problems important to the reserves.

Conflict of interest

The authors declare that the research was conducted in the absence of any commercial or financial relationships that could be construed as a potential conflict of interest.

Publisher's note

All claims expressed in this article are solely those of the authors and do not necessarily represent those of their affiliated organizations, or those of the publisher, the editors and the reviewers. Any product that may be evaluated in this article, or claim that may be made by its manufacturer, is not guaranteed or endorsed by the publisher.

Supplementary material

The Supplementary Material for this article can be found online at: https://www.frontiersin.org/articles/10.3389/fmars.2022.930440/full#supplementary-material

References

Alexander, M. A., Bladé, I., Newman, M., Lanzante, J. R., Lau, N.-C., and Scott, J. D. (2002). The atmospheric bridge: The influence of ENSO teleconnections on air–Sea interaction over the global oceans. *J. Clim.* 15, 2205–2231. doi: 10.1175/1520-0442(2002)015<2205:TABTIO>2.0.CO;2

Baptista, A. M. (1989). *Salinity in coos bay* (Oregon: U.S. Army Engineer District).

Barnard, P. L., Hoover, D., Hubbard, D. M., Snyder, A., Ludka, B. C., Allan, J., et al. (2017). Extreme oceanographic forcing and coastal response due to the 2015-2016 El niño. *Nat. Commun.* 8, 6–13. doi: 10.1038/ncomms14365

Basilio, A., Searcy, S., and Thompson, A. R. (2017). Effects of the blob on settlement of spotted sand bass, paralabrax maculatofasciatus, to mission bay, San Diego, CA. *PloS One* 12, 6–8. doi: 10.1371/journal.pone.0188449

Beca-Carretero, P., Olesen, B., Marbà, N., and Krause-Jensen, D. (2018). Response to experimental warming in northern eelgrass populations: Comparison across a range of temperature adaptations. *Mar. Ecol. Prog. Ser.* 589, 59–72. doi: 10.3354/meps12439

Bi, H., Peterson, W. T., and Strub, P. T. (2011). Transport and coastal zooplankton communities in the northern California current system. *Geophys. Res. Lett.* 38, 1–5. doi: 10.1029/2011GL047927

Black, B. A., Sydeman, W. J., Frank, D. C., Griffin, D., Stahle, D. W., Garcia-Reyes, M., et al. (2014). Six centuries of variability and extremes in a coupled marine-terrestrial ecosystem. *Science* 345, 1498–1502. doi: 10.1126/science.1253209

Black, B. A., van der Sleen, P., Di Lorenzo, E., Griffin, D., Sydeman, W. J., Dunham, J. B., et al. (2018). Rising synchrony controls western north American ecosystems. *Glob. Change Biol.* 24, 2305–2314. doi: 10.1111/gcb.14128

Bond, N. A., Cronin, M. F., Freeland, H., and Mantua, N. (2015). Causes and impacts of the 2014 warm anomaly in the NE pacific. *Geophys. Res. Lett.* 42, 3414–3420. doi: 10.1002/2015GL063306

Borde, A. B., Thom, R. M., Rumrill, S., and Miller, L. M. (2003). Geospatial habitat change analysis in pacific Northwest coastal estuaries. *Estuaries* 26, 1104–1116. doi: 10.1007/bf02803367

Capotondi, A., Sardeshmukh, P. D., Di Lorenzo, E., Subramanian, A. C., and Miller, A. J. (2019). Predictability of US West coast ocean temperatures is not solely due to ENSO. *Sci. Rep.* 9, 1–10. doi: 10.1038/s41598-019-47400-4

Chhak, K., and Di Lorenzo, E. (2007). Decadal variations in the California current upwelling cells. *Geophys. Res. Lett.* 34, 1–6. doi: 10.1029/2007GL030203

Clinton, P. J., Young, D. R., Specht, D. T., and Lee, I. I. ,. H. (2007). *A guide to mapping intertidal eelgrass and nonvegetated habitats in estuaries of the pacific Northwest USA* (National Health and Environmental Effects Research Laboratory (NHEERL) Office of Research and D. Newport OR. by Project Officer: Walter G . Nelson.

Cloern, J. E., Jassby, A. D., Schraga, T. S., Nejad, E., and Martin, C. (2017). Ecosystem variability along the estuarine salinity gradient: Examples from long-term study of San Francisco bay. *Limnol. Oceanogr.* S272–S291. doi: 10.1002/lno.10537

Conroy, T., Sutherland, D. A., and Ralston, D. K. (2020). Estuarine exchange flow variability in a seasonal, segmented estuary. *J. Phys. Oceanogr.* 50, 595–613. doi: 10.1175/JPO-D-19-0108.1

Costanza, R., D'Arge, R., de Groot, R., Farber, S., Grasso, M., Hannon, B., et al. (1997). The value of the world's ecosystem services and natural capital. *Nature* 387, 253–260. doi: 10.1038/387253a0

Daly, E. A., Brodeur, R. D., and Auth, T. D. (2017). Anomalous ocean conditions in 2015: Impacts on spring Chinook salmon and their prey field. *Mar. Ecol. Prog. Ser.* 566, 168–182. doi: 10.3354/meps12021

Davis, K. A., Banas, N. S., Giddings, S. N., Siedlecki, S. A., MacCready, P., Lessard, E. J., et al. (2014). Estuary-enhanced upwelling of marine nutrients fuels coastal productivity in the U.S. pacific Northwest. *J. Geophys. Res. Ocean.* 119 (12), 8778–8799. doi: 10.1002/2014JC010248

Delefosse, M., Povidisa, K., Poncet, D., Kristensen, E., and Olesen, B. (2016). Variation in size and chemical composition of seeds from the seagrass *Zostera marina*-ecological implications. *Aquat. Bot.* 131, 7–14. doi: 10.1016/j.aquabot.2016.02.003

Di Lorenzo, E., Fiechter, J., Schneider, N., Braceo, A., Miller, A. J., Franks, P. J. S., et al. (2009). Nutrient and salinity decadal variations in the central and eastern north pacific. *Geophys. Res. Lett.* 36, 2003–2008. doi: 10.1029/2009GL038261

Di Lorenzo, E., Liguori, G., Schneider, N., Furtado, J. C., Anderson, B. T., and Alexander, M. A. (2015). ENSO and meridional modes: A null hypothesis for pacific climate variability. *Geophys. Res. Lett.* 42, 9440–9448. doi: 10.1002/2015GL066281

Di Lorenzo, E., and Mantua, N. (2016). Multi-year persistence of the 2014/15 north pacific marine heatwave. *Nat. Clim. Change* 6, 1042–1047. doi: 10.1038/nclimate3082

Di Lorenzo, E., Schneider, N., Cobb, K. M., Franks, P. J. S., Chhak, K., Miller, A. J., et al. (2008). North pacific gyre oscillation links ocean climate and ecosystem change. *Geophys. Res. Lett.* 35, 2–7. doi: 10.1029/2007GL032838

Echavarria-Heras, H. A., Solana-Arellano, E., and Franco-Vizcaíno, E. (2006). The role of increased Sea surface temperature on eelgrass leaf dynamics: Onset of El niño as a proxy for global climate change in San quintín bay, Baja California. *Bull. South. Calif. Acad. Sci.* 105, 113–127. doi: 10.3160/0038-3872(2006)105[113:TROISS]2.0.CO;2

Eidam, E. F., Sutherland, D. A. A., Ralston, D. K. K., Dye, B., Conroy, T., Schmitt, J., et al. (2020). Impacts of 150 years of shoreline and bathymetric change in the coos estuary, Oregon, USA. *Estuaries Coasts* 1170–1188. doi: 10.1007/s12237-020-00732-1

Emmett, R., Llansó, R., Newton, J., Thom, R. M., Hornberger, M., Morgan, C., et al. (2000). Geographic signatures of north American West coast estuaries. *Estuaries* 23, 765. doi: 10.2307/1352998

Evans, E. C., McGregor, G. R., and Petts, G. E. (1998). River energy budgets with special reference to river bed processes. *Hydrol. Process.* 12, 575–595. doi: 10.1002/(SICI)1099-1085(19980330)12:4<575::AID-HYP595>3.0.CO;2-Y

Frischknecht, M., Münnich, M., and Gruber, N. (2015). Remote versus local influence of ENSO on the California current system. *J. Geophys. Res. Ocean.* 120, 1353–1374. doi: 10.1002/2014JC010531

Gao, Y., Fang, J., Du, M., Fang, J., Jiang, W., and Jiang, Z. (2017). Response of the eelgrass (*Zostera marina* l.) to the combined effects of high temperatures and the herbicide, atrazine. *Aquat. Bot.* 142, 41–47. doi: 10.1016/j.aquabot.2017.06.005

Gentemann, C. L., Fewings, M. R., and García-Reyes, M. (2017). Satellite sea surface temperatures along the West coast of the united states during the 2014–2016 northeast pacific marine heat wave. *Geophys. Res. Lett.* 44, 312–319. doi: 10.1002/2016GL071039

Goodman, A. C., Thorne, K. M., Buffington, K. J., Freeman, C. M., and Janousek, C. N. (2018). El Niño increases high-tide flooding in tidal wetlands along the U.S. pacific coast. *J. Geophys. Res. Biogeosciences* 123, 3162–3177. doi: 10.1029/2018JG004677

Groner, M., Eisenlord, M., Yoshioka, R., Fiorenza, E., Dawkins, P., Graham, O., et al. (2021). Warming sea surface temperatures fuel summer epidemics of eelgrass wasting disease. *Mar. Ecol. Prog. Ser.* 679, 47–58. doi: 10.3354/meps13902

Groth, S., and Rumrill, S. (2009). History of Olympia oysters (ostrea lurida carpenter 1864) in Oregon estuaries, and a description of recovering populations in coos bay. *J. Shellfish Res.* 28, 51–58. doi: 10.2983/035.028.0111

Hessing-Lewis, M. L., Hacker, S. D., Menge, B. A., and Rumrill, S. S. (2011). Context-dependent eelgrass-macroalgae interactions along an estuarine gradient in the pacific Northwest, USA. *Estuaries Coasts* 34, 1169–1181. doi: 10.1007/s12237-011-9412-8

Hickey, B. M., and Banas, N. S. (2003). Oceanography of the U. S. doi: 10.1007/bf02803360

Hickey, B. M., Zhang, X., and Banas, N. S. (2003). Coupling between the California current system and a coastal plain estuary in low riverflow conditions. *J. Geophys. Res.* 108, 1–20. doi: 10.1029/2002JC001737

Hosack, G. R., Dumbauld, B. R., Ruesink, J. L., and Armstrong, D. A. (2006). Habitat associations of estuarine species: Comparisons of intertidal mudflat, seagrass (*Zostera marina*), and oyster (Crassostrea gigas) habitats. *Estuaries Coasts* 29, 1150–1160. doi: 10.1007/BF02781816

Huyer, A. (1983). Coastal upwelling in the California current system. *Prog. Oceanogr.* 12, 259–284. doi: 10.1016/0079-6611(83)90010-1

Huyer, A., Smith, R. L., and Fleischbein, J. (2002). The coastal ocean off Oregon and northern California during the 1997-8 El niño. *Prog. Oceanogr.* 54, 311–341. doi: 10.1016/S0079-6611(02)00056-3

Huyer, A., Wheeler, P. A., Strub, P. T., Smith, R. L., Letelier, R., and Kosro, P. M. (2007). Progress in oceanography the Newport line off Oregon – studies in the north East pacific 75 (2), 126–160. doi: 10.1016/j.pocean.2007.08.003

Jackson, J. M., Johnson, G. C., Dosser, H. V., and Ross, T. (2018). Warming from recent marine heatwave lingers in deep British Columbia fjord. *Geophys. Res. Lett.* 45, 9757–9764. doi: 10.1029/2018GL078971

Jacox, M. G., Hazen, E. L., Zaba, K. D., Rudnick, D. L., Edwards, C. A., Moore, A. M., et al. (2016). Impacts of the 2015–2016 El niño on the California current system: Early assessment and comparison to past events. *Geophys. Res. Lett.* 43, 7072–7080. doi: 10.1002/2016GL069716

Jarvis, J. C., Moore, K. A., and Kenworthy, W. J. (2012). Characterization and ecological implication of eelgrass life history strategies near the species' southern limit in the western north Atlantic. *Mar. Ecol. Prog. Ser.* 444, 43–56. doi: 10.3354/meps09428

Johnson, M. R., Williams, S. L., Lieberman, C. H., and Solbak, A. (2003). Changes in the abundance of the seagrasses *Zostera marina* l. (eelgrass) and ruppia maritima l. (widgeongrass) in San Diego, California, following an El niño event. *Estuaries* 26, 106–115. doi: 10.1007/BF02691698

Kaldy, J. (2012). Influence of light, temperature and salinity on dissolved organic carbon exudation rates in *Zostera marina* l. *Aquat. Biosyst.* 8, 1–12. doi: 10.1186/2046-9063-8-19

Kaldy, J. E. (2014). Effect of temperature and nutrient manipulations on eelgrass *Zostera marina* l. from the pacific Northwest, USA. *J. Exp. Mar. Bio. Ecol.* 453, 108–115. doi: 10.1016/j.jembe.2013.12.020

Kalnay, E., Kanamitsu, M., Kistler, R., Collins, W., Deaven, D., Gandin, L., et al. (1996). The NCEP/NCAR 40-year reanalysis project. *Bull. Am. Meteorol. Soc* 77, 437–471. doi: 10.1175/1520-0477(1996)077<0437:TNYRP>2.0.CO;2

Large, W. G., and Pond, S. (1981). Open Ocean Momentum Flux Measurements in Moderate to Strong Winds. *J. Phys. Oceanogr.* 11, 324–336. doi: 10.1175/1520-0485(1981)011<0324.

Lee, H. II, and Brown, C. A. (eds.) (2009). *Classification of Regional Patterns of Environmental Drivers And Benthic Habitats in Pacific Northwest Estuaries*. U.S. EPA, Office of Research and Development, National Health and Environmental Effects Research Laboratory, Western Ecology Division.

Lee, K. S., Park, S. R., and Kim, Y. K. (2007). Effects of irradiance, temperature, and nutrients on growth dynamics of seagrasses: A review. *J. Exp. Mar. Bio. Ecol.* 350, 144–175. doi: 10.1016/j.jembe.2007.06.016

Logerwell, E. A., Mantua, N., Lawson, P. W., Francis, R. C., and Agostini, V. N. (2003). Tracking environmental processes in the coastal zone for understanding and predicting Oregon coho (Oncorhynchus kisutch) marine survival. *Fish. Oceanogr.* 12, 554–568. doi: 10.1046/j.1365-2419.2003.00238.x

Magel, C. L., Chan, F., Hessing-Lewis, M., and Hacker, S. D. (2022). Differential responses of eelgrass and macroalgae in pacific Northwest estuaries following an unprecedented NE pacific ocean marine heatwave. *Front. Mar. Sci.* 9. doi: 10.3389/fmars.2022.838967

McKay, P., and Iorio, D. (2008). Heat budget for a shallow, sinuous salt marsh estuary. *Cont. Shelf Res.* 28, 1740–1753. doi: 10.1016/j.csr.2008.04.008

Milcu, A. I., Hanspach, J., Abson, D., and Fischer, J. (2013). Cultural ecosystem services: A literature review and prospects for future research. *Ecol. Soc* 18. doi: 10.5751/ES-05790-180344

Miller, J. A., and Shanks, A. L. (2004). Ocean-estuary coupling in the Oregon upwelling region: Abundance and transport of juvenile fish and of crab megalopae. *Mar. Ecol. Prog. Ser.* 271, 267–279. doi: 10.3354/meps271267

Nejrup, L. B., and Pedersen, M. F. (2008). Effects of salinity and water temperature on the ecological performance of *Zostera marina*. *Aquat. Bot.* 88, 239–246. doi: 10.1016/j.aquabot.2007.10.006

Nixon, S. W., Granger, S., Buckley, B. A., Lamont, M., and Rowell, B. (2004). A one hundred and seventeen year coastal water temperature record from woods hole, Massachusetts. *Estuaries* 27, 397–404. doi: 10.1007/BF02803532

NOAA National Estuarine Research Reserve System (NERRS) (2020) *System-wide monitoring program* (NOAA NERRS Cent. Data Manag. Off). Available at: http://www.nerrsdata.org (Accessed June 11, 2020).

Officer, C. B., Biggs, R. B., Taft, J. L., Cronin, L. E., Tyler, M. A., and Boynton, W. R. (1984). Chesapeake Bay anoxia: Origin, development, and significance. *Science* 223, 22–27. doi: 10.1126/science.223.4631.22

Peterson, W. T., Fisher, J. L., Strub, P. T., Du, X., Risien, C., Peterson, J., et al. (2017). The pelagic ecosystem in the northern California current off Oregon during the 2014-2016 warm anomalies within the context of the past 20 years. *J. Geophys. Res. Ocean.* 122, 7267–7290. doi: 10.1002/2017JC012952

Phillips, R. C. (1984). The ecology of eelgrass meadows in the pacific Northwest: a community profile. *US Fish Wildl. Serv*.

Phillips, R. C., McMillan, C., and Bridges, K. W. (1983). Phenology of eelgrass, *Zostera marina* l., along latitudinal gradients in north America. *Aquat. Bot.* 15, 145–156. doi: 10.1016/0304-3770(83)90025-6

Pierce, S. D., Barth, J. A., Thomas, R. E., and Fleischer, G. W. (2006). Anomalously warm July 2005 in the northern California current: Historical context and the significance of cumulative wind stress. *Geophys. Res. Lett.* 33, 2–7. doi: 10.1029/2006GL027149

Preston, B. L. (2004). Observed winter warming of the Chesapeake bay estuary, (1949-2002): Implications for ecosystem management. *Environ. Manage.* 34, 125–139. doi: 10.1007/s00267-004-0159-x

Raimonet, M., and Cloern, J. E. (2017). Estuary–ocean connectivity: fast physics, slow biology. *Glob. Change Biol.* 23, 2345–2357. doi: 10.1111/gcb.13546

Roegner, G. C., Hickey, B. M., Newton, J. A., Shanks, A. L., and Armstrong, D. A. (2002). Wind-induced plume and bloom intrusions into willapa bay, Washington. *Limnol. Oceanogr.* 47, 1033–1042. doi: 10.4319/lo.2002.47.4.1033

Roegner, G. C., Needoba, J. A., and Baptista, A. M. (2011). Coastal upwelling supplies oxygen-depleted water to the columbia river estuary. *PloS One* 6. doi: 10.1371/journal.pone.0018672

Roegner, G. C., and Shanks, A. L. (2001). Import of coastally-derived chlorophyll a to south Slough, Oregon. *Estuaries* 244, 244–256. doi: 10.2307/1352948

Salo, T., and Pedersen, M. F. (2014). Synergistic effects of altered salinity and temperature on estuarine eelgrass (*Zostera marina*) seedlings and clonal shoots. *J. Exp. Mar. Bio. Ecol.* 457, 143–150. doi: 10.1016/j.jembe.2014.04.008

Schneider, S. (1993). ""Scenarios of global warming,"," in *Biotic interactions and global change*. Eds. P. Kareiva, J. Kingsolver and R. Huey (Sunderland, MA: Sinauer Associates), 9–23.

Seekell, D. A., and Pace, M. L. (2011). Climate change drives warming in the Hudson river estuary, new York (USA). *J. Environ. Monit.* 13, 2321–2327. doi: 10.1039/c1em10053j

Seppelt, R., Dormann, C. F., Eppink, F. V., Lautenbach, S., and Schmidt, S. (2011). A quantitative review of ecosystem service studies: Approaches, shortcomings and the road ahead. *J. Appl. Ecol.* 48, 630–636. doi: 10.1111/j.1365-2664.2010.01952.x

Shanks, A. L., Rasmuson, L. K., Valley, J. R., Jarvis, M. A., Salant, C., Sutherland, D. A., et al. (2020). Marine heat waves, climate change, and failed spawning by coastal invertebrates. *Limnol. Oceanogr.* 65, 627–636. doi: 10.1002/lno.11331

Sherman, K., and DeBruyckere, L. A. (2018) *Eelgrass habitats on the U.S. West coast. state of the knowledge of eelgrass ecosystem services and eelgrass extent*. Available at: http://www.pacificfishhabitat.org/wp-content/uploads/2017/09/EelGrass_Report_Final_ForPrint_web.pdfeation%2020180109.pdf.

Short, F. T., and Coles, R. G. (2001). *Global seagrass research methods*. Eds. F. T. Short and R. G. Coles (Elsevier: Amsterdam, The Netherlands).

Short, F. T., McKenzie, L. J., Coles, R. G., Vidler, K. P., and Gaeckle, J. L. (2006). *SeagrassNet Manual for Scientific Monitoring of Seagrass Habitat, Worldwide* edition. University of New Hampshire Publication. 75

Smith, N. P. (1983). A comparison of winter and summer temperature variations in a shallow bar-built estuary. *Estuaries* 6, 2–9. doi: 10.2307/1351801

Steele, M. O., Chang, H., Reusser, D. A., Brown, C. A., and Jung, I.-W. (2012). Potential climate-induced runoff changes and associated uncertainty in four Pacific Northwest estuaries: *U.S. Geological Survey Open-File Report 2012-1274*, 63. doi: 10.3133/ofr20121274

Stevenson, J. W., and Niiler, P. P. (1983). Upper ocean heat budget during the Hawaii-to-Tahiti shuttle experiment. *J. Phys. Oceanogr.* 13, 1894–1907. doi: 10.1175/1520-0485(1983)013<1894:UOHBDT>2.0.CO;2

Strub, P. T., Allen, J. S., Huyer, A., Smith, R. L., and Beardsley, R. C. (1987). Seasonal cycles of currents, temperatures, winds, and sea level over the northeast pacific continental shelf: 35°N to 48°N. *J. Geophys. Res.* 92, 1507. doi: 10.1029/JC092iC02p01507

Sutherland, D. A., and O'Neill, M. A. (2016). Hydrographic and dissolved oxygen variability in a seasonal pacific Northwest estuary. *Estuar. Coast. Shelf Sci.* 172, 47–59. doi: 10.1016/j.ecss.2016.01.042

Thom, R. M., and Albright, R. G. (1990). Dynamics of benthic vegetation standing-stock, irradiance, and water properties in central Puget Sound. *Mar. Biol.* 104, 129–141. doi: 10.1007/BF01313166

Thom, R. M., Borde, A. B., Rumrill, S., Woodruff, D. L., Williams, G. D., Southard, J. A., et al. (2003). Factors influencing spatial and annual variability in eelgrass (*Zostera marina* l.) meadows in willapa bay, Washington, and coos bay, Oregon, estuaries. *Estuaries* 26, 1117–1129. doi: 10.1007/BF02803368

Thom, R. M., Gaeckle, J., Buenau, K., Borde, A., Vavrinec, J., Aston, L., et al. (2018). Eelgrass (*Zostera marina* L.) restoration in Puget Sound: development of a site suitability assessment process. *Restor. Ecol.* 26, 1066–1074. doi: 10.1111/rec.12702

Wang, S.-Y., Hipps, L., Gillies, R. R., and Yoon, J.-H. (2014). Probable causes of the abnormal ridge accompanying the 2013-2014 California drought: ENSO precursor and anthropogenic warming footprint. *Geophys. Res. Lett.* 41, 3220–3226. doi: 10.1002/2014GL059748

Wyrtki, K. (1984). The slope of sea level along the equator during the 1982/1983 El nino. *J. Geophys. Res.* 89, 10419–10424. doi: 10.1029/JC089iC06p10419

Zapata, C., Puente, A., Garca, A., Garcia-Alba, J., and Espinoza, J. (2018). Assessment of ecosystem services of an urbanized tropical estuary with a focus on habitats and scenarios. *PloS One* 13, 1–19. doi: 10.1371/journal.pone.0203927

Zimmerman, R. C., Smith, R. D., and Alberte, R. S. (1989). Thermal acclimation and whole-plant carbon balance in *Zostera marina* L. (eelgrass). *J. Exp. Mar. Bio. Ecol.* 130, 93–109. doi: 10.1016/0022-0981(89)90197-4

frontiers | Frontiers in Marine Science

TYPE Original Research
PUBLISHED 14 December 2022
DOI 10.3389/fmars.2022.898080

OPEN ACCESS

EDITED BY
Juan Jose Munoz-Perez,
University of Cádiz, Spain

REVIEWED BY
Xiaoxia Zhang,
Dalian University of Technology, China
Samantha Chapman,
Villanova University, United States

*CORRESPONDENCE
Svenja Reents
svenja.reents@awi.de

SPECIALTY SECTION
This article was submitted to Coastal Ocean Processes, a section of the journal Frontiers in Marine Science

RECEIVED 16 March 2022
ACCEPTED 21 November 2022
PUBLISHED 14 December 2022

CITATION
Reents S, Möller I, Evans BR, Schoutens K, Jensen K, Paul M, Bouma TJ, Temmerman S, Lustig J, Kudella M and Nolte S (2022) Species-specific and seasonal differences in the resistance of salt-marsh vegetation to wave impact.
Front. Mar. Sci. 9:898080.
doi: 10.3389/fmars.2022.898080

Species-specific and seasonal differences in the resistance of salt-marsh vegetation to wave impact

Svenja Reents[1,2]*, Iris Möller[3], Ben R. Evans[4], Ken Schoutens[5], Kai Jensen[1], Maike Paul[6,7], Tjeerd J. Bouma[8,9], Stijn Temmerman[5], Jennifer Lustig[10], Matthias Kudella[11] and Stefanie Nolte[12,13]

[1]Applied Plant Ecology, Institute of Plant Science and Microbiology, University of Hamburg, Hamburg, Germany, [2]Alfred Wegener Institute, Helmholtz Centre for Polar and Marine Research, Wadden Sea Research Station, List, Germany, [3]Department of Geography, School of Natural Sciences, Trinity College Dublin, Dublin, Ireland, [4]British Antarctic Survey, Cambridge, United Kingdom, [5]Ecosphere, University of Antwerp, Antwerp, Belgium, [6]Landscape Ecology and Environmental Systems Analysis, Institute of Geoecology, Technische Universität Braunschweig, Braunschweig, Germany, [7]Leibniz University Hannover, Ludwig Franzius Institute of Hydraulic, Estuarine and Coastal Engineering, Hannover, Germany, [8]Department of Estuarine and Delta Systems, Royal Netherlands Institute for Sea Research (NIOZ), Yerseke, Netherlands, [9]Faculty of Geosciences, Department of Physical Geography, Utrecht University, Utrecht, Netherlands, [10]BioConsult SH GmbH & Co. KG, Husum, Germany, [11]Forschungszentrum Küste (FZK), Hannover, Germany, [12]School of Environmental Sciences, University of East Anglia, Norwich, United Kingdom, [13]Center for Environment, Fisheries and Aquaculture Science (Cefas), Lowestoft, United Kingdom

The coastal protection function provided by the vegetation of tidal wetlands (e.g. salt marshes) will play an important role in defending coastlines against storm surges in the future and depend on how these systems respond to such forcing. Extreme wave events may induce vegetation failure and thereby risking loss of functionality in coastal protection. However, crucial knowledge on how hydrodynamic forces affect salt-marsh vegetation and whether plant properties might influence plant resistance is missing. In a true-to-scale flume experiment, we exposed two salt-marsh species to extreme hydrodynamic conditions and quantified wave-induced changes in plant frontal area, which was used to estimate plant damage. Moreover, half of the plants were artificially weakened to induce senescence, thus allowing us to examine potential seasonal effects on plant resistance. Morphological, biomechanical as well as biochemical plant properties were assessed to better explain potential differences in wave-induced plant damage. Our results indicate that the plants were more robust than expected, with pioneer species *Spartina anglica* showing a higher resistance than the high-marsh species *Elymus athericus*. Furthermore, wave-induced plant damage mostly occurred in the upper part of the vegetation canopy and thus higher canopies (i.e. *Elymus athericus*) were more vulnerable to damage. Besides a taller canopy, *Elymus athericus* had weaker stems than *Spartina anglica*, suggesting that biomechanical properties (flexural stiffness) also played a role in defining plant resistance. Under the highest wave conditions, we also found seasonal differences in the vulnerability to plant damage but only for *Elymus athericus*. Although we found higher concentrations of a strengthening

compound (biogenic silica) in the plant material of the weakened plants, the flexibility of the plant material was not affected indicating that the treatment might not has been applied long enough. Nevertheless, this study yields important implications since we demonstrate a high robustness of the salt-marsh vegetation as well as species-specific and seasonal differences in the vulnerability to plant damage.

KEYWORDS

salt marshes, flume experiment, wave-induced damage, plant properties, seasonality

Introduction

Salt marshes are intertidal wetlands that are widely distributed along the coastlines from middle to high latitudes. They are increasingly recognized as contributing to the provision of valuable ecosystem services such as climate change mitigation through long-term carbon sequestration (Mcleod et al., 2011) or coastal protection through wave attenuation (Möller et al., 2014). To a great extent, the provision of these ecosystem services is determined by the vegetation of salt marshes which mainly consists of highly specialized grasses, herbs and shrubs that are adapted to high salinities and regular flooding (Adam, 2002). Despite their value, the persistence of salt marshes is threatened by anthropogenic pressures like their embankment, land-use change, eutrophication and climate change, leading to a salt marsh loss of 1-2% of the global area per year (Duarte et al., 2013). From all climate change factors, so far the impact of accelerated sea level rise on marshes has been most widely studied (Spencer et al., 2016; Schuerch et al., 2018), while other climate change effects such as the projected changes in storm intensities and thus hydrodynamic forcing has still received relatively less attention (Leonardi et al., 2018; Armitage et al., 2020).

Previous research examining the interaction of hydrodynamic forces and salt-marsh vegetation mainly focused on the wave attenuation capacity of salt marshes, i.e. the effect of vegetation on waves. These studies compared the wave attenuation capacity of different plant species as well as whole ecosystems, or aimed to find determinants of effective reduction in wave energy (Möller et al., 2003; Pinsky et al., 2013; Anderson and Smith, 2014). In a true-to-scale flume experiment, Möller et al. (2014) showed that the vegetation of NW European salt marshes is able to reduce significant wave height by between 15% and 60% over a 40 m distance under storm surge conditions. Additionally, the authors observed that the behavior of the tall grass *Elymus athericus* under the action of waves differed from that of the much shorter *Puccinellia maritima*, suggesting that plant-wave interactions and thereby wave attenuation capacity is dependent on species-specific traits (Rupprecht et al., 2017). These species traits include e.g. length, width, number or rigidity of plant stems and leaves, all influencing vegetation properties known to affect wave attenuation such as aboveground biomass (Bouma et al., 2010; Ysebaert et al., 2011), plant frontal area (Zhang and Nepf, 2021), stem density (Bouma et al., 2005; Anderson and Smith, 2014) and biomechanical properties (Riffe et al., 2011; Paul et al., 2016). However, the vegetation's ability to reduce wave energy is also depending on hydrodynamic conditions like inundation depth and wave orbital velocity (Koch et al., 2009; Gedan et al., 2011; Garzon et al., 2019). For example, above certain values of orbital velocity, stem breakage and biomass loss may lead to a decrease in wave attenuation (Rupprecht et al., 2017; Vuik et al., 2018). Yet, studies investigating these limits, i.e. defining hydrodynamic conditions above which salt-marsh vegetation experiences severe physical damage, as well as factors that influence plants resistance, are rare.

The few studies that focused on physical damage induced by waves all suggest that the plant damage is species-specific (Coops and van der Velde, 1996; Heuner et al., 2015; Vuik et al., 2018; Schoutens et al., 2021). Furthermore, the observed differences between species have been attributed to differences in stem flexibility (Coops and van der Velde, 1996; Heuner et al., 2015; Vuik et al., 2018) and plant height (Vuik et al., 2018) and, in the case of seedling survival, stem diameter (Schoutens et al., 2021). A theoretical approach by Duan et al. (2002) showed that the position of stem breakage was dependent on the ratio of the top to base stem diameter. With increasing ratio, the position of steam breakage moved further up the stem, a finding that was in line with field observations by Groeneveld and French (1995). Moreover, a stem breakage model developed by Vuik et al. (2018) combined plant morphology (stem height and diameter), flexural strength of the stems and wave-induced bending stress to determine hydrodynamic forces above which stems break or fold. Vuik et al. (2018) found that shorter species were more flexible than taller ones and have a lower probability of stem breakage. However, a species-specific validation remains indispensable.

Apart from species-specific differences, seasonality in vegetation properties needs to be considered when evaluating

the resistance of salt-marsh vegetation and their role for wave attenuation capacity (Schoutens et al., 2019; Zhang et al., 2022). In temperate and boreal regions, aboveground parts of many salt-marsh species die-off in autumn, but remain as dead standing biomass in winter until storms (and thus wave action) induce breakage of stems or leaves and eventually carry the litter away. While transforming from a vital to senescent or even dead state, the plant material undergoes major physiological changes that affect biomechanical properties like stem flexibility (Coops and van der Velde, 1996; Schulze et al., 2019; Zhu et al., 2020). The seasonal vegetation response was also confirmed by the stem breakage model of Vuik et al. (2018), which suggested that the salt marsh grass *Spartina anglica* is more vulnerable to stem breakage in November compared to December or April. During the storm surge season in temperate regions (from autumn until early spring), the coastal protection provided by salt marshes is most needed. However, the protection capacity in winter might be hampered due to changes in plant resistance and wave-induced damage. To our knowledge, it has never been experimentally tested whether seasonal changes in biomechanical or even morphological vegetation properties directly affect plant resistance to extreme wave conditions.

To improve our understanding on how plant's vulnerability to wave-induced damage differs between species and seasonal conditions, we thus conducted a controlled flume experiment. We exposed two NW European salt marsh grass species (*Spartina anglica*, *Elymus athericus*) to progressively increased wave energies and measured plant response as well as biomechanical, biochemical and morphological plant properties. Since *Spartina anglica* usually grows in the pioneer zone of the marsh (low elevations, at the marsh edge), we expected a higher resistance to hydrodynamic forcing and thus lower vulnerability to wave-induced plant damage than for *Elymus athericus*, which typically grows at higher elevations that are less frequently flooded. Furthermore, prior to wave exposure, we induced senescence in half of the plants to create a weakened 'autumn treatment'. We hypothesized that the plant's resistance to hydrodynamic forcing is negatively affected by the autumn treatment due to changes in their biomechanical properties.

Material & methods

This flume experiment was conducted in the Large Wave Flume (Großer Wellenkanal (GWK) of the Forschungszentrum Küste (FZK), Hanover, Germany) in which salt-marsh plants, that have been previously collected in the field, were exposed to extreme hydrodynamic conditions. In addition to recordings of plant response to wave exposure (i.e. wave-induced plant damage), plant properties were assessed.

Plant material

For this study we used *Spartina anglica* (C. E. Hubb) and *Elymus athericus* (Link) Kerguélen, two clonal grass species that are widely distributed in NW European salt marshes. In March 2018, plants were collected in salt marshes of Paulinaschor (*Spartina anglica*, 51°20'56.2"N 3°43'37.4"E) and Zuidgors (*Elymus athericus*, 51°23'13.6"N 3°49'18.5"E) along the Western Scheldt estuary in the Netherlands. They were excavated in sods (20 cm x 20 cm) and transported to the Royal Netherlands Institute for Sea Research (NIOZ) in Yerseke, the Netherlands, where they were kept in the greenhouse until they were planted. Before planting the sods, boxes (120 cm x 80 cm x 40 cm, hereafter referred to as pallets) were lined with an impermeable foil and filled with sediment taken from a marsh of the Scheldt estuary (see Schoutens et al. (2021) for soil properties). Ten holes (2 mm diameter) on each side of the pallet were drilled to allow for drainage after inundation. In April, six sods per pallet were arranged together to create a dense canopy, leading to stem densities of 741 ± 123 stems/m^2 for *Spartina anglica* and 1108 ± 176 stems/m^2 for *Elymus athericus* (mean ± SD). The sods were planted at one end of the pallet to allow the waves to run up over an unvegetated strip before reaching the vegetation (see Figure 1 and Supplementary Material Figures 1A, B).

To assess seasonal differences in plant response to hydrodynamic forces, half of the plants were subjected to an 'autumn treatment' while the others remained as 'summer treatment'. The 'autumn' treatment was achieved by creating a drought, since the plant stress response (e.g. to drought) shares many similarities with the process of natural plant senescence at the end of the growing season (Gepstein and Glick, 2013; Sade et al., 2018). Furthermore, it has been reported that several plant species showed a significant accelerated maturity in response to water limitation (Desclaux and Roumet, 1996; Talukdar, 2013; Cseresnyés et al., 2020). To create a drought, pallets of the 'autumn treatment' were covered for six weeks prior to the flume experiment to exclude rainfall while the 'summer treatment' pallets were kept irrigated with freshwater (Schoutens et al., 2021). Hereafter, the term treatment is used to refer to the condition of the vegetation (summer/autumn).

Flume set up

The experiment in the Large Wave Flume (300 m x 5 m x 7 m) was carried out over three weeks in August 2018. For addressing different research questions within the RESIST project, five zones in total (10 m apart, Figure 1) were used to investigate the effect of increased hydrodynamic forces on different types of marsh vegetation as well as their soil surface.

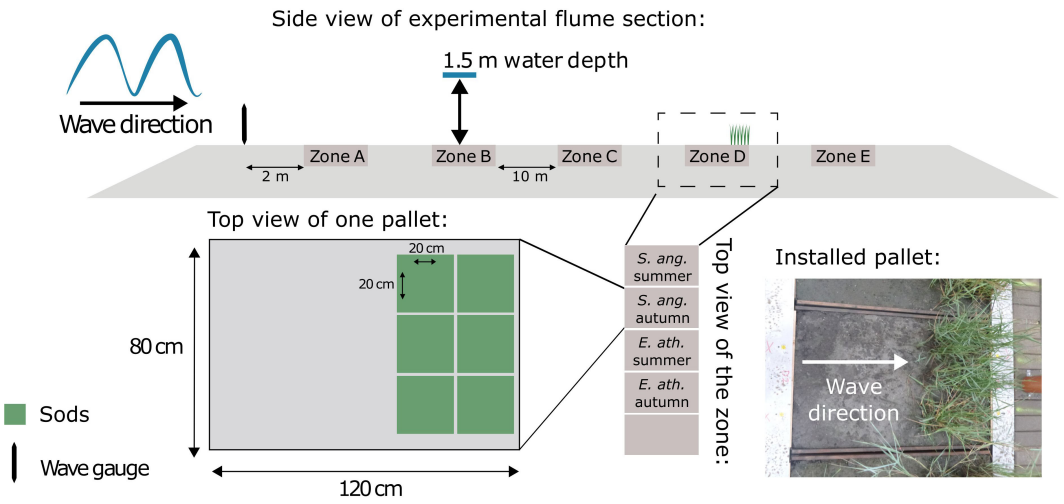

FIGURE 1
Schematic figure illustrating the experimental set up in the flume. The side view of the experimental platform shows the positions of the zones and wave gauges. The top views below visualize the arrangement of the pallets within zone D as well as the sods within a pallet (*S. ang.* = *Spartina anglica*, *E. ath.* = *Elymus athericus*). The figure was adapted from Schoutens et al. (2021).

For instance, in Schoutens et al. (2021), we reported the results for one specific zone where we tested the resistance of seedlings to strong waves. Within each zone five pallets were placed next to each other over the flume width and between concrete blocks which had the same height as the pallets (see Figure 1 and Supplementary Material Figure 1C). The present study only focusses on one other zone, where we specifically tested the resistance of mature shoots of *Spartina anglica* and *Elymus athericus*, both in summer and autumn treatment, resulting in four pallets within this zone, while one pallet was left empty. Each Monday for the three weeks of the experiment, we replaced all pallets with a new set and carried out baseline measurements.

Hydrodynamic conditions

Hydrodynamic conditions were the same as reported in Schoutens et al. (2021). Each day from Tuesday to Friday, we created a sequence of waves that are hereafter referred to as 'wave runs'. Wave runs consisted of 1000 randomly generated waves (JONSWAP spectrum, Hasselmann et al., 1973) that were monitored with wave gauges and from which we calculated significant wave height (H_s) and significant wave period (T_s). The wave gauge array was installed on the flume wall, 2 m in front of the first zone (zone A, Figure 1). The still water level was 1.5 m above the sediment surface for all wave runs. We increased bed orbital velocity by increasing wave height and/or wave period in subsequent wave runs over the course of days and weeks (Table 1), which also implies a cumulative wave exposure experienced by the vegetation and sediment per week. In the third week, pallets were moved to zone A and thus closer to the wave paddle (Figure 1) to further increase hydrodynamic forces. The wave conditions generated in this flume experiment were comparable to natural storm surge conditions in temperate regions (this study: H_s = 0.78 m, h = 1.5 m; field: H_s = 0.58-1.0 m, h = 1.39-3.85 m; H_s = significant wave height, h = inundation depth, Schoutens et al., 2021). After each wave run, we slowly drained the flume to record potential impacts of hydrodynamic forcing on the vegetation (details in next section).

Vegetation response: Δ frontal area and mean vegetation height

To measure plant damage non-destructively, we used the photo-method described by Möller (2006). Every day after the wave run and draining of the flume, a red screen with a scale attached was placed behind the vegetation to increase contrast between vegetation and background (see Supplementary Material Figure 2A). Side-on photographs (Supplementary Material Figure 2B) were taken of the vegetation with a calibrated camera and from the back of the pallet (i.e. facing the back of the flume) always at the same position, height and distance to the screen. Photographs were cropped and corrected for distortion in MATLAB (The MathWorks Inc., 2019) before pixels were classified into either vegetation or background pixel using an unsupervised classification tool and followed by manual class allocation in ArcGIS (ESRI, 2020). Similarly to Rupprecht et al. (2015), these obtained binary images (Supplementary Material Figure 2C) were used to perform further program routines in

TABLE 1 Wave conditions measured in front of the first zone generated in this flume experiment and shown per week and wave run.

		Significant wave height (H_s, in m)			Significant wave period (T_s, in seconds)		
		Week 1	Week 2	Week 3	Week 1	Week 2	Week 3
Wave run	1	0.30	0.68	0.68	2.58	3.80	4.02
	2	0.40	0.68	0.77	4.22	3.80	5.63
	3	0.58	0.78	0.78	3.56	5.66	5.63
	4	0.69	0.78	*0.71*	5.23	5.63	*6.00*

All wave runs consisted of randomly generated waves except for the last wave run (wave run 4 in week 3, italic), where monochromatic waves were used to increase bed shear stress beyond that which can be generated by random wave sequences [see also Schoutens et al. (2021)].

MATLAB to generate information on vegetation structure, adapting the protocol developed by Möller (2006, MATLAB program available on request). Vegetation structure parameters included projected plant frontal area (projected area of vegetation pixel (mm^2) normalized by the horizontal extent of the image (mm)) as well as the vegetation profile (highest vegetation pixel per pixel column). In this study, plant frontal area is given per pixel column and per vertical subsections (0-20 cm, 20-40 cm and >40 cm from soil surface). While projected plant frontal area per pixel column was further processed as described below, plant frontal area per vertical subsections was used to illustrate potential changes in the vertical distribution of the vegetation in each photograph.

Projected plant frontal area per pixel column was spatially referenced and converted into 1 cm wide columns (starting from the bottom left of the image). The data was averaged over 5 cm wide vertical subsections. Every second subsection, as well as the left and right outer edges (6 cm each), were removed to reduce potential impacts from adjacent subsections and pallets, respectively. To detect potential changes in plant frontal area due to wave exposure (indicating plant damage), we calculated the difference between projected plant frontal area prior to (Monday) and after wave exposure (Friday) per week (designated as Δ plant frontal area). It should be noted that changes in plant surface area might result from plant damage but also from reconfiguration of shoots and leaves. Estimations for vegetation height were obtained from vegetation profile data of the photographs taken prior to wave exposure. That data was averaged over the same 5 cm wide vertical subsections as for Δ plant frontal area and designated as mean vegetation height.

Biomechanical plant properties

Three-point bending tests were performed to measure stem flexibility as potential explanatory factor of plant damage under hydrodynamic forcing. Each week prior to and after wave exposure, five stems per species-treatment combination were cut at random at the soil surface. The bottom part of the stem was shortened to a length that was not exceeding a stem diameter-to-length ratio of 1:15 to avoid shear stress while testing (Niklas, 1992). Bending tests were performed with a universal test machine, including flexure fixture and a 5 kN load cell (Instron Corporation, Canton, MA, USA). Following Rupprecht et al. (2015) and Schulze et al. (2019), a force-displacement curve was created to determine the linear slope indicating elastic behavior that was then used to calculate flexural stiffness. Flexural stiffness or flexural rigidity describes the ability of the stem to resist bending, i.e. high values indicate high stem stiffness and thus low flexibility. It combines the information on the stem's material property expressed by the Young's bending modulus and the stem's morphology expressed by the second moment of area which both contribute to overall flexural stiffness. The second moment of area is a term to include stem morphology (i.e. shape and diameter). Since the second moment of area can be derived from the stem's dimensions, we were able to calculate Young's bending modulus, which is only describing the flexibility of the material but without taking stem morphology into account. Equations for calculating flexural stiffness, second moment of area and Young's bending modulus can be found in the Supplementary Material.

Biochemical plant properties

Biogenic silica, lignin and cellulose are known to affect the rigidity of plant tissue (Turner et al., 2001; Schoelynck et al., 2010; Schoelynck et al., 2012) and thus Young's bending modulus. Potential differences in concentrations of these strengthening compounds could provide additional explanations for differences in stem flexibility and therefore plant resistance to hydrodynamic forcing. Plant material that was harvested for flexibility measurements was dried for 72 hours at 70°C and afterwards ground with a mixer mill (MM400, Retsch, Germany). For analyzing lignin and cellulose content, we used the Van Soest method (Van Soest 1963) whereas the biogenic silica content was determined by applying the DeMaster alkaline extraction method (DeMaster 1981).

Statistical analyses

To test whether Δ plant frontal area (difference between projected plant frontal area prior to and after wave exposure),

flexibility parameters (Young's bending modulus, flexural stiffness) and concentration of strengthening compounds (cellulose, lignin, biogenic silica) differed between species, treatments and weeks, factorial ANOVAs were applied. Accordingly, species, treatment, and week, as well as their interactions, were set as explanatory variables. After visually checking ANOVA assumptions following Zuur et al. (2010), flexibility parameters (Young's bending modulus, flexural stiffness) were log transformed to meet normality assumptions. Plant material that was harvested for flexibility measurements and biochemical analyses was tested for differences between the two harvesting days (Monday and Friday). Since we did not find any differences, we merged the data per week. To detect significant differences between species, treatments, and weeks, *post hoc* tests (Tukey's HSD, honest significant difference) were applied. A linear regression was performed to examine the relationship between Δ plant frontal area and mean vegetation height for the entire data set and separately for each species-treatment combination. To test whether biogenic silica concentration affect the flexibility of the plant material (Young's bending modulus) another linear regression with these two variables was conducted. For this regression, Young's bending modulus needed to be averaged over the five stems measured per day since there was not enough plant material of the single samples for the chemical analyses. All statistical analyses were performed using R version 4.1.1. (R Core Team, 2021).

Results

Plant damage under wave exposure

In this study, we used Δ plant frontal area to indicate wave-induced plant damage. Although reconfiguration of plant material might have influenced plant frontal area, we did observe plant damage in the form of torn-off material in the flume after draining (see Supplementary Material Figures 3, 4) which consisted of plant parts (e.g. leaves or inflorescences) as well as whole plants which broke off at soil surface level. Moreover, the quantity of the torn-off plant material reflected the overall trends we found for Δ plant frontal area. However, allocation of torn-off plant material to single pallets or zones was not possible. Δ plant frontal area differed significantly between species, treatments, and weeks (Table 2). Additionally, the three-way-interaction of these factors had a significant effect on Δ plant frontal area as well. In general, *Elymus athericus* showed a stronger reduction in frontal area compared to *Spartina anglica* (*Elymus*: -985.31 ± 950.66 mm^2/mm, *Spartina*: -6.44 ± 499.91 mm^2/mm, Figure 2, mean ± SD), implying that *Elymus athericus* lost more biomass due to wave exposure than *Spartina anglica*. Summer and autumn treatments of *Spartina anglica* showed similar response in Δ plant frontal area and decreased from week to week. This decrease was also found for *Elymus athericus* in autumn condition, but in comparison with *Spartina anglica* it was much more pronounced in *Elymus athericus*. In the third week, the difference in Δ plant frontal area between the summer and autumn treatment of *Elymus athericus* was highly significant (Figure 2) while differences between summer and autumn treatment were not significant for all other weeks for *Elymus athericus* and were never significant for *Spartina anglica*.

Considering the spatial distribution of the vegetation in each photograph (Figure 3), the area from the bottom of the photograph to 20 cm height was completely saturated with vegetation for both species. For *Elymus athericus*, the area from 20 to 40 cm was likewise saturated, while wave-induced changes in frontal area became visible in this section on photographs of *Spartina anglica*. However, most changes in frontal area were detected in the upper section (>40 cm) for all species-treatment combinations. Here, frontal area tended to decrease over the course of days and weeks, which was most pronounced in the autumn treatment of *Elymus athericus*, indicating that plant damage was restricted to biomass removal from the top of the vegetation.

TABLE 2 Summary statistics of factorial ANOVAs for testing the effect of species, treatment and week (and their interaction) on Δ plant frontal area, Young's bending modulus (MPa), flexural stiffness (Nm^2) and biogenic silica concentration (mg/g dry weight).

	Δ plant frontal area		Young's bendingmodulus		Flexural stiffness		Biogenic silica	
	F value	p value	F value	p value	F value	p value	F value	p value
Species	54.83	<0.001	64.98	<0.001	111.41	<0.001	50.99	<0.001
Treatment	6.72	<0.05	1.98	n.s.	2.63	n.s.	16.00	<0.01
Week	11.77	<0.001	20.05	<0.001	7.05	<0.01	10.25	<0.01
Species x treatment	7.44	<0.01	3.43	n.s.	0.09	n.s.	3.52	n.s.
Treatment x week	10.48	<0.001	0.27	n.s.	0.38	n.s.	2.45	n.s.
Species x week	1.45	n.s.	2.21	n.s.	9.32	<0.001	1.99	n.s.
Species x treatment x week	9.04	<0.001	2.05	n.s.	0.32	n.s.	0.16	n.s.

Cellulose and lignin are not included since no significant effects were detected (n.s., not significant).

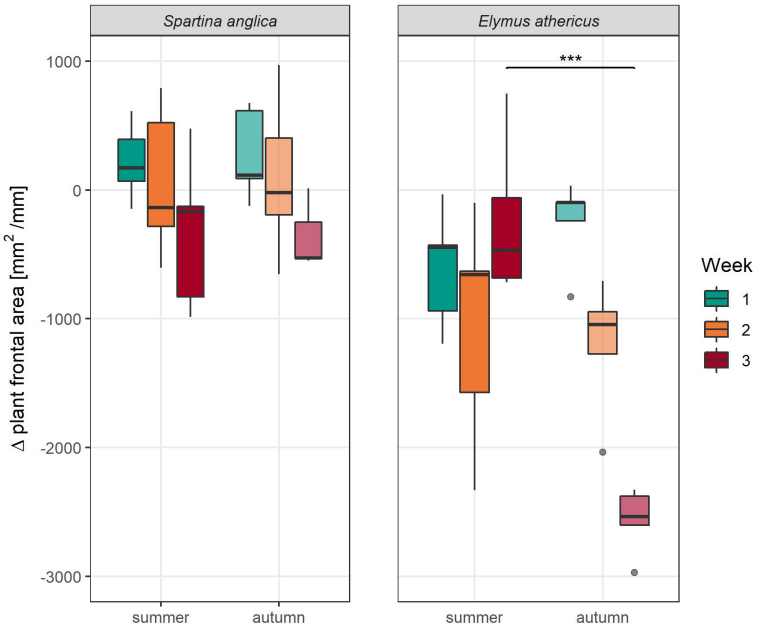

FIGURE 2
Δ plant frontal area (difference between prior to and after wave exposure) per week of *Spartina anglica* and *Elymus athericus* in summer and *autumn condition*. Asterisks show significant differences between the summer and autumn treatment within the same species and week based on Tukey's HSD *post hoc* test (***p < 0.001).

Morphological properties and plant damage

The linear regression between mean vegetation height (in mm) and Δ plant frontal area showed a negative relationship (R^2 = 0.36, p <0.001, Table 3) indicating an increase in plant damage (as Δ plant frontal area decreased) with increasing vegetation height (Figure 4). Additionally, mean vegetation height clearly differed between both species, i.e. *Elymus athericus* being taller than *Spartina anglica* (Figure 4). For both species, autumn treatments were slightly taller than summer treatments (*Spartina anglica*: 624.1 ± 98.5 mm (summer) and 658.9 ± 145.6 mm (autumn), *Elymus athericus*: 832.7 ± 121.3 mm (summer) and 929.9 ± 92.4 mm (autumn)). However, no significant linear relationships between mean vegetation height and Δ plant frontal area were found for single species-treatment combinations except for the summer treatment of *Elymus athericus* (Table 3).

Biomechanical properties and plant resistance

Young's bending modulus differed significantly between species and weeks, but no significant effects of treatment and the interactions between factors were found (Table 2). In general, Young's bending modulus of *Elymus athericus* was twice as high as that of *Spartina anglica* (*Elymus*: 1169.82 ± 646.86 MPa, *Spartina*: 553.74 ± 315.04 MPa, Figure 5), indicating a higher stiffness of the plant material of *Elymus athericus*. From week to week, Young's bending modulus increased, a trend that was more pronounced for *Elymus athericus*.

Similarly, flexural stiffness, which describes the absolute strength of plant stems (material stiffness + stem morphology), differed significantly between species and weeks (Table 2). Furthermore, the interaction of species and week had a significant effect on flexural stiffness of the vegetation. Flexural stiffness of *Spartina anglica* was four times higher than of *Elymus athericus* (*Spartina*: 6.56 ± 4.39 Nm^2*10^{-3}, *Elymus*: 1.61 ± 1.59 Nm^2*10^{-3}), indicating that *Spartina anglica* stems had a higher resistance to bending than the ones of *Elymus athericus*. Yet no clear trend was recognizable for *Spartina anglica*, we found a slight increase in flexural stiffness for *Elymus athericus* from week to week (Figure 6).

Biochemical properties and plant resistance

We found no significant effects of species, treatment or week on the lignin and cellulose concentration of the plant material harvested in our flume experiment. Biogenic silica concentration, however, was

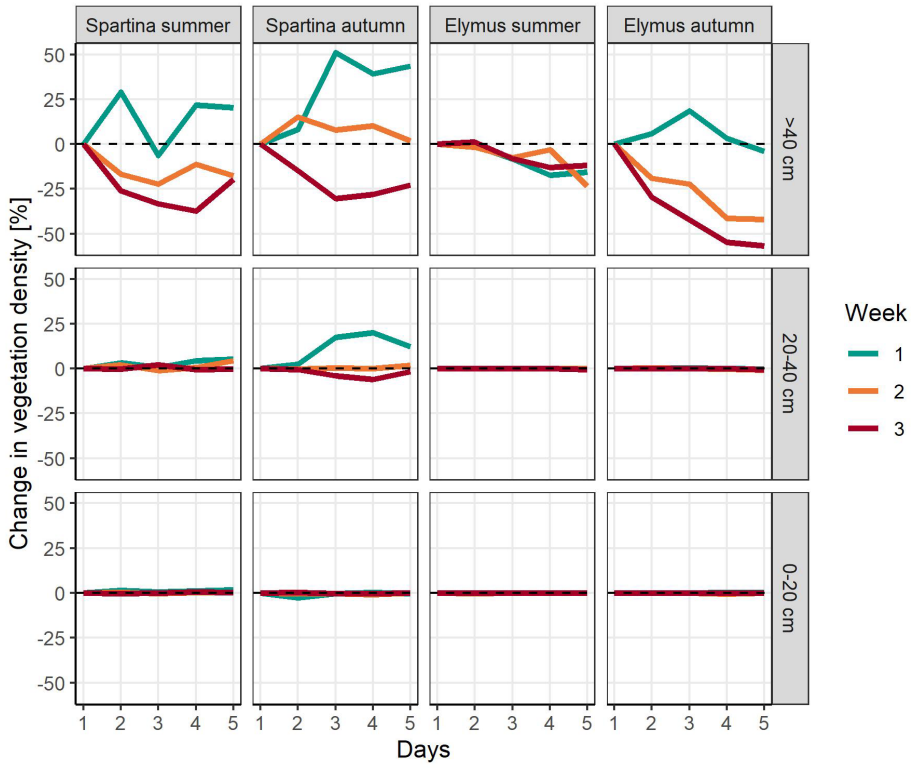

FIGURE 3
Change in projected plant frontal area in percent (relative to the condition prior to wave exposure on day 1) of three different vertical subsections shown per day, week and species-treatment combination. Dashed lines indicate a plant frontal area equivalent to the initial state on day 1 of the experimental week (i.e. 100%).

significantly affected by species, treatment, and week but no significant interaction was found (Table 2). Biogenic silica concentration in the plant material of *Elymus athericus* was almost twice as high as of *Spartina anglica* (*Elymus*: 7.14 ± 1.66 mg/g dry weight, *Spartina*: 4.84 ± 0.85 mg/g dry weight). Plants that had been exposed to the autumn treatment had higher biogenic silica concentrations than those of the summer treatment, but this was only significant in *Elymus athericus* (Table 4). Regardless of the species-treatment combinations, biogenic silica concentrations of the third week were significantly higher than those measured in the first and second week (*1*: 5.50 ± 1.99 mg/g dry weight, *2*: 5.45 ± 1.07 mg/g dry weight, *3*: 7.02 ± 1.75 mg/g dry weight). Highest concentrations for biogenic silica were detected in the autumn treatment of *Elymus athericus* (Table 4). The biogenic silica concentration and Young's bending modulus showed a significant positive relationship, indicating an increase in the stiffness of the plant material with increasing biogenic silica concentration (Figure 7).

Discussion

Our study investigated the resistance of salt-marsh vegetation to wave-induced plant damage, which is a relevant question as climate change may induce changes in wave forcing

TABLE 3 Results of linear regression analyses testing the relationship between mean vegetation height and Δ plant frontal area for the different species-treatment combinations as well as the entire data set (n.s. = not significant).

Species	Treatment	Estimate	Std. Error	t value	Pr(>|t|)
Spartina anglica	summer	-0.769	1.467	-0.524	n.s.
	autumn	-1.594	0.823	-1.938	n.s.
Elymus athericus	summer	-3.306	1.355	-2.440	<0.05
	autumn	-1.066	3.128	-0.341	n.s.
All data		-3.184	0.557	-5.718	<0.001

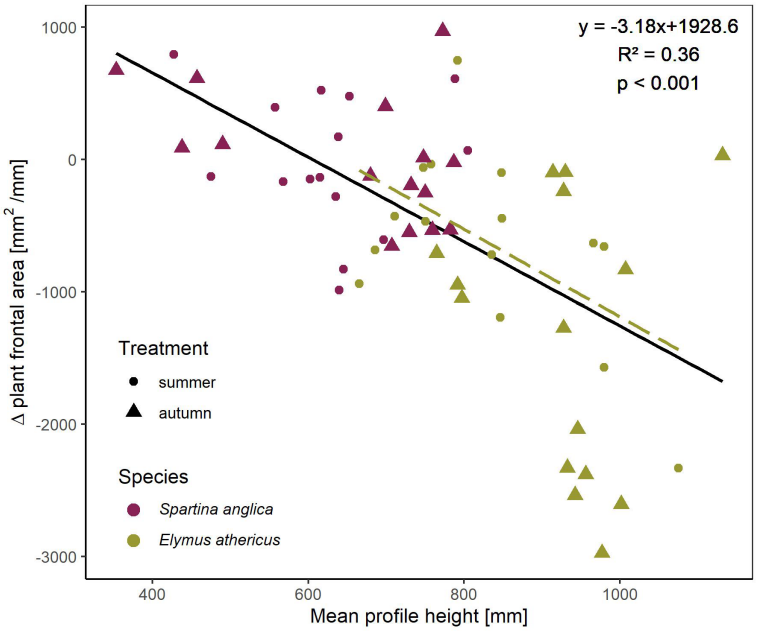

FIGURE 4
Linear regression showing the significant negative relationship between mean vegetation height (in mm, measured prior to wave exposure) and Δ plant frontal area of the entire data set (black line, *Spartina anglica* and *Elymus athericus* including both summer and autumn treatment). The dashed line indicates the significant linear relationship between mean vegetation height and Δ plant frontal area of the summer treatment of *Elymus athericus* only, while the ones of the other species-treatment combinations were not significant (Table 3) and therefore not shown here.

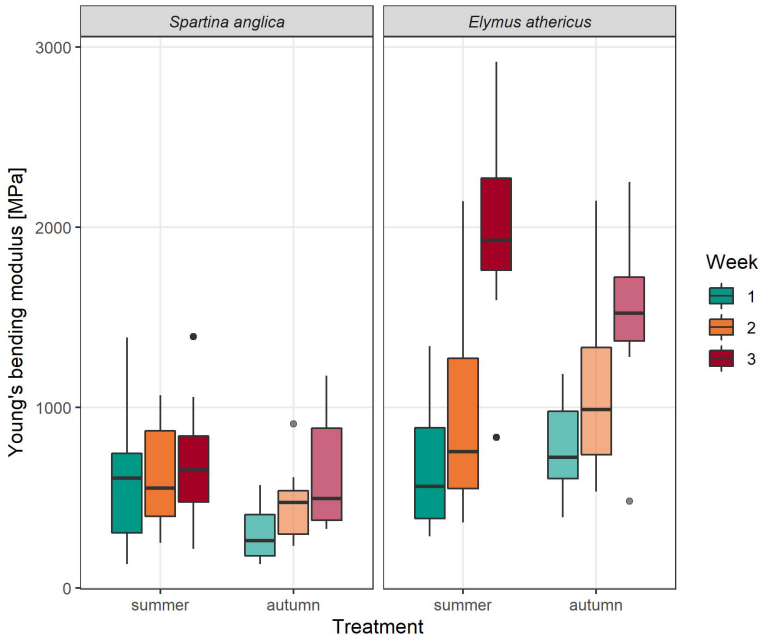

FIGURE 5
Young's bending modulus (MPa) per week of *Spartina anglica* and *Elymus athericus* in summer and autumn condition.

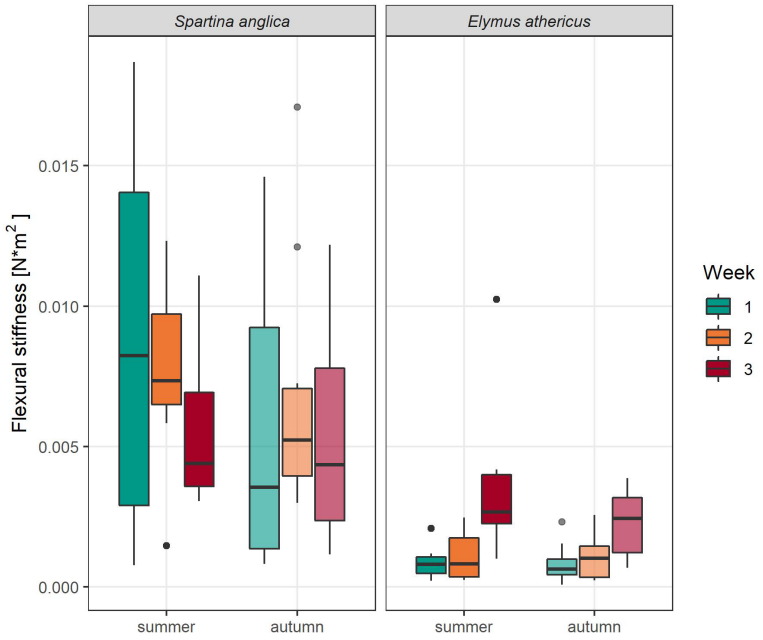

FIGURE 6
Flexural stiffness (Nm^2) per week of *Spartina anglica* and *Elymus athericus* in summer and autumn condition.

on marshes, and as damage to marsh vegetation may imply loss of valuable ecosystem services. So far, studies investigating how hydrodynamic forces affect marsh vegetation focused exclusively on vital vegetation (Heuner et al., 2015; Rupprecht et al., 2017). Seasonal differences in vegetation condition were only accounted for in modelling studies (Vuik et al., 2018) and in field studies (Schulze et al., 2019; Schoutens et al., 2019; Zhu et al., 2020) not directly quantifying plant damage. This flume experiment was designed to compare wave-induced plant damage of two salt-marsh species under both summer (vital) and autumn (weakened) conditions. Furthermore, we aimed to assess whether species-specific or seasonal differences in plant damage are caused by potential differences in biomechanical, biochemical and/or morphological plant properties. In accordance with our first hypothesis, the wave forcing caused significantly more damage (measured as Δ plant frontal area) to *Elymus athericus*, than to *Spartina anglica*. Moreover, we found indications of higher plant damage in the autumn treatment compared to the summer treatment in *Elymus athericus*, but not in *Spartina anglica*, only partly supporting our second hypothesis. In the following paragraphs, we will discuss factors that may have affected our results, focusing on measured variables (canopy height, biomechanical and biochemical plant properties) and whether they are suitable determinants of plant resistance to wave-induce plant damage.

In comparison with *Elymus athericus*, the plant damage of *Spartina anglica* was relatively low. *Spartina anglica* is typically growing in pioneer marsh zones and is therefore regularly exposed to higher wave intensities, which may lead to a higher resistance, as compared to *Elymus athericus*, which grows typically in high, wave-sheltered marsh zones (Suchrow and Jensen, 2010). This adaptation mechanism has also been suggested as a possible explanation for thicker reed (*Phragmites* spp) stems at an exposed site on the southern shore of the Baltic Sea (Möller et al., 2011) and has been

TABLE 4 Strengthening compound concentration of plant material of two salt-marsh species in summer and autumn condition averaged over weeks (mean ± SD in mg/g dry weight).

	Spartina anglica		*Elymus athericus*	
Compound	**summer**	**autumn**	**summer**	**autumn**
Cellulose	276.75 ± 16.16^{a}	240.08 ± 90.34^{a}	214.72 ± 28.88^{a}	246.46 ± 25.55^{a}
Lignin	42.44 ± 26.29^{a}	29.84 ± 20.67^{a}	31.28 ± 12.20^{a}	29.47 ± 9.67^{a}
BSi	4.50 ± 0.80^{a}	5.18 ± 0.82^{ab}	6.20 ± 1.06^{b}	8.09 ± 1.66^{c}

Different letters indicate significant differences between species-treatment combinations according to a Tukey test at $p < 0.05$.

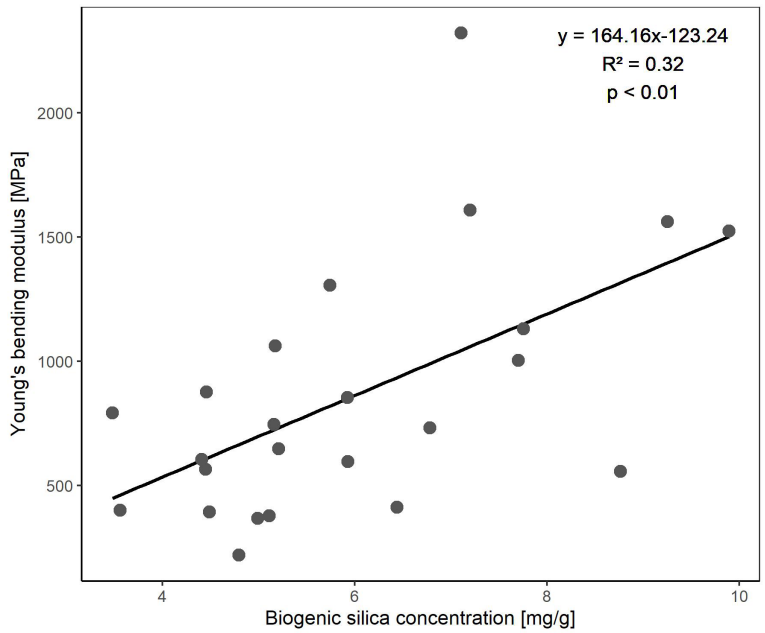

FIGURE 7
Linear regression showing the significant positive relationship between Young's bending modulus and biogenic silica concentration. The data includes both species, treatments and all three weeks.

shown to exist for other marsh pioneer species (Silinski et al., 2018). Interestingly, for other species it has been shown that the opposite mechanism (i.e. a reduction in rigidity) is beneficial as it allows plants to bend under the flow, thereby reducing drag forces acting on plants (Schoutens et al., 2020). Even seedlings display different levels of plant resistance to hydrodynamic forcing depending on their site of origin, with salt-marsh species being less damaged by hydrodynamic forcing than brackish marsh species (Schoutens et al., 2021).

Vegetation height

Our results indicate that wave-induced plant damage mostly occurs in the upper part of the vegetation canopy (Figure 3) and that higher vegetation canopies (e.g. *Elymus athericus*) are more vulnerable to damage (Figure 4). An increase in plant damage with increasing plant height was also described in modelling studies by Vuik et al. (2018) and Duan et al. (2002). Taller plants might be more affected by wave impact because wave orbital motion and thereby wave energy is greatest at the water surface and decreases with water depth (Anderson and Smith, 2014; Möller and Christie, 2019). As Duan et al. (2002) found that the ratio of the top to base stem diameter can affect the position of plant damage along the stem this ratio might have given another possible explanation for our observation but unfortunately this has not been assessed in this study. Although plants under the autumn treatment were slightly taller than under the summer treatment, these differences might not have been big enough to affect the plants vulnerability to plant damage since we have not found significant relationships through our linear regression analyses (except for *Elymus athericus* in summer condition, Table 3). This suggest that vegetation height alone did not entirely explain observed pattern e.g. the higher plant damage in the autumn treatment compared to the summer treatment of *Elymus athericus*. However, it should be noted that one value of *Elymus athericus* under the autumn treatment stands out (mean vegetation height = 1131.68 mm, Δ plant frontal area = 31.89 mm^2/mm, Figure 4) which might have affected the insignificance of the relationship.

Biomechanical plant properties and plant resistance

Canopy height may correlate with biomechanical plant properties because taller species tend to have stiffer stems than shorter ones (Zhu et al., 2020). In our study, this difference between taller and shorter species was only true for Young's bending modulus, which describes the stiffness of plant material itself without taking stem morphology into account. Here the plant material of the taller species (*Elymus athericus*) was indeed stiffer. However, when considering the absolute strength of the stems by integrating stem morphology (i.e. flexural stiffness), the taller species *Elymus athericus* had weaker stems than the shorter

Spartina anglica (Figure 6), which might have contributed to the higher vulnerability to wave-induced plant damage found for *Elymus athericus*. Flexural stiffness of *Elymus athericus* (1.61 ± 1.59 Nm^2*10^{-3}) was similar to values Rupprecht et al. (2015) reported for salt marshes in the Dengie Peninsula, England, (1.23 ± 0.64 Nm^2*10^{-3}). Nevertheless, flexural stiffness of *Spartina anglica* (6.56 ± 4.39 Nm^2*10^{-3}) was much higher in our study compared to Rupprecht et al. (2015) (3.51 ± 0.58 Nm^2*10^{-3}). Interestingly, flexural stiffness increased from week to week but only for *Elymus athericus*, while we see a decreasing tendency for *Spartina anglica*. This significant interaction effect of weeks and species on flexural stiffness might reflect different aging pattern as the plants of week two and three had more time to mature before they placed in the flume. Consequently, an adaptation to wave exposure can be neglected because we used new sets of plants every week. Neither Young's bending modulus nor flexural stiffness were affected by the summer and autumn treatments (Table 2). Since the increase in Young's bending modulus over the weeks was also present in the autumn treatments, it might suggest that the peak in plant stiffness with further maturation was not reached and the drought treatment was not long enough.

Biochemical plant properties and plant resistance

We have not found any significant differences between species nor treatments in strengthening compounds except for biogenic silica. Biogenic silica increases rigidity and, in contrast to cellulose and lignin, its incorporation is at lower energetic costs (Schoelynck et al., 2010). In comparison with *Spartina anglica*, biogenic silica concentrations were much higher for *Elymus athericus*, which might have resulted in the higher stiffness of the plant material (Young's bending modulus) since a positive relationship between these two variables has been shown to exist for the entire data set (Figure 7). We also found significant higher biogenic silica concentrations in the plant material of the autumn treatment in comparison with the summer treatment (Tables 2 and 4). However, these differences between the treatments cannot directly be translated into a higher stiffness of the plant material since we have not found an effect of the treatment on Young's bending modulus. The seasonal differences in biogenic silica concentration might have contributed to a higher stiffness of the plant material, if the drought treatment were to have been applied for longer.

Methodological considerations

Autumn treatment – Applying a drought to create an autumn treatment seems to have worked well for *Elymus athericus* since biomechanical properties of the autumn treatment correspond well with data gathered in the field in early spring i.e. before the onset of plant growth (flexural stiffness, our study: 1.40 ± 1.09 Nm^2*10^{-3}, field: 1.54 ± 0.58 Nm^2*10^{-3}, Schulze et al., 2019). In contrast, *Spartina anglica* seemed to be barely affected by the drought treatment. This could be explained by *Spartina anglica* being a C4 plant, which generally results in higher water use efficiency and tolerance against drought (Taylor et al., 2014). Considering the circumstances of our experimental set up, the drought treatment turned out as a good method to create the weakened autumn condition. However, for future studies, we suggest to conduct a flume study with vegetation collected in autumn to support our findings. Alternatively, and if available, climate rooms could be used to induce an autumn condition by reducing light availability and temperature.

Photo method – For our study, using the photo method for detecting plant damage fast and non-destructively generated relatively good results. This is especially true for higher wave intensities resulting in major changes in plant frontal area which was also noticeable in the amount of torn-off plant material after wave exposure (Supplementary Material Figure 3). Nevertheless, reconfiguration, which is likely to be height-dependent, cannot be excluded as contributing factor to changes in plant frontal area. In the first week, this became visible when wave intensities were not high enough to cause distinguishable damage but rather caused a rearrangement and straightening of the vegetation under inundation, which eventually led to positive values in Δ plant frontal area. Since the bottom sections of the vegetation photographs were saturated with vegetation pixels and plant parts were overlapping, changes in plant frontal area might not be as recognizable there as at the top (where vegetation was less dense). For future research on wave-induced plant damage, we recommend to use less dense vegetation if it is not possible/desirable to create extreme wave conditions. Additionally, more investigations should be conducted on the flexibility as well as concentration of strengthening compounds of the plant leaves since they contribute to plant frontal area (Zhang and Nepf, 2021) and have not been determined in this study.

Effect of weeks – Lastly, plant damage of both species increased (i.e. Δ plant frontal area decreased) from week to week (Figure 2). This can be explained by the hydrodynamic forces, which were set to increase successively. Moving of the pallets in the direction of the wave paddle in the third week further increased hydrodynamic forces potentially resulting in an amplification of plant damage, which was observed for *Elymus athericus* (in autumn condition) and perhaps even implies a threshold effect for this particular species-treatment combination. However, we noticed upward trends from week to week also in other variables that were independent of wave conditions such as Young's bending modulus, flexural stiffness and biogenic silica concentration. These trends might be due to natural development as plants matured outside the wave flume prior to the placement on the flume test section, which

was inevitable but should be born in mind when interpreting our results.

Although we created storm surge conditions that are typical for the NW European salt marshes, the vegetation was more robust than expected. This finding is of great importance as it provides additional support for the high resilience of salt marshes to storm impact. A species-specific characterization with respect to the vegetation's vulnerability to wave-induced damage is important to faster assess the status and predict future responses of a salt marsh, and of course adapt management if necessary. Furthermore, we need to investigate how climate change (e.g. increased warming) affects biomechanical and morphological plant properties, which have been shown to clearly affect plant's vulnerability to wave-induced damage. It is interesting to note here that recent studies report that *Elymus athericus* has formed a new genotype that is growing at lower elevations and appears to be better adapted to higher flooding frequencies (Veeneklaas et al., 2013; Reents et al., 2021). *Elymus athericus* is highly competitive and has, due to the new genotype, the potential to outcompete other species and further establish in lower parts of the marsh. Investigations on whether this genotype exhibits a higher resistance against increased hydrodynamic forces, is required to improve predictions on potential shifts in species composition and thereby marsh resilience in the future.

However, it is worth noting that, over longer (decadal) time scales, the susceptibility of aboveground biomass to breakage or loss may in fact reduce the risk for uprooting and hence allow the belowground biomass to remain intact during severe storm impact, as noted by Schoutens et al. (2021). Without removal of the aboveground parts of the plant, wave-forces can translate into stresses at the water/sediment interface around the plant stem that may produce scour, associated loss of sediment, and ultimately the potential uprooting of the plant itself. Following this, another focus for future studies should be to investigate whether wave-induced plant damage and thus aboveground biomass loss ultimately have a positive or negative effect on the longer-term survival chances of the vegetation and thereby provision of wave attenuation under altered future environmental conditions.

Data availability statement

The raw data supporting the conclusions of this article will be made available by the authors, without undue reservation.

Author contributions

SR conducted vegetation measurements, analyzed the data and wrote the first draft. JL conducted the three-point bending tests. BE wrote the MATLAB program for the image analysis. All authors designed the study, contributed to the article and approved the submitted version.

Funding

The work described in this publication was supported by the European Community's Horizon 2020 Research and Innovation Programme through the grant to HYDRALAB-PLUS (contract no. 654110). SR was funded by the German Research Foundation (DFG, Deutsche Forschungsgemeinschaft, project no. 401564364) and KS by the Research Foundation Flanders, Belgium (FWO, PhD fellowship for fundamental research, 1116319 N). Additional support was provided by the RESIST-UK project (UKRI Natural Environment Research Council grant no. NE/R01082X/1). We acknowledge support by the Open Access Publication Funds of Alfred-Wegener-Institut Helmholtz-Zentrum für Polar- und Meeresforschung.

Acknowledgments

We would like to thank the team from the Forschungszentrum Küste (FZK) as well as Meline Brendel, Helen Brooks, Haobing Cao, Elizabeth Christie, Rachael Dennis, Anke van Eggermond, Grazia Doronzo and Lennart van IJzerloo.

Conflict of interest

Author JL is employed by BioConsult SH GmbH & Co. KG. The remaining authors declare that the research was conducted in the absence of any commercial or financial relationships that could be construed as a potential conflict of interest.

Publisher's note

Supplementary material

The Supplementary Material for this article can be found online at: https://www.frontiersin.org/articles/10.3389/fmars.2022.898080/full#supplementary-material

References

Adam, P. (2002). Saltmarshes in a time of change. *Envir. Conserv.* 29, 39–61. doi: 10.1017/S0376892902000048

Anderson, M. E., and Smith, J. M. (2014). Wave attenuation by flexible, idealized salt marsh vegetation. *Coast. Eng.* 83, 82–92. doi: 10.1016/j.coastaleng.2013.10.004

Armitage, A. R., Weaver, C. A., Kominoski, J. S., and Pennings, S. C. (2020). Resistance to hurricane effects varies among wetland vegetation types in the marsh–mangrove ecotone. *Estuaries. Coasts.* 43, 960–970. doi: 10.1007/s12237-019-00577-3

Bouma, T. J., Vries, M.B. de, and Herman, P. M. J. (2010). Comparing ecosystem engineering efficiency of two plant species with contrasting growth strategies. *Ecology* 91, 2696–2704. doi: 10.1890/09-0690.1

Bouma, T. J., Vries, M.B.de, Low, E., Peralta, G., Tánczos, I. C., van de Koppel, J., et al. (2005). Trade-offs related to ecosystem engineering: A case study on stiffness of emerging macrophytes. *Ecology* 86, 2187–2199. doi: 10.1890/04-1588

Coops, H., and van der Velde, G. (1996). Effects of waves on helophyte stands: mechanical characteristics of stems of *Phragmites australis* and *Scirpus lacustris*. *Aquat. Bot.* 53, 175–185. doi: 10.1016/0304-3770(96)01026-1

Cseresnyés, I., Rajkai, K., Szitár, K., Radimszky, L., Ónodi, G., and Kröel-Dulay, G. (2020). Root capacitance measurements allow non-intrusive in-situ monitoring of the seasonal dynamics and drought response of root activity in two grassland species. *Plant Soil* 449, 423–437. doi: 10.1007/s11104-020-04505-4

Desclaux, D., and Roumet, P. (1996). Impact of drought stress on the phenology of two soybean (*Glycine max* L. Merr) cultivars. *Field Crops Res.* 46, 61–70. doi: 10.1016/0378-4290(95)00086-0

Duan, J. G., French, R. H., and Miller, J. (2002). The lodging velocity for emergent aquatic plants in open channels. *J. Am. Water Resour. Assoc.* 38, 255–263. doi: 10.1111/j.1752-1688.2002.tb01549.x

Duarte, C. M., Losada, I. J., Hendriks, I. E., Mazarrasa, I., and Marbà, N. (2013). The role of coastal plant communities for climate change mitigation and adaptation. *Nat. Clim. Change* 3, 961–968. doi: 10.1038/nclimate1970

ESRI (2020). *ArcGIS desktop* (Version 10.8: Redlands, California).

Garzon, J. L., Maza, M., Ferreira, C. M., Lara, J. L., and Losada, I. J. (2019). Wave attenuation by *Spartina* saltmarshes in the Chesapeake bay under storm surge conditions. *J. Geophys. Res. Oceans.* 124, 5220–5243. doi: 10.1029/2018JC014865

Gedan, K. B., Kirwan, M. L., Wolanski, E., Barbier, E. B., and Silliman, B. R. (2011). The present and future role of coastal wetland vegetation in protecting shorelines: answering recent challenges to the paradigm. *Climatic. Change* 106, 7–29. doi: 10.1007/s10584-010-0003-7

Gepstein, S., and Glick, B. R. (2013). Strategies to ameliorate abiotic stress-induced plant senescence. *Plant Mol. Biol.* 82, 623–633. doi: 10.1007/s11103-013-0038-z

Groeneveld, D. P., and French, R. H. (1995). Hydrodynamic control of an emergent aquatic plant (Scirpus acutus) in open channels. *J. Am. Water Resour. Assoc.* 31, 505–514. doi: 10.1111/j.1752-1688.1995.tb04037.x

Hasselmann, K., Barnett, T. P., Bouws, E., Carlson, H., Cartwright, D. E., Enke, K., et al. (1973). Measurements of wind-wave growth and swell decay during the joint north Sea wave project (JONSWAP). *Ergänzungsheft. zur Deutschen Hydrographischen. Zeitschrift. Reihe. A Nr.* 12, 1–95.

Heuner, M., Silinski, A., Schoelynck, J., Bouma, T. J., Puijalon, S., Troch, P., et al. (2015). Ecosystem engineering by plants on wave-exposed intertidal flats is governed by relationships between effect and response traits. *PloS One* 10, e0138086. doi: 10.1371/journal.pone.0138086

Koch, E. W., Barbier, E. B., Silliman, B. R., Reed, D. J., Perillo, G. M. E., Hacker, S. D., et al. (2009). Non-linearity in ecosystem services: temporal and spatial variability in coastal protection. *Front. Ecol. Environ.* 7, 29–37. doi: 10.1890/080126

Leonardi, N., Carnacina, I., Donatelli, C., Ganju, N. K., Plater, A. J., Schuerch, M., et al. (2018). Dynamic interactions between coastal storms and salt marshes: A review. *Geomorphology* 301, 92–107. doi: 10.1016/j.geomorph.2017.11.001

Mcleod, E., Chmura, G. L., Bouillon, S., Salm, R., Björk, M., Duarte, C. M., et al. (2011). A blueprint for blue carbon: Toward an improved understanding of the role of vegetated coastal habitats in sequestering CO 2. *Front. Ecol. Environ.* 9, 552–560. doi: 10.1890/110004

Möller, I. (2006). Quantifying saltmarsh vegetation and its effect on wave height dissipation: Results from a UK East coast saltmarsh. *Estuarine. Coast. Shelf. Sci.* 69, 337–351. doi: 10.1016/j.ecss.2006.05.003

Möller, I., and Christie, E. (2019). "Hydrodynamics and modeling of water flow in coastal wetlands," in *Coastal wetlands* (Amsterdam (NL), Oxford (UK), Cambridge (USA): Elsevier), 289–323.

Möller, I., Kudella, M., Rupprecht, F., Spencer, T., Paul, M., van Wesenbeeck, B. K., et al. (2014). Wave attenuation over coastal salt marshes under storm surge conditions. *Nat. Geosci.* 7, 727–731. doi: 10.1038/ngeo2251

Möller, I., Mantilla-Contreras, J., Spencer, T., and Hayes, A. (2011). Micro-tidal coastal reed beds: Hydro-morphological insights and observations on wave transformation from the southern Baltic Sea. *Estuarine. Coast. Shelf. Sci.* 92, 424–436. doi: 10.1016/j.ecss.2011.01.016

Möller, I., Spencer, T., and Rawson, J. (2003). "Spatial and temporal variability of wave attenuation over a UK saltmarsh," in *Coastal Engineering 2002:* Proceedings of the 28th international conference - Coastal Engineering. (Singapore (SGP), New Jersey (USA), London (UK)) *World Scientific.* 651–663.

Niklas, K. J. (1992). *Plant biomechanics: An engineering approach to plant form and function* (Chicago & London: The University of Chicago Press).

Paul, M., Rupprecht, F., Möller, I., Bouma, T. J., Spencer, T., Kudella, M., et al. (2016). Plant stiffness and biomass as drivers for drag forces under extreme wave loading: A flume study on mimics. *Coast. Eng.* 117, 70–78. doi: 10.1016/j.coastaleng.2016.07.004

Pinsky, M. L., Guannel, G., and Arkema, K. K. (2013). Quantifying wave attenuation to inform coastal habitat conservation. *Ecosphere* 4, 1–16. doi: 10.1890/ES13-00080.1

R Core Team (2021). *R: A language and environment for statistical* (Vienna, Austria: R Foundation for Statistical Computing).

Reents, S., Mueller, P., Tang, H., Jensen, K., and Nolte, S. (2021). Plant genotype determines biomass response to flooding frequency in tidal wetlands. *Biogeosciences* 18, 403–411. doi: 10.5194/bg-18-403-2021

Riffe, K. C., Henderson, S. M., and Mullarney, J. C. (2011). Wave dissipation by flexible vegetation. *Geophys. Res. Lett.* 38, 1–5. doi: 10.1029/2011GL048773

Rupprecht, F., Möller, I., Evans, B., Spencer, T., and Jensen, K. (2015). Biophysical properties of salt marsh canopies — Quantifying plant stem flexibility and above ground biomass. *Coast. Eng.* 100, 48–57. doi: 10.1016/j.coastaleng.2015.03.009

Rupprecht, F., Möller, I., Paul, M., Kudella, M., Spencer, T., van Wesenbeeck, B. K., et al. (2017). Vegetation-wave interactions in salt marshes under storm surge conditions. *Ecol. Eng.* 100, 301–315. doi: 10.1016/j.ecoleng.2016.12.030

Sade, N., Del Mar Rubio-Wilhelmi, M., Umnajkitikorn, K., and Blumwald, E. (2018). Stress-induced senescence and plant tolerance to abiotic stress. *J. Exp. Bot.* 69, 845–853. doi: 10.1093/jxb/erx235

Schoelynck, J., Bal, K., Backx, H., Okruszko, T., Meire, P., and Struyf, E. (2010). Silica uptake in aquatic and wetland macrophytes: A strategic choice between silica, lignin and cellulose? *New Phytol.* 186, 385–391. doi: 10.1111/j.1469-8137.2009.03176.x

Schoelynck, J., Bal, K., Puijalon, S., Meire, P., and Struyf, E. (2012). Hydrodynamically mediated macrophyte silica dynamics. *Plant Biol. (Stuttg)* 14, 997–1005. doi: 10.1111/j.1438-8677.2012.00583.x

Schoutens, K., Heuner, M., Fuchs, E., Minden, V., Schulte-Ostermann, T., Belliard, J.-P., et al. (2020). Nature-based shoreline protection by tidal marsh plants depends on trade-offs between avoidance and attenuation of hydrodynamic forces. *Estuarine. Coast. Shelf. Sci.* 236, 106645. doi: 10.1016/j.ecss.2020.106645

Schoutens, K., Heuner, M., Minden, V., Schulte Ostermann, T., Silinski, A., Belliard, J.-P., et al. (2019). How effective are tidal marshes as nature-based shoreline protection throughout seasons? *Limnol. Oceanogr.* 64, 1750–1762. doi: 10.1002/lno.11149

Schoutens, K., Reents, S., Nolte, S., Evans, B., Paul, M., Kudella, M., et al. (2021). Survival of the thickest? impacts of extreme wave-forcing on marsh seedlings are mediated by species morphology. *Limnol. Oceanogr.* 66, 2936–2951. doi: 10.1002/lno.11850

Schuerch, M., Spencer, T., Temmerman, S., Kirwan, M. L., Wolff, C., Lincke, D., et al. (2018). Future response of global coastal wetlands to sea-level rise. *Nature* 561, 231–234. doi: 10.1038/s41586-018-0476-5

Schulze, D., Rupprecht, F., Nolte, S., and Jensen, K. (2019). Seasonal and spatial within-marsh differences of biophysical plant properties: Implications for wave attenuation capacity of salt marshes. *Aquat. Sci.* 81, 1–11. doi: 10.1007/s00027-019-0660-1

Silinski, A., Schoutens, K., Puijalon, S., Schoelynck, J., Luyckx, D., Troch, P., et al. (2018). Coping with waves: Plasticity in tidal marsh plants as self-adapting coastal ecosystem engineers. *Limnol. Oceanogr.* 63, 799–815. doi: 10.1002/lno.10671

Spencer, T., Schuerch, M., Nicholls, R. J., Hinkel, J., Lincke, D., Vafeidis, A. T., et al. (2016). Global coastal wetland change under sea-level rise and related stresses: The DIVA wetland change model. *Global Planetary. Change* 139, 15–30. doi: 10.1016/j.gloplacha.2015.12.018

Suchrow, S., and Jensen, K. (2010). Plant species responses to an elevational gradient in German North Sea salt marshes. *Wetlands* 30, 735–746. doi: 10.1007/s13157-010-0073-3

Talukdar, D. (2013). Comparative morpho-physiological and biochemical responses of lentil and grass pea genotypes under water stress. *J. Nat. Sci. Biol. Med.* 4, 396–402. doi: 10.4103/0976-9668.116983

Taylor, S. H., Ripley, B. S., Martin, T., De-Wet, L.-A., Woodward, F. I., and Osborne, C. P. (2014). Physiological advantages of C4 grasses in the field: A comparative experiment demonstrating the importance of drought. *Glob. Chang. Biol.* 20, 1992–2003. doi: 10.1111/gcb.12498

The MathWorks Inc. (2019). *MATLAB* (Version R2019a: Natick, Massachusetts).

Turner, S. R., Taylor, N., and Jones, L. (2001). "Mutations of the secondary cell wall," in *Plant cell walls*. Eds. N. C. Carpita, M. Campbell and M. Tierney (Dordrecht: Springer Netherlands), 209–219.

Veeneklaas, R. M., Dijkema, K. S., Hecker, N., and Bakker, J. P. (2013). Spatio-temporal dynamics of the invasive plant species *Elytrigia atherica* on natural salt marshes. *Appl. Veg. Sci.* 16, 205–216. doi: 10.1111/j.1654-109X.2012.01228.x

Vuik, V., Suh Heo, H. Y., Zhu, Z., Borsje, B. W., and Jonkman, S. N. (2018). Stem breakage of salt marsh vegetation under wave forcing: A field and model study. *Estuarine. Coast. Shelf. Sci.* 200, 41–58. doi: 10.1016/j.ecss.2017.09.028

Ysebaert, T., Yang, S.-L., Zhang, L., He, Q., Bouma, T. J., and Herman, P. M. J. (2011). Wave attenuation by two contrasting ecosystem engineering salt marsh macrophytes in the intertidal pioneer zone. *Wetlands* 31, 1043–1054. doi: 10.1007/s13157-011-0240-1

Zhang, W., Ge, Z.-M., Li, S.-H., Tan, L.-S., Zhou, K., Li, Y.-L., et al. (2022). The role of seasonal vegetation properties in determining the wave attenuation capacity of coastal marshes: Implications for building natural defenses. *Ecol. Eng.* 175, 106494. doi: 10.1016/j.ecoleng.2021.106494

Zhang, X., and Nepf, H. (2021). Wave-induced reconfiguration of and drag on marsh plants. *J. Fluids. Structures* 100, 103192. doi: 10.1016/j.jfluidstructs.2020.103192

Zhu, Z., Yang, Z., and Bouma, T. J. (2020). Biomechanical properties of marsh vegetation in space and time: Effects of salinity, inundation and seasonality. *Ann. Bot.* 125, 277–290. doi: 10.1093/aob/mcz063

Zuur, A. F., Ieno, E. N., and Elphick, C. S. (2010). A protocol for data exploration to avoid common statistical problems. *Methods Ecol. Evol.* 1, 3–14. doi: 10.1111/j.2041-210X.2009.00001.x

Frontiers in Marine Science

Explores ocean-based solutions for emerging global challenges

The third most-cited marine and freshwater biology journal, advancing our understanding of marine systems and addressing global challenges including overfishing, pollution, and climate change.

Discover the latest Research Topics

See more →

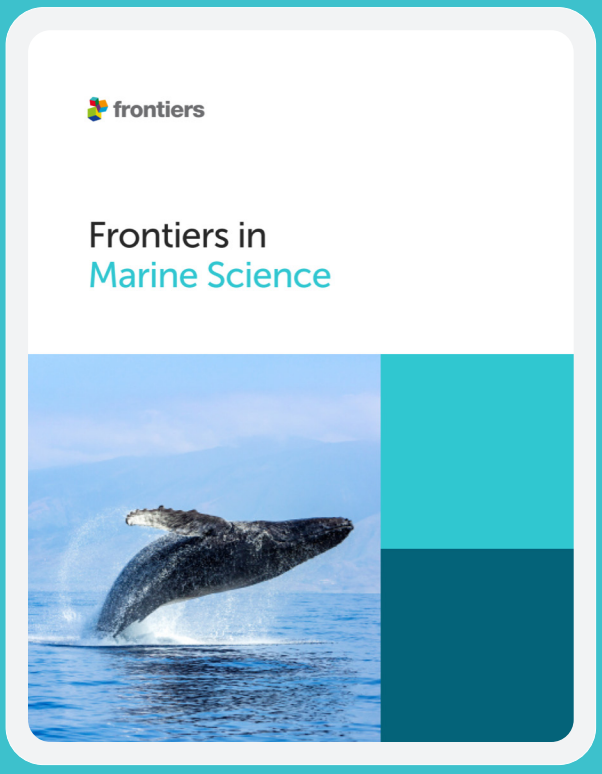

Frontiers

Avenue du Tribunal-Fédéral 34
1005 Lausanne, Switzerland
frontiersin.org

Contact us

+41 (0)21 510 17 00
frontiersin.org/about/contact